Simple monocyclic aromatic compounds from a global scale perspective

Carlos David Cabrera Perez

geboren in Madrid

Dissertation zur Erlangung des akademischen Grades "Doctor rerum naturalium (Dr. rer. nat.)"

am

Institut für Physik der Atmosphäre

am Fachbereich Physik, Mathematik und Informatik der Johannes Gutenberg-Universität Mainz

March 2017

Abstract

In this thesis mono-cyclic aromatic compounds in the atmosphere are chemically characterized at a global scale. Atmospheric budgets, impacts on atmospheric photo-chemistry, and past and future trends of aromatic compounds are estimated using numerical simulations.

The Modular ECHAM/MESSy Atmospheric Chemistry (EMAC) model with an aromatic compound oxidation mechanism was used in this thesis. Emissions from biomass burning, anthropogenic sources, and biogenic sources were incorporated, allowing us simulate sources, sinks, and mixing ratios of aromatic compounds.

The model simulation was compared with a set of observations compiled from surface and aircraft measurements. We found good spatial and temporal agreement of numerically simulated concentrations of benzene; good agreement at the surface, but a large underestimation in the free troposphere for toluene, and even larger discrepancies for xylenes. The budget of most aromatic compounds is driven by anthropogenic emissions—which constitute the largest source of aromatics ($\simeq 23$ TgC year^{-1})—as well as by photochemical decomposition, which is responsible for the removal of $\simeq 27$ TgC year^{-1}. Biomass burning is the second-largest source of aromatic compounds ($\simeq 5$ TgC year^{-1}), followed by the simulated chemical production of aromatics, which accounts for $\simeq 5$ TgC year^{-1}. Wet and dry deposition are responsible for a small sink of $\simeq 4$ TgC year^{-1}, and the global atmospheric burden of aromatics amounts to 0.3 TgC.

A comparison of simulation scenarios including and excluding aromatic compounds revealed that they cause a net annual global mean decrease in OH and O_3 mixing ratios. However, an increase in OH and O_3 mixing ratios is found in the high NO_x mixing ratios areas. NO_x mixing ratios decreased globally due to the partial transfer of the NO_x atmospheric burden into nitrogenated aromatic species. Among VOCs, glyoxal was most strongly affected by the inclusion of aromatics in the chemical mechanism, with mixing ratios increasing by 20%.

Finally, we studied trends in atmospheric mixing ratios between 1950 and 2050, through a series of simulations covering past, present, and future projections. At the global scale, mixing ratios of most aromatic compounds increased steadily for the entire 100-year period, with a small decrease towards 2050. At the regional scale, the mixing ratios in Europe and North America increased from 1950 to 2010, followed by a strong decrease until 2050. In contrast, a continuous increase was found in Southeast Asia and over the Arabian Peninsula.

Contents

Chapter 1

Introduction

1.1 The role of volatile organic compounds in the atmosphere

The lowest layer of Earth's atmosphere, the troposphere, contains 75% of the total atmospheric mass. The troposphere is almost entirely composed of nitrogen (78.09%), oxygen (20.95%), and argon (0.93%), with the remaining 0.03% containing more than ten thousand trace gases. Within this large number of species, hydrocarbons are a highly relevant group. *Hydrocarbons* are defined as any chemical compound formed by carbon and hydrogen molecules, which excludes compounds containing oxygen, sulphur, or nitrogen. For this reason, in the present thesis, the broader term *volatile organic compound* (VOC), defined as "organic compounds having pressure greater than 10 Pa at 25°C, a boiling point of up to 260°C at atmospheric pressure, and 15 or less carbon atoms" is used (Koppmann, 2008). This definition is not universal. For example, the World Health Organization (WHO) defines a VOC as any organic compound whose boiling point is within the range of (50°C to 100°C) to (240°C to 260° C), i.e. a saturation vapour pressure greater than 100 kPa at 25°C. Another definition is given by the Iowa Department of Natural Resources (DNR), which defines a VOC as any compound of carbon—excluding carbon monoxide, carbon dioxide, carbonic acid, metallic carbides or carbonates, and ammonium carbonate—which participates in atmospheric photochemical reactions.

Carbon dioxide, carbon monoxide, and methane are the most abundant VOCs in the troposphere; carbon dioxide has a mixing ratio of around 370 ppmv (10^{-6} mol/mol), methane (1.8 ppmv), and carbon monoxide (0.15 ppmv). However, although they are the most abundant, these species are not the most reactive, and there are a large number of reactive organic compounds with mixing ratios ranging from nmol/mol to pmol/mol.

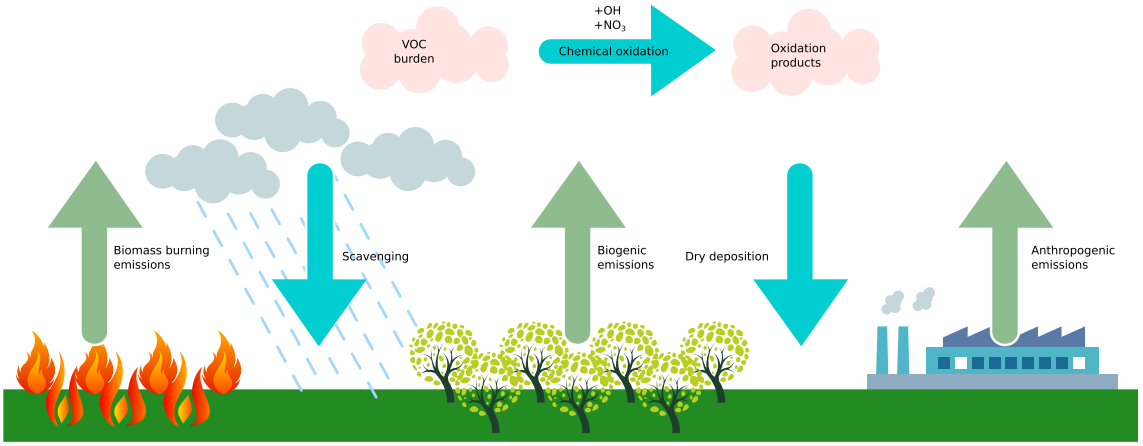

FIGURE 1.1: Schematic of sources and sinks of aromatic compounds in the atmosphere.

Volatile organic compounds have a large impact on the atmosphere despite their low concentrations, and can be considered a source of the oxidative power of the atmosphere. They have therefore been the subject of numerous studies for several decades. In addition to their sizeable influence on atmospheric photochemistry from the local to the global scale, VOCs have the potential to affect climate change both directly and indirectly. VOCs can lead to aerosol formation upon chemical oxidation, meaning that they can form products that have sufficiently low vapour pressure such that they partition into the condensed phase (Kroll and Seinfeld, 2008).

Atmospheric VOC sources are classified into four types: anthropogenic, biomass burning, biogenic, and oceanic. Cooking; natural fires; human, animal, and plant respiration; fossil fuel burning by engines; and refineries are only a few examples of the vast number of processes that release organic compounds into the atmosphere (Andreae and Merlet, 2001; McDonald et al., 2003; Barker et al., 2006; Na et al., 2004). An enormous variety of VOCs are released, including carbonyls, alcohols, alkenes, alkanes, esters, aromatics, ethers, and amides. Together, all of these sources release approximately 1.7 Pg/year of VOCs. Table 1.1 summarizes the reactive-carbon emissions (i.e. carbon monoxide, methane and VOCs) sorted by sources. Total VOC emissions are larger than methane emissions and in the same order of magnitude as carbon monoxide emissions.

The biosphere is of great importance for emissions of organic compounds. As photosynthesis converts carbon dioxide into biomass, some of this carbon is released into the atmosphere in the form of VOCs, most commonly as isoprene and terpenes. The amount of organic matter released depends on physical parameters such as temperature, moisture, and light, as well as the type, health, and age of the plant (Guenther, 2002). The biosphere also uses air as a communication medium, with insects and plants emitting specific organic species to signal information or repel potential threats (Cremer et al., 2002;

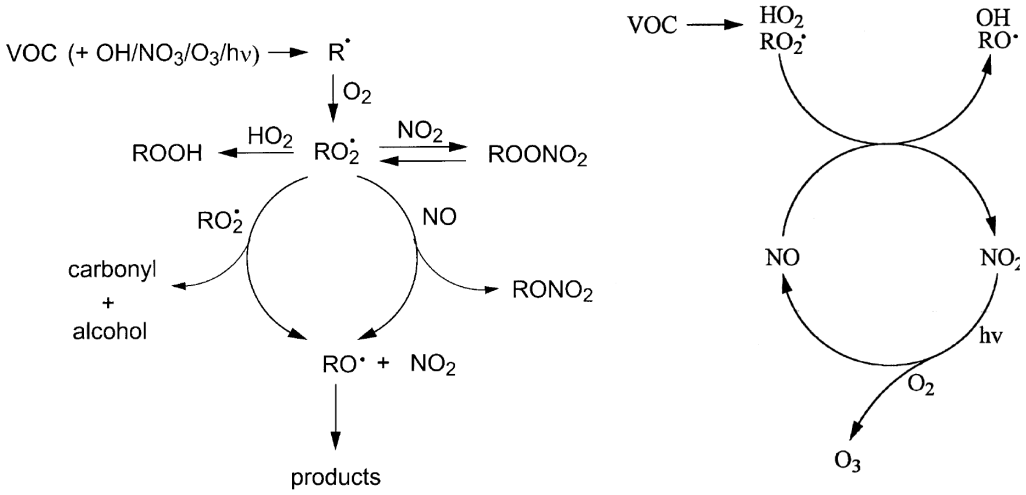

FIGURE 1.2: Left: VOC general degradation scheme. Right: Scheme of ozone formation, including the main chemical compounds involved. The schemes were taken from (Atkinson and Arey, 2003).

Shiojiri et al., 2002). The estimated global VOC emissions from vegetation are about 1.2 Pg/year (Guenther, 2002).

Although there are a large number of anthropogenic sources, they are dominated by processes related to fossil fuels (i.e. coal, oil, and gas). Coal production principally releases methane, along with small fractions of ethane and propane. Thus, a large variety of VOCs are emitted to the atmosphere through the production, storage, and distribution of liquid fossil fuel (Koppmann, 2008). The most relevant sources of VOCs due to processing liquid fossil fuel are catalytic cracking and asphalt blowing (Friedrich and Obermeier, 1999). Evaporation and leaking also take place in engines and service stations. In addition to fossil fuels, other sources of VOCs include industrial processes; paints and solvents; biofuel combustion, which is the primary anthropogenic source of VOCs for developing countries, and which is mostly used for heating and cooking; and waste management (Koppmann, 2008). Global anthropogenic VOC emissions amount to around 130 Tg/year (Lamarque et al., 2010).

A third important source of VOCs into the atmosphere is biomass burning. The influence of biomass burning is strong in the tropics during the dry season (September - October). Fires are used to clean up remnants after harvests and to maintain pastures (Akagi et al., 2011) and are common in rural agricultural regions and peri-urban areas (Andreae and Merlet, 2001). Emissions of VOCs are vegetation dependent and are usually classified into groups such as savannah, tropical forest, extra-tropical forest, peatlands, and agriculture (Van der Werf et al., 2010; Kaiser et al., 2012). Biomass burning emissions release approximately 400 Tg/year of VOCs (Akagi et al., 2011).

TABLE 1.1: Emission of the reactive carbon in the atmosphere split in source types. Oceanic emissions are included in the biogenic sources. Units are $Tg\,year^{-1}$.

	Anthropogenic	Biomass burning	Biogenic	Chemical oxidation	Total	Reference
CO	476	675	186	1368	2705	(Granier et al., 2000)
CH_4	286	50	189		525	(Bousquet et al., 2006)
VOCs	130	400	1200		1700	(Lamarque et al., 2010), (Guenther, 2002), (Akagi et al., 2011)

The last source of VOCs is oceans, which are a strong source of dimethyl sulphide (DMS) (Groene, 1995) and methyl iodide (Lovelock, 1975), oxygenated VOCs (OVOCs, e.g. methanol or acetone) (Millet et al., 2008; Jacob et al., 2002), as well as a minor source of alkanes and alkenes (Broadgate et al., 1997).

VOCs are removed from the atmosphere through photochemical and physical processes. In the first process, the reaction between VOCs and the hydroxyl radical (OH) is usually a major sink; reactions with ozone O_3 or nitrate NO_3 are a minor sink. When some organic compounds absorb sunlight, they are susceptible to photolysis, which leads to a fragmentation of their chemical structure. Certain compounds are physically removed by dry deposition onto vegetation, oceans, or aerosol surfaces. For instance, some organic species can be removed through biological uptake, although the efficiency of this process depends on ambient concentration. Another physical process is wet deposition in rain, although the efficiency of this process is highly dependent on the organic species. Figure 1.1 shows a simple schematic of the typical sources and sinks for VOCs in the atmosphere.

1.2 VOCs oxidation, HO_x and NO_x cycles

The various classes of VOCs have common oxidation paths. Initial reactions of VOCs with OH or NO_3 radicals form alkyl or substituted alkyl (R^*) radicals. The resulting alkyl radicals then react with O_2 to form an alkyl peroxy radical (RO_2^*).

$$VOC + OH/O_3/NO_3/h\nu \rightarrow RO_2 \tag{R1}$$

Alkenes and VOCs containing >C=C< bonds react with O_3, forming organic peroxy radicals (RO_2^*). Figure 1.2 shows the general degradation scheme valid for most VOCs and illustrates the role of the intermediate radicals: alkyl or substituted alkyl (R^*), organic peroxy radicals (RO_2^*), and alkoxy (or substituted alkoxy) radicals (RO^*). Oxidation-relevant reactions in the troposphere of RO_2^* take place with nitric oxide (NO) and hydroperoxyl (HO_2) radicals, leading to the formation of relatively long-lived organic nitrates

($RONO_2$) and hydroperoxides (ROOH).

$$RO_2^* + NO + M \rightarrow RONO_2 + M \tag{R2}$$

$$RO_2^* + HO_2 \rightarrow ROOH + O_2 \tag{R3}$$

During the night, reactions between NO_3 with organic peroxy radicals become important, as the nitrate radical photolyzes rapidly during day time (Atkinson, 2000).

$$RO_2^* + NO_3 \rightarrow RO^* + NO_2 + O_2 \tag{R4}$$

Hence, VOC oxidation is dependent on both the $HO_x(OH + HO_2)$ and $NO_x(NO + NO_2)$ cycles. The reaction of NO either with HO_2 or RO_2 produces NO_2.

$$HO_2 + NO \rightarrow OH + NO_2 \tag{R5}$$

$$RO_2^* + NO \rightarrow RO^* + NO_2 \tag{R6}$$

Photolysis of NO_2 produces O_3 through reactions R7-R9 (Atkinson, 2000). This is the main process of ozone formation in the troposphere. The efficiency of this catalytic process is dependent on the VOC and NO_x concentrations and ratio (Kleinman, 1994). A diagram showing the main species involved in ozone formation is presented in Figure 1.2 (right).

$$NO_2 + h\nu + (O_2) \rightarrow O_3 + NO \tag{R7}$$

$$O_3 + h\nu \rightarrow O(^1D) + O_2 \tag{R8}$$

$$O(^1D) + H_2O \rightarrow 2OH \tag{R9}$$

The production of ozone through the oxidation of organic species in the presence of NO_x or sunlight was first understood in the early 1950s (Haagen-Smit, 1952). Tropospheric ozone is toxic to terrestrial life, and is currently a major air quality issue in areas such as China (Akimoto, 2003) and the Mediterranean (Lelieveld et al., 2002). Ozone can also modify radiative forcing, as it functions as a greenhouse in the troposphere, as well as blocking a large amount of UV radiation from the sun in the stratosphere (Ramaswamy et al., 2001).

The NO_x cycle is completed by NO_2 reacting with OH to form HNO_3 (reaction R10),

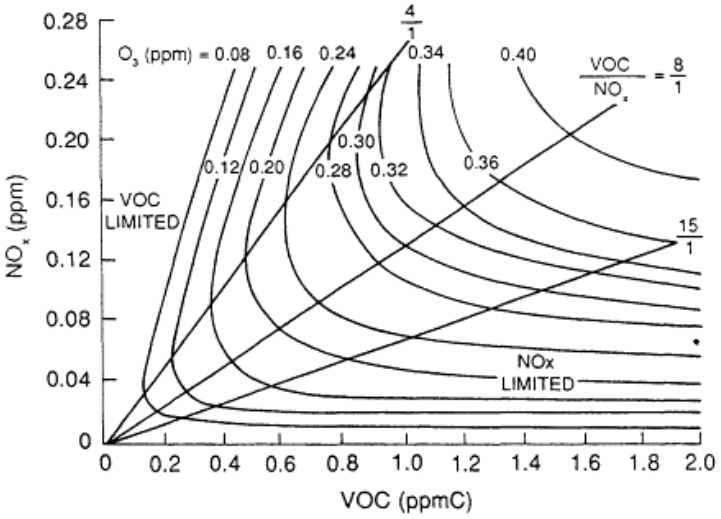

FIGURE 1.3: EKMA diagram, illustrating the ozone formation under different ozone and NO_x regimes. Scheme taken from NRC (1991), adapted from Dodge (1977).

which can be scavenged or lead to a slow photodissociation, making HNO_3 a relatively long-lived compound and the end of the NO chain (Finlayson-Pitts and Pitts Jr, 1986). The photolysis of NO_2 leads to O_3 formation and NO recycling.

$$NO_2 + OH \rightarrow HNO3 \tag{R10}$$

Simultaneously to the NO_x cycle, in the HO_x ($HO_2 + OH$) cycle OH radicals react with O_3 to form HO_2. The reaction of O_3 with HO_2 produces OH.

$$OH + O_3 \rightarrow HO_2 + (O_2) \tag{R11}$$

$$HO_2 + O_3 \rightarrow OH + (2O_2) \tag{R12}$$

Self-reaction of HO_2 produces H_2O_2 (reaction R13), which under photolysis recycles OH (reactions R14 and R15). However, the efficiency of this recycling process is low because H_2O_2 is rapidly scavenged.

$$HO_2 + HO_2 \rightarrow H_2O_2 + (O_2) \tag{R13}$$

$$H_2O_2 + OH \rightarrow HO_2 + (H_2O) \tag{R14}$$

$$H_2O_2 + h\nu \rightarrow 2OH \tag{R15}$$

As HO_x and NO_x cycles and the VOC degradation are interconnected, changes in VOC concentrations directly affect the balance and feedback between the cycles.

Whether net ozone formation or destruction takes place is determined by the competition between the reactions that destroy (R11+R12+R13) or produce (R5+R6) it. Figure 1.3 shows the relationship between VOCs and NO_x concentrations, and the capacity to form ozone, indicating that the different regimes can be detached from the VOC to NO_x ratio. In the low NO_x regime, ozone production is limited by the reactive nitrogen, independent of the VOC concentrations. In the low NO_x conditions, net ozone loss takes place; this can be considered the default regime for rural environments. In contrast, the high NO_x regime is limited by the VOC concentration. This regime describes urban environments, which results in net ozone formation.

An accurate description of the yields of organic nitrates and hydroxyl radicals is crucial to ensure accurate models (Atkinson, 2000).

1.3 Aromatic VOC

Volatile Organic Compounds (VOCs) play a significant role in the chemistry of the troposphere and in ozone formation (Atkinson, 2000; Seinfeld and Pandis, 2012). Within the VOC class, aromatic compounds form a subgroup of special interest. *Aromatics* can be defined as organic compounds that are ring-shaped and that have a planar (i.e. flat) structure, with six carbon atoms and three double bonds. Aromatics are more stable than other compounds with the same atomic composition. The name *aromatic* refers to their sweet smell, reminiscent of, for example, cherries, peaches, and, almonds (all of which contain benzaldehyde), or of Tolu balsam (which contains toluene). By 1825, Michael Faraday had isolated the hydrocarbon that would be called benzol or benzene, drawing it out of compressed illuminating gas (Faraday, 1825). However, the term *aromatic* did not appear until 1855, when August Wilhelm Hofmann used it to specify the chemical rather than the olfactory nature of these compounds (Hofmann, 1856; Rocke, 2015).

In the troposphere of urban and semi-urban areas, aromatic hydrocarbons comprise a major fraction (up to 60%) of the VOCs (Lee et al., 2002; Ran et al., 2009). They are therefore highly relevant for ozone formation in these areas (Kansal, 2009; Barletta et al., 2005; Koppmann, 2008), as they can be responsible for up to 50% of the total ozone formation potential (Tan et al., 2012). Even in rural areas, high levels of aromatics have been reported, summing up to 35% of the total VOCs (Guo et al., 2006; You et al., 2008). Typical benzene and toluene mixing ratios fall within the 0.1–10 pmol/mol range, and estimated lifetimes are two days for toluene and two weeks for benzene (Koppmann,

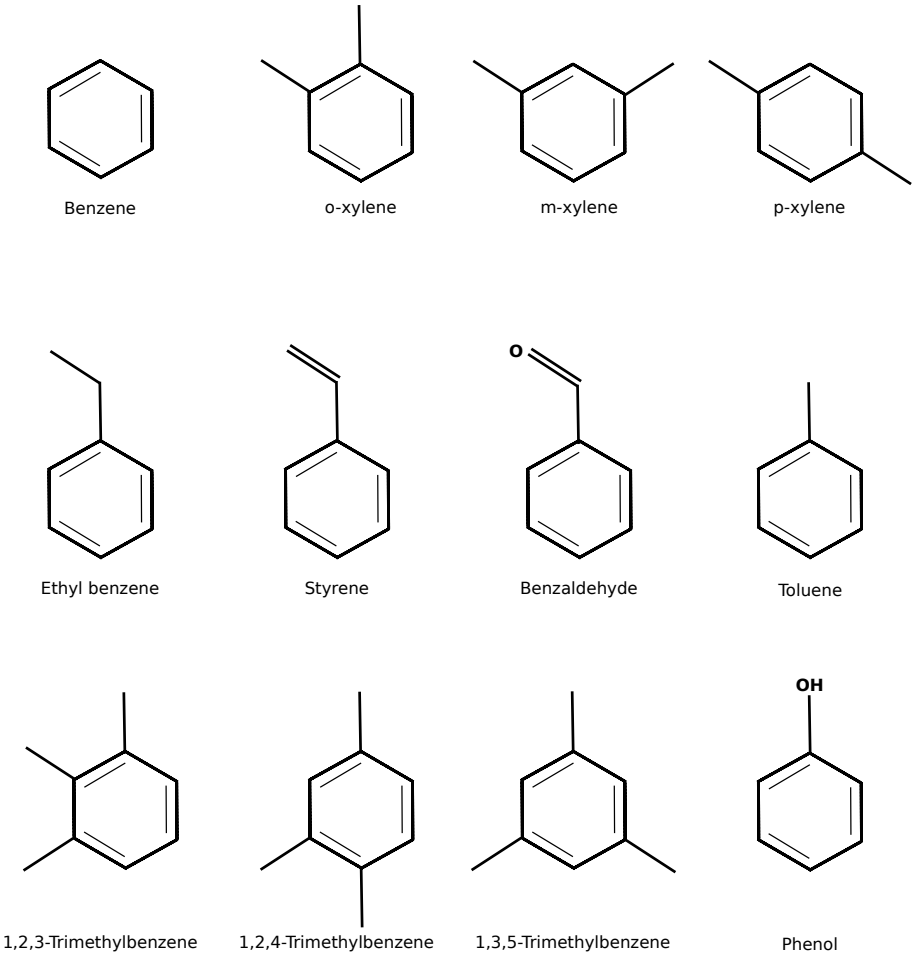

FIGURE 1.4: Structure of the aromatic compounds studied in this thesis

2008). These lifetimes are long enough to allow the compounds to reach downwind areas far from sources, with the Sahara Desert being a striking example (Yassaa et al., 2011).

Aromatic VOCs are emitted by a range of sources. They form a relevant fraction of fossil fuels, and they are released into the atmosphere by combustion (i.e. gasoline and diesel engines), gasoline evaporation, solvent usage, and spillage (Sack et al., 1992; Kim and Kim, 2002; Na et al., 2004; Baek and Jenkins, 2004). Benzene, toluene, ethylbenzene, xylenes, styrene, and trimethylbenzenes are highly present in urban air masses (Koppmann, 2008). After anthropogenic emissions, biofuel and biomass burning are the second-largest sources of aromatics. They are also important sources of benzene, toluene, and phenol in tropical and boreal areas (Fu et al., 2008; Henze et al., 2008; Andreae and Merlet, 2001). While, of all of these compounds, only toluene is known to be biogenically emitted (Sindelarova et al., 2014), a recent study found that biogenic emissions of aromatics could be equal in strength to anthropogenic emissions (Misztal et al., 2015).

The primary atmospheric oxidation pathway of benzene and alkyl-substituted benzenes is via their reaction with OH, followed by their reaction with NO_3 (Atkinson, 2000, and

references therein). The oxidation products of aromatic compounds contribute to ozone formation and to the production of secondary organic aerosol (SOA) (Odum et al., 1997; Butler et al., 2011).

A variety of chemical processes in the atmosphere also involve aromatic oxidation products, which can influence OH recycling in the atmosphere. For instance, *ortho*-nitrophenols are species of interest due to their HONO-production upon photolysis (Bejan et al., 2006; Chen et al., 2011), and nitrophenols are emitted directly into the atmosphere by both traffic and biomass burning (Tremp et al., 1993; Mohr et al., 2013).

Many aromatic compounds can be dangerous for humans, animal life, and plants (Ciarrocca et al., 2012; Snyder et al., 1993). For instance, benzene is known to be carcinogenic (Snyder et al., 1993), toluene and xylenes can have severe effects on the neural system (WMO, 2000; Sarigiannis and Gotti, 2008), and nitrophenols are acutely toxic to humans and plants (Natangelo et al., 1999; Michałowicz and Duda, 2007). Due to their high noxiousness and atmospheric impacts, aromatics have been the subject of monitoring and measurement campaigns (see Table 4.2 in Chapter 4) aiming to establish control strategies for environmental and human health protection.

1.4 Scientific questions

This thesis focuses on the gas-phase chemistry of mono-cyclic aromatics. Although there are countless aromatic compounds in the atmosphere, this work focuses on benzene (C_6H_6), toluene (C_7H_8), xylenes (C_8H_{10}), phenol (C_6H_6O), styrene (C_8H_8), ethylbenzene (C_8H_{10}), trimethylbenzenes (C_9H_{12}), and benzaldehydes (C_7H_6O), as well as on the higher aromatics (i.e. aromatic compounds with more than 9 carbon atoms).

For the purposes of this thesis we disregard SOA production, except for in the chapter on the chemical impacts of aromatics (a detailed explanation of the SOA treatment is given in Chapter 5). Other global studies such as Henze et al. (2008) did not omit SOA production, although they focused on better understanding the aerosol phase.

The addition of a detailed understanding of aromatic compound oxidation in a global model is necessary to accurately simulate and study the impacts and characteristics of these compounds, thus improving our understanding of their photochemical production yields (Lewis et al. (2000)). The following questions will therefore be the object of discussion in this thesis:

1. How can we accurately represent the oxidation of aromatic compounds in global models?

There are several degradation schemes that describe the atmospheric chemical interactions among the cycles of the most important compounds (i.e. OH and ozone) and cycles (i.e. HO_x and NO_x), as well as how they interact with VOCs. The different mechanisms range from relatively simple models (e.g. Model for Ozone and Related chemical Tracers version 4 (MOZART-4), Emmons et al. (2010)) to very complex ones (e.g. Master Chemical Mechanism v3.1 (MCM3.1), Bloss et al. (2005b)). Naturally, increasing the complexity of the system leads to a more detailed description, which implies more reactions and species to be employed. However, this complexity can be a drawback, especially in the case of global models, as it decreases the computational efficiency, which can have a dramatic impact on high resolution simulations. Thus, a compromise between accuracy and efficiency must be achieved. In Chapter 2, a chemical mechanism development suited for global models is described.

2. Do the current emission inventories cover the sources of aromatics?

   If we want to consistently simulate aromatic compounds in a global model, emissions are a key factor, and should be treated carefully. As aromatics are emitted by anthropogenic, biogenic, and biomass burning sources, these sources have been revised in the current model. Often, anthropogenic emission inventories do not provide VOC speciation, or only provide this for a few key compounds. To include the nine aromatic compounds discussed, a general strategy to define the emissions in any inventory is used in the present thesis, following a mass conservative approach. For biogenic emissions, we reviewed the MEGAN model (as a submodel) in EMAC, and for biomass burning emissions, we developed a new submodel to more easily represent these types of emissions.

3. How accurately can we reproduce atmospheric observations of aromatic compounds?

   Before answering further questions, we first need to compare different simulation results with observations from campaigns, stations, and other sources to determine how well the models represent actual observations. This comparison will also help us to understand the current state of knowledge of aromatics, identifying what factors are already well captured and which require further study.

4. What are the relative strengths of the different atmospheric sources and sinks of aromatic compounds?

   Numerous laboratory studies have been conducted with the aim of better understanding the products of aromatic oxidation and their reaction rates; there have also been field campaigns around the world into the concentrations of aromatics, and some regional-level modelling. However, a global perspective on these processes is still lacking, and, if it were provided, would help us to understand the relative strengths of sources and sinks. Although a number of global-level studies have been

conducted on the most important aliphatic hydrocarbons budgets (e.g. ethanol, acetaldehyde, PAN, glyoxal) (Fischer et al., 2014; Fu et al., 2008; Millet et al., 2010; Pozzer et al., 2010; Naik et al., 2010), the budget for aromatics remains unresolved, probably due to its chemical complexity. A detailed study on the atmospheric budget of the aromatic compounds discussed in this chapter is presented in Chapter 4.

5. How do aromatics affect key atmospheric species (e.g. OH and NO_2)?

   Aromatic compounds are relatively short-lived species, characterized by their high reactivity and mainly emitted by human-related activates. They can react with OH or ozone, and, depending on the NO_x regime, they can lead to either the recycling or net consumption of OH and ozone. These processes are studied in depth in Chapter 5.

6. How do aromatics affect VOCs?

   A number of important organic compounds are formed through aromatic oxidation (e.g. formaldehyde and glyoxal). In extension with the preceding question, this thesis will help to shed light on the relevance of aromatics at the global scale.

7. How has the concentration of aromatic compounds changed in recent decades, and what do future scenarios of emissions look like?

   Aromatics are of great concern as they pertain to ozone formation and health in urban areas. It is therefore important to understand how concentrations of aromatics have changed and what we can expect in the future. Chapter 6 will explore the long-term forecast.

1.5 Outline of this thesis

This thesis aims to improve our understanding of how aromatic compounds are distributed in the troposphere, and to shed light on the atmospheric impacts of aromatics on key atmospheric species and other VOCs, from a global-scale point of view. This is achieved with the help of a global atmospheric-chemistry general circulation model (AC-GCM). The thesis is structured in two parts. The first part covers Chapters 2 and 3. Chapter 2 first describes the AC-GCM EMAC model, including the submodels used in this thesis. This chapter also presents the details of the aromatic oxidation chemical mechanism. In Chapter 3, developments in the submodels dealing with anthropogenic, biogenic, and biomass burning emissions are presented. This chapter includes the methodology to create speciations for anthropogenic emissions, updates on biogenic sources in the model, and a new model for biomass burning emissions. The second part—Chapters 4 to 6—presents

the different simulation results. Chapter 4 contains a study on the global budget of aromatic compounds, describing the relative importance of the different emissions and sinks, followed by the atmospheric distribution of the most abundant aromatic compounds in the atmosphere. This chapter also contains a detailed evaluation of the model simulations, with a comparison between model output and observational data. In Chapter 5, the tropospheric chemical changes imposed by the presence of aromatic compounds are discussed for OH, ozone, NO_x, VOCs, and CO. In Chapter 6 atmospheric past–future trends of aromatic compounds are described. Finally, the conclusions, final remarks, and outlook of the thesis are presented in Chapter 7.

Chapter 2

Model description and aromatic mechanism

In order to study aromatic compounds at global scale, we use the three dimensional state-of-the-art atmospheric chemistry general circulation model (AC-GCM) system EMAC (ECHAM5/MESSy Atmospheric Chemistry). In this chapter a comprehensive overview of the model system is presented, including a description of the main physical and chemical aspects which are intrinsic of this work.

The first part of this chapter describes the meteorological base model (ECHAM5), the Modular Earth Submodel System (MESSy), and the sub-models used for the purposes of this thesis. The last section covers the description the chemical mechanism development and its evaluation.

2.1 General circulation model: ECHAM5

ECHAM5 serves as the meteorological base model for MESSy. ECHAM5 was created by the Max Planck Institute for Meteorology in Hamburg. It is an atmospheric general circulation model based on the EMCWF (European Centre for Medium-Range Weather Forecasts) model. For this thesis we use the ECHAM5 (5th generation) version 5.3.02 (Roeckner et al., 2003, 2006; Manzini et al., 2006; Roesch and Roeckner, 2006; Hagemann et al., 2006; Wild and Roeckner, 2006).

The fundamental equations of the atmospheric dynamics are solved in ECHAM5 in order to reproduce the dynamics and thermodynamics of the atmosphere. By applying the "spectral transform method", i.e. using grid and spectral representations, the solutions of

TABLE 2.1: ECHAM5 horizontal resolutions and corresponding time steps.

Resolution	# of longitudes	# of latitudes	Approximate box width (degrees)	Approximate of box width (km)	Time step (s)
T21L19	64	32	5.62 x 5.62	626 x 626	2400
T31L31	96	48	3.75 x 3.75	417 x 417	1800
T42L31	128	64	2.81 x 2.81	313 x 313	1200
T63L31	192	96	1.87 x 1.87	209 x 209	720
T85L31	256	128	1.41 x 1.41	156 x 156	480
T106L31	320	160	1.12 x 1.12	125 x 125	360
T159L31	480	240	0.75 x 0.75	83 x 83	180

the fundamental equations are obtained. Triangular truncations are used at wave numbers corresponding to those of the horizontal resolutions. Typical triangular horizontal resolutions are 21, 31, 42, 63, 85, 106, and 159. The vertical coordinates are described by hybrid pressure levels. Therefore, in the stratosphere there are constant pressure levels to progressively become terrain following profile at surface. Two possible vertical configurations are available: the standard, in which the vertical axis reach up to 10 hPa (30 Km, mid of uppermost layer) containing 19 or 31 levels. The second is the *middle atmosphere* configuration, where the model describes the atmosphere up to 0.01 hPa (80 Km, mid of uppermost layer) with 39 or 90 vertical layers.

The maximum time step applicable is dependent on the horizontal and vertical resolution. The possible resolutions are resumed in Tab. 2.1. The Courant-Friedrich-Levi (CFL) criterion (Courant et al., 1928) is satisfied in order avoid instabilities.

A semi-implicit time-centered integration scheme, so called *leapfrog-scheme*, is adopted. In order to keep the numeral stability in the integration scheme, the Robert-Asselin time filter (Robert, 1969; Asselin, 1972) is also applied, so the growth of spurious computational modes is avoided. The CFL criterion and the Robert-Asselin time filter allows relatively long time steps. A semi-lagrangian (FFSL) scheme developed by Lin and Rood (1996) is used for the advection of tracers. For the convection, the scheme created by Tiedtke (1989) is used in combination with the additions of Nordeng (1994).

2.2 Data Assimilation

The *Nudging* system can be used in the ECHAM5 model, which consist in the assimilation of observational data in order to "gentle push" the model towards observations (Jeuken et al., 1996; van Aalst et al., 2004). The purpose of nudging is to represent realistic synoptic conditions in the model. The observational data used is that from the ECMWF analysis or reanalysis data (ERA-Interim, ERA20CM) which contains temperature, surface pressure, vorticity and divergence fields. The nudging of the fields in the

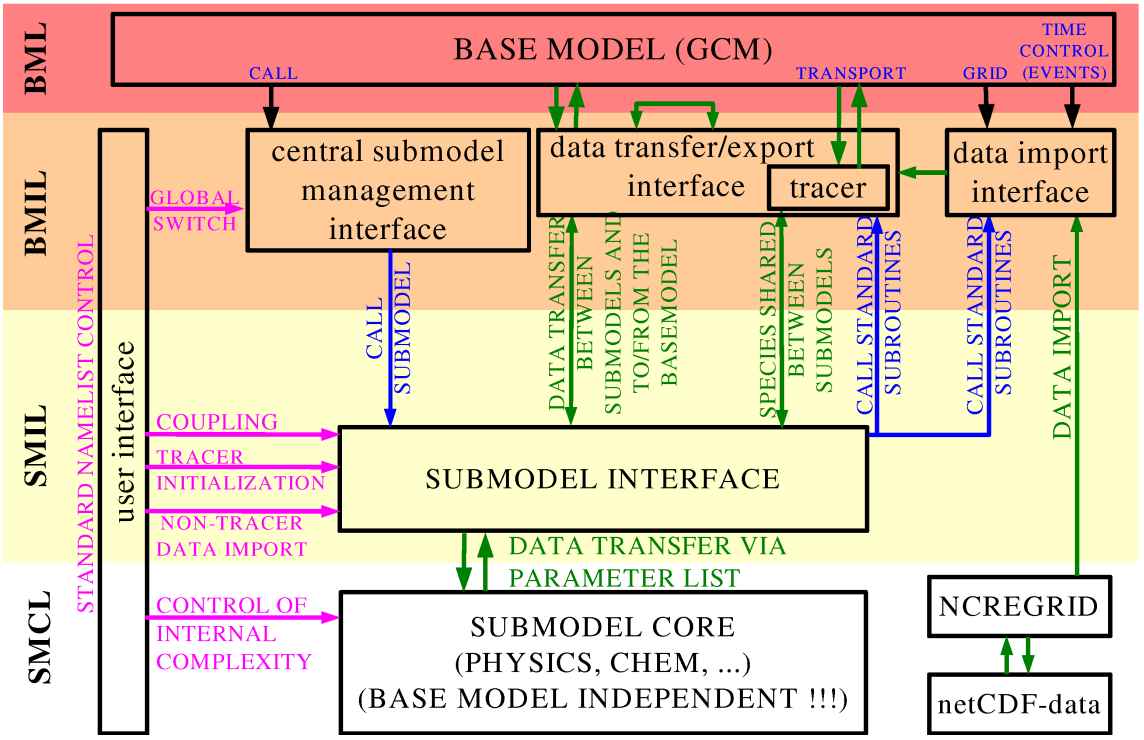

FIGURE 2.1: The MESSy interface scheme showing the communication and levels of the system. From Jöckel et al. (2005).

model occurs upon the addition of an artificial tendency $(\partial X/\partial t)_{nudge}$ to each prognostic variable. The tendency is the product of the difference between input data X_{obs} and the simulated values X_{mod}, multiplied by a relaxation coefficient $G(X)$ (Lelieveld et al., 2007; Buchholz, 2005).

$$\frac{\partial X_{mod}}{\partial t} = G(X_{obs} - X_{mod}) \tag{2.1}$$

The relaxation term is an artificial contribution which sets the strength of the nudging. Therefore, G should be enough strong to commit its purpose but without leading to instabilities or inconsistent model states (Bengtsson et al., 2004; Hack, 1994). Nudging is applied in every time step and for each vertical layer a specific relaxation coefficient is used.

Nudging has been widely used in EMAC (Jöckel et al., 2006; Lelieveld et al., 2007; Pozzer et al., 2012) as well as for this thesis.

2.3 MESSy

The Modular Earth Submodel System (MESSy) is a highly flexible combination of submodels together with a structured interface. Integrated in a General Circulation Model (GCM) it becomes an Atmospheric Chemistry General Circulation model (AC-GCM)(Jöckel et al., 2005). The MESSy submodels brings the possibility to represent emissions, transport, physical (deposition) and chemical (chemical oxidation, aqueous, gas, heterogeneous phase) processes.

Each submodel represent an individual process which is linked to the central interface. This allows the feedback between the different submodels, i.e. feedback between different physical and chemical processes when necessary. Because of the coupling between MESSy and ECHAM5, the submodels can take the meteorological variables. In the MESSy website `www.messy-interface.org` and in Jöckel et al. (2010) can be found the description and current status of each MESSy submodel.

The MESSy interface is conformed in four different layers, a scheme is shown in figure 2.1. The Base Model Layer (BML), is the base model which for this thesis is the ECHAM5 model. Then, the Base Model Interface Layer (BMIL), permit the communication between submodels and the base model. Moreover serves as central manager of the interface. The Submodel Interface Layer (SMIL) transfers the the data from the individual submodels to the BMIL. Last, The Submodel Core Layer (SMCL) comprises the individual routines for each of the submodels.

For this work the MESSy version 2.50 has been used. To accomplish the goals of this thesis, this MESSy version has been modified, with the extension of the current available chemical mechanism and the development of new submodel to represent biomass burning emissions.

2.3.1 MESSy submodels

The MESSy submodels used for this thesis are described below. The table 2.2 lists the submodels used and its main function. The MESSy website contains detailed information about the complete set of submodels.

Aerosol optics: AEROPT

Aerosol optical properties are calculated with the diagnostic AERosol OPTical submodel (AEROPT). The submodel uses in pre-calculated lookup-tables including the extinction coefficient σ_{sw}, the single scattering albedo ω_{sw} and the asymmetry factor γ_{sw} in the shortwave (sw) regime and the extinction coefficient σ_{lw} in the longwave regime. This is

TABLE 2.2: List of Messy submodels used in the different simulations of this thesis.

Submodel	Function	Reference
AEROPT	Aerosol optical depth	(Jöckel et al., 2006)
AIRSEA	Ocean-atmosphere exchange	(Pozzer et al., 2006)
BIOBURN	Biomass burning emissions	This thesis
CLOUD	Cloud processes and cover	(Jöckel et al., 2006)
CLOUDOPT	Cloud optical properties	(Dietmüller et al., 2016)
CONVECT	Convection processes	(Tost et al., 2006b)
CVTRANS	Convection transport of tracers	(Tost et al., 2006b)
DDEP	Dry deposition	(Kerkweg et al., 2006a)
JVAL	Photolysis rate coefficients	(Jöckel et al., 2006)
LNOX	NOx lighting production	(Tost et al., 2007)
MECCA	Tropospheric chemistry	(Sander et al., 2011)
MEGAN	Biogenic emissions	(Guenther et al., 2012)
OFFEMIS	Off-line emissions	(Kerkweg et al., 2006b)
ONEMIS	On-line emissions	(Kerkweg et al., 2006b)
ORBIT	Orbital parameters	(Dietmüller et al., 2016)
PTRAC	Pseudo tracers	(Jöckel et al., 2008)
RAD	Radiation	(Dietmüller et al., 2016)
SCAV	Wet deposition	(Tost et al., 2006a)
SEDI	Aerosol sedimentation	(Kerkweg et al., 2006a)
SURFACE	Surface processes	(Jöckel et al., 2016)
TNUDGE	Tracer nudging	(Kerkweg et al., 2006b)
TROPOP	Tropopause calculation	(Jöckel et al., 2006)

based on the scheme developed by Lauer et al. (2007) and uses predefined lognormal modes (mode width and mean radius). AEROPT calculates the optical properties for several sort of aerosols including water soluble compounds (water soluble inorganic ions, aerosol water, black carbon, particulate organic matter, sea salt, and dust), aerosol water, black carbon, organic carbon, dust and sea spray (Pozzer et al., 2012). The values of the lookup tables are estimated with LIBRADTRAN (Mayer and Kylling, 2005) for the different aerosol types. The refractive indices for the compounds mentioned above are obtained from several data bases, e.g., HITRAN2004 (Pozzer et al., 2012). During the simulation the volume-weighted mean complex refractive index is determined for each mode. Then, the Mie size parameter (which depends on the mean radius of the mode) is calculated for each wavelength. These parameters (Mie size parameter, complex refractive index, and mode mean radius) allow the calculation of σ_{sw}, ω_{sw}, γ_{sw} and σ_{lw} for the lookup table. The values are estimated for 32 predefined bands, 16 in the shortwave and 16 in the longwave spectrum. The bands do not necessarily match the bands in the radiation scheme of the base model (ECHAM5), therefore weighted interpolation is used between the predefined and the radiation scheme bands. Finally, the aerosol optical depth (AOD) is calculated in the following way: first, for a particle the extinction coefficient is estimated (for each mode), then in each layer the extinction coefficient is multiplied by the number of particles

per grid cell. The vertical integration provides the total atmospheric AOD per grid cell (Pozzer et al., 2012).

Air-Sea exchange: AIRSEA

This submodel represents the bidirectional transfer of tracers between the atmosphere and the ocean. AIRSEA is relevant for the representation of some organic compounds, as for example the global budgets of tracers such as methanol and acetone. The submodel is based on a two-layer approach to simulate the bi-directional exchange of VOCs and their oxidation products (Jöckel et al., 2006). It is based in two assumptions: first, fluids are well mixed close to the air-sea interface, and second, molecular diffusion is the only driving force within the interface between water and air. A detailed description of the submodel can be found in Pozzer et al. (2006).

Biomass burning emissions: BIOBURN

Emissions of trace gases from biomass burning are estimated with the submodel BIOBURN. This submodel has been developed as a part of this thesis and a detailed description can be found in chapter 3.

Cloud processes: CLOUD

CLOUD is the MESSy modularized version of the original ECHAM5 scheme (Roeckner et al., 2003) and calculates cloud cover, microphysics, and precipitation processes. The microphysics scheme created by Lohmann and Roeckner (1996) uses cloud water and cloud ice as prognostic variables. Hence prognostic equations are given for the aqueous phases. The scheme is conformed by phase changes between the water components, precipitation processes (autoconversion, accretion, aggregation), the evaporation of rain, the melting of snow, and the sedimentation of ice. The cloud cover parametrization is based on the work by Tompkins (2002). This scheme works with a probability density function (beta-distribution based) which involves the total water content (water vapor, cloud water, and cloud ice mixing ratios). The prognostic variables calculated in the microphysics will modify the phase density function accordingly. Therefore, deep convection, large-scale condensation or turbulence processes contribute to the fluctuations in the total water content and the phase density function. The cloud fraction is obtained by integrating the supersaturated part of the phase density function.

Cloud processes: CLOUDOPT

Cloud optical properties are calculated in the CLOUDOPT submodel (Dietmüller et al., 2016). The submodel uses the following input variables for the estimation of optical properties: cloud cover, cloud liquid, and cloud ice water, and cloud nuclei concentration.

Then, the optical depth, the asymmetry factor, and the single scattering albedo of cloud particles both for shortwave and longwave are diagnosed for different wavelength bands.

Convection processes: CONVECT

Based on the ECHAM5 scheme, the CONVECT submodel estimates the convection and convective precipitation. Because of the relatively large grid sizes of global models the convection schemes are parametrized. The CONVECT submodel is based on the mass-flux approach parametrization from Tiedtke (1989) with the adjustment from Nordeng (1994). In the original scheme developed by Arakawa and Schubert (1974), convection is treated as an ensemble of several sized clouds (spectral cloud ensemble). However, in MESSy, a bulk formulation is used (Yanai et al., 1973), avoiding to calculate an explicit solution. The formulation calculates deep, shallow and midlevel convections, including entrainment and detrainment processes. The convection mechanism operates at the level of free convection when it is satisfied the condition of an increase of 0.5k difference between air parcel and enclosing area. In addition, the modification from Nordenq assumes a dependency between updraft mass-flux and convective available potential energy to regulate the closure. An extensive comparison of different possible parametrizations in MESSy can be found in Tost et al. (2006b).

Convective tracer transport: CVTRANS

The convective transport of tracers is calculated with the CVTRANS submodel (Tost et al., 2010), using the bulk approach from Lawrence and Rasch (2005). Tracer mass fluxes for updrafts and downdrafts are estimated, and also entrainment and detrainment. For the model consistency, CVTRANS includes a monotonic, positive definite, and mass conserving approach. In Tost et al. (2006b) detailed information can be found.

Dry deposition: DDEP

The dry deposition (DDEP) submodel calculates the atmospheric removal of trace gases and aerosols by uptake or by turbulent transfer onto the Earth's surface in the absence of clouds and precipitation. The submodel was developed by Kerkweg et al. (2006a), based on the big leaf scheme for gases (Ganzeveld and Lelieveld, 1995; Ganzeveld et al., 1998) and for aerosols (Stier et al., 2005). The dry deposition flux, F_D, is calculated in the lowermost layer of the model by the following equation,

$$F_D = c(x) \times V_D(x) \tag{2.2}$$

where c(x) represents the concentration of the tracer x and $V_D(x)$ the dry deposition velocity, with the flux expressed in $mlc/m^2/s$. The dry deposition velocity is defined as

$$v_D = \frac{1}{R_a + R_{qbr}(x) + Rs(x)} \tag{2.3}$$

where R_a is the aerodynamic resistance that depends on the physical state of the atmosphere, R_s, the surface resistance that is function of the molecular diffusion, and R_{qbr}, the quasi-laminar resistance boundary layer which is controlled by the chemical, physical, and biological characteristics of the surface. The different resistances are calculated for the following surfaces: ice/snow water, bare soil, vegetation and wet skin (i.e. wetted fraction of vegetation or bare soil). For the gas phase deposition the solubility for each tracer (i.e Henry's law constant) must be declared as well as the reactivity, which is an scaling between ozone and sulphur dioxide reactivities. Then, the velocities are calculated for land and water (combining the surfaces mentioned beforehand) which depend consequently on the surface type and trace gas properties. Thus, in each grid cell the deposition is the sum the deposition velocities of each surface type. For aerosols the same scheme is used with the exception that only three surfaces (bare soil/snow, vegetation, and water) are taken into account.

Photolysis rate coefficients: JVAL

The MECCA submodel calculates photolysis reactions using the precalculated photolysis rates from the JVAL (J-values) submodel. JVAL uses the scheme from (Landgraf and Crutzen, 1998), which depends on the wavelength λ, the absorption cross section σ_X, the quantum yield Φ_X and the actinic flux $F(\lambda)$ over the integration range I. The equation for the calculation of the photolysis rates of a tracer (X) in the integration range of 178.6-752.5 nm is the following,

$$J_X = \int_I \sigma_X(\lambda)\Phi_X(\lambda)\ F(\lambda) \tag{2.4}$$

The numerical approximation of the previous equations is

$$J_X \approx \sum_{i=1}^{N} \sigma_X(\lambda_i)\Phi_X(\lambda_i)\ F(\lambda_i)d\lambda_i \tag{2.5}$$

Eight intervals are defined for the active spectral range, where only the first is in the Schumann-Runge band (178.6-202.0 nm).

Cloud particles, gas phase species, and aerosols modify the actinic flux. Considering only an absorptive atmosphere (not in the Schumann-Runge region), the actinic flux $F^a(\lambda_i)$ can be expressed as

TABLE 2.3: Subdivision of the spectral range 178.6-752.5nm; λ_a and λ_b are the lower and the upper wavelengths of the bands, λ_i is the fixed wavelength used in 2.4. From Landgraf and Crutzen (1998).

Interval	λ_a (nm)	λ_b(nm)	λ_i(nm)
1	178.6	202.0	
2	202.0	241.0	205.1
3	241.0	289.9	287.9
4	289.9	305.5	302.0
5	305.5	313.5	309.0
6	313.5	337.5	320.0
7	337.5	422.5	370.0
8	422.5	752.5	580.0

$$F(\lambda_i) = F^a(\lambda_i) \times \delta_i \tag{2.6}$$

where δ_i is a factor dependent on the wavelength. In the Schumann-Runge band the absorption of O_2 is large enough to neglect scattering effects. Hence, J_X approximation is:

$$J_X \approx J^a_{i,X} + \sum_{i=2}^{8} J^a_{i,X} \cdot \delta_i \tag{2.7}$$

Under the mentioned assumptions, $F^a(\lambda_i)$ is offline calculated and δ_i is online calculated. Table 2.3 presents the wavelength intervals used in JVAL.

NOx lightning production: LNOX

The LNOX submodel calculates NO_x formation due to lightning (Tost et al., 2007). Four different schemes are available (e.g. Price and Rind (1994); Pickering et al. (1998)). In this study we use the parametrization from Grewe et al. (2001), which links the vertical velocity with flash frequency. The flash frequency and NO_x production per single flash are scaled in order to agree with literature estimates (Jöckel et al., 2006).

Gas phase chemistry: MECCA

The atmospheric chemistry model MECCA (Module Efficiently Calculating the Chemistry of the Atmosphere) is in charge of calculating the evolution of atmospheric tracer concentrations upon chemical reactions (Sander et al., 2005, 2011). The submodel covers stratospheric and tropospheric chemistry, although for this thesis only the latter has been used, as the stratosphere has not been included in the vertical domain. MECCA incorporates a detailed chemical mechanism that includes fundamental HO_x, NO_x, CH_4 and O_3 reactions. Moreover, the mechanism contains VOC chemistry up to isoprene, although the

set of reactions have been expanded in this thesis to include aromatic compounds. Details about the aromatic development can be found in the section 2.5. Currently, the model uses Mainz Isoprene Mechanism (MIM2) developed by Taraborrelli et al. (2008), which replaced the former the Mainz Isoprene Mechanism (MIM) by Pöschl et al. (2000). MIM2 is mass-conserved with respect to carbon. Before simulations, the set of chemical species and reactions must be chosen. Then the Kinetic PreProcessor (KPP) (Damian et al., 2002; Sandu and Sander, 2006) creates the routines. In each step of the global model, MECCA solves the chemical equations to determine the new species concentration. The model uses substeps in order to keep the stability of the equation system.

Biogenic emissions: MEGAN

The Model of Emissions of Gases and Aerosols from Nature (MEGAN version 2.04) (Guenther et al., 2012) has been adapted and modularized to become part of the MESSy submodels. The submodel estimates the emissions fluxes of biogenic organic compounds between terrestrial ecosystems and the atmosphere. In order to involve the major processes that controls biogenic emissions the model applies a simple mechanistic approach. A exhaustive description of this model can be found in the next chapter in addition with the estimation of the global emissions of aromatic VOCs in the EMAC model.

Offline emissions: OFFEMIS

The OFFEMIS (OFFline EMISsions) submodel deals with input files containing prescribed emissions (Kerkweg et al., 2006b). This submodel allows an independent management of the emissions for each compound (every single species can be switched on/off) and no code addition is necessary in order to expand the number of species emitted. Moreover, OFFEMIS uses the NCREGRID tool (Jöckel et al., 2006) to transform the resolution of any emission input file to the model resolution. OFFEMIS provides three types of emissions:

Surface emissions (2D): For emissions placed directly at the lowermost layer of the atmosphere. Input files contain emission fluxes in molecules $m^{-2}s^{-1}$.

Multilayer emissions (Nx2D): This case is used when the emissions are released at different heights above the surface. The input files contain three-dimensional fields (with fluxes in molecules $m^{-2}s^{-1}$) at specific (arbitrary) heights. The heights are defined at the import namelist. In the case of the anthropogenic emissions for our study, tracers are released at six heights.

Volume emissions (3-D): To use in case of vertically distributed emissions with no predefined heights. The input files contain three-dimensional emission rates in

molecules $m^{-3}s^{-1}$. This *type* is used for instance with aircrafts and/or volcanic emissions.

Besides the emission types, OFFEMIS provides three *methods*. In the first one, emissions are not linked to atmospherics tracers. Therefore, no changes will take place on tracers due to emissions. In the second method changes on mixing ratios of atmospheric tracers are calculated. In the third method a lower boundary condition for the vertical diffusive flux F_{vdiff} is calculated from the prescribed emission.

On-line emissions: ONEMIS

The ONEMIS (ONlin EMIssions) submodel calculates emissions that depend on the current state of the model i.e wind speed, soil properties, radiation, and precipitation (Kerkweg et al., 2006b). This submodel treats in a different manner gas and aerosol emissions. In the case of gas phase tracers, same *methods* as in OFFEMIS can be used. However, for aerosols the emissions cannot be directly linked to the corresponding tracer because in an intermediate step another submodel must process the particle number distribution.

Orbital parameters: ORBIT

The ORBIT submodel is in charge of the orbital parameter calculations (Dietmüller et al., 2016). These parameters depend on the time of the day and the year. The Kepler equation is solved here for the eccentric anomaly and the distance of the sun to the earth, the cosines of the zenith angle, and the relative day length.

Prognostic tracers: PTRAC

The PTRAC submodel is used to generate tracers unlinked to the chemical mechanism (Jöckel et al., 2008) but to be used for any other submodel. This is particularly useful for the QTCM mode (see section 2.4). It can be used to define either trace gases or aerosols.

Radiation: RAD

In the MESSy model, radiation is calculated by the RAD model (Dietmüller et al., 2016; Jöckel et al., 2006). RAD implementation is based on the ECHAM5 routines, which have been adapted to the MESSy coding standards. This submodel calculates the coupling between dynamics and chemistry i.e. the tendencies of the shortwave and longwave radiation fluxes. The calculation depends on the radiatively active tracers (CO_2, CH_4, O_3, N_2O, $CFCl_3$, and CF_2Cl_2), the cloud cover (provided by the CLOUD submodel), the water vapour, the cloud water content, and cloud ice. For the aerosols a combined scheme is used, integrating the original ECHAM5 aerosol climatology (Tanre et al., 1984) and the AEROPT submodel.

Wet deposition: SCAV

SCAV submodel has two functions, it calculates liquid phase chemistry inside clouds and precipitation, and solves the wet deposition of atmospheric tracers and aerosols. Scavenging is an important removal process at global scale for highly soluble species and small aerosols. The submodel distinguishes the following processes, nucleation scavenging (NS) and impaction scavenging (IS). The removal during the nucleation and growth of cloud droplets is calculated by *nucleation scavenging*. Impaction scavenging is defined as the aerosols or gases phase tracer uptake by droplets while precipitate. The scavenging calculations begin at the uppermost layer where a cloud occurs (NS). In the subsequent layers, *IS* is calculated for the precipitation flux coming from the upper layers. In the order of the calculations IS goes before NS. In the case of lack of clouds, the calculation of NS is neglected. On the other hand, if a cell is partially filled by clouds, the representative fraction of cloud cover is taken into account for the scavenging.

There are two possibilities in terms of gas phase scavenging calculations. The first approach uses prescribed scavenging coefficients (calculated based on former studies and Henrys law coefficients). In the second approach the processes are calculated with the help of a set of coupled Ordinary Differential Equations (ODE). The advantage of the first method is its computational efficiency, however in the latter the coupling between multi-phase chemistry and transport processes is resolved. For the second case a numerical solver is needed, thus KPP (the Kinetic PreProcessor) is used. SCAV has subdivision of time steps with respect to the global model since the last have too long time steps for chemical integrations. In this thesis case we use the Rosenbrock solver with automatic time step control in order to avoid problems with stiff ODE (Sandu and Sander, 2006).

Droplet uptake and release of trace gases is described by Henry's equilibrium law with the addition of a correction for gas phase diffusion limitation and the accommodation coefficients (Tost et al., 2006a). The liquid phase reaction set is based on that described by Sander et al. (2005) and Ervens et al. (2003). For the calculations of the reaction rates temperature, pressure, and liquid water content are needed at each model time step and grid box. For each time step the entire tropospheric column needs to be considered because the tracer uptake is limited by the amount dissolved in the precipitation. In the same manner as in the the gas phase treatment, two approaches can be used for determining the scavenging coefficients (fixed or online) of aerosols.

When complete evaporation of cloud or falling rain droplets takes place dissolved species are released. Consequently, any dissolved neutral volatile compound is discharged to the gas phase. In the case of scavenged aerosol particles, redistribution into the aerosol distribution takes place. Moreover, ions are taken into account so to avoid mass conserving

inconsistencies during the process. A full description of the SCAV submodel can be found in (Tost et al., 2006a).

Surface processes: SURFACE

The SURFACE submodel represents surface processes, i.e. it calculates surface heat and water budgets, lake temperatures and ice thickness (Jöckel et al., 2016). Based on the thermal diffusion equation the soil temperature profile and its evolution can be estimated. Lake-ice temperature and sea-ice temperature are calculated prognostically. SURFACE is the modularization from the ECHAM5 routines (Roeckner et al., 2003).

Tracer nudging: TNUDGE

The tracer-nudging, TNUDGE, submodel is used for the addition of pseudo sources/sinks of tracers (Kerkweg et al., 2006b). A second purpose of the submodel is to nudge mixing ratios to prescribed values, as for example CFC or methane, whose lifetimes are long and mixing ratios are well known. It also may be used for specific regions (e.g. stratospheric ozone in simulations focused on the troposphere).

Tropopause calculation: TROPOP

The submodel TROPOP (Jöckel et al., 2006) is a diagnostic tool in charge of the calculation of the tropopause height (and its corresponding model level). In addition, the submodel diagnose the planetary boundary layer height. The tropopause definition is that from the WMO based on temperature lapse rate (WMO, 1992) for latitudes between 30°N-30°S or as a potential vorticity iso-surface for latitudes above 30°N or 30°S.

2.4 QCTM mode

In order to study the feedbacks in the Earth system, the use of global chemistry-climate models results is as it combines feedbacks between radiation, chemistry, and atmospheric dynamics. Nevertheless, such feedbacks hinder, for example, the analysis of the effects of emissions on short lived compounds. In the hypothetical case of two simulations, including feedback between chemistry and dynamics, initiated with identical meteorological conditions but with slightly different emissions of certain tracers, the meteorological conditions between simulations will diverge after some time steps due to the intrinsic chaos of the system. Consequently, the two different meteorological systems will affect the chemistry of each simulation in a different way. Although in the long term the dynamical variables average may be barely modified, the sequence of meteorological weather patterns can be entirely different between simulations. Hence, there is strong noise in the mixing ratios

for the different simulations. This is of particular concern when there are changes in the emission sources.

The idea behind the "quasi chemistry-transport mode" (QCTM) within a global chemistry-climate model (CCM) is that there is no feedback of model chemistry in the model dynamics. Thus, two simulations with different tracer emissions would generate identical meteorological conditions. In consequence, the QCTM mode (Deckert et al., 2011) sets the correct conditions for meaningful sensitivity studies on the effects from small chemical perturbations. In order to make the QCTM mode effective, the model namelists of RAD, TNUDGE and PTRAC have to be modified.

For this thesis, the QCTM is used in all simulations, because in the studies of the budget estimation (chapter 4) and the chemical influence of aromatic compounds in the troposphere in chapter 5, several simulations are performed in order to test different emission scenarios. The steps needed in order to decouple carbon dioxide, methane, ozone, and CFC from the online chemistry calculations to radiation are the following: first, pseudo-tracers are created with PTRAC and linked to prescribed values, then nudged with TNUDGE, and finally connected to the RAD submodel.

2.5 Aromatic mechanism

In order to perform simulations with the EMAC model including aromatic compounds, the addition of a descriptive mechanism of the atmospheric oxidation of such compounds is needed. Building up an entire new mechanism is a complex task, which requires laboratory data, model development, and evaluation. This is out of the scope of this thesis. Therefore, our aim is to expand the current chemical mechanism of EMAC, the Mainz Isoprene Mechanism (MIM2, Taraborrelli et al. (2008)), which contains organic species up to isoprene. MIM2 is a reduced version of the Master Chemical Mechanism (MCM, Saunders et al. (2003); Bloss et al. (2005a)) and is suitable for regional and global modelling. The expansion of the MIM2 mechanism is done through the integration of an available and evaluated chemical mechanism containing aromatic compounds. So the procedure is to first select the most suitable mechanism and then optimize it to the needs of our studies. As it is desired to reproduce the atmospheric chemistry as realistic as possible, to select a complex detailed mechanism is highly preferred. Therefore mechanisms as MOZART4 (Emmons et al., 2010), RADM2 (Stockwell et al., 1990), RACM (Stockwell et al., 1997), RACM2 (Goliff et al., 2013), CBM-IV (Gery et al., 1989), and CB05 (Yarwood et al., 2005) were discarded, as they do not include aromatics or do it in a simple way (i.e less than 60 species involved and 140 reactions in total), and, moreover, they present a highly lumped structure, which leaves small room for modifications within the mechanism and

usually implies lack of carbon mass conservation. Consequently, the potential selection is reduced to the MCMv3.2 and the Common Representative Intermediates (CRIv2, Jenkin et al. (2008)).

A detailed work on the degradation mechanism was done for aromatics (in the MCM) by Jenkin et al. (2003). MCM is a near-explicit mechanism describing the oxidation for 125 VOCs (1884 organic species involved and 5621 reactions). The mechanism gathers all information available about kinetics and elementary reactions. It contains a consistent treatment of the VOC oxidation (independently whether there is lack of experimental data available for certain steps). Thus, VOCs are degraded into first generation products, and the oxidation will take place successively for products under the same general structure. The process is repeated up to CO_2 formation.

The CRI mechanism is a reduced version of MCM. It reproduces the chemistry of 115 NMVOC and methane. It contains 559 reactions and 189 species in total (10% of MCM size). The main assumption on the methodology of the mechanism is the following: for each VOC the ozone formation potential is correlated to the number of reactive bonds contained in the molecule (C-C and C-H bonds). This classification allows the generations of general intermediate species that can be used as *common representatives* for different tracers (with the same index). The mechanism is tuned to reproduce similar results to MCM.

The reason to adapt the MCM mechanism into similar CRI's size instead of using CRI itself is the approximation. In CRI, all intermediates are representative lumped species, this means that a molar mass cannot be defined for those species. Moreover, the mechanism is not carbon mass conservative and due to its structure it is not possible to apply further modifications on the mechanism. On the other hand, a reduced version of MCM can be easily updated or expanded, and it keeps the carbon-conservative approach.

A complete list of chemical equations and species involved can be found in appendix A. The mechanism reduction has been performed according to the following procedure:

1. The oxidation mechanisms for benzene and toluene were taken from MCM because of their relatively high abundance in the atmosphere in comparison with the other aromatics. Therefore, these two species are described with the highest available accuracy.

2. For the other aromatics, the first oxidation step is taken from the MCM, and the second oxidation step is linked to that of toluene because of the similar chemical structure.

3. Intermediates having a lifetime always below one second are replaced by their products with the corresponding reactions being removed.

4. Xylenes and trimethylbenzenes have been lumped, assuming equal proportions of single isomers.

   In the case of xylenes (**LXYL**), for the reaction with NO_3, LXYL + NO_3, the rate constant is the average of the -m, -p, -o rate constants.

$$Rc = (4.10 \cdot 10^{-16} + 2.60 \cdot 10^{-16} + 5.00 \cdot 10^{-16})/3 = 3.9 \cdot 10^{-16} \tag{2.8}$$

   For the reaction with OH (LXYL + OH) a different approach is taken. The rate constant is estimated by the average of the rate constant times the branching ratio.

   - **A.** for the OXYBIPERO2, MXYBIPERO2 and PXYBIPERO2 channels
     -*O* $1.36 \cdot 10^{-11} \cdot 0.55 = 0.748 \cdot 10^{-11}$
     -*M* $2.31 \cdot 10^{-11} \cdot 0.50 = 1.155 \cdot 10^{-11}$
     -*P* $1.43 \cdot 10^{-11} \cdot 0.625 = 0.894 \cdot 10^{-11}$

     Rc(average)= $0.932 \cdot 10^{-11} \cdot$

   - **B.** for the OXYEPOXMUC, MXYEPOXMUC and PXYEPOXMUC channels
     -*O* $1.36 \cdot 10^{-11} \cdot 0.24 = 0.326 \cdot 10^{-11}$
     -*M* $2.31 \cdot 10^{-11} \cdot 0.29 = 0.670 \cdot 10^{-11}$
     -*P* $1.43 \cdot 10^{-11} \cdot 0.155 = 0.221 \cdot 10^{-11}$

     Rc(ave)= $0.406 \cdot 10^{-11}$

   - **C.** for the OXYLO2, MXYLO2 and PXYLO2 channels
     -*O* $1.36 \cdot 10^{-11} \cdot 0.05 = 0.068 \cdot 10^{-11}$
     -*M* $2.31 \cdot 10^{-11} \cdot 0.04 = 0.092 \cdot 10^{-11}$
     -*P* $1.43 \cdot 10^{-11} \cdot 0.10 = 0.143 \cdot 10^{-11}$

     Rc(ave)= $0.101 \cdot 10^{-11}$

   - **D.** for the OXYLOL, MXYLOL and PXYLOL channels
     -*O* $1.36 \cdot 10^{-11} \cdot 0.16 = 0.218 \cdot 10^{-11}$
     -*M* $2.31 \cdot 10^{-11} \cdot 0.17 = 0.393 \cdot 10^{-11}$
     -*P* $1.43 \cdot 10^{-11} \cdot 0.12 = = 0.172 \cdot 10^{-11}$

Rc(ave)= 0.261 $\cdot 10^{-11}$

In the case of trimethylbenzenes (**LTMB:**), the same procedure is followed. Thus, for the reaction LTMB + NO_3 the rate constant is:

$$Rc = (1.90 \cdot 10^{-15} + 1.80 \cdot 10^{-15} + 0.88 \cdot 10^{-15})/3 = 1.52 \cdot 10^{-15} \qquad (2.9)$$

For the reaction with OH, an analogous procedure as for xylenes is used:

- **A.** for the TM123BPRO2, TM124BPRO2 and TM135BPRO2 channels
  -*TM123* 3.27·10^{-11}· 0.70 = 2.289 ·10^{-11}
  -*TM124* 3.25·10^{-11}· 0.61 = 1.983 ·10^{-11}
  -*TM135* 5.67·10^{-11}· 0.79 = 4.479 ·10^{-11}

  Rc (ave)= 2.917 ·10^{-11}

- **B.** for the TM123OXMUC, TM124OXMUC and TM135OXMUC channels
  -*TM123* 3.27·10^{-11}· 0.21 = 0.687 ·10^{-11}
  -*TM124* 3.25·10^{-11}· 0.30 = 1.005 ·10^{-11}
  -*TM135* 5.67·10^{-11}· 0.14 = 0.794 ·10^{-11}

  Rc (ave)= 0.827 ·10^{-11}

- **C.** for the TM123BO2, TM124BO2 and TMBO2 channels
  -*TM123* 3.27·10^{-11}· 0.06 = 0.196 ·10^{-11}
  -*TM124* 3.25·10^{-11}· 0.06 = 0.201 ·10^{-11}
  -*TM135* 5.67·10^{-11}· 0.03 = 0.170 ·10^{-11}

  Rc(ave)= 0.189 ·10^{-11}

- **D.** for the TM123BOL, TM124OL and TM135BZOL channels
  -*TM123* 3.27·10^{-11}· 0.03 = 0.098 ·10^{-11}
  -*TM124* 3.25·10^{-11}· 0.03 = 0.100 ·10^{-11}
  -*TM135* 5.67·10^{-11}· 0.04 = 0.226 ·10^{-11}

  Rc (ave)= 0.141 ·10^{-11}

Moreover, the photolysis rate of benzaldehyde is updated following IUPAC recommendations (http://iupac.pole-ether.fr), and *ortho*-nitrophenols have a new photolysis channel leading to HONO formation (Veerecken, personal communication). The resulting oxidation mechanism for aromatics contains 666 reactions and 229 species.

A comparison between MCM, CRI and the aromatic mechanism created for this thesis (for simplicity, called MAM "Mainz aromatic Mechanism") was performed. Two simulations for each mechanism were run, one with low NO_x conditions and a second one in the high NO_x regime. All the simulations started on 1st August 2000, at midnight and simulated five days. The relative humidity and the pressure were set to be 70% and 101 325 Pa, respectively, simulating atmospheric conditions on polluted regions on the south of China. A diurnal cycle for light was applied. The temperature used was 301 K. In all simulations we used the same emission fluxes: ozone $5 \cdot 10^{10}$ molecule/cm^2/s (as representative of transport between grid boxes), benzene $6.66 \cdot 10^{10}$ molecule/cm^2/s, toluene $3.66 \cdot 10^{11}$ molecule/cm^2/s, phenol $6.66 \cdot 10^{10}$ molecule/cm^2/s, and NO (for the high NO_x regime) $6.66 \cdot 10^{11}$ molecule/cm^2/s. Figure 2.2 shows the comparison between the different mechanisms for the high NO_x regime. We chose MCM as reference mechanism since it has been evaluated against chamber data and the other mechanisms have been developed around MCM. For ozone, CRI and MAM overestimates MCM, although MAM is closer to MCM. The bias (figure 2.3) for CRI is approximately 25% and for MAM 10%. Similar patterns can be observed for OH and HO_2, with MAM closer to MCM than CRI. Although the bias for HO_2 and OH can be more than 100%, it corresponds to small absolute bias when the mixing ratios are at night close to zero. Also analogous to ozone, NO_x shows similar mixing ratios for all mechanisms, and large bias only occurs at night time. An important difference between CRI and MAM can be found for glyoxal (GLYOX) and methylglyoxal (MGLYOX). CRI neglects the formation of these compounds because of the high number of lumped species does not lead to formation of such compounds. MAM reproduces the mixing ratios simulated by MCM well. On the other hand, opposite behaviour is found for acetaldehyde, where no formation takes place from the aromatic oxidation in MCM and MAM, but increases are observed for CRI. In the case of formaldehyde, its production in CRI is higher with respect to MCM and MAM. A remarkable feature of MAM is the enhanced HONO formation due to the photolysis of nitrophenols. During day time, differences rises up to 50%, and at night time the bias shows increases by more than 400% with respect to MCM (although this is again due to differences in very low mixing ratios).

Figures 2.4 and 2.5 show simulation results in a low NO_x environment. For this simulation we use an NO emission flux of $3.33 \cdot 10^{11}$ molecule/cm^2/s. The emission fluxes for the other compounds remain the same as in the high NO_x regime. In the low NO_x regime, larger discrepancies (than the previous regime) for several sepcies are found between the different mechanisms. For OH, CRI overestimates MCM and in contrast, MAM underestimates

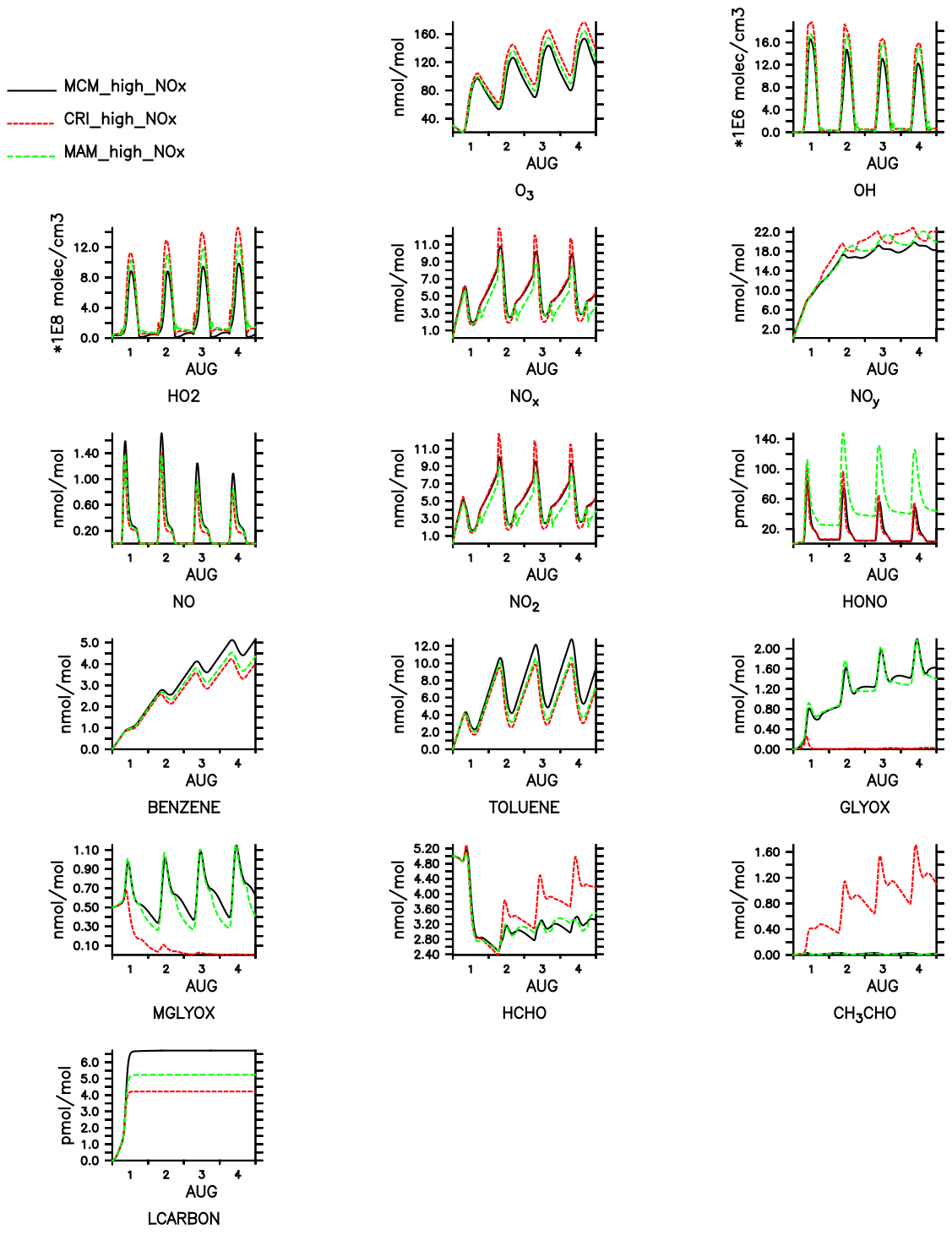

FIGURE 2.2: Comparison between MCM, CRI and MAM in a high NO_x environment.

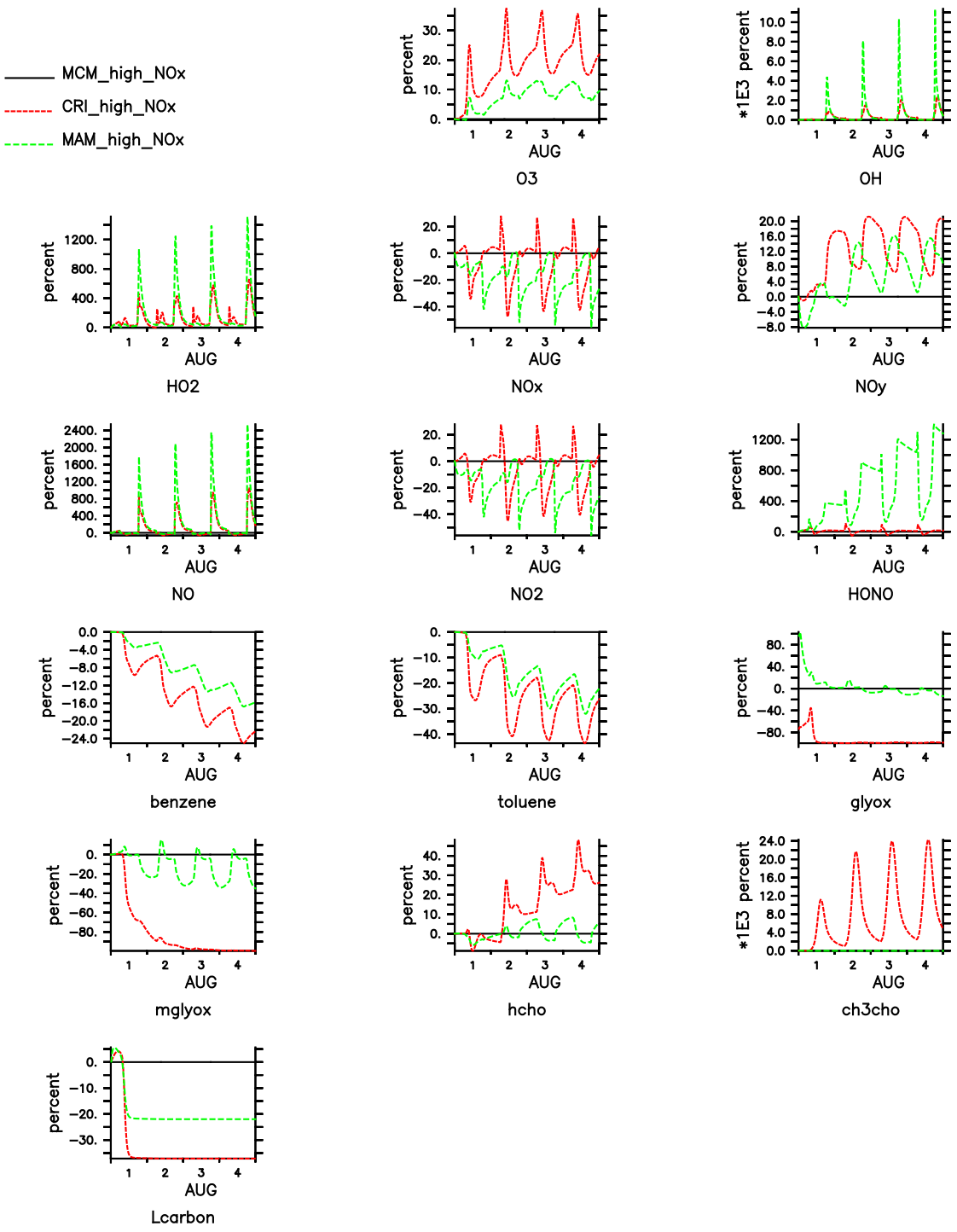

FIGURE 2.3: Bias of CRI and MAM with respect to MCM mechanism for high NO_x simulation.

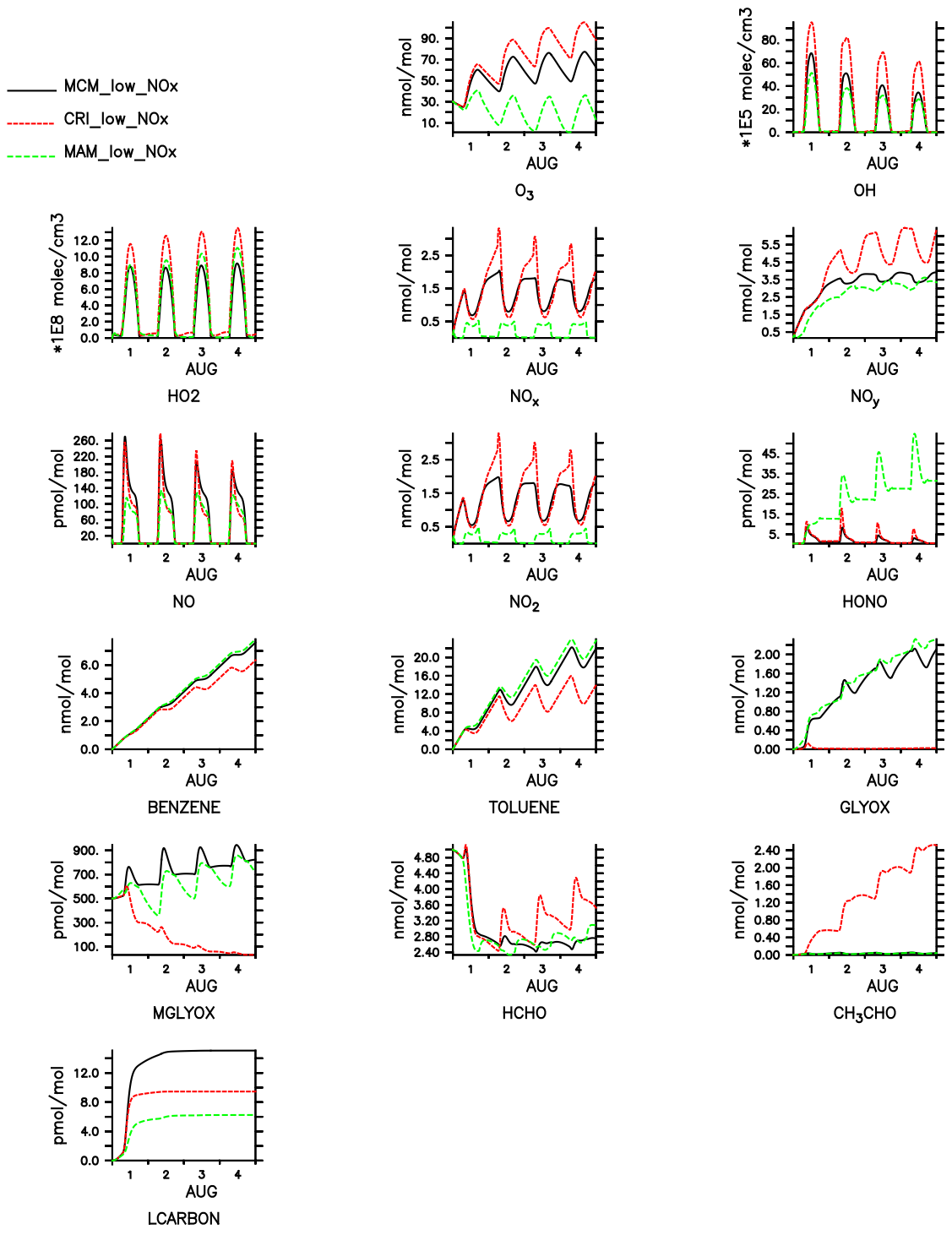

FIGURE 2.4: Comparison between MCM, CRI and MAM in a low NO_x environment.

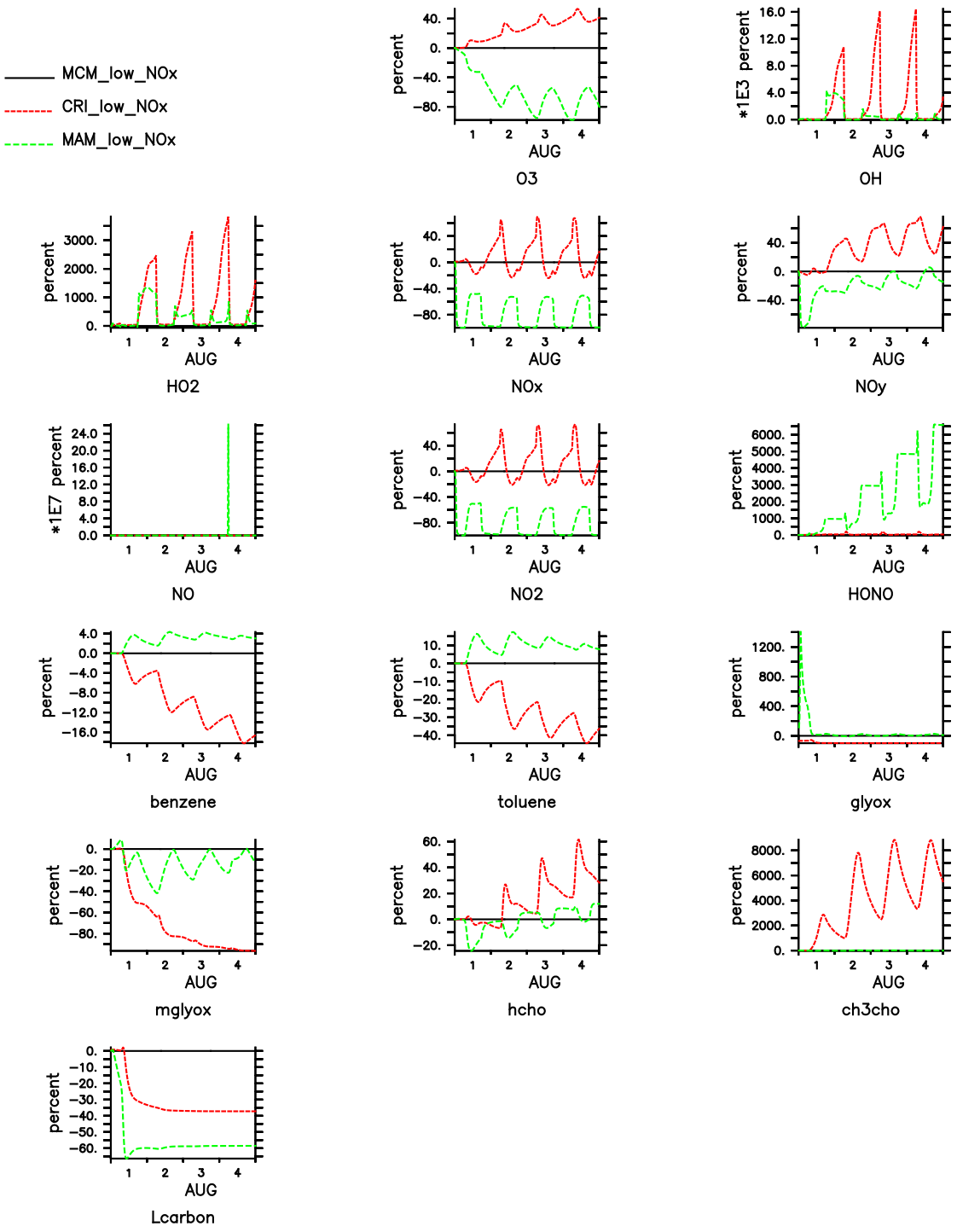

FIGURE 2.5: Bias of CRI and MAM with respect to MCM mechanism for low NO_x simulation.

MCM. For glyoxal, methylglyoxal, formaldehyde and acetaldehyde results are very similar to those in the high NO_x regime, where MAM presents small differences with respect to MCM. HONO mixing ratios are again higher than CRI and MCM, with an increase of one order of magnitude. A feature that is not present in the high NO_x regime, is the depletion of NO_x at night-time and lower mixing ratios than MCM at day time. The depletion on NO_2 explains the decrease on ozone mixing ratios in comparison with MCM. The NO_x depletion is due phenoxy radical reactions with NO_2 (Jagiella and Zabel, 2007), which leads to NO_3 formation in combination with the photolysis of nitrophenols (Bejan et al., 2006). Both channels are new with respect to the MCM code. As a result of the phenoxy radical channel addition there is a net nitrogen shift from NO_2 to NO_3.

Thus, we conclude that MAM is consistent with MCM results, and, furthermore, MAM includes new features. In chapter 5, the characteristic of this new mechanism is evaluated at a global scale with a GCM.

2.5.1 Henry's law coefficient

The addition of new chemical species in the system implies the implementation of Henry's law coefficient for those species. This is relevant for dry deposition and scavenging processes, as mentioned in the section 2.3.1. There are plenty of studies focused on Henry's law coefficients for numerous organic and inorganic species, for instance a large overview of Henry's law coefficient can be found in Sander (1999). However, there are only measurements of Henry's law values of the primary aromatic compounds, whereas the oxidation products (more than 200) remain unknown. Thus, in order to define the Henry's law values for all the aromatic species, we follow a simple approach. We select several organic species with well known Henry's values as reference (each of the chosen species contains different groups as alcohols, phenols, etc). Then, we compare each aromatic species with the reference species and then select the structure which is the most similar, consequently we create groups by affinity with the reference species (with known Henry's law constant). Finally, we add the coefficients on the SCAV and DDEP submodels. The full list of Henry's law coefficients for aromatics can be found in the appendix B.

Chapter 3

Emissions of aromatic VOCs in the MESSy model

In this chapter we present a series of updates on several MESSy submodels that calculate the emission fluxes of tracers (including aromatic VOCs) into the atmosphere. These updates pertain to the submodels of biogenic, anthropogenic, and biomass burning emissions. With respect to biomass burning emissions, a detailed explanation of our development of the new submodel BioBurn is presented. For biogenic emissions, we study the dependency of the MEGAN submodel on MESSy model resolution, and we propose an approach to overcome this issue. For anthropogenic emissions, we present a general VOC speciation and tuning approach that is valid for any anthropogenic emission database available.

3.1 Biomass Burning

Biomass burning can be defined as the incineration of living or dead flora. Fires can be ignited by natural causes or by human activity. Ignition by nature is mostly due to lightning strikes. Fires caused by human activity have a range of possibilities, from deliberate deforestation activities aimed at transforming forest into agricultural land, to carelessness around campfires or cigarettes (Crutzen and Andreae, 1990). Biomass burning emissions release a large number of chemical species, as well as large amounts of aerosols. Among the trace gases emitted, carbon monoxide (CO) and oxides of nitrogen (NO_x) are particularly large; short-lived species are also common (e.g. VOCs, including aromatic compounds). Approximately 400 Tg of VOCs are emitted annually (Akagi et al., 2011), and extensive research has shown that biomass burning emissions have an effect on both climate and on regional–global air quality (Andrés-Hernández et al., 2009; Sanford et al., 1985; Andreae and Merlet, 2001); these emissions may also alter both the carbon and

the nitrogen cycles (Crutzen and Andreae, 1990). In general, biomass burning emissions are strongly dependant on fuel properties, such as the fuel's type, amount, and degree of dryness. The fire state (i.e. a combination of the physical and chemical mechanisms at work during combustion) also plays a strong role (Lobert and Warnatz, 1993; Yokelson et al., 1996, 1997).

3.1.1 GFAS

One of the available datasets that estimates biomass burning emissions is the Global Fire Assimilation System (GFASv1.0). This system uses different satellites to retrieve Fire Radiative Power (FRP) observations through the Moderate Resolution Imaging Spectroradiometer (MODIS) instrument. Lack of data due to cloud cover is corrected, and volcanoes, gas flares, and other industrial activity are filtered out, as they cause false FRP measurements. GFAS presents daily temporal and 0.5°x0.5° spatial resolutions, covering the time span of 2003–2016 (Kaiser et al., 2012). The system results are consistent with alternative representations of biomass burning emissions, such as the Global Fire Emission Database version 3.1 (GFED3.1) (Van der Werf et al., 2010).

Biomass burning emits thermal radiation in the 3.9–11 μm wavelength range. This radiation is measured using the MODIS instruments contained in the polar-orbiting satellites Aqua and Terra. The fire radiative power and the binary active fire flag are contained in the MOD14 (Justice et al., 2002; Giglio, 2010) NASA product. Both combustion rates and aerosol emission rates have been linked to the FRP (Wooster et al., 2005; Ichoku and Kaufman, 2005). Typically, FRP units for observed fires are in Watt for each satellite pixel. All observations are then collected by GFAS to produce an FRP map with a 0.5° resolution grid, covering the entire globe.

The FRP products must be converted into dry matter combustion rates. This conversion is obtained by multiplying the FRP by a factor of 0.368 kg/MJ, as proposed by Wooster et al. (2005). Ground-based experiments have been carried out linking FRP measurements of small-scale fires and fuel consumption, to estimate the conversion factor. However, MODIS FRP underestimates small-fire fuel consumption (with no correction for it by default); GFAS FRP is therefore tuned to represent more realistic fuel consumption. GFAS uses a conversion factor of 1.37 kg/MJ, which is based on a comparison of the global emission budgets from GFED2 (Kaiser et al., 2009).

The emission rate densities, F, with units of (Kg/m^2/s), are calculated using the following equation:

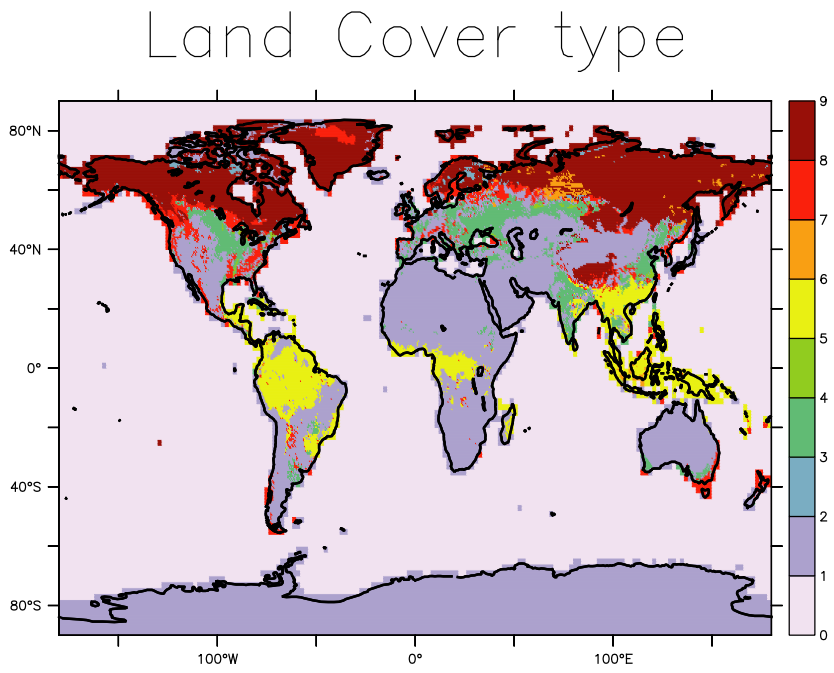

FIGURE 3.1: Land cover type used in GFAS: 1. savannah, 2. savannah with organic soil, 3. agriculture, 4. agriculture with organic soil, 5. tropical forest, 6. peat, 7. extratropical forest, 8. extratropical forest with organic soil.

$$F = EF(c) \times DM \tag{3.1}$$

Where EF are the emission factors, dependent on the land cover type. Figure 3.1 presents the distribution of the different land covers, which comprise savannah, tropical forest, boreal forest, agriculture, and peat. DM refers to the dry matter combustion flux, in units of $g(fuel)/s/m^2$. An example of the annual distribution of the dry matter burned is given in Figure 3.2.

A description of two different methods that can be used to quantify emission factors was summarized by Andreae and Merlet (2001). The first method, *Emission Ratios*, pairs the emissions of a specific tracer to that of a reference species (e.g. CO_2 or CO). The second method, *Emission factors*, is based on the amount of mass released (of certain compound X) with respect to the amount of dry fuel burned. The emission factor (EF) has units of *g(of species X)/kg(dry matter burned)*, and is estimated based on the carbon content of the biomass burned and the carbon budget of the fire. However, determining these parameters in the field is, naturally, more complicated than in laboratory studies. The sum of the concentrations of CO_2, CO, hydrocarbons, and black carbon is used to estimate the total amount of carbon released. The EF can therefore be expressed as:

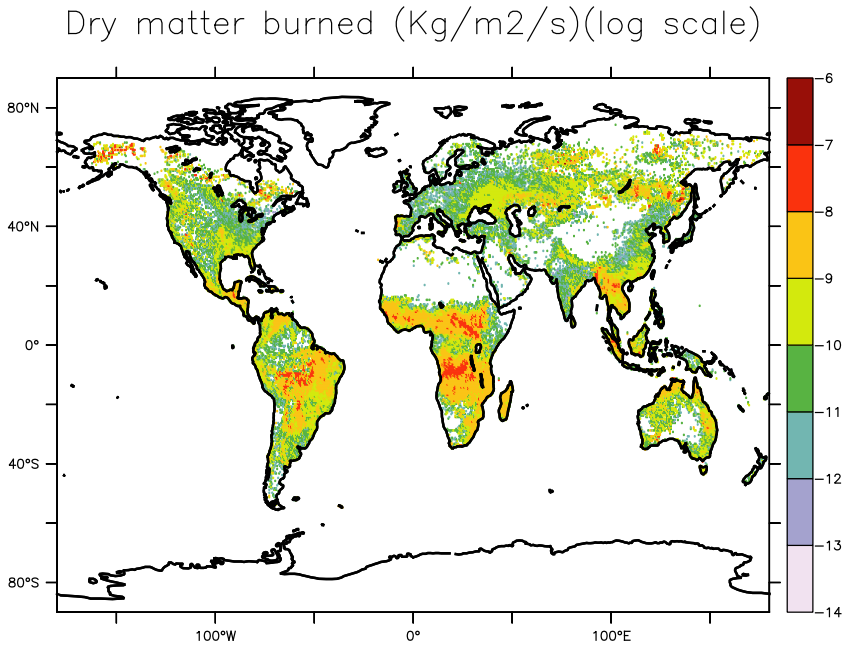

FIGURE 3.2: Annual average dry matter burned fluxes in Kg/m^2/s for the year 2005. Note the logarithmic scale.

$$EF_X = \frac{M_x}{M_{biomass}} = \frac{M_x}{M_C}[C]_{biomass} \tag{3.2}$$

$$EF_X \cong \frac{[x]}{\sum([CO_2] + [CO] + [CH_4] + [VOC] + ...)}[C]_{biomass} \tag{3.3}$$

where M_x represents the mass of carbon released, $[C]_{biomass}$ is the carbon concentration in the biomass burned, [x] is the concentration of tracer x, and $[CO_2]$, $[CO]$, $[CH_4]$ are the concentrations of the different gases in the smoke.

3.1.2 BioBurn

Traditionally, biomass burning emissions in MESSy are pre-processed files in net-CDF format that are linked directly to OFFEMIS or ONEMIS submodels (depending on user needs). However, this method limits flexibility. For instance, some biomass burning emission datasets are only available for certain species, or it is not possible to control the emission factors used to estimate mass fluxes. In other cases, it is possible to modify the emission factors, but calculating the biomass-burning fluxes requires an external script. To combine full control over the choice of emission factors and avoid having to pre-calculate

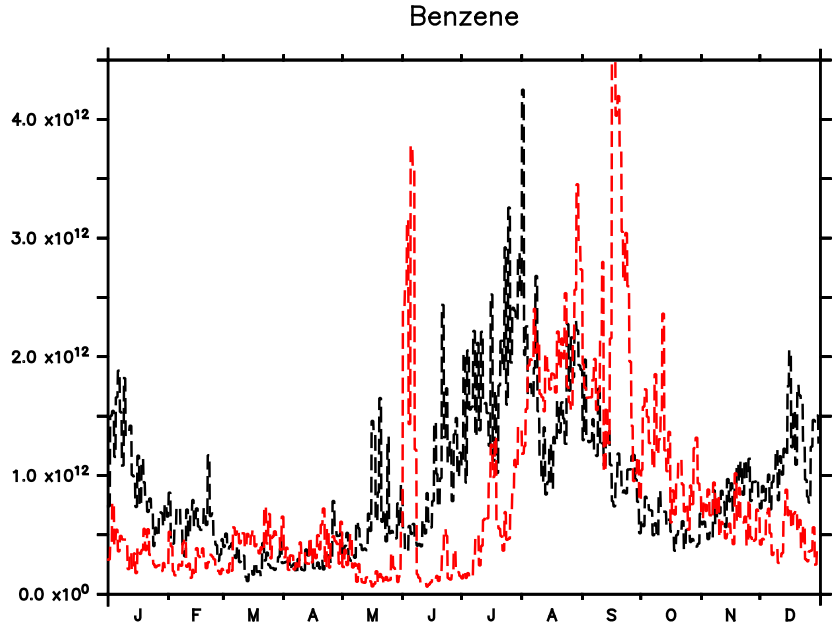

FIGURE 3.3: Benzene emissions for the year 2005, in mlc/m^2/s. In black, averaged emissions for the northern hemisphere; in red, averaged emissions for the southern hemisphere.

the emission fluxes, a new submodel was created, called *BioBurn*. This submodel is suitable for representing biomass burning emissions from the GFAS database.

Bioburn is controlled via namelist, whereby species can be added or removed by simply adding (or removing, respectively) a line of code containing the molar mass of the species and the emission factors for the different land-cover types. The user can also choose whether the emission fluxes are in mlc/m^2/s or gr(species)/m^2/s, and emissions can be coupled to ONEMIS and OFFEMIS submodels. *Bioburn* uses a GFAS-prescribed file containing dry-matter-burned fluxes and land-cover-type fields. Both fields are re-gridded by MESSy to adapt them to the model resolution. The re-gridding from fine to coarse resolution can lead to loss of information due to the averaging of values of the different grid boxes making up the coarse grid; this method is therefore suitable for calculating the amount of dry matter burned, but not for examining land cover type, as the latter would entail averaging indices. We therefore used IFX re-gridding for the land-cover-type fields. The IFX method is especially well-suited for re-gridding indices and for conserving the proportion of the different indices. The equation used to estimate the fluxes in *Bioburn* is based on 3.1:

TABLE 3.1: Biomass burning emission factors for the BIOBURN submodel. Emission factors are given in units of g (species) /kg (dry matter burned). The last column presents the global biomass burning emissions for the year 2005.

Specie	**Savanna**	**Tropical forest**	**Boreal forest**	**agriculture**	**peat**	reference	emissions (Tg/yr)
Benzene	0.20	0.39	1.11	0.15	1.21	(Akagi et al., 2011)	1.49
Toluene	0.08	0.26	0.48	0.19	2.46	(Akagi et al., 2011)	0.91
Xylene	0.05	0.11	0.18	0.01	0.00	(Andreae and Merlet, 2001) (Akagi et al., 2011)	0.29
Phenol	0.52	0.45	0.48	0.52	4.36	(Akagi et al., 2011)	1.86
Styrene	0.02	0.03	0.13	0.03	0.00	(Andreae and Merlet, 2001)	0.14
Ethylbenzene	0.13	0.02	0.05	0.03	0.00	(Andreae and Merlet, 2001)	0.08
Trimethyl-benzene	0.00	0.00	0.12	0.00	0.00	(Yokelson et al., 2013)	0.05
Benzaldehyde	0.03	0.03	0.04	0.01	0.00	(Andreae and Merlet, 2001) (Yokelson et al., 2013)	0.10

$$F_c = EF_c(i) \times DM \times GS_c \tag{3.4}$$

where GS is a global scaling factor for tuning emissions and sensitivity studies. C represents the tracer and i the land-cover type. One limitation in *BioBurn* is the constraint imposed by the number of emission factors available, as they are often missing for certain species or for some land-cover types. The emission factors are given in several studies e.g. (Akagi et al., 2011; Yokelson et al., 2013; Andreae and Merlet, 2001). The emissions have low resolution dependency (less than 3% between T85 and T42 resolutions) due to the combination of the land-cover types with the re-gridded dry matter burned.

3.1.3 Biomass burning emissions of aromatics

We used the *BioBurn* submodel to calculate the emission fluxes of the most-emitted monocyclic aromatic compounds. Figure 3.4 shows the annual mean biomass burning fluxes and Table 3.1 presents the emission factors used for each compound and land-cover type, as well as the total annual emissions of each species. More Benzene is emitted in the southern hemisphere than in the northern hemisphere, with Amazonian and Central African fires being the largest sources. In the northern hemisphere, the strongest sources are located in the boreal forests of Canada, the US, Russia, northern China, and the Indochina Peninsula. In such regions, the emission fluxes reach approximately 10^{14} mlc/m^2/s and the total annual emissions of benzene reach 1.49 Tg/yr. A similar strength and distribution of toluene fluxes is found in the northern hemisphere, but toluene emissions are weaker than benzene in the southern hemisphere, particularly in Central Africa. The total emissions of toluene amount to 0.91 Tg/yr. Xylenes, styrene, benzaldehyde, and ethylbenzene

all present a very similar distribution of emissions. The sum of the emissions for these compounds does not exceed 0.66 Tg/yr. Phenol is strongly emitted in the southern hemisphere and is the mono-cycle aromatic compound with the largest biomass burning emissions, amounting to 1.86 Tg/yr.

Figure 3.3 shows the daily average hemispheric emissions for benzene (i.e. the northern and southern hemispheres separately). We omit other species, as their annual hemispheric emissions distribution is very similar to that of benzene.

Emissions in the northern hemisphere exhibit an annual cycle, ranging from approximately 0.2–1$\times 10^{12}$ mlc/m^2/s between January and June. Emissions then reach their maximum during July and August, when fluxes rise to more than 4$\times 10^{12}$ mlc/m^2/s. Emissions then decrease, reaching a minimum in October. In the southern hemisphere, emissions remain below 10^{12} mlc/m^2/s from January to June. From July to October emissions range between 1–4$\times 10^{12}$ mlc/m^2/s, then decrease until December.

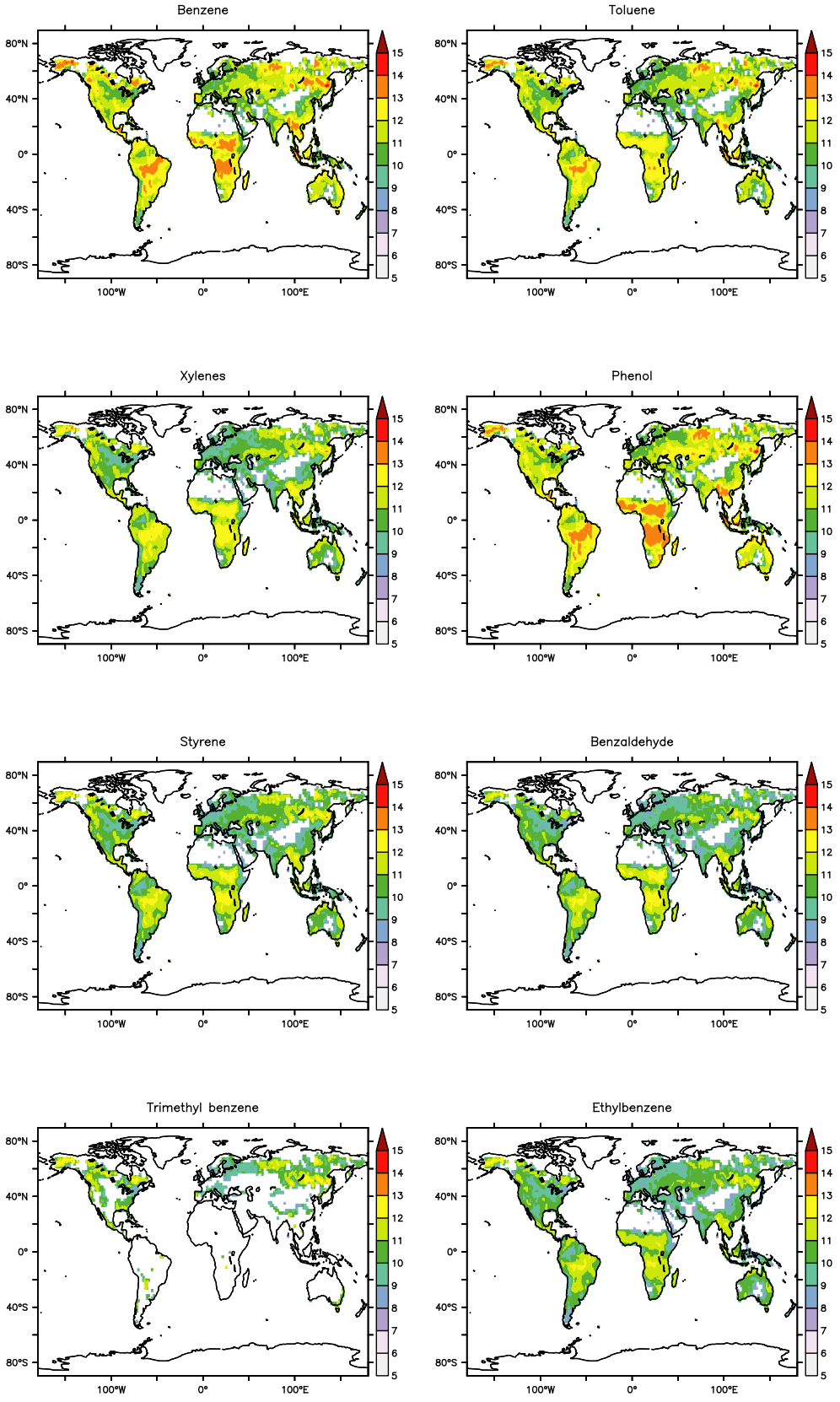

FIGURE 3.4: Annual average biomass burning emissions for the different aromatic compounds studied in this thesis for the year 2005. The fluxes are in mlc/m^2/s. Note the logarithmic scale.

3.2 Biogenic emissions

Organic compounds emitted by the biosphere (which involves soil, oceans, and microorganisms) are called Biogenic VOCs (BVOCs). Biogenic emissions include a vast number of compounds, including isoprenoids (e.g. isoprene and monoterpenes) as well as alkanes, alkenes, carbonyls, alcohols, esters, ethers, and acids (Kesselmeier and Staudt, 1999). However, two compounds dominate fluxes at the global scale, methane and isoprene. The first is predominately produced by microbial sources, the second by plant foliage (which is the source of more than 90% of the total isoprene produced). Other biogenic sources of isoprene are microbes (e.g. aquatic organisms) and animals (including humans) (Wagner et al., 1999). Methane and isoprene account for approximately one-third of all types of VOC emissions (which, again, include biogenic, biomass-burning, and anthropogenic sources). Biogenic VOC emissions were first known to be relevant for the atmosphere in the 1960s (e.g. Isoprene and terpenoids Went (1960); Sanadze (1957)). The large number of VOC species emitted by vegetation was discovered later (Zimmerman, 1979). The first attempts at calculating emission fluxes at a global scale were performed by Dignon and Logan (1990) and (Müller, 1992). A comprehensive model involving isoprene, monoterpene, and VOC emissions (called G95) was formulated by Guenther et al. (1995) under the direction of the International Global Atmospheric Chemistry and the (IGAC) Global Emissions Inventory Activity (GEIA) working groups. There have also been several regional biogenic models, such as the Biogenic Emissions Inventory System (BEIS) developed by Pierce and Waldruff (1991). Later, the different versions of BEIS and G95 models were replaced by the Model of Emissions of Gases and Aerosols from Nature (MEGAN) (Guenther et al., 2006).

3.2.1 MEGAN model description

The MEGAN model calculates the net emission fluxes of isoprene (as well as that of many other organic compounds and aerosols) above the canopy level from biogenic environments to the atmosphere. Fluxes are given in units of mg(species)/m^2/h. The main equation driving the fluxes is:

$$Emission = [\varepsilon][\gamma][\rho] \tag{3.5}$$

where ε (mg/m^2/h) is an emission factor dependent on the compound, and which accounts for the emission of a species into the canopy under standard conditions. γ (as a normalized ratio) is an emission activity factor representing the emission modifications due to

deviations from standard conditions and ρ (normalized ratio) is a factor that accounts for production and loss plant canopies.

Emission factor, ε

Emission factors in MEGAN are regionally characterized with the help of databases containing Plant Functional Types (PFT). As each PFT is associated with an emission factor, the emission factor depends on both the species and the PFT. In the PFT approach used, each surface grid cell contains the information about the fraction covered by each PFT (including non-vegetated surfaces). Thus, MEGAN simulates different canopy environments (e.g., broadleaf trees, needle trees), allowing it to represent different light and temperature distributions. MEGAN provides 4 different PFT schemes. The one used in EMAC [PFT-4] is the most suitable for global simulations, as it includes the following canopy environments: needle evergreen tree; broadleaf evergreen tree; shrub; and grass, crops, and other ground cover.

The PFT geographical distributions are dynamic over the time. The PFT distributions must therefore be representative of the simulation period to correctly estimate emissions.

Emission activity factor, γ

Physiological and phenological activities lead to changes in isoprene emission fluxes. These changes are taken into account through the emission activity factor γ. This dimensionless factor is the product of different emission activity factors, which are equal to unity under standard conditions:

$$\gamma = \gamma_{CE} \times \gamma_{age} \times \gamma_{SM} \tag{3.6}$$

where γ_{CE} accounts for the variation due to light, temperature, humidity, wind, and leaf area index (LAI) conditions under the canopy environment. LAI represents the fraction of land covered by plants; this fraction is time dependent and is necessary to correctly simulate seasonal variations in leaf biomass and age distribution. γ_{age} describes adjustments for effects of leaf age, and γ_{SM} represents direct changes in γ due to changes in soil moisture.

MEGAN provides two approaches to estimate γ_{CE}. The first uses a detailed canopy environment model to estimate light and temperature within different canopy layers. The second is a parametrized approach based on the previous system, called the parametrized canopy environment emission activity (PCEEA) algorithm. The PCEEA approach for the calculation of the canopy environment emission activity factor is:

TABLE 3.2: These values belong to the year 2000, based on the year 2000 climatological data. No nudging was used. All vertical resolutions were L31ECMWF (except for T21, which used L19). All emission are in Tg/year.

Specie	T21	T42	T63	T85	T106
CO	88.11	97.36	106.30	108.50	110.40
C2H4	19.09	21.10	23.03	23.43	23.92
C2H6	0.39	0.32	0.35	0.36	0.37
C3H6	11.75	12.98	14.17	14.42	14.72
C3H8	0.15	0.16	0.18	0.18	0.18
C4H10	0.22	0.24	0.27	0.27	0.28
CH3COCH3	28.14	31.62	34.97	35.11	35.85
CH3COOH	2.85	3.15	3.44	3.49	3.57
CH3OH	87.66	96.91	106.70	109.50	112.90
HCOOH	2.85	3.15	3.44	3.49	3.57
ISOP	582.80	653.00	749.80	740.60	762.80

$$\gamma_{CE} = \gamma_{LAI} \times \gamma_P \times \gamma_T \tag{3.7}$$

where γ_{LAI}, γ_P, and γ_T describe variations associated with LAI, photosynthetic photon flux density (PPFD), and temperature, respectively. A detailed explanation of the model can be found in (Guenther et al., 2006).

Canopy environment

MEGAN calculates the net canopy emission flux, which differs from the total net flux. For instance, the canopy loss factor for isoprene, $\rho_{ISO,ISO}$, is the ratio between the emissions of isoprene above canopy to the isoprene flux into the canopy atmosphere. Moreover, isoprene oxidation within the canopy produce other species that may enter the gas or aerosol phases. For instance, the canopy production factor of formaldehyde, $\rho_{CH2O,ISO}$, is the ratio between the formaldehyde formed by isoprene oxidation above the canopy and the isoprene emitted in the canopy.

3.2.2 Resolution and approach

The MEGAN model was implemented as a submodel in the MESSy model. For this thesis, the MEGAN model has been tested under different vertical and horizontal model resolutions. As MEGAN is a non-linear system that is strongly dependent on PPFD, cloud cover, and temperature, MEGAN fluxes are dependent on the model setup and resolution used. The ECHAM5 model results are also sensitive to vertical and horizontal resolutions (Roeckner et al., 2006). For example, in Figure 3.5 we present the surface temperature (right) and SFRL (left) for two different resolutions at an identical time step. The upper

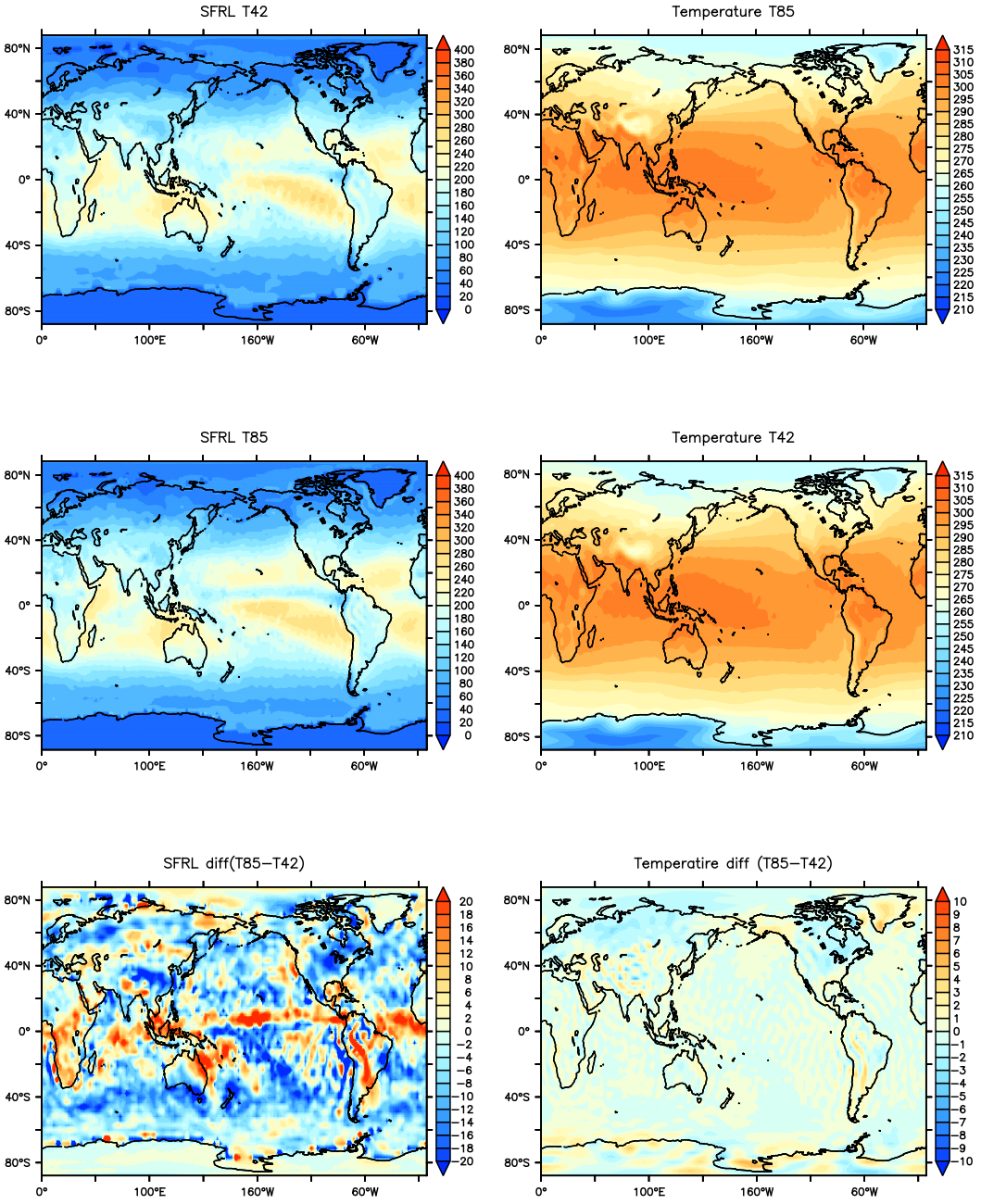

FIGURE 3.5: Left, annual average of the SFRL in units of W/m^2 at surface in the resolutions T42, T85 and absolute differences. Right, surface temperature in K for the resolutions T42, T85 and absolute differences.

figure (SFRL) shows similar but not identical patterns in the Pacific ocean; in the bottom figure (temperature) the patterns for continental areas such as China are similar but not identical. Thus, the aim of this section is to determine whether there is a convergence of the solution with resolution, to quantify the bias, and to determine the appropriate reference resolution.

TABLE 3.3: Increases (in %) for each species with respect to T21 resolution.

	Scaled on	T21	T42	T42L39	T63	T63 nudge	T85	T106
CO	CO	1.000	1.105	1.115	1.206	1.203	1.227	1.253
C2H4	CO	1.000	1.105	1.115	1.206	1.203	1.227	1.253
C2H6	CO	1.000	1.105	1.115	1.206	1.203	1.227	1.253
C3H6	CO	1.000	1.105	1.115	1.206	1.203	1.227	1.253
C3H8	CO	1.000	1.105	1.117	1.207	1.203	1.227	1.252
C4H10	CO	1.000	1.105	1.115	1.207	1.203	1.227	1.253
CH3COCH3	ACTO	1.000	1.124	1.125	1.243	1.231	1.248	1.274
CH3COOH	FORM	1.000	1.105	1.115	1.207	1.203	1.227	1.253
CH3OH	MEOH	1.000	1.106	1.133	1.217	1.224	1.249	1.288
HCOOH	FORM	1.000	1.105	1.115	1.207	1.203	1.227	1.253
ISOP	ISOP	1.000	1.120	1.155	1.287	1.316	1.271	1.309

To achieve these aims, we performed a series of identical simulation set ups, varying only the horizontal and vertical resolutions. Tables 3.2 and 3.3 present the biogenic emission fluxes for different species and several resolutions, taking the arbitrary resolution of T21 as the reference. Model results are in line with estimates from other studies; for example, isoprene has been shown to have emissions ranging between 500–750 Tg/year (Guenther et al., 2006; Arneth et al., 2008), similar to the 582–762Tg/year of EMAC. Another example is CO, whose emissions in EMAC range from 88 to 110 Tg/year, in agreement with the 90 Tg/year reported by Sindelarova et al. (2014). Furthermore, the annual emission fluxes rose when increasing the horizontal or vertical resolution. For a horizontal resolution of T42, increases in most cases of 10% with respect to T21 were observed, while for the T106 resolution, the increases reached up to 25%. For all species the emission rates converged with increased resolution. For the T63 resolution, we also performed a test including nudging. For most of the species the difference remained below 1%; however, in the case of isoprene, this difference was larger, up to 3%.

To correct these differences and to obtain similar total annual fluxes for all resolutions, we added a global scale emission factor (G), which tunes the net annual flux of any species. The G factor has a double purpose: firstly, to allow sensitivity simulations by scaling biogenic emissions, and secondly, to fix the emissions of any species (e.g. if it is known that certain species are over or underestimated by the model). Therefore, the equation 3.5, in MESSy is now:

$$Emission = [\varepsilon] \cdot [\gamma] \cdot [\rho] \cdot G \tag{3.8}$$

where G is defined for each species in the namelist. The scaling to a reference from the Table 3.2, is therefore defined as:

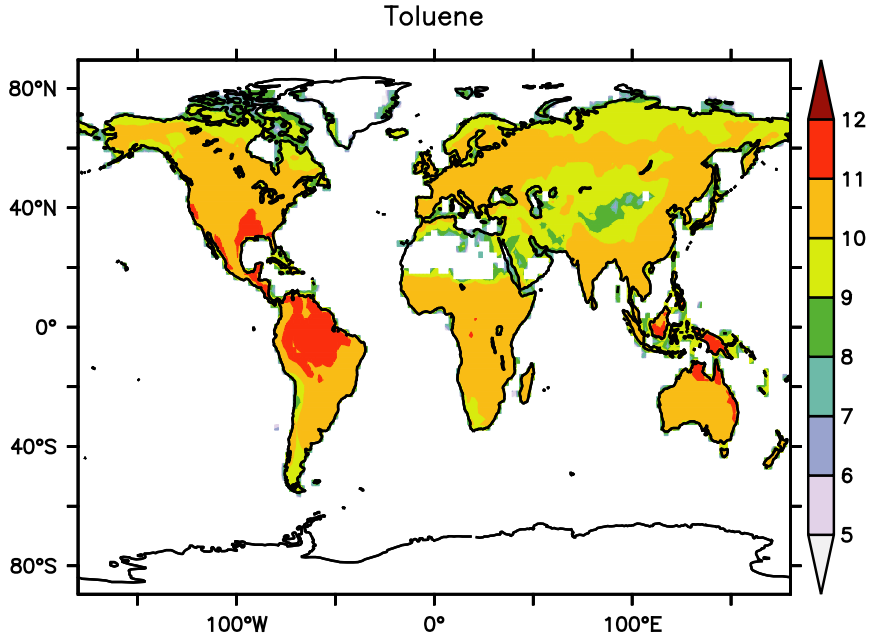

FIGURE 3.6: Annual average surface emission fluxes of toluene from biogenic sources for the year 2000. The fluxes are in mlc/m^2/s. Note the logarithmic scale.

$$G = \frac{Reference\,emissions\,for\,X\,(Literature)}{Estimated\,emissions\,for\,X\,(any\,resolution)} \tag{3.9}$$

where *Estimated emissions* are the emissions for the compound X at any specified resolution, the reference emissions can be obtained from literature estimates, and X is a chemical species.

3.2.3 Biogenic emissions of aromatics

The only simple mono-cycle aromatic compound for which biogenic emissions are known is toluene (Heiden et al., 1999b). Figure 3.6 shows the annual averaged surface emission fluxes of toluene. These fluxes are, in most areas, on the order of 10^{10} mlc/m^2/s, such as, for instance, in Africa, Europe, and continental Asia. In some equatorial regions—i.e. the Amazonian forest, Central America, and Southeast Asia—these emissions fluxes reach 10^{11} mlc/m^2/s.

3.3 Anthropogenic emissions

The term *anthropogenic emissions* comprises a range of different sources, such as fuel production, industrial and domestic combustion of fossil fuel and biofuel, transportation (i.e. road, rail, air, and ships), waste disposal, industrial activities, solvent production and use, and agriculture. There currently exist several anthropogenic emission inventories that provide information about past, present, and future emissions of chemically active species. These emission datasets differ in the number and choice of species treated (e.g., some, like GEIAv1, include few species, while others include a large number of species, including VOCs), the area (i.e. regional or global), and the time span covered. In recent years, an effort has been made to generate datasets (e.g. RCP, ACCMIP) that contain a large number of chemical species and that offer a high resolution at a global scale. Although a sharp contrast remains between inventories from developed and developing countries with respect to the amount of information available (e.g. emission factors), these datasets are particularly important for rapidly developing economies such as China and India (Lamarque et al., 2010; Granier et al., 2004).

In general, most inventories use the following formula to determine emission fluxes:

$$Emission\,flux = AR \times EF \times P_{i,i=1...} \tag{3.10}$$

where AR represents the activity rate of a source (e.g. the mass of coal burned in a power plant), EF accounts for the uncontrolled emission factor (i.e. amount of emissions per unit of activity) by fuel, sector, technology, and compound, and the P_i factor is the parameter that applies to specific abatement options, source types, and species. Typical species included are ozone, nitrogen oxides (NO_x), carbon monoxide, methane, VOCs, sulphur dioxide, ammonia, and organic and black carbon (Granier et al., 2011).

3.3.1 VOC speciation

In most of these inventories, VOC emissions are provided as total VOC emissions (i.e. the sum of all the species listed as VOCs). While some inventories have tried to characterize the different VOC species by fractioning the total VOC emissions into different subgroups and/or species, these inventories have major uncertainties:

- The emission fluxes of each VOC compound are variable in space and time, and they do not necessarily follow the same patterns with respect to the total VOC emissions: i.e. an increase in the total VOC emissions in a specific location does not

necessarily conserve the same ratio with respect to a specific compound. The same uncertainty occurs for the different sectors [1]. There is also temporal variability to emissions, on scales such as seasonal or inter-annual. Some databases have made an effort to specify country-dependant speciations (van Vuuren et al., 2011), although such speciations does not capture any spatio-temporal variability within individual countries.

- Speciation is a complex and time-consuming task (Granier et al., 2011). Unlike species like CO_2, CH_4, or SO_2, for which inventories already contain information about each sector and activity rate, there is not enough global data about VOCs to create such speciations.

A correct speciation is necessary to correctly simulate the atmospheric mixing ratios of VOCs. Knowing the total amount of each VOC that is emitted into the atmosphere is especially important to avoid net under or overestimation. For this reason, we developed a tool for tuning the global annual emissions of any anthropogenic inventory. Several key steps in creating this tool are explained in detail in the following subsections.

3.3.2 Literature review

The first step in developing a tool for tuning the global annual emissions of any anthropogenic inventory was to generate a collection of references containing the global annual emission estimates for VOCs, and then to define a general strategy to create a *Best Estimate* of the emissions for each species. Table 3.4 presents a compilation of emission estimates for the most important VOC compounds (15 species), as well as the *best estimate* for each compound and the range of the emissions. To select the *best estimate*, emissions were prioritized based on (Pozzer et al., 2012), who evaluated the mixing ratios simulated by the EMAC model as they compared to observations. If the species was not evaluated in EMAC, we chose the reference that evaluated the mixing ratios based on direct observations using a model other than EMAC. If a specific compound had never been evaluated in this way, we selected the emission estimate used in the largest number of studies. An extended table including references and best estimates for biogenic and biomass burning emissions is available in Appendix C.

[1] sector refers to a sub-classification of the anthropogenic sources by origin (e.g. transportation, residential, agricultural, industrial, etc.)

TABLE 3.4: Annual average emissions for important VOCs. Units are Tg/yr.

Species	TgC/yr (Range)	Tg(tracer)/yr (Range)	Best Estimate Tg/yr (range)
Ethane – C2H6			9.2 (4 – 10.6)
Ayddin et al 2011	(6.39-7.98)	(8-10)	
Pozzer et al 2010	7.3	9.2	
Etiope et al2009	4.5	5.7	
Xiao et al 2008	8.5	10.6	
Pozzer et al 2007	7.3	9.17	
Folberth et al 2006	3.18	4.0	
Von Kuhlman et al 2003	4.6	5.7	
Granier et al 2001	4.6	5.75	
Bey et al 2001	6.6	8.25	
Poisson et al 2000	4	5	
Propane – C3H8			10.5 (5.75 – 14.1)
Pozzer et al 2010	8.6	10.5	
Etiope et al 2009	5.3	6.51	
Fu et al 2008	11.5	14.1	
Pozzer et al 2007	8.8	10.78	
Folberth et al 2006	6.95	8.5	
Von Kuhlman et 2003	5.4	6.6	
Granier et al 2001	5.5	6.72	
Bey 2001	7	8.1	
Poisson et al 2000	4.7	5.75	
Acetone – CH3COCH3			1.5 (0.6 – 4.98)
Fischer et al 2012	-	0.73	
Fu et al 2008	0.9	1.5	
Pozzer et al 2007	3.1	4.98	
Folberth et al 2006	0.63	1.0	
Von Kuhlman et al2003a,b	1.2	2	
Jacob et al 2002	0.7	1.1	
Bey et al 2001	1.1	1.8	
Singh et al 2000	1.24 (0.62 – 1.86)	2 (1-3)	
Reissell et al 99	-	-	
Collins et al 99	1.9	3	
Brasseur et al 98	1.2	2	
Wang et al 98a	1.2	2	
Singh et al 94	0.5 (0.37- 0.62)	0.8 (0.6-1.0)	
Methanol – CH3OH			8 (1 – 11)
Pozzer et al 2007	3.6	9.71	
Folberth et al 2006	-	-	
Jacob et al 2005	1.48 (0.37 – 3.7)	4 (1-10)	
Tie et al 2003	-	-	
von Kuhlman et al 2003a,b	0.7	2	
Heikes et al 2002	2.96 (1.85 – 4.07)	8 (5-11)	
Galbally and Kirstine 2002	1.48 (1.11 – 1.85)	4 (3-5)	

Singh et al 2000	1.11 (0.74 – 1.48)	3 (2-4)	
Ethene – C2H4			5.4 (5.2 – 9.01)
Pozzer et al 2007	7.7	9.01	
Fu et al 2008	4.6	5.4	
Folberth et al 2006	4.45	5.2	
Poisson et al 2000	4.7	5.5	
Propene – C3H6			4.26 (2 – 4.26)
Pozzer et al 2007	3.6	4.26	
Folberth et al 2006	1.68	2.0	
Poisson et al 2000	2.1	2.5	
Butanes(lumped) – C4H10			73.7 (45.9 – 84.7)
Pozzer et al 2007	60.8	73.7	
von Kuhlman et al 2003a,b	37.9	45.9	
Poisson et al 2000	70	84.7	
Formic Acid – HCOOH	*Gmol/yr		3.56 (0.46 – 3.56)
Paulot et al 2011	(10-28.5)	(0.46-1.31)	
Ito et al. 2007	-	-	
Pozzer et al 2007	77.3	3.56	
Lathiere et al 2006	-	-	
von Kuhlmann 2003a,b	-	-	
Kesselmeier&Staudt99	-	-	
Kesselmeier'98b	-	-	
Acetic Acid – CH3COOH	*Gmol/yr		6.52 (7.3-16.5)
Paulot et al 2011	(121.5-281)	(7.3 – 16.5)	
Pozzer et al 2007	108.6	6.52	
Ito et al. 2007	-	-	
Lathiere et al 2006	-	-	
von Kuhlmann 2003a,b	-	-	
Kesselmeier'98b	-	-	
Bode et al '97	-	-	
Acetaldehyde – CH3CHO			2 (1-2)
Millet et al 2010	1.1	2	
Singh et al 2004	0.5	<1	
Benzene – C6H6			3.4 (2.9 – 3.4)
Fu et al 2008	3.7	3.4	
Henze et al 2008	3.1	2.9	
Toluene - C7H8			5.8 (4.8 – 5.8)
Fu et al 2008	6.4	5.8	
Henze et al 2008	5.3	4.8	
Xylene – C6H4(CH3)2			4.35 (3.6 – 4.35)
Fu et al 2008	4.8	4.35	
Henze et al 2008	4	3.6	
Formaldehyde –HCHO			4.5(0.63-4.5)
Pozzer et al 2007	1.79	4.5	
Folberth et al 2006	0.3	0.63	

Von Kuhlman et 2003	0.5	1.2	
MEK			1 (0-4.68)
Pozzer et al 2007		4.68	
Singh et al 2004		<1	
Von Kuhlman et 2003 (Mek + ketones)	1.8	2.7	

3.3.3 Speciation method

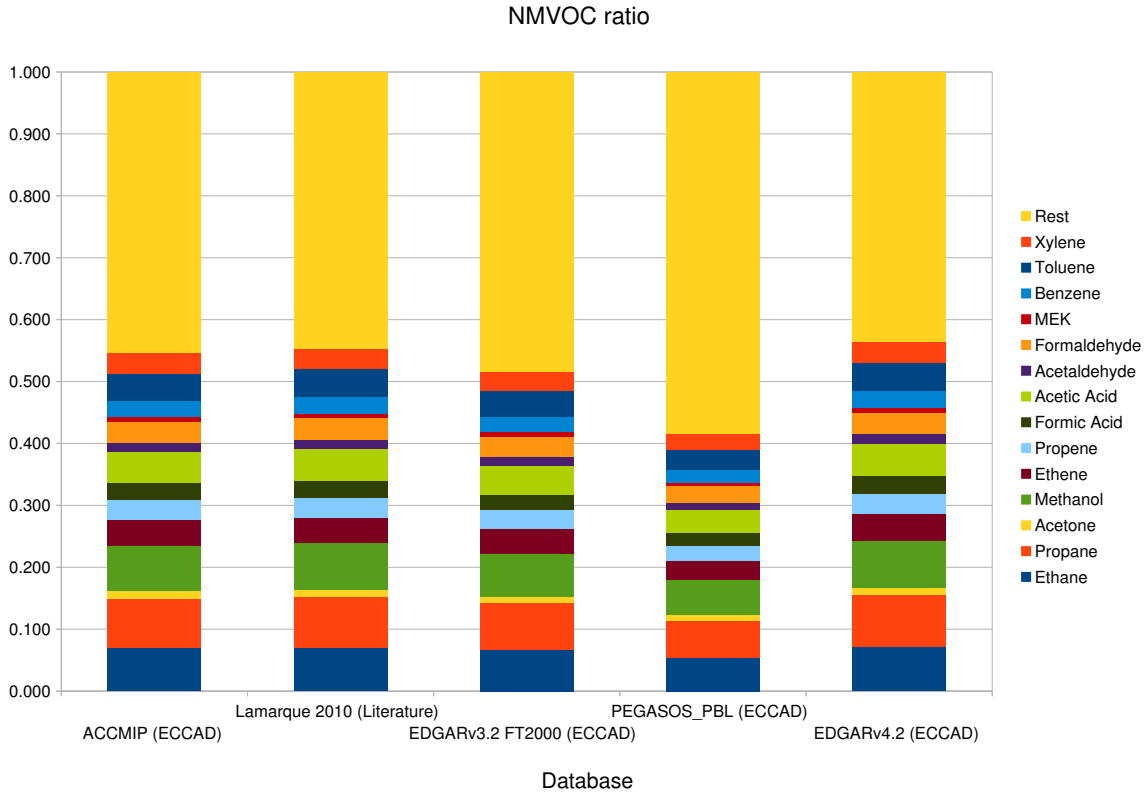

FIGURE 3.7: VOC fractioning for five databases.

Our main goal was to create a simple method that could be used for VOC speciation or for tuning any database. Such a method had to conserve the mass of the total anthropogenic VOC emissions: i.e. independent of the database and the species selected, the total VOC flux had to remain unaltered. Depending on the database, speciation could consist of identifying chosen VOC species and specifying the total annual flux; or, if the database provided VOC speciation, this method could be used to tune the emissions. Considering a database that already provides VOC speciation, but for which we want to tune the total emissions of each species, the method is based on the following equations:

$$Scaling\ fraction_i = \frac{X_{i,Literature}}{X_{i,Database}} \tag{3.11}$$

$$Rest = \frac{\sum VOC_{Database} - \sum VOC_{Literature}}{\sum VOC_{Database}} \tag{3.12}$$

where $X_{i,Literature}$ is the global annual emission of the compound i retrieved from the literature (table 3.4), $X_{i,Database}$ is the global annual emission of the compound i from the selected database, $VOC_{Database}$ is the total annual emission of VOCs for the specified database, and $VOC_{Literature}$ is the total annual emission of VOCs from the literature. A similar procedure can be followed if the database does not provide VOC speciation, by simply substituting $X_{i,Database}$ for $VOC_{Database}$.

Figure 3.7 shows identical VOC speciation applied to several databases and the scaling fractions generated with Equations 3.11 and 3.12. For each VOC, the speciation generates the same annual flux on any database. Changes in the fractions between databases are due to the fact that each of these databases has different total VOC emissions. The only species whose total flux does not remain constant across the databases is the *rest* group. Usually, *rest* is characterized as butanes. Due to the nature of the approximation used, the total mass is always conserved, and the sum of the fractions is always equal to one. As the EDGAR and PEGASOS databases do not include VOC speciation, the plot in these cases shows the results of the new VOC speciation.

It should be stressed that VOC speciation provided by scaling the total VOC flux has an important drawback, as it does not account for the different spatial variability of each VOC. Therefore, while the total amount of each VOC is correct in terms of annual emissions, at the local scale the speciation under or overestimates depending on the ratio of the tracer to total VOCs. Comparisons of observations with model results could therefore lead to undesired discrepancies. For this reason, in this thesis we used a database that already featured VOC speciation.

3.3.4 Anthropogenic emissions of aromatics

Figure 3.8 presents the annual averaged anthropogenic emissions from the RCP8.5 database. We used the original speciation provided by the database, because it reproduces relatively well simulated mixing ratios for the species shown in Figure 3.8 (the evaluation of the model results is studied in detail in Chapter 4). For benzene (upper left), we observe that the largest amount of emissions are located in Asia, mainly in the Arabic Peninsula, China, and India with fluxes of approximately 10^{13} mlc/m^2/s. Fluxes at this level are

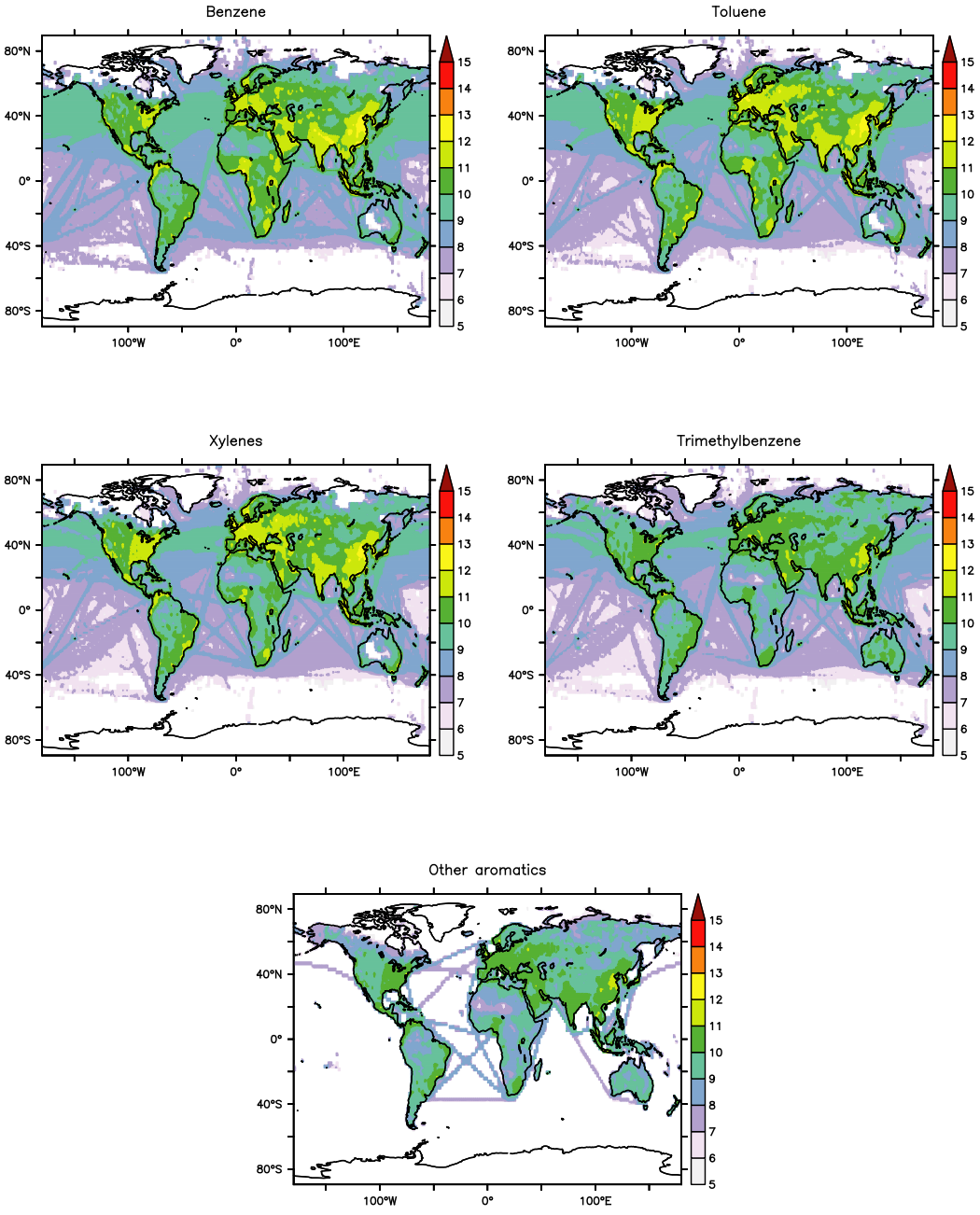

FIGURE 3.8: Annual average anthropogenic emissions for the different aromatic compounds studied in this thesis for the year 2005 from the RCP8.5 database. The fluxes are in mlc/m^2/s. Note the logarithmic scale.

also found in some areas of Europe, North America, Central America, and Africa. Emissions in Africa and South America generally range between $10^{10} - 10^{12}$ mlc/m^2/s. In the case of toluene (upper right) emissions appear to have a similar spatial distribution for flux strength as for benzene. Xylenes (mid left) also presents a similar spatial distribution to toluene, although emissions are overall weaker. Emission fluxes in the Arabic Peninsula are remarkably different, as the emissions of xylenes are one order of magnitude

lower than for benzene and toluene. In the case of trimethylbenzene (mid right), fluxes are generally one order of magnitude lower than for benzene. Other aromatics (bottom) represent a lump species containing other aromatics that were not explicitly calculated. These lumped species will be used to characterize the emissions of compounds such as benzaldehyde in the following chapter. The strength distribution of the fluxes of other aromatics is somewhat similar to trimethylbenzenes.

Chapter 4

Global budget of simple mono-cycle aromatic compounds

In this chapter, simple mono-cycle aromatic compounds are studied from the global scale perspective. The global atmospheric budget and distribution of monocyclic aromatic compounds is estimated, using the EMAC model. Simulation results are evaluated with an ensemble of surface and aircraft observations with the goal of understanding emission, production and removal of these compounds.

In section 4.2, we present the model setup, including a detailed description of the chemical oxidation mechanism created for the aromatic compounds, emissions and sinks. A detailed description of the observations used for the model evaluation is given in section 4.6. Then, an overview of the ability of the model to reproduce observations is shown (Sec. 4.7). Finally, we discuss the atmospheric budget of aromatic compounds in terms of sources, sinks and spatial distribution (Sec. 4.8), followed by the conclusions and outlook.

This chapter is based on the published paper (Cabrera-Perez et al., 2016).

4.1 Introduction

As shown before, the number of aromatic compounds in the atmosphere is countless, and in this work we focus on those with less than nine carbon atoms and the most abundant: benzene, toluene, xylene, phenol, styrene, ethylbenzene, trimethyl-benzenes, benzaldehydes and higher aromatics. The purpose of this study is to:

1. Simulate the aromatic compounds in the atmosphere with an atmospheric chemistry general circulation model.

2. Evaluate the model results by comparing different simulated emission scenarios with atmospheric observations from a number of surface and aircraft campaigns and monitoring stations.

3. Provide an estimate of the global atmospheric budget of the most abundant aromatic species in the atmosphere.

4.2 Methods

For this study, we use the EMAC model with a resolution of T63L31ECMWF, which corresponds to a horizontal resolution of T63 with spherical truncation (i.e., a Gaussian grid of approx. 210km × 210km in latitude and longitude). In this setup, the model has 31 vertical hybrid pressure layers up to 10 hPa. The simulation was nudged towards ECMWF analysis data for a realistic representation of tropospheric meteorology (Jeuken et al., 1996). In order to have the same atmospheric dynamics in all sensitivity simulations, the feedback between chemistry and dynamics is switched off (Chemical Transport Model mode, (Deckert et al., 2011)).

We performed a 24-month simulation from January 2004 to December 2005. The first 12 months are used as spin-up, and only the results for 2005 are used for the analysis.

Two different scenarios have been simulated, differing only with respect to anthropogenic emissions. A detailed description of the scenarios can be found in the following section. A summary of the scenarios and the emissions of the different species can be found in Table 4.1.

In addition, box model simulations have been performed in order to better understand the chemical mechanism used in this work.

4.3 Emissions of aromatics

4.3.1 Anthropogenic

Emissions of aromatics are primarily anthropogenic, coming from numerous sources, including fuel evaporation and combustion, spillage, solvent use, refining of gasoline, landfill wastes and coal-fired stations (Kansal, 2009).

In our study, emissions due to human activities are taken from the Representative Concentration Pathways (RCP) inventory (van Vuuren et al., 2011). The RCP dataset was used

TABLE 4.1: Total annual anthropogenic emissions for the different emission scenarios in $\mathrm{TgC\,year^{-1}}$.

Scenario	Benzene	Toluene	Xylenes	reference
RCP	6.35	6.68	5.66	Lamarque et al. (2010)
LIT	3.24	5.48	4.13	Fu et al. (2008)

in the IPCC's Fifth Assessment Report and consists of a set of four emission scenarios, developed by four different modelling groups (van Vuuren et al., 2008). Each scenario has a specific radiative forcing for the year 2100 (2.6, 4.5, 6.0, and $8.5\,\mathrm{W\,m^{-2}}$) (van Vuuren et al., 2011). We selected the RCP8.5 pathway (Riahi et al., 2007). Granier et al. (2011) indicate that this assumption is reasonable for the time span 2000–2010. The dataset has a yearly resolution and no seasonal variation. We adopted a vertical distribution of emissions based on the work of Pozzer et al. (2009).

Two simulations with identical meteorology and different anthropogenic emissions have been performed. One scenario has the default emissions developed by the IPCC (denoted as "RCP"). The second scenario, called "LIT", has scaled RCP emissions, which are adapted to reproduce the total annual anthropogenic emissions reported by Fu et al. (2008). A summary of the scenarios and their total emissions for the different species can be found in Table 4.1. The scenarios are only different for benzene, toluene and xylenes, since no literature studies have been found for other species. Both scenarios are compared with surface and tropospheric observations, as described in Sect. 4.7.

In the RCP simulation, 23 TgC of aromatics are released into the atmosphere, which represents 18 % of the total anthropogenic VOC emissions. In the LIT scenario, 16 TgC are emitted, and the aromatics represent 13 % of the total anthropogenic VOC emissions. When looking into the sectors provided by the RCP, we found for benzene 49 % of the emissions originate in the residential sector, followed by the energy sector (29 %). In the case of toluene, emissions are evenly split for transportation, energy, solvents and residential. Xylenes emission are similarly distributed as for toluene, however solvents are the leading source with 30 % of the emissions and residential only 7 %. Trimethylbenzenes are abundantly emitted by the transportation sector (90 %), as well as other aromatics (60 %).

4.3.2 Biomass burning

Biomass burning presents a large source of VOCs for the atmosphere (Lamarque et al., 2010). This contribution is represented by the BIOBURN submodel. BIOBURN calculates the emission fluxes, based on the Global Fire Assimilation System (GFAS) datasets

(Kaiser et al., 2012). The details on the BIOBRUN structure and development can be found in chapter 3.

For each aromatic species, we applied emission factors retrieved from literature (Yokelson et al., 2013; Andreae and Merlet, 2001; Akagi et al., 2011). The emission factors used in this work are listed in Table 3.1 in chapter 3. For other VOCs, we selected evaluated factors as in Pozzer et al. (2010).

Akagi et al. (2011) showed that at least 400 $\mathrm{Tg\,year^{-1}}$ of VOCs are emitted into the atmosphere from biomass burning. Approximately 5 $\mathrm{TgC\,year^{-1}}$ are aromatics, which consequently represent less than 2 % of the total biomass burning VOC emissions. It is worth mentioning the study of Johnson et al. (2013), who estimated an emission of 10.19 $\mathrm{TgC\,year^{-1}}$ for phenol. These emissions are dominated by open cooking, although it remains unclear how calculations were done. In the present study open cooking emissions are included within anthropogenic sources but the RCP database does not present such large phenol emissions.

4.3.3 Biogenic

Biogenic emissions have been reported for more than 25 aromatic species (Misztal et al., 2015), although at low amounts. Moreover, most compounds have complex structures (polycyclic aromatics) or more than eight carbon atoms. These compounds are out of the scope of this paper, since only emissions of simple monoaromatic compounds, such as toluene, have been considered here. Toluene fluxes from plants have been measured. The production mechanism is not clear (Heiden et al., 1999a) but a considerable source of toluene from vegetation of more than 1 $\mathrm{TgC\,year^{-1}}$ has been reported (Sindelarova et al., 2014). In this study, biogenic emissions are calculated online by the MEGAN model (v2.04, Guenther et al., 2012). For toluene, the model yields an emission rate of $\simeq 0.32\,\mathrm{TgC\,year^{-1}}$.

4.4 Chemistry

Reaction with OH is the major removal process of aromatic compounds in the troposphere, followed by a small contribution via reaction with NO_3 radicals (Atkinson, 2000). For benzene and the alkyl-substituted benzenes there are two possible pathways concerning the OH reaction, the first and most prominent is the OH radical addition, which amounts to about 90% of the reactions, and the other 10% correspond to H-atom abstraction (Atkinson, 2000). Only for styrene, which contains a non-aromatic double bond, the

reaction with O_3 is relevant. Phenol undergoes mostly OH-addition, while benzaldehyde reacts almost exclusively via H-abstraction (Clifford et al., 2005). In our model, chemical kinetics calculations are done with the MECCA submodel (Sander et al., 2011) which uses the Kinetic PreProcessor (KPP, Sandu and Sander (2006)). For this study, a new reaction mechanism for aromatics has been developed and added to MECCA (Taraborrelli et al, manuscript in preparation). It describes the chemistry of benzene, toluene, xylenes, phenol, styrene, ethylbenzene, trimethylbenzenes, benzaldehydes and higher aromatics (lumped alkyl-substituted benzenes with 10 or more carbon atoms). The new scheme is based on the Master Chemical Mechanism (MCMv3.2), the most detailed oxidation mechanism available for aromatics with 3788 reactions and 1271 species (Bloss et al., 2005b). However, since the MCM is too computationally expensive for global models, it had to be reduced to 666 reactions and 229 species. A complete list of chemical equations and species involved can be found in the appendix A. The details of the chemical mechanism development can be found in chapter 2.

Atmospheric oxidation of some aromatic compounds can result in a major production (or sink) of other (aromatic) compounds. For instance, when benzene reacts with OH, more than 50% is transformed to phenol. Due to the large amount of benzene that is released into the atmosphere, up to 4 Tg/yr of phenol is produced by this pathway, which represents more than 50% of the global phenol source (see Table 4.4). Additionally, benzaldehyde is produced from several oxidation pathways, which together constitute more than 50% of the total benzaldehyde source.

4.5 Sinks

4.5.1 Scavenging and dry deposition

Because of the hydrophobic nature of aromatic hydrocarbons, scavenging is a minor sink in the atmosphere. However, most oxidation products of aromatics have a strong hydrophilic character. Therefore, wet deposition is a removal process of minor importance for aromatics but essential for its oxidation products.

In the model, dry deposition velocities are calculated using an algorithm based on the big leaf approach (Wesely, 1989; Ganzeveld and Lelieveld, 1995). To account for scavenging, the aqueous and gas-phase chemistry is coupled with physical processes related to clouds and precipitation, which represents the wet deposition (Tost et al., 2006a).

Scavenging and dry deposition are calculated in the MESSy submodels SCAV (Tost et al., 2006a) and DDEP (Kerkweg et al., 2006a), respectively. The Henry's law constants used

in these calculations are listed in the appendix B and a detailed explanation of the method for choosing the Henry's law constants is described in chapter 2

4.6 Observations

To evaluate the model simulations (Sec. 4.7), we collected a set of observations from aircraft and surface campaigns, and from monitoring stations. Table 4.2 summarizes the locations and periods of the different campaigns.

using surface observations is the examination of large scale features (e.g. seasonal cycles and spatial gradients). Observations include data from:

- *CARIBIC*: the CARIBIC project (Civil Aircraft for the Regular Investigation of the atmosphere Based on an Instrument Container) is a long-term monitoring program, based on atmospheric measurements on board of a passenger aircraft (Lufthansa A340-600) (Brenninkmeijer et al., 2007; Baker et al., 2010). Cruising altitudes are 10–12 km and, on average, 50 % in the upper troposphere and 50 % in the lowermost stratosphere. The data span from 2005 to 2012. CARIBIC flights take off from Frankfurt (Germany) on routes to India, East Asia, South America and North America.

- *EMEP*: the European Monitoring and Evaluation Programme (EMEP) (Tørseth et al., 2012) is a network of monitoring sites over Europe and includes measurements of a wide number of species. One of its principal aims is to quantify the long-range transmission of air pollutants, and their fluxes across boundaries. The Chemical Coordinating Centre at NILU (Norwegian Institute for Air Research) is responsible for the data harmonisation after the data have successfully passed quality controls. EMEP sites are located in such a way that local influences are minimal, and consequently the observations are representative of large regional areas.

- *EEA*: data provided by the European Environmental Agency (EEA) are based on the public air quality database AirBase. EEA gathers information from a large network of monitoring stations in urban, semi-urban and background areas. However, only rural background stations are used for the comparison because the simulation horizontal scale is not representative for traffic or industrial influenced stations. Moreover, for the comparison, annual averages for each station have been used. We selected observations from the year 2005. However, the number of stations that is feasible for this study is small.

TABLE 4.2: Aircraft and surface measurements of aromatics that are used for comparison with model simulations.

Site name	Time	Location	Reference
	Surface measurements		
Karachi	Dec 1998–Jan 1999	Pakistan	(Barletta et al., 2002)
43 cities	Jan–Feb 2001	China	(Barletta et al., 2005)
28 cities	1999–2005	US	(Baker et al., 2008)
12 sites	1996	UK	(Derwent et al., 2000)
Rome	1992–1993	Italy	(Brocco et al., 1997)
Antwerp	Sep 2003–Oct 2005	Belgium	(Buczynska et al., 2009)
Paris	2010	France	(Dolgorouky et al., 2012)
Kolkata	Mar–Jun 2006	India	(Dutta et al., 2009)
Pear River Delta	Aug 2001–Dec 2002	China	(Guo et al., 2006)
Boreal forest	Apr 2000–Apr 2002	Finland	(Hakola et al., 2003)
Mount Tai	June 2006	China	(Inomata et al., 2010)
Welgegund	Feb 2011–Feb 2012	South Africa	(Jaars et al., 2014)
Oil refinery	1997	Greece	(Kalabokas et al., 2002)
Kathmandu	Jan–Feb 2003	Nepal	(Yu et al., 2008)
Algiers	Nov 1999	Algeria	(Kerbachi et al., 2006)
Rio de Janeiro	Jan 2001	Brazil	(Martins et al., 2007)
Windsor	2004–2006	Canada	(Miller et al., 2012)
Delhi	Oct 2001–Sep 2002	India	(Hoque et al., 2008)
Ankara	Jan–Jun 2008	Turkey	(Yurdakul et al., 2013)
Bangkok	Jul 2008	Thailand	(Suthawaree et al., 2012)
6 sites	Nov 1999	Sahara desert	(Yassaa et al., 2011)
EMEP	2005	Europe	(Tørseth et al., 2012)
EEA	2005	Europe	http://www.eea.europa.eu/data-and-maps/data/
	Aircraft measurements		
Caribic aircraft (∼11 km)	2005–2012	global/multiple locations	(Baker et al., 2008)

- *Literature*: A compilation of measurements from the literature, covering multiple parts of the globe in multiple campaigns, is summarized in Table 4.2. The table provides detailed information on the location and the time span of the observational dataset. The data cover the years 1995–2012 for 111 surface sites located in rural, semi-urban and urban areas. Each observation represents a different period, ranging from months to years (e.g., Barletta et al., 2005), which can be a source of error in the comparison.

4.7 Results

In this section the model results for benzene, toluene and xylenes are evaluated by comparison with observations. Comparisons for other aromatic compounds cannot be made

due to lack of a consistent set of global measurements. The full set of figures can be found in the Appendix D.

Model results for the year 2005 were chosen for the comparison with observations, assuming that interannual variability is not a significant source of error and that emissions of aromatics were rather constant over the period 1995–2010. For the RCP dataset, this is true, having the emissions with a relative increase of 3 %.

Table 4.3 summarizes the statistics of the model-measurement comparison for the three species mentioned above and for the monitoring networks described in Sect. 4.6. To calculate the statistics, model results were sampled within the geographical locations of the observations.

We follow the criteria of Barna and Lamb (2000) and Pozzer et al. (2012) for the analysis of the model performance. A ratio of RMS (root mean square error) to SD (standard deviation of observations) below 1 is taken as the criterion to establish good modelling quality. In general, the ratio RMS / SD gives a better agreement for the RCP simulation than for the LIT simulation, but both simulations give ratios close to one, meaning relatively good agreement. As a final note, comparisons with station observations must be taken cautiously, as they could be influenced by local emissions and consequently not fully representative for background air, which would be best suited for comparison with large-scale models as the one used in this work.

4.7.1 Benzene

EEA: this set of 22 stations with observations for 2005 shows annually averaged mixing ratios of 194 pmol mol^{-1} (see Table 4.3). In general, the model underestimates observations by a factor of 3.1 in the LIT simulation and by 1.7 in the RCP simulation. As expected due to the coarse model resolution, the simulated spatial variability of simulations (with standard deviations of 15 and 29 pmol mol^{-1} for LIT and RCP, respectively) is lower than that of the observations (118 pmol mol^{-1}). The RMS shows better agreement for the RCP than for the LIT simulation. In addition, RCP and LIT show good spatial agreement for all stations, except for one station in central Europe (figures can be found in the appendix D). In conclusion, this comparison suggests that emissions from the RCP scenario give better results in Europe.

EMEP: this dataset has a daily resolution for 14 stations located in Europe. In this work only monthly values estimated from the database are used. In Fig. 4.1, the RCP simulation results for benzene are compared with observations from six stations. It can be noticed that mixing ratios are better captured by the model in summer than in winter,

TABLE 4.3: Summary of the statistical comparison of observed and simulated mixing ratios. Arithmetic means and standard deviations are shown in pmol/mol. M*LIT*, M*RCP* and MObs represent the mean values for the *LIT* simulation, the *RCP* simulation and the observations, respectively. S*LIT*, S*RCP* and SObs are the standard deviations of the previously mentioned cases.

Species	Network	Number of locations	Time resolution	M*LIT*	S*LIT*	M*RCP*	S*RCP*	MObs	SObs	/M*LIT* MObs	/M*RCP* MObs	RMS (*LIT*)	RMS (*RCP*)	*RCP*: RMS /SObs	*LIT*: RMS /SObs
Benzene	CARIBIC	1241	Instantaneous	6.6	2.1	13.4	3.9	16.0	15.8	0.41	0.83	18.0	15.5	1.0	1.1
	EEA	22	Annual mean	62.2	14.9	117.1	29.3	194.0	118.4	0.32	0.60	178.2	144.9	1.2	1.5
	EMEP	14	Monthly	50.1	22.4	93.3	40.5	166.4	71.7	0.30	0.56	146.3	107.2	1.5	2.0
	*LIT*ERATURE	105	Campaign dependent	205.6	173.8	393.2	339.5	1500.0	1968.0	0.14	0.26	2301.0	2168.0	1.1	1.2
Toluene	CARIBIC	789	Instantaneous	0.7	0.5	0.8	0.6	3.6	7.5	0.19	0.23	8.0	7.9	1.1	1.1
	EEA	6	Annual mean	118.5	65.0	144.0	79.1	240.3	59.4	0.49	0.60	134.4	116.5	2.0	2.3
	EMEP	12	Monthly	91.8	37.0	111.5	44.8	133.1	66.2	0.69	0.84	100.2	102.8	1.6	1.5
	LITERATURE	105	Campaign dependent	290.3	200.3	352.1	243.4	2454.0	3499.0	0.12	0.14	4100.0	4066.0	1.2	1.2
Xylenes	EMEP	8	Monthly	55.5	24.7	75.7	33.5	42.3	41.9	1.31	1.79	79.4	101.8	2.4	1.9
	LITERATURE	53	Campaign dependent	120.7	78.1	164.8	106.8	2026.0	6149.0	0.06	0.08	6452.0	6445.0	1.0	1.0

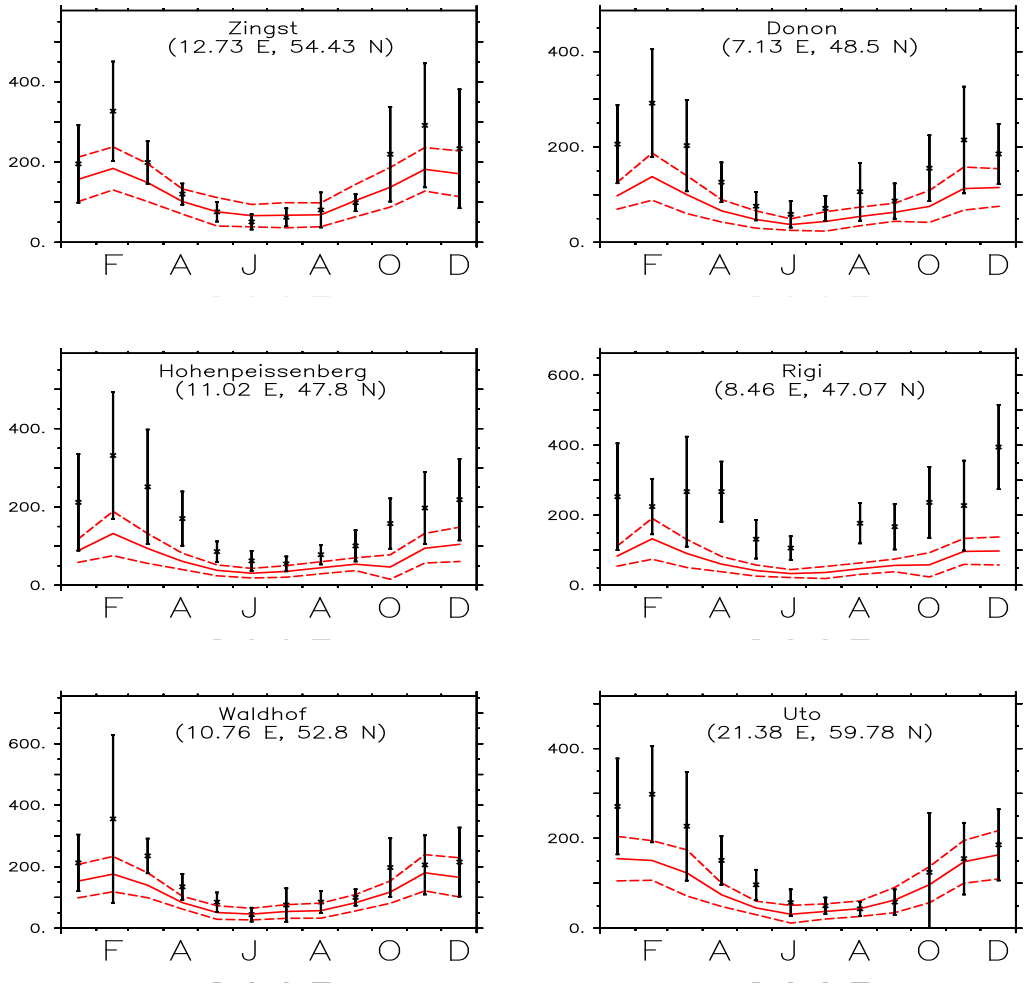

FIGURE 4.1: EMEP observations of benzene for six different locations for the year 2005 (monthly average) (in black) and the simulated toluene mixing ratios for the RCP simulation (in red), both in pmol mol^{-1} . Error bars show standard deviation of the observations and red dashes show the standard deviation of the model simulation.

which is a feature that has been previously observed in EMAC for other simpler VOCs (Pozzer et al., 2007). The RCP simulation yields an amplitude of the annual cycle that is closer to the observations than that of the LIT simulation (see Table 4.3). In addition, the observations show larger standard deviations than the simulations, with the ratio between the observed standard deviation and the RCP standard deviation being 1.8. The ratio RMS(RCP) / SD(OBS) is above 1, but the temporal correlation between the observations and the RCP scenario is very good (above 0.8 in most cases; Fig. 4.2). This supports the good representation of the observations by the RCP simulation. On the other hand, the RCP simulation underestimates the annual average systematically (44 %) compared to the EMEP dataset, which is consistent with underestimation compared to the EEA dataset (40 %).

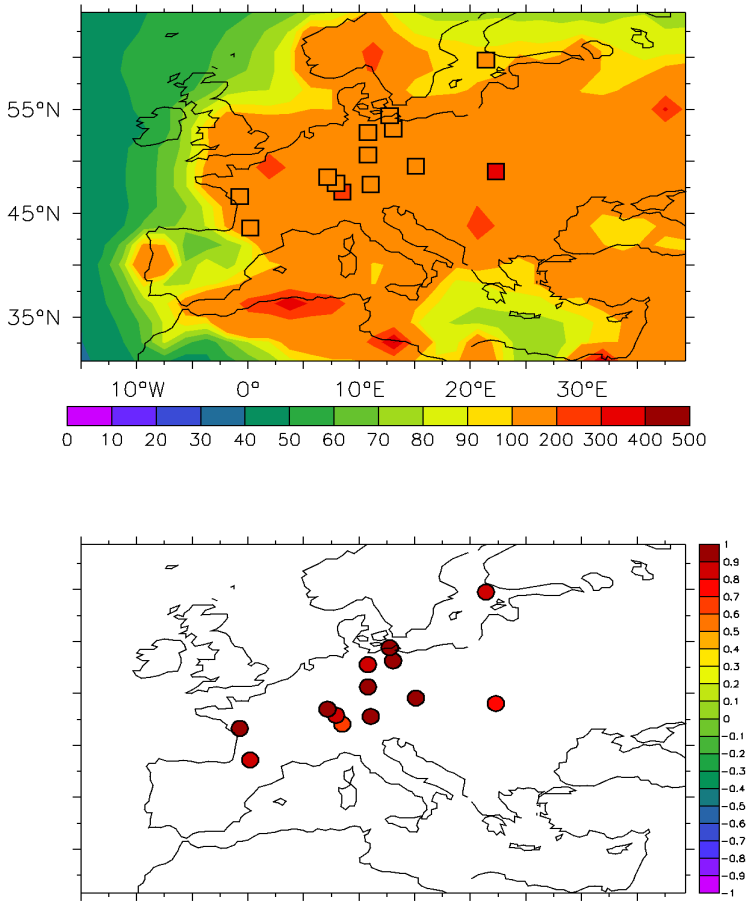

FIGURE 4.2: Top: Annually averaged surface mixing ratios of benzene (pmol mol^{-1}) for the RCP simulation. Circles depict observations from literature. Bottom: Correlations between observations and model results. In red for the LIT scenario, in black for RCP scenario.

Literature: statistics cannot be calculated for these data, because in general the measurements were not performed in rural background areas and time spans of the studies are not suitable for comparison. Nevertheless, they are useful for a qualitative interpretation. In particular, this set of observations helps to better understand spatial performance of the model in regions of America, Africa and Asia (see Fig. 4.3). Observations for 28 US cities (Baker et al., 2008) were taken during summer months in background locations (thus excluding New York, Philadelphia and Salt Lake city). Chicago and Detroit are strong industrialised cities, and therefore the model is biased low in both simulations. Despite the low resolution of the model, in the rest of US cities the simulation is clearly able to capture spatial gradients towards the urban areas. When comparing with the RCP simulation for the month of July, we find an underestimation of 48 % on average. In China, benzene was measured in different areas (mainly residential, commercial, and industrial) in 48 cities

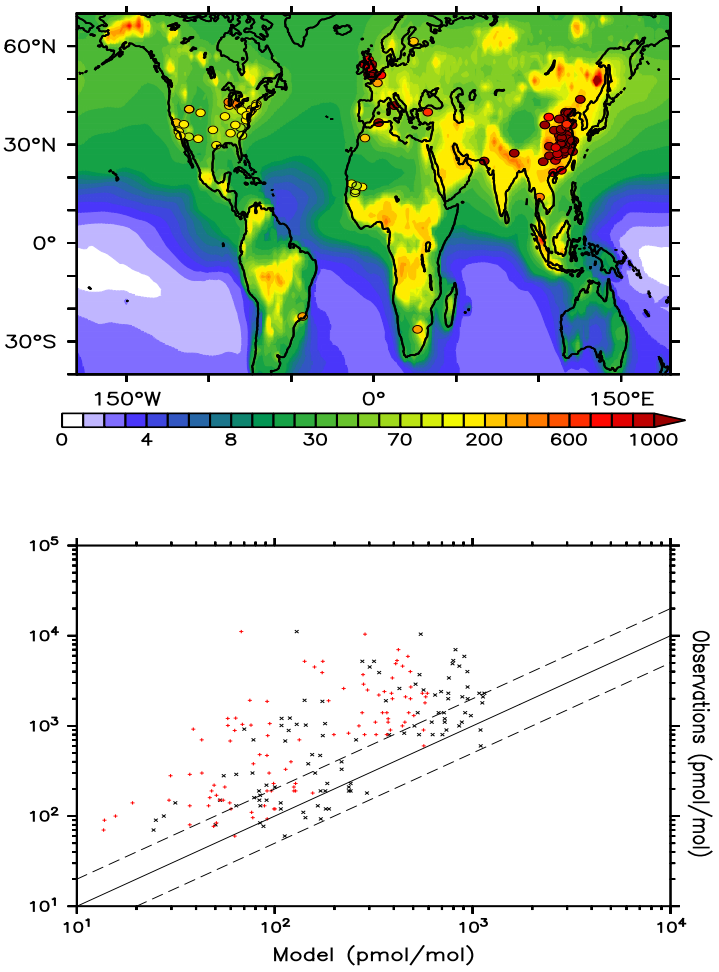

FIGURE 4.3: Annually averaged surface mixing ratios of benzene (pmol/mol) for the *RCP* simulation . Circles depict observations from literature.

during the winter season (Barletta et al., 2005). Both simulations reproduce the observed spatial gradient well, but strongly underestimate the mixing ratios, probably because the instruments were located close to sources. In general the RCP simulation is closer to the observations. At six different locations in the Sahara desert region, observations show mixing ratios on the order of tens of $\mathrm{pmol\,mol^{-1}}$ for the winter months in background remote locations (Yassaa et al., 2011). The RCP simulation consistently reproduces those mixing ratios during the winter. Compared to the observations at a regional background station in South Africa (Jaars et al., 2014), the model shows again a low bias (88 % lower than the observations) but within a reasonable range. The model is able to represent the mixing ratios peak in Rio de Janeiro (Brazil) (Martins et al., 2007).

CARIBIC: model results have been sampled along the flight tracks, and observations within the 200–300 hPa levels are compared to the annual mean of the simulation in the

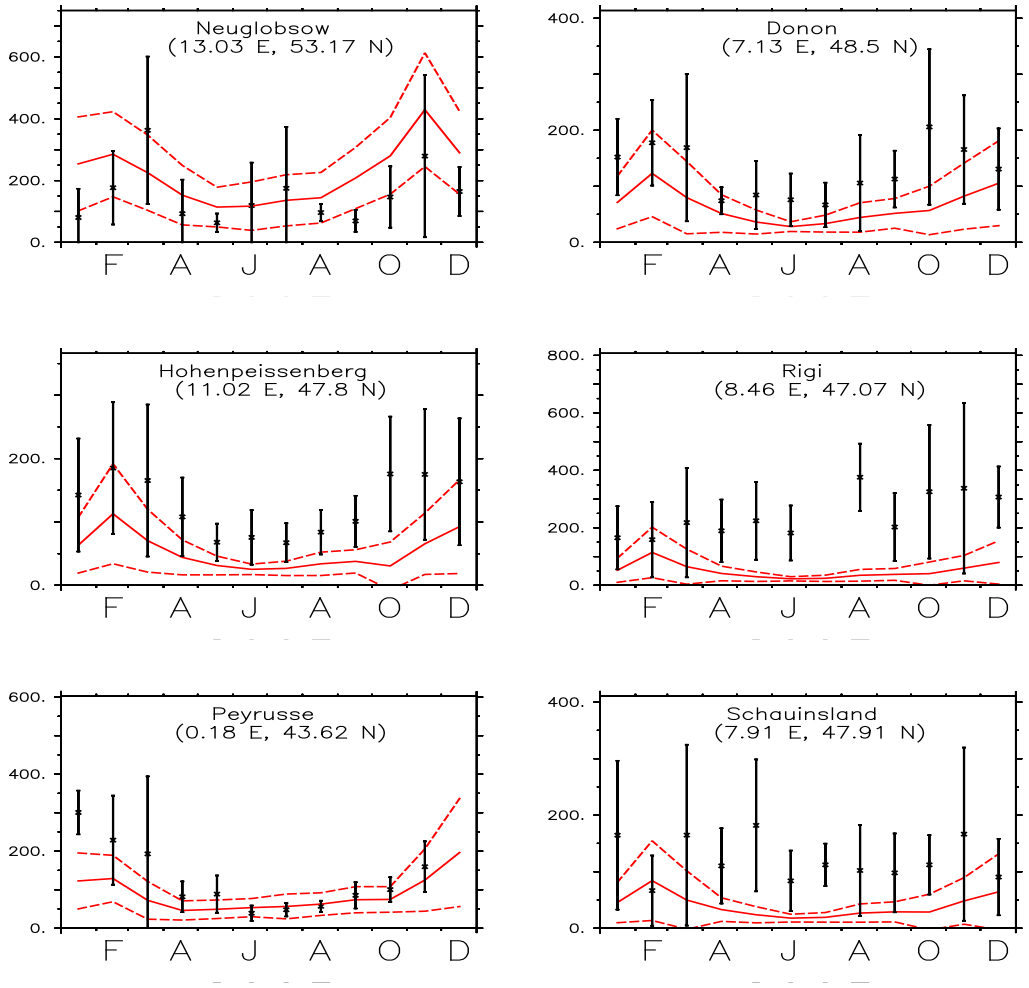

FIGURE 4.4: EMEP observations of toluene for six different locations for the year 2005 (monthly average) (in black) and the simulated toluene mixing ratios for the RCP simulation (in red), both in pmol mol^{-1}. Error bars show standard deviation of the observations and red dashes show the standard deviation of the model simulation.

250 hPA level. The LIT simulation shows a stronger underestimation than RCP, with the RCP simulation underestimating tropospheric benzene mixing ratios by 20 % and the LIT simulation by more than 100 %. For the RCP scenario, the underestimations appear to be lower in the free troposphere than at the surface (RCP simulation underestimates observations of EMEP by 34 % and EEA by 35 %). Despite the large annual variability in benzene mixing ratios, the model is able to capture the gradients along the Africa and Europe-Brasil paths. For the North America-Europe-Asia tracks, the high variability of the measurements makes it hard to compare them with the simulations. In general, the model shows smaller spatial variability than the measurements and an RMS / SD ratio slightly above one, as for the *EEA* and *Literature* data.

4.7.2 Toluene

EEA: toluene mixing ratios for the European stations used in this study show an average annual value of 240 pmol mol^{-1}. Compared to observations, model results from the LIT simulation show an underestimation of 51 %, while the model results from the RCP simulation have a low bias of 40 %. Contrary to the case of benzene, simulated mixing ratios have a larger standard deviation than observations, meaning larger simulated spatial variability.

EMEP: similar to the comparison with the EEA database, model results from the LIT simulation are closer to the EMEP observations than those from the RCP simulation, with annual average underestimations of 31 and 16 %, respectively. Additionally, the RMS / STD ratio is for both simulations lower than in the comparison with the EEA database, which means that there is a better spatio-temporal correlation. The temporal correlation for some stations is weaker than for benzene (see appendix D). Model results from both simulations reproduce the annual cycle; in the case of the RCP simulation, the agreement is in general higher (see RCP case in Fig. 4.4). As opposed to benzene, the variability of the model results from the RCP simulation is 33 % lower than that of the observations.

Literature: generally, the performance of the model for the observations from the literature of toluene is similar to the one of benzene, and spatial gradients and large urban areas are correctly simulated. Nevertheless, for the same reasons as for benzene, the model is showing a general underestimation for both simulations; RCP results are biased low by more than 3 times for benzene and almost 8 times for toluene. Both simulations capture the spatial distributions reasonably well, compared to the observations during summer for the US and during winter for the Sahara and China. The stronger discrepancies for toluene compared to benzene can be explained by the short lifetime of toluene in combination with the short distance from sources of the observation sites. In addition, we also compared the toluene to benzene ratios for the RCP scenario with the *Literature* observations. We found that the model captures well the areas where the observed ratios are higher or lower than one (appendix D). The agreement is in general good in America, Europe and East Asia regions, although the ratios are underestimated.

CARIBIC: in contrast to benzene, toluene annual average mixing ratios are underestimated greatly in both simulations, by more than 4 times (3.6 pmol mol^{-1} for observations and 0.8 pmol mol^{-1} for the RCP scenario). In contrast to the surface observations, the RCP simulation is closer to observations in the troposphere than the LIT simulation. Spatial gradients are best captured in the European-African and European-Asian tracks. Geographical variability is larger than for benzene, due to the shorter lifetime of toluene.

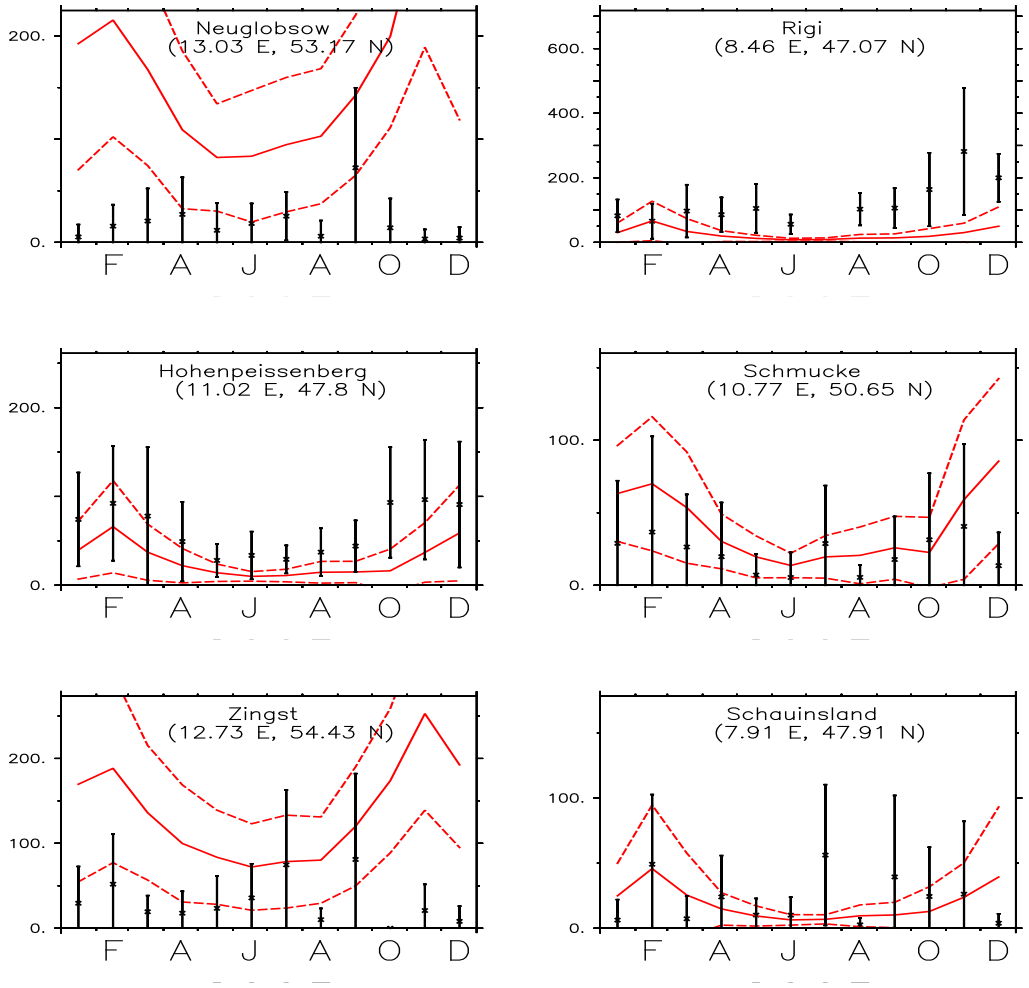

FIGURE 4.5: Mixing ratios of xylenes (pmol mol^{-1}) from EMEP observations in the year 2005 (monthly average) (in black), and from the LIT simulation (in red). Error bars show the standard deviation of the observations, red dashes show the standard deviation of the model simulation.

In the simulations toluene is almost depleted above the planetary boundary layer, which suggests too strong model sinks in those regions. However, as pointed out by Helsel (1990), the underestimation due to the large number of measurements under the instrumental detection limit (1 pmol mol^{-1}) is a source of error, since it artificially causes too high values in the observations. In this case, 46 % of the CARIBIC observations for toluene is below detection limit, which partially explains the bias. We only use the other 54 % of the data for the calculations in Table 4.3. As for benzene, the ratio RMS / STD is somewhat above one for both simulations.

4.7.3 Xylene

EEA: due to the low number of stations available for this dataset (only 2), the results may be not representative and therefore we did not include them in Table 4.3. However, for the two stations, mixing ratios from the LIT and RCP simulations are 66 and 100 % higher than the observations, respectively.

EMEP: a comparison with model results of this set of eight stations shows a similar result as the comparison for toluene. Figure 4.5 shows observations and model results from the LIT simulation. Results from both simulations are poorly correlated with observations in terms of time and space (see appendix D). Model results from the LIT simulation are closer to the measurements than those from RCP, but in both cases the RMS / STD ratio is relatively high, which points at a low consistency in reproducing spatio-temporal features. EMEP observations are overestimated by 31 and 79 % by results from the LIT and RCP simulations, respectively.

Literature: observations of xylenes are only available for the US and for one location in China. As for other species, xylenes are well represented in the US, with the exception of some cities. In China, the model reproduces the increase in mixing ratios towards the Hong Kong area. In the Southern Hemisphere, the model reproduces the polluted spots in South Africa and Rio de Janeiro. We also compared the ratio of xylenes to benzene. The simulation agrees better for xylenes/benzene ratio than for the toluene/benzene, this can observed clearly observed in US regions (see appendix D).

4.8 Global budget

TABLE 4.4: Global atmospheric budget of aromatic compounds from the RCP simulation. Units are TgC/yr in all cases, unless noted otherwise.

	Benzene	Toluene	Xylene	Phenol	Styrene	Ethylbezene	TMB	Benzaldehyde
Sources (TgC/yr)								
Biomass burning	1.5	0.9	0.3	1.9	0.1	0.1	0.1	0.1
Anthropogenic	6.3	6.7	5.7	0.5	0.7	0.7	1.4	0.6
Biogenic		0.3						
Chemical production	0.01			3.4				1.3
Total Sources	7.8	7.9	5.9	5.8	0.8	0.8	1.4	2.0
Sinks (TgC/yr)								
Dry Depostion	1.4	1.1	0.6	0.2	0.0	0.1	0.1	0.1
Oxidation by OH	6.4	6.7	5.1	3.2	0.2	0.6	1.2	0.5
Oxidation by NO_3			0.1	1.8	0.3	0.0	0.0	0.1
Oxidation by O_3					0.1			
Photolysis								1.5
Total Sinks	8.3	7.8	5.8	5.2	0.7	0.8	1.3	2.2
Burden (GgC)	213	57	20	2	0	5	3	2
Lifetime (days)	8.3	1.0	0.5	0.1	0.1	1.2	0.2	0.1

Table 4.4 summarizes the global budget of aromatic compounds for the RCP simulation. This simulation has been selected because it reproduces benzene and toluene observations in terms of annual average mixing ratios, yearly cycle and spatial variations better than the LIT simulation. Moreover, the differences for xylenes are not significant between the two simulations.

For benzene, the total global primary emission of 7.8 $\mathrm{TgC\,year^{-1}}$ is composed of anthropogenic emissions (81 %), biomass burning emissions (19 %) and chemical production (< 1 %). The sources are balanced by the sinks due to OH oxidation (87 %), and dry deposition (13 %). As expected due to the strong hydrophobicity of aromatic compounds, wet deposition has been found to be a negligible process for the budget.

Figure 4.6 shows modelled annually averaged mixing ratios of benzene, toluene and xylenes. For benzene (upper left panel), the surface mixing ratios are as high as 300–400 $\mathrm{pmol\,mol^{-1}}$ in highly urbanised and industrialised areas in the Northern Hemisphere (US, Europa, China). Western Asia shows similar mixing ratios, probably due to the large petrol industry. The highest modelled mixing ratios can be found in India and China, due to large anthropogenic emissions. Central Africa and Northern Asia mixing ratios are mainly driven by biomass burning emissions. In general, areas with high mixing ratios of benzene are located close to sources, due to its relatively short lifetime. Over the oceans, mixing ratios vary between 20 and 70 $\mathrm{pmol\,mol^{-1}}$ (due to ship emissions). In southern hemispheric continental areas, we find mixing ratios in the 100–300 $\mathrm{pmol\,mol^{-1}}$ range. The highest mixing ratios are found in Africa, due to the strong biomass burning season. Continental background areas show mixing ratios between 10–50 $\mathrm{pmol\,mol^{-1}}$. Lowest mixing ratios (1–5 $\mathrm{pmol\,mol^{-1}}$) are found in oceanic areas due to the far distances to sources.

Figure 4.6 (upper right panel) shows the modelled annual zonal mean benzene mixing ratios. Note the strong north–south gradient and the averaged mixing ratios of 60–100 $\mathrm{pmol\,mol^{-1}}$ for the free troposphere. The highest values are found at the surface in the Northern Hemisphere.

Toluene emissions sum up to 7.9 $\mathrm{TgC\,year^{-1}}$, a number similar to that of benzene emissions. Anthropogenic emissions (84 % of the total) play a larger role for this compound than the biomass burning emissions (11 % of the total). Additionally, the model estimates 4 % of emissions from biogenic sources. Sinks are dominated by OH oxidation (85 %), and the remaining 15 % is removed by dry deposition.

Mixing ratios at the surface are in the order of 20–200 $\mathrm{pmol\,mol^{-1}}$ in continental areas (Fig. 4.6, middle left panel), which are larger than for benzene for specific urban regions urban (Europe), due to large anthropogenic emissions. However, in the free troposphere

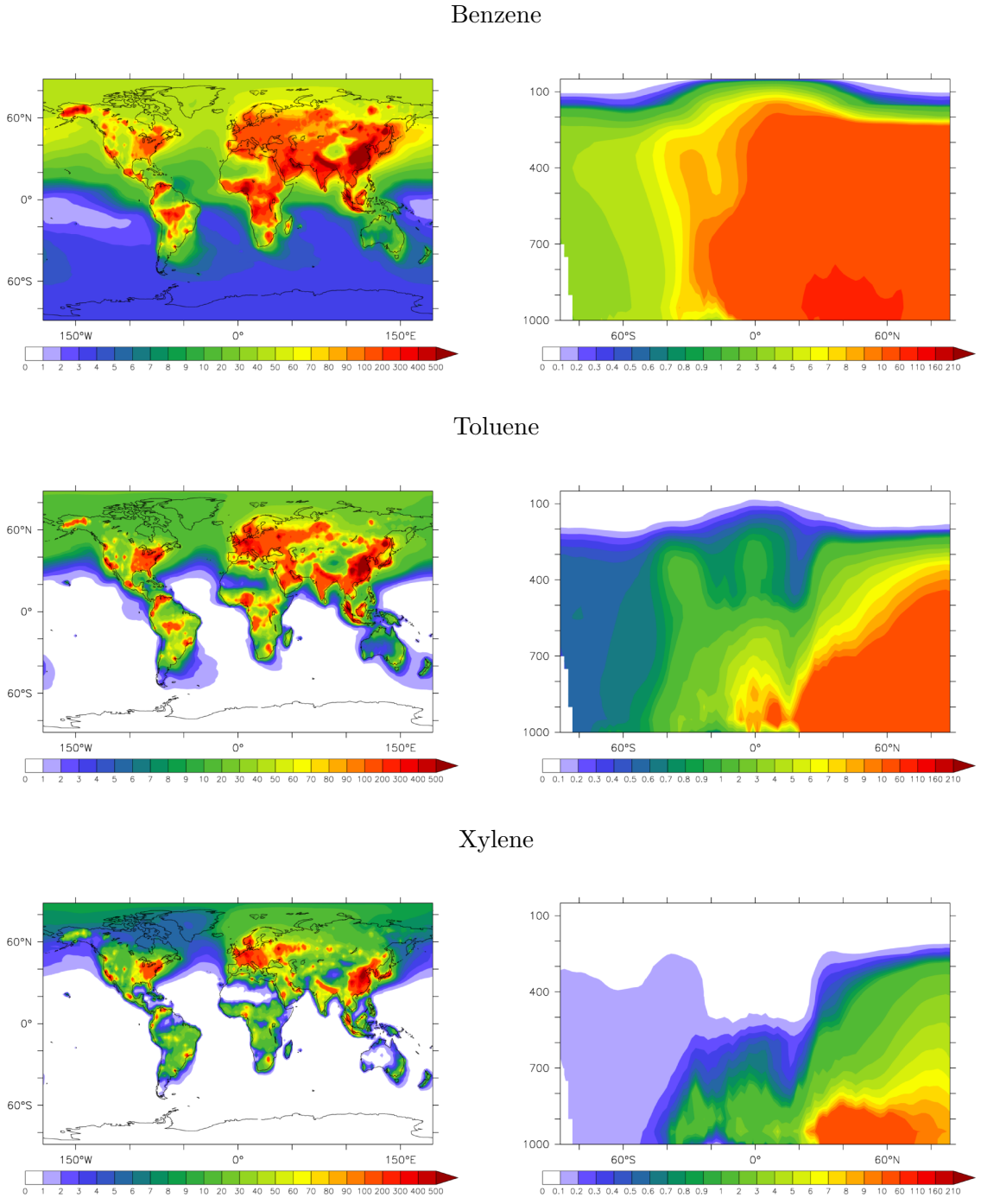

FIGURE 4.6: The left column shows annually averaged surface mixing ratios (pmol/mol) for the *RCP* simulation. The right column shows the annual zonal average. Upper plots show benzene, the middle toluene and the bottom plots show xylenes. Figures for other species can be found in the appendix A.

we find low mixing ratios (a few pmol mol^{-1}), due to the short lifetime of toluene. Background areas (oceans, deserts) show surface mixing ratios below pmol mol^{-1} levels for the same reason.

More than 95 % of xylenes are emitted by anthropogenic sources. Total emissions sump up 5.9 TgC year^{-1}, from which 88 % is removed by OH, 11 % by dry deposition and the remainder (< 1 %) by reaction with NO_3. Very low mixing ratios are present at the surface in the Southern Hemisphere (Fig. 4.6, bottom left panel), except for a few specific locations (i.e. Indonesia, Nigeria, São Paulo in Brazil). In the free troposphere, mixing ratios are below pmol mol^{-1} levels in the Southern Hemisphere, even in the lowermost levels.

Phenol has a different distribution of sources compared to other aromatics. The main source is the atmospheric oxidation of benzene with OH, which produces 3.4 TgC year^{-1} (59 % of total sources). The second important source of phenol is the primary emission from biomass burning, which represents 32 % of the total emissions. Anthropogenic emissions are only 9 % of the total. Nevertheless, mixing ratios of phenol in the atmosphere are low because of its short lifetime.

Emissions of benzaldehyde, styrene and trimethylbenzenes sum up to 3.2 TgC year^{-1}. Their spatial patterns resemble those of toluene, with most emissions, and hence higher mixing ratios, located in the Northern Hemisphere. Nevertheless, their mixing ratios are almost 1 order of magnitude lower than those of toluene at the surface and in the free troposphere. For this reason, they have only been measured in few campaigns (Baker et al., 2008; Yurdakul et al., 2013).

Consistent with their main sink (i.e. reaction with OH), which is weaker during winter (NDJ months) and the main region of their emission (i.e. the Northern Hemisphere), the burden of most species shows a clear annual cycle, with higher mixing ratios in winter than in summer. As an exception, phenol and styrene have an annual cycle with a small amplitude. The specific pattern in their atmospheric burden is caused by their very short lifetimes and the relative high strength of the biomass burning emissions during autumn.

The atmospheric aromatic burden totals 0.3 TgC. Benzene contributes 70 % to the total mass, toluene and xylenes 25 % and the remaining species 5 %.

Estimated lifetimes of aromatics are for most species on the order of a day or less (except for benzene, toluene and ethylbenzene), and can be found in Table 4.4. Estimated lifetimes are in line with values of the literature Atkinson (2000).

4.9 Conclusions

The 3-D atmospheric chemistry general circulation model EMAC and an ensemble of airborne and surface observations were used to evaluate our current understanding of

the global atmospheric budget of monoaromatic compounds, including benzene, toluene, xylenes, phenol, styrene, ethylbenzene, trimethylbenzenes and benzaldehyde.

We extended the chemical mechanism of MECCA in order to accurately describe the chemical reactions of aromatic compounds. Emissions of simple aromatics were included in the model, considering biomass burning, anthropogenic activities and natural sources. As sinks, wet and dry deposition were included.

Simulations with two different sets of anthropogenic emissions were evaluated against observations. The comparison with surface and aircraft observations shows that for benzene, the model seems to underestimate mixing ratios consistently at the surface and in the free troposphere, while the spatial distributions and seasonal cycles are well reproduced. The model captures the spatial variability and averaged mixing ratios at the surface of toluene well, but it does not accurately reproduce the seasonal cycle and considerably underestimates mixing ratios in the free troposphere. This suggests an overestimation of the efficiency of the chemical removal processes, of which the chemical reaction with OH is the most important. The uncertainty of the rate constant for the reaction of toluene + OH is about $5.6 \pm 0.9 \times 10^{-12}\,\mathrm{cm^3\,molecule^{-1}\,s^{-1}}$ at 298 K, which implies a 30 % error on the chemical sink estimate. Additionally, the relative bias of the observations, due to the large number of observations below the instrumental detection limit of the aircraft measurements, can partially explain the disagreement in the upper troposphere. The model shows large temporal discrepancies for mixing ratios of xylenes, although they remain within an acceptable range. We can conclude that the RCP scenario captures better total amounts of aromatics released to the atmosphere than the LIT. Nevertheless, in both scenarios we observed underestimation of the observations which could indicate an underestimation on the emission ratios.

Because of the low mixing ratios of some species (phenol, styrene, ethylbenzene, trimethylbenzenes and benzaldehydes) in the atmosphere, and the limitations of the present instrumentation, a model-measurement comparison was not possible for all species. Therefore, a wider array of samples would be helpful to assess the model's accuracy in remote regions and constrain the respective global atmospheric budgets.

The budget of the studied aromatic compounds is characterized by a total emission rate of $33\,\mathrm{TgC\,year^{-1}}$ (including 1 $\mathrm{TgC\,year^{-1}}$ from higher aromatics). For most species, with the exception of phenol, anthropogenic emissions are the main source. Large emissions are located in industrialised and heavily populated areas, such as Asia and Europe. Emissions from biomass burning play a secondary role on the global scale, although they can be the strongest source of aromatics in specific areas such as Central Africa, South America and boreal areas.

The chemical production generates 4.7 $TgC\,year^{-1}$ of aromatics (mainly phenol), making them nearly ubiquitous. Biogenic emissions form only a small fraction of the total toluene source (4 %), although other studies suggest that this fraction could be larger (Sindelarova et al., 2014). Photochemical reaction with OH is the most important removal process of aromatics from the atmosphere, followed by dry deposition. As an exception, styrene and benzaldehyde also react with O_3 and NO_3, respectively, as their primary sink.

Chapter 5

Atmospheric impacts

Aromatic compounds are reactive species that influence ozone formation, OH *reactivity, and organic aerosol formation. The aim of this chapter is to explore the relationship between aromatic compounds and their influence on gas-phase composition on a global scale. To determine the effects of aromatic compounds on* HO_x*,* NO_x*, and VOCs, we compared simulated scenarios produced by the general circulation atmospheric-chemistry model EMAC.*

5.1 Model set-up

In this thesis a resolution of T63L31ECMWF was used, which corresponds to a horizontal resolution of $1.875° \times 1.875°$ and a vertical resolution of 31 hybrid-pressure levels, extending up to the tropopause. The simulated period covers the years 2004–2005, with the first year being used as spin-up, and the year 2005 being used for the analysis. The feedback between radiation and chemistry was decoupled to avoid any influence of chemistry on the dynamics (QCTM mode (Deckert et al., 2011)). As a consequence, every simulation discussed here has identical meteorology (i.e. binary identical transport).

To analyze the influence of aromatic compounds on atmospheric composition, we performed a comparison between two scenarios. The baseline scenario, called *REF* scenario, excludes the emissions of aromatic compounds. The second scenario, called *AROM* scenario, includes all emissions from anthropogenic, biogenic, and biomass burning sources of the following aromatic compounds: benzene, toluene, xylenes (lumped), phenol, styrene, ethylbenzene, trimethylbenzenes (lumped), benzaldehydes, and higher aromatics (as representative of aromatics with more than nine carbon atoms). Both scenarios are identical aside from emissions (in the baseline case there is no chemistry of aromatic species).

TABLE 5.1: List of aromatic compounds included in this study and the respective annual emissions. This emissions are the same as in chapter 4 but for higher aromatics.

Species	Emissions (TgC/yr)
Benzene	7.8
Toluene	7.9
Xylenes	5.9
Ethylbenzene	0.8
Benzaldehyde	2.0
Phenol	5.8
Styrene	0.8
Trimethyl-benzene	1.4
Higher aromatics	3.4
Total	35.0

We used the Representative Concentration Pathways (RCP) inventory for anthropogenic emissions (van Vuuren et al., 2011), the MEGAN model for biogenic emissions, (Guenther et al., 2012), and the MESSy submodel Bioburn—which integrates the Global Fire Assimilation system (GFAS) inventory (Kaiser et al., 2012)—for biomass burning. In the *AROM* scenario, emissions are identical to those in Chapter 4, except for the emissions of *higher aromatics*. In this chapter, emissions of *higher aromatics* were expanded to include biomass burning emissions. Emissions of aromatics sum to 35 TgC/yr, of which 3.4 TgC/yr are higher aromatics (the details of the emission factors used can be found in the Appendix E). The atmospheric oxidation of aromatic compounds is performed by the MECCA sub-model (Sander et al., 2011). The complete description of the model setup—including emissions, the chemical mechanism used, and the evaluation of the *AROM* scenario—are included in Chapters 2, 3, and 4.

The products from the oxidation of aromatic compounds have low volatility, allowing them to partition into the aerosol phase and to form secondary organic aerosols (SOA). This removal process of aromatic trace gases can significantly reduce the mixing ratios of the aromatic oxidation products. Since SOA formation is outside the scope of this work, additional channels in the chemical mechanism have been added to account for loss via SOA formation, using the yields from Ng et al. (2007). The modifications in the chemical mechanism are described in Appendix E. This approach avoids a possible overestimation of atmospheric concentrations of aromatic oxidation products.

5.2 Results discussion

Figure 5.1 shows the mixing ratios of the sum of all aromatic compounds included in the numerical simulation, on an annual average basis. The mixing ratios are higher in continental areas and close to surface. The highest mixing ratios are found in Asia, as well as in parts of Europe and the US, reaching ppb levels. The background mean mixing ratios in oceanic areas of the Southern Hemisphere are on the order of a few ppt.

In this section we compare the aforementioned scenarios. For clarity, we will always compare the *AROM* scenario to the baseline *REF* scenario.

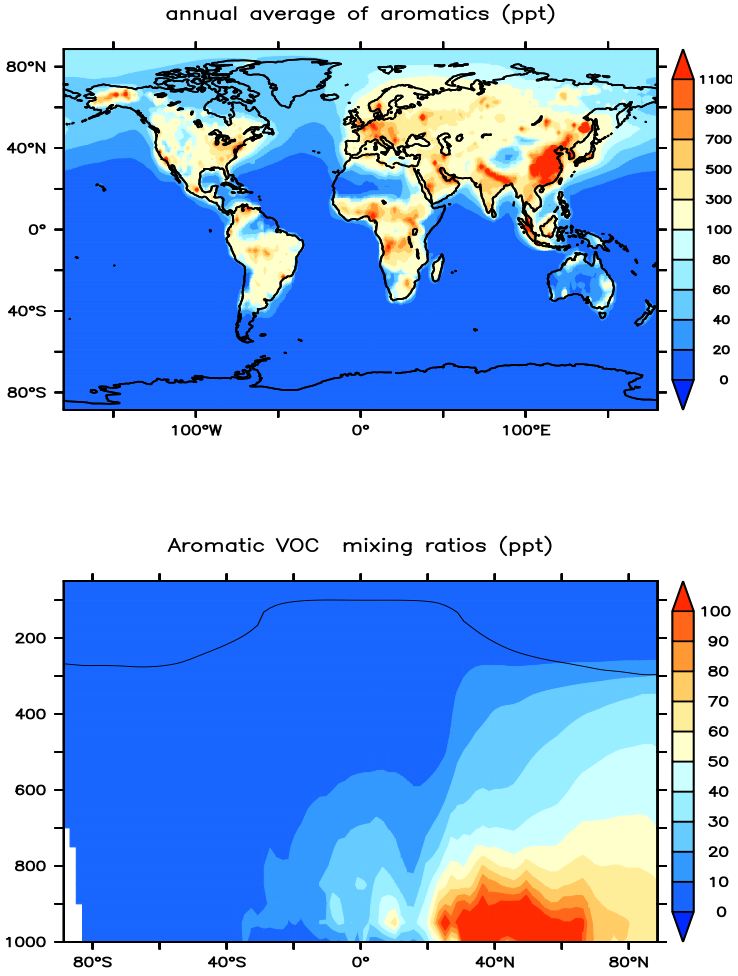

FIGURE 5.1: Top, Annual average surface mixing ratios of aromatics in ppt. Bottom, zonal annual mean.

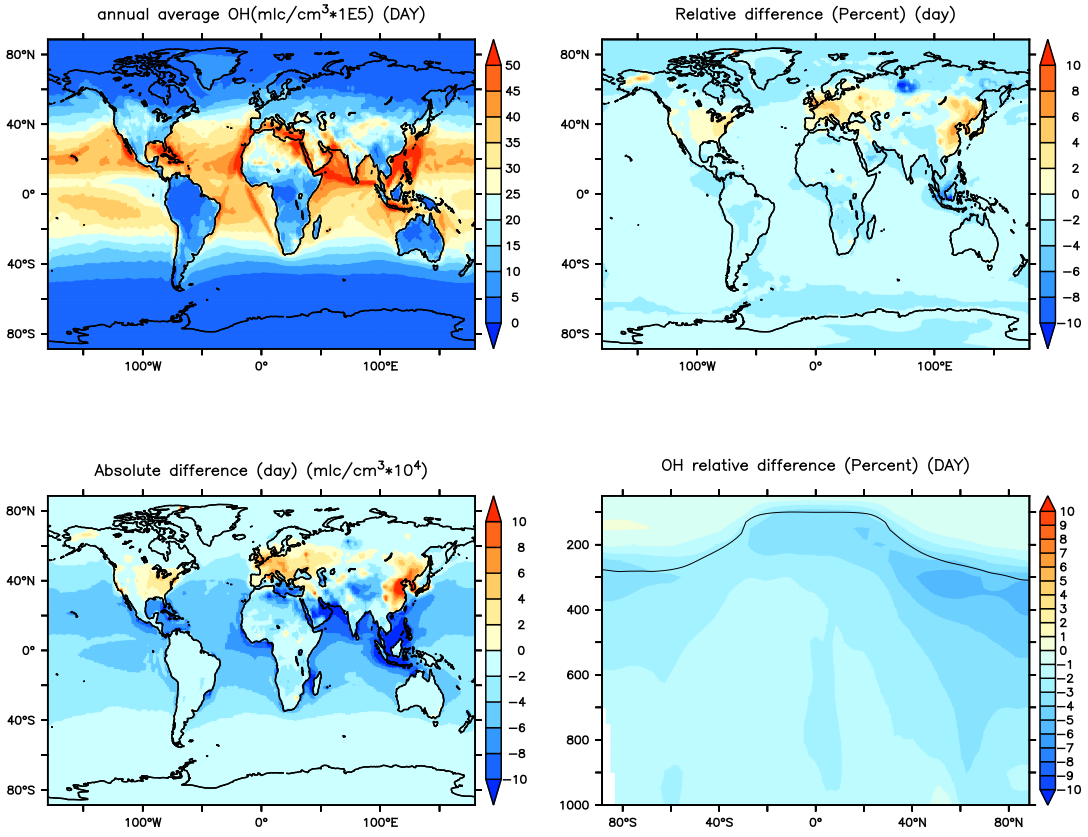

FIGURE 5.2: On the upper left panel, annual average surface concentrations of OH during day time (*REF* scenario). On the upper right, surface OH relative difference between aromatic and no-aromatic scenarios expressed in %. On the lower left, OH absolute difference between mentioned scenarios. On the lower right, zonal relative differences (in %).

5.2.1 Hydroxyl radical (OH)

Figure 5.2 (upper right) shows the relative difference (in %) in annually averaged daytime OH surface concentrations between the *REF* and *AROM* scenarios. Eastern Asia, Europe, and the eastern coast of the US show increased OH concentrations. The relative difference in OH is up to 8% higher in Eastern Asia, 6% higher in Europe, and 4% higher in the US. Comparing the OH concentrations (Figure 5.2, upper left) with the relative and absolute differences, we observe that regions with the maximum (relative and absolute) difference (Figure 5.2, upper right and bottom left) match the territories where OH is quickly removed from the atmosphere, as a result of the large anthropogenic VOC emissions. Everywhere else, we found a net depletion of OH. Indonesia and its surrounding areas, and continental areas on the equatorial belt both had the strongest OH depletion.

On the seasonal level, we found higher OH formation over continental areas during the winter and spring (especially in winter) than in summer and autumn (see Appendix F).

TABLE 5.2: Estimated global averaged OH concentrations in the boundary layer by three different approximations Lawrence et al. (2001) and global lifetime of methane. Estimations are calculated for the reference scenario and the aromatic scenario. Relative and absolute difference is between both scenarios.

In the planet boundary layer	Lifetime CH4 (years)	OH concentration (VOL) x $10^6 mlc/cm^3$	OH concentration (MASS) x$10^6 mlc/cm^3$	OH concentration (CH4) x $10^6 mlc/cm^3$
		No aromatics		
Global	4.45	1.30	1.27	1.46
Global day	2.46	2.33	2.29	2.58
Global night	236	0.03	0.02	0.03
		Aromatics		
Global	4.53	1.28	1.25	1.43
Global day	2.51	2.29	2.24	2.53
Global night	235	0.03	0.02	0.03
		Relative Difference (%)		
Global	1.91	-1.87	-1.86	-1.88
Global day	1.95	-1.89	-1.88	-1.90
Global night	0.21	0.51	0.56	.20
		Absolute Difference ($10^4 mlc/cm^3$)		
Global	0.08	-2.42	-2.37	-4.10
Global day	0.05	-4.40	-4.30	-7.25
Global night	-0.50	0.01	0.01	<0.01

During the northern hemisphere winter, the relative increase in OH exceeds 50% (e.g. China). In summer, Europe is the only region where OH concentrations in aromatics increase, although not exceeding 10%. However, it is not convenient to look at the relative error because at low OH concentrations, small variations between simulations lead to a large relative difference. We therefore looked at the absolute differences, finding increases of approximately 10×10^4 mlc/cm^3 in China and West Asia, and of less than 6×10^4 mlc/cm^3 in the US, Europe, and most continental territories of Asia. The increase of OH production via $NO + HO_2$ is likely the result of an increase in HO_2 due to aromatic oxidation. Although there is a decrease in NO_x, this does not seem to limit OH formation. In the southern hemisphere and in oceanic areas the net effect of introducing aromatic compounds into the system results in a net depletion of OH.

The changes in OH concentrations can be attributed to the NO_x regimes, in combination with increases in CO concentrations and changes in VOC mixing ratios as a consequence of aromatic oxidation. In areas with high NO_x and VOC mixing ratios, ozone is formed, which under photolysis produces OH (R7 in Chapter 1). In contrast, in regions with low NO_x concentrations OH recycling is limited by NO_x, forcing the aromatic oxidation products to react with HO_2 or peroxy radicals (RO_2) (Reactions R5 and R6 in Chapter 1). Hence, reactions R5 and R6 act as a net sink for OH. At the same time, CO is formed from the oxidation of aromatics (its main sink is reaction with OH), strengthening the removal of OH. Moreover, the oxidation chain of aromatics includes a large number of reactions involving OH. Therefore, positive changes in OH concentrations take place in continental areas with large NO_x emissions, unlike, for example oceanic areas, where NO_x is rapidly scavenged when HNO_3 is formed.

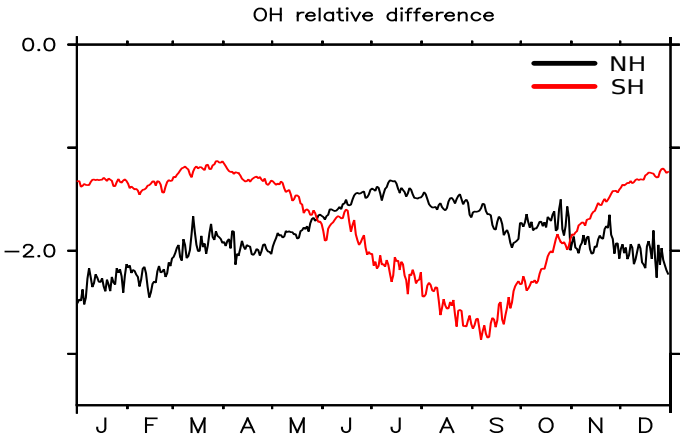

FIGURE 5.3: OH relative difference (expressed in a percent) in the boundary layer between *AROM* and *REF* scenarios. In black, values for the northern hemisphere. In red, values for the southern hemisphere.

At night, OH absolute differences showed a decrease of 1×10^3 mlc/cm^3 in India and Central Africa (approximately 8–10%). We also studied the maximum instantaneous OH relative differences during the day, observing increases of more than 100% in the northern hemisphere continental areas during the winter, spring, and fall seasons. The absolute differences reveal peaks of increase by more than 20×10^5 mlc/cm^3 in Eastern China and Central Africa.

Figure 5.3 shows the seasonal cycle of the relative difference between both scenarios for the northern and southern hemispheres. We found that the relative difference varies between -3.5% for winter months up to -1.5% in summer months. The cycle is reversed for the southern hemisphere, where the changes in OH concentrations are due to transported species (mostly CO), making changes relatively homogeneous. However, the relative difference increases in summer months due to strong biomass burning.

Table 5.2 shows OH concentrations for the *REF* and *AROM* scenarios, and the relative and absolute difference averaged globally at surface. We found an enhancement of 2–3% in the atmospheric lifetime of methane, along with a decrease in OH concentration. Methane is a long-lived species whose breakdown is driven by OH (Crutzen and Zimmermann, 1991); its lifetime can therefore be used to estimate OH concentration (Prather and Spivakovsky, 1990). The decrease in the OH concentration thus explains methane's increased lifetime. OH concentrations are also in line with values estimated by Lawrence et al. (2001), although estimated methane lifetimes are shorter, as these lifetimes were estimated only for the boundary layer. Tropospheric methane lifetimes were close to literature estimates: The *REF* scenario presents a methane lifetime of 9.74 years, and *AROM* a methane lifetime of 10.05 years. Literature estimates vary between 7.1 and 10.6 years

(Voulgarakis et al., 2013; Lawrence et al., 2001). The introduction of aromatics perturbs OH concentration, mostly during the day (∼ 2%, independent of the weighting method), while during the night only a small decrease in OH concentrations (<1%) is observed.

During the day in the northern hemisphere the annual zonal mean of the relative differences (fig 5.2, bottom right) globally decreased, with a (negative) gradient towards the free troposphere, reaching the maximum decrease at 200–300 hPa. During the night, similar patterns are observed in the free troposphere.

For HO_2 a relative increase of less than 1% in atmospheric mixing ratios was observed; at the regional scale, only Europe and East Asia had relative increases between 2% and 10%. The oxidation of carbon monoxide by OH is the main source of HO_2 (Lightfoot et al., 1992), serving as a buffer for OH. The updated benzaldehyde photolysis used in this study was also more efficient than the one previously used, making it a significant source of HO_2 radicals. The small impact of aromatics observed on the HO_x budget was expected, since this budget is well buffered against perturbations (Montzka et al., 2011; Lelieveld et al., 2016).

Contrary to expectations, we found large increases of HONO mixing ratios in continental areas, with the sign of this change opposite that of OH. These relative changes reached more than 100%. The reason for this pattern is explained by the photolysis of nitrophenols, which leads to HONO formation (Bejan et al., 2006; Cheng et al., 2009). In the *AROM* scenario, approximately 54% of the HONO formation is directly related to nitrophenol photolysis. Nevertheless, the net effect on the atmospheric burden is a daytime depletion of around 0.5% and a nighttime depletion of around 3%.

5.2.2 Ozone

Surface ozone mixing ratio differences between *AROM* and *REF* are shown in fig. 5.4 (upper right and bottom left). In general, surface ozone depletion occurs globally. Maximum depletion occurs in equatorial areas, of between 10°N–20°S (down to 4%, a drop of approximately 5 ppbv). In contrast, some regions of Europe and China present small increases (less than 5%); these areas match the regions with the largest NO_x annual mean mixing ratios. In Central African and Indonesian territories, where strong biomass burning takes place (i.e. large emissions of VOCs), significant decreases in ozone formation are observed.

No significant differences between daytime and nighttime surface ozone mixing ratios were found, due to the relatively long lifetime of ozone (22 days), which is several times longer than the lifetime of aromatics (Stevenson et al., 2006). On the other hand, large relative

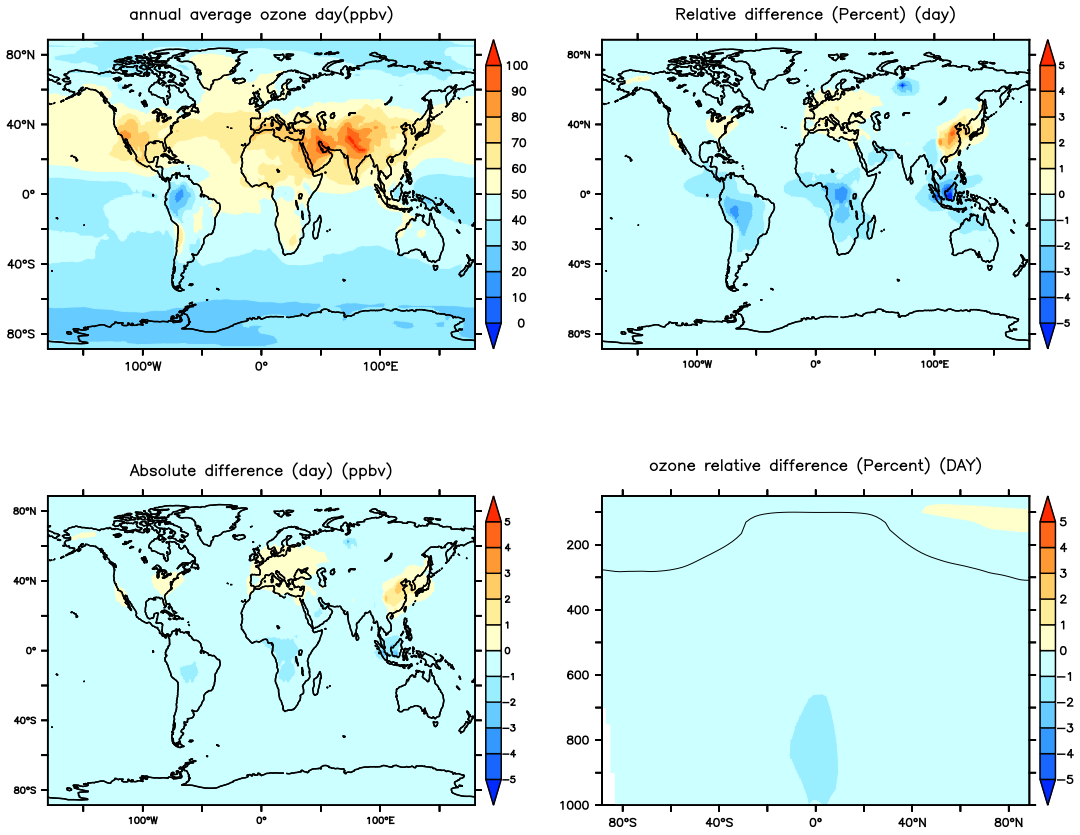

FIGURE 5.4: On the upper left panel, annual average surface concentrations of O_3 during day time (*REF* scenario). On the upper right, surface O_3 relative difference between aromatic and no-aromatic scenarios expressed in %. On the lower left, O_3 absolute difference between mentioned scenarios. On the lower right, zonal relative differences (in %).

TABLE 5.3: Estimated global averaged ozone mixing ratios in the boundary layer (mass weighted) Lawrence et al. (2001). Relative and absolute difference is between both scenarios.

	O_3 mixing ratio ppb
	No aromatics
Global	1.11
Global day	1.05
Global night	1.18
	Aromatics
Global	1.10
Global day	1.05
Global night	1.17
	Relative Difference (%)
Global	-0.72
Global day	-0.57
Global night	-1.76
	Absolute Difference (ppb)
Global	-0.69
Global day	-0.63
Global night	-0.78

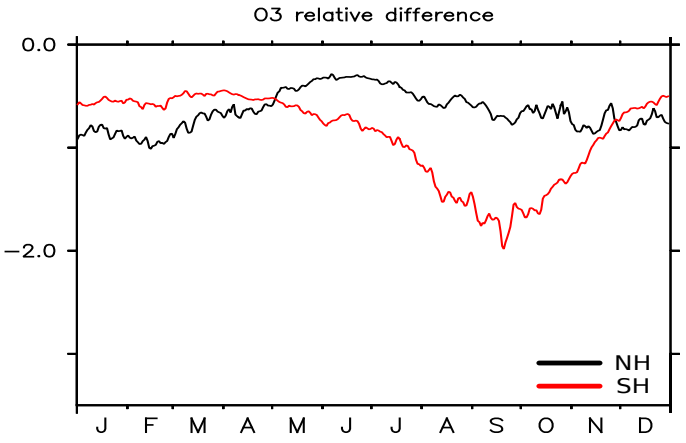

FIGURE 5.5: Same as in fig. 5.3 for ozone.

differences at surface are revealed at the seasonal level. During the winter months, a relative growth of more than 10% is observed in China, and of 1–4% in Europe and the US. China had increased ozone mixing ratios for almost the entire year (excluding the summer months), and ozone depletion in central Africa remained relatively constant year-round. During the summer and fall seasons, the strongest depletion is observed in the southern hemisphere (approximately 7%).

Maximum relative changes of ozone increased more than 10% over the northern hemisphere. In the US, Europe, and China ozone mixing ratios rose by more than 20%. Large peaks were also observed in Central Africa, due to strong biomass-burning events.

Relative changes in tropospheric ozone were found to be homogeneous within the northern hemisphere (fig. 5.4, bottom right). There did not appear to be any differences between day and night, with decreases below 2% in the boundary layer and lower part of the free troposphere (up to 7 km). Above 7km height, the relative differences decrease.

Table 5.3 presents annual global mean ozone mixing ratios in the boundary layer for both scenarios—weighted by two different methods, but only mass weighted is shown, as both methods present the same values—as well as the relative and absolute differences. Both methods show good agreement in the mixing ratios. Relative differences are approximately 1%. During nighttime, relative differences increase by 1.8%. Compared to OH, relative differences are lower for ozone, suggesting that ozone recycling is less affected by aromatics than OH.

The seasonal distribution of the relative differences (fig. 5.10) shows lower amplitude than for OH, but similar patterns. In the northern hemisphere, greater relative differences occurred between scenarios in the winter months than in the summer months; in the

southern hemisphere this pattern was reversed. The relative differences range within 1%–2%. In the southern hemisphere a maximum difference of 2% was found over biomass burning activity regions. Ozone depletion is due to (i) aromatic decomposition, which involves a number of reactions that efficiently consume ozone, and to (ii) increasing radical production (OH, HO_2, and RO_2) in ozone-depleting regimes, which speeds up the reactions of O_3 with HO_2 and OH. Growth in ozone mixing ratios is observed in regions of high NO_x mixing ratios, where the limiting factor for ozone formation is hydrocarbon mixing ratios.

5.2.3 NO_x

The simulated NO_x mixing ratios were slightly lower in the *AROM* scenario than in the *REF* scenario. One reason why NO_x decreased was the addition of chemical species containing nitrogen (e.g. nitrophenols) in the *AROM* scenario, thereby transferring part of the NO_x burden to the nitrogenated species. Thus, aromatic nitrogenated species become channels for the deposition of nitrogen.

The comparison between the *AROM* and the *REF* model results showed significant NO_x depletion in central Africa, the Amazon forest, China, and Indonesia, with relative differences reaching approximately 10% (fig. 5.6). In Europe, the US, and the Arabian Peninsula, reductions in NO_x mixing ratios did not exceed 5%. Oceanic areas showed small decrease, although NO_x mixing ratios were several orders of magnitude lower than over continental territories, with absolute changes not exceeding 1 ppt levels. We observed large relative and absolute differences in the northern hemisphere during the winter season, consistent with changes observed for ozone and the hydroxyl radical. At the global scale, NO_x mixing ratios decreased by 5% in the *AROM* scenario.

5.2.4 NO_3

NO_3 mixing ratios had a global increase of 1.2% during the nighttime and 4.5% during the daytime. At the regional scale, the largest daytime changes occurred in northern Africa, the Arabian Peninsula, and northern Asia, with increases of 20–30%. An increase of more than 30% was also observed over the Tibetan plateau, although mixing ratios in this area are generally low. Decreases of up to 10% were observed in central Africa and in the Amazonian areas. During nighttime, the contrast between the scenarios became larger, with a 30% decrease in mixing ratios in central Africa and the Amazonian areas, an increase of more than 30% in the Tibetan plateau and northern Asia, and no change in northern Africa with respect to daytime.

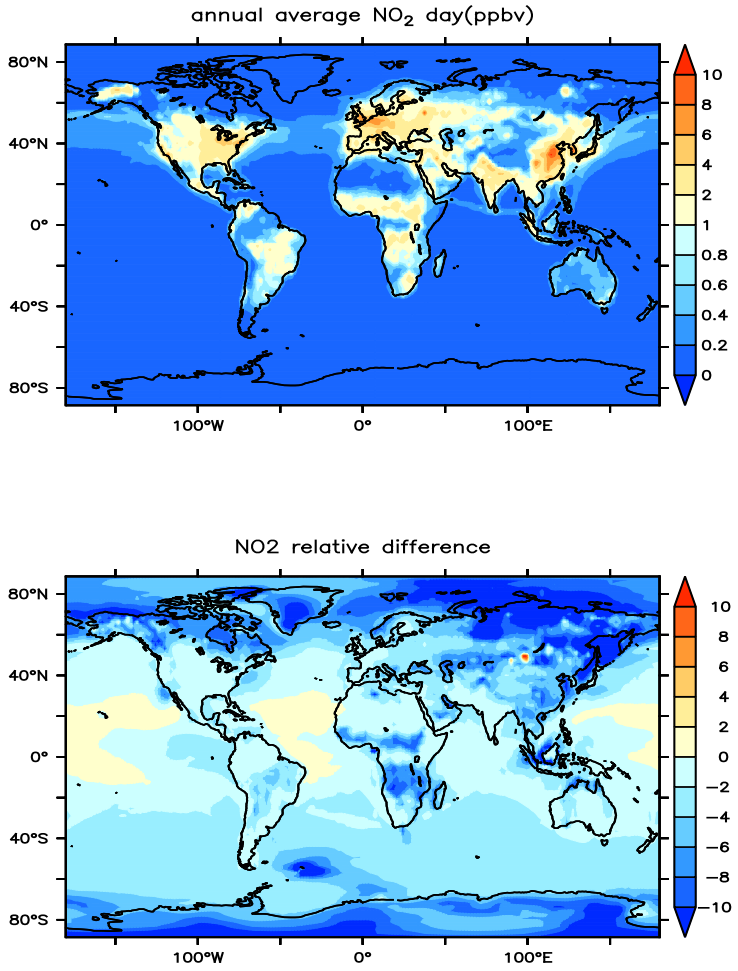

FIGURE 5.6: Same as in fig. 5.3 for NO_2.

For HNO_3, mixing ratios decreased by 1% in the *AROM* scenario.

5.2.5 VOC

5.2.5.1 Formaldehyde

The main photochemical source of formaldehyde in the background troposphere is methane oxidation; in continental areas, VOC (including aromatic compounds) oxidation is the main source, and its main sink is reactions with OH. Comparing our two scenarios, we found a depletion in the formaldehyde mixing ratios (on an annual basis) in the Amazonian and central African regions—two areas that typically have higher formaldehyde mixing ratios (Figure 5.8). This decrease reaches 10% in South America and 5% in Africa. In contrast, we observed increases of up to 6% in these mixing ratios in China and Europe. On the global level there was a decrease in the atmospheric burden of formaldehyde of

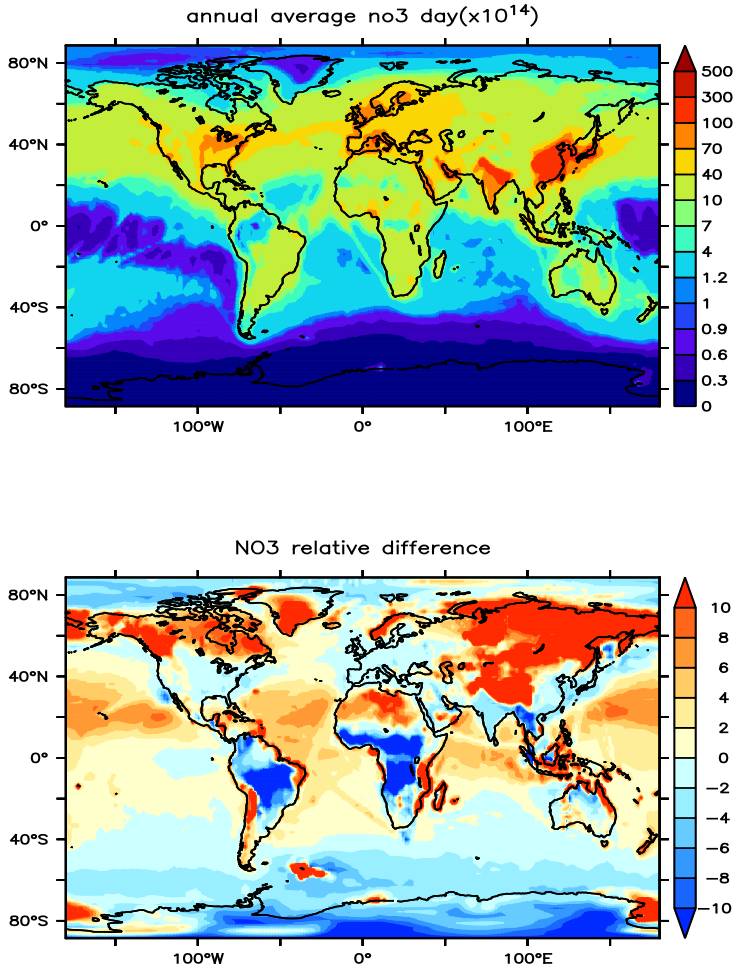

FIGURE 5.7: Same as in fig. 5.3 for NO_3.

1.6%. These changes in the formaldehyde distribution can be explained by changes in the OH mixing ratios, as well as the formaldehyde production from the aromatic oxidation. For instance, large urban areas have high levels of aromatics, which leads to increases in formaldehyde formation. In regions where aromatics deplete OH, methane and other VOCs then form less formaldehyde.

5.2.5.2 Glyoxal

With respect to glyoxal, we found a global increase of 20% on the simulated mixing ratios at surface. At the regional scale, China had the strongest absolute difference, with an increase of approximately 70 ppt (80%); this was followed by India and the Arabian Peninsula, where increases rose by more than 40 ppt. In Figure 5.9 (bottom), increases larger than 20% can be observed in oceanic areas; however, this high relative change is

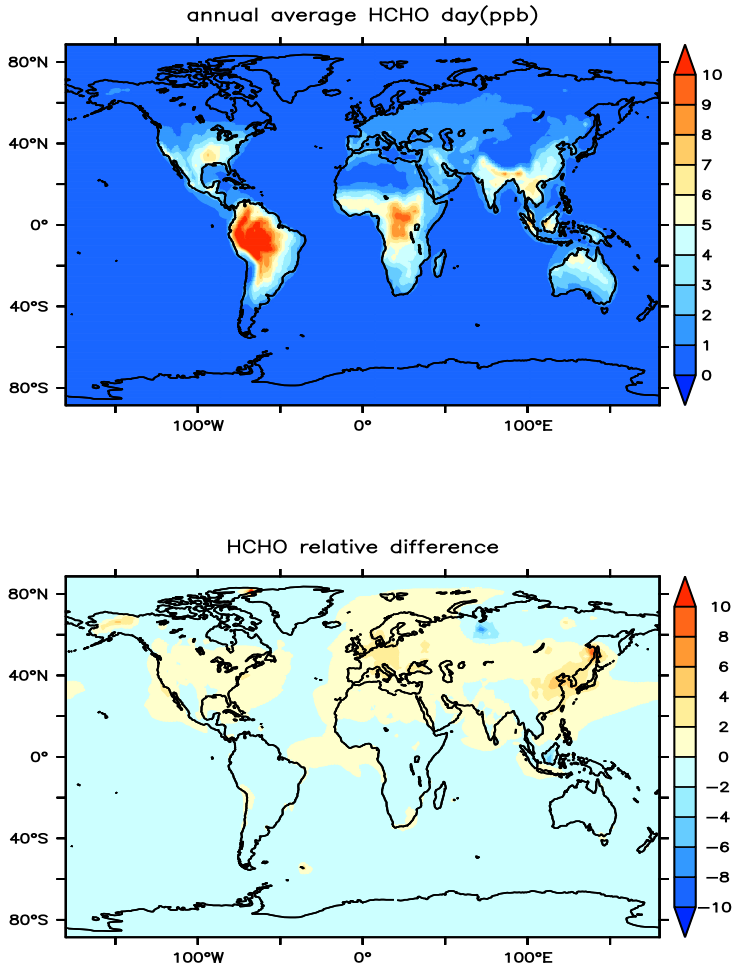

FIGURE 5.8: Same as in fig. 5.3 for HCHO.

caused by very low mixing ratios (less than 1 ppt). In continental areas over the northern hemisphere, increases of more than 10% were found. Relative increases were lower in the southern hemisphere than in the northern hemisphere, because the main source of glyoxal in the southern hemisphere is isoprene (Fu et al., 2008). Only in some regions of Africa and the Amazon forest was a decrease (less than 2%) observed; this was caused by a depletion of OH, and by isoprene being almost the only source of glyoxal. The atmospheric burden of glyoxal had a net increase of approximately 10%. Nevertheless, the burden (62 Gg in the *REF* scenario) seems to be much larger than in Fu et al. (2008); Myriokefalitakis et al. (2008) (15–20 Gg). This discrepancy is attributed to the missing channel leading to SOA formation, an important sink of glyoxal.

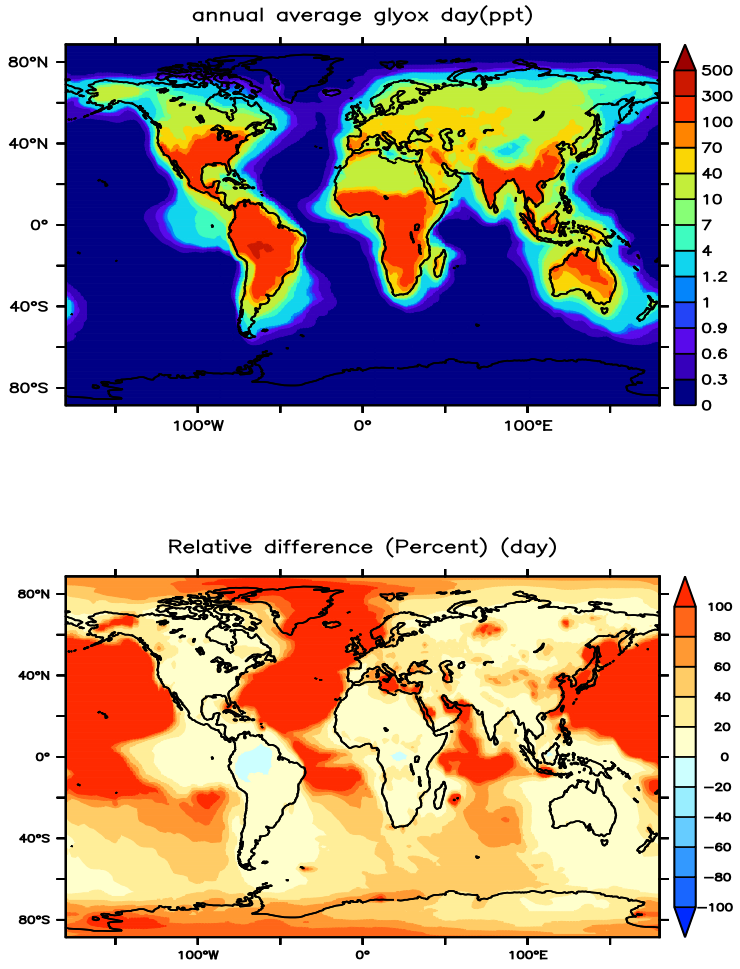

FIGURE 5.9: Top. Annual average surface mixing ratios of glyoxal in ppt. Bottom, relative difference in %

5.2.5.3 Carbon monoxide

The reaction chain in the oxidative process of aromatics produces carbon monoxide (CO), a relatively long-lived molecule (1–2 months). CO can travel long distances from its source, although this lifetime is not long enough to allow it to cross hemispheres (Daniel and Solomon, 1998). CO mixing ratios generally increased on the global scale, indicating a small growth in the carbon budget. When comparing both scenarios, we observed an increase of 7% in the atmospheric burden of CO, which corresponds to an increase of 30 Tg. The CO burden estimated by the model in the *REF* scenario is 535 Tg.

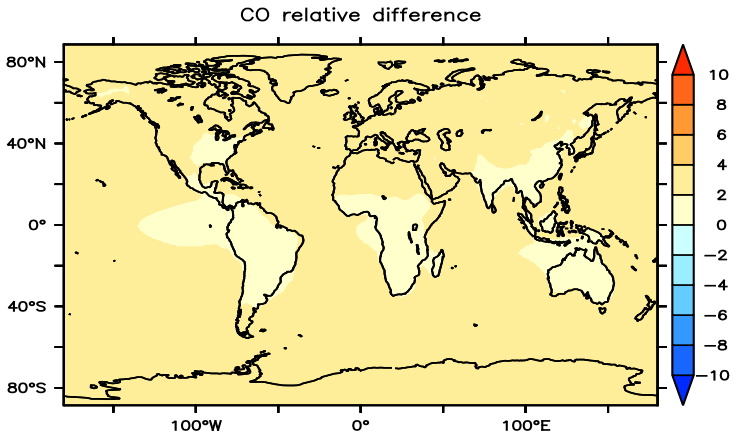

FIGURE 5.10: Same as in fig. 5.3 for CO.

5.3 Sources of uncertainty

There were a number of sources of uncertainty in this estimation of the impact of aromatics on tropospheric chemistry. Firstly, emissions of aromatics have high uncertainties. One reason for this is that few databases provide anthropogenic speciation of aromatic VOCs. In the case of the RCP database (van Vuuren et al., 2008), speciation entails fractioning the total VOC flux into different species (a top-down approach) (Moss et al., 2008). In the case of biomass burning emissions, information regarding the emission factors for each vegetation type is not always available for all species. With regard to biogenic emissions in the present study, only toluene was included, despite the fact that this source is of minor relevance as compared to other sources. The emissions fluxes calculated by the MEGAN model are strongly dependent on input data: e.g., on temperature or incoming radiation (Guenther et al., 2012) (see Chapter 3).

Atmospheric changes produced by aromatics are strongly dependent on NO_x mixing ratios. The model's tendency to underestimate NO_x mixing ratios (Jöckel et al., 2006) has previously been acknowledged as a possible source for underestimating ozone formation. Finally, it must be stressed that the EMAC model overestimates ozone mixing ratios (Jöckel et al., 2006). The scenario that includes aromatic compounds slightly improves ozone mixing ratios with respect to observations, although it clearly shows that the main overestimation has different causes.

Another source of error was due to the chemical oxidation mechanism (based on MCMv3.1), which overestimates peak ozone mixing ratios and underestimates OH formation and NO

oxidation rates Bloss et al. (2005b). In the case of OH, our version of the chemical mechanism includes new formation channels from nitrophenol photolysis; underestimation of daytime OH formation is therefore lower than in the original MCM.

In the mechanism used in this work, the oxidation of benzene and toluene was explicitly taken from MCM. For the rest of the aromatics that were included, the second oxidation products are directly linked to those of toluene. This approximation implies a less accurate representation of the oxidation of those species. However, comparison of simulation results with observations show relatively good agreement for benzene and toluene (Cabrera-Perez et al., 2016), although the model has difficulty reproducing xylene mixing ratios (see Chapter 4).

The largest uncertainty was generated by the treatment of SOA formation. Although a theoretical limit of 30 Tg/yr of SOA from aromatics can be formed (Henze et al., 2008), there are large uncertainties in the yields, and in whether they can be used to simulate real atmospheric conditions. We consider it to be a plausible assumption that we can create channels to account for SOA formation right after the first oxidation step, although this assumption implies that all secondary reactions are equally affected. However, it is hard to estimate whether this methodological choice leads to an underestimation or overestimation of the effects of aromatic compounds on atmospheric species.

5.4 Summary

This thesis investigated the effect of aromatic compounds on the chemistry of the troposphere at the global scale, with the help of the global circulation atmospheric chemistry model EMAC. A baseline case scenario and a sensitivity run were compared, with the first excluding aromatic compound emissions and second including them. To accurately describe the oxidation chain of the species involved (all of which were simple mono-cycle aromatic compounds) we used a detailed chemical mechanism based on MCM.

At the global scale, OH concentrations decrease by 2–3% once aromatics were included. On the regional scale, areas with high levels of aromatics had decreases of more than 10%, while regions with large NO_x mixing ratios showed increases of up to 10%. Similar results are found for ozone, with a global net decrease of 1%. However, the relative importance of aromatics at the regional scale can cause increases or decreases of more than 10% during the winter season. This decrease in OH mixing ratios can then alter VOC mixing distribution. For example, large changes are observed for glyoxal, with an observed increase of 20% in the mixing ratios. In the case of formaldehyde, a net decrease of 1.2% in the atmospheric burden was found.

When aromatic compounds are included, increases in carbon-containing compound emissions lead to growth in the carbon monoxide burden. This increase explains the net decrease in OH concentrations over remote regions. NO_x is also depleted due to absorption of nitrogen by aromatics, with this nitrogen later being deposited. The depletion of NO_x in combination with the increase in CO leads to OH depletion.

We conclude that, although aromatic compound chemistry at the global scale has relatively low relevance, its omission could lead to an overestimation of ozone and OH concentrations. However, at a regional scale, the impacts of aromatics in the troposphere can be important, as they can be responsible for relatively large OH, ozone, and, especially, glyoxal formation. We therefore recommend including detailed chemistry in regional simulations; at the global scale, a simpler mechanism would be sufficient.

To better constrain OH and ozone mixing ratios in global models, further improvements to the representation of the chemistry and emissions of VOCs are necessary.

Chapter 6

Trends

This chapter presents trends in aromatic compound mixing ratios for 1950–2050. The aim is to better understand the evolution of aromatic mixing ratios starting from 1950—the beginning of a period of rapid industrial growth—and ending in 2050, which allows us to envision possible future scenarios. We also focus on the influence of emissions on mixing ratios and on the evolution of different emission sources.

6.1 Methods

For this study, we used the EMAC model with a T42L31ECMWF resolution, which represents a Gaussian grid of approximately 300km × 300km at the equator and 31 vertical levels up to the top of the troposphere (i.e. 10hPa). Although the period covered was from 1950 to 2050, simulating this entire time period was too expensive. Instead, we led a series of six time-slice experiments every 20 years, starting in 1950 and ending in 2050 (i.e. we simulated 1950, 1970, 1990, 2010, 2030, and 2050). All simulations ran for two years (e.g. 1950–1951), with the first year used as the spin up and the second year for the analysis.

Biomass burning and anthropogenic emissions were taken from the RCP8.5 database. The RCP provides a basis for both long- and short-term modelling experiments. The dataset was constructed based on the idea that climate research is based on socio-economic and emission scenarios, and its aim is to provide a plausible characterization of how future socio-economic and technological changes, energy and land use, and emissions of greenhouse gases and air pollutants may affect the climate. Atmospheric emissions were also harmonized across models and scenarios to ensure consistency with historical observations. This dataset has high spatial (0.5×0.5 degree) resolution. Emissions are classified

by sector: air transportation, international shipping, other transportation (i.e. surface transport), energy (i.e. electric power plants; energy conversion, extraction, and distribution), solvents, waste (i.e. landfill, waste water, non-energy incineration), industry (i.e. combustion and process emissions), domestic (i.e. residential and commercial buildings), agricultural waste burning on fields, agriculture (i.e. agricultural soil emissions, other agricultural processes), savannah burning, and forest burning (van Vuuren et al., 2011).

Unlike in previous chapters, the GFAS inventory was not employed, because it does not cover the time frame of 1950–2050; instead, we used the biomass burning emissions from the RCP8.5 dataset. Biogenic emissions were calculated using the MEGAN model (Guenther et al., 2012).

Simulations were not nudged due to a lack of nudging data. We therefore relied on the model capability to correctly reproduce the climatology fields. Furthermore, as our aim was to study aromatics on the global scale, we did not need to know the meteorological conditions of any specific location. We applied the QCTM mode to avoid feedbacks between physical and chemical processes.

We employed the previously evaluated chemical mechanism developed in this thesis for aromatic compounds (detailed information in Chapters 2 and 4).

6.2 Results

6.2.1 Trends on concentrations and emissions

Trends in surface annual mean mixing ratios and emissions, the percent increase or decrease of emissions relative to the year 1951, and the ratio between biomass burning and anthropogenic emissions for the aromatic compounds studied in this thesis are shown in Figure 6.1. The mixing ratios of all species had similar patterns, with increases from 1951 to 1991, followed by a stable-state regime from 1990 to 2010, and ending in 2050 with a drop in mixing ratios. When mixing ratios were divided into hemispheres, two different trends were found: In the southern hemisphere we observed a slight increase in mixing ratios during the entire period, as a consequence of relatively constant biomass burning emissions, in addition to increasing anthropogenic emissions. The northern hemisphere exhibited the same patterns as were observed globally, as a result of the higher emissions in the northern hemisphere as compared to the southern hemisphere. Figure 6.1 (third row) demonstrates that, in both hemispheres, anthropogenic emissions were greater than biomass burning sources, with the exception of phenol. Mixing ratios closely followed the patterns of the emissions, as sinks were generally constant in all simulations. Emission

FIGURE 6.1: First row: Emissions (anthropogenic and biomass burning) of aromatic compounds (global, northern and southern hemisphere). Second row: The percent of increase/decrease of the emissions with respect 1951 (global, northern and southern hemisphere). Third row: ratio between biomass burning and anthropogenic emissions (global, northern and southern hemisphere). Fourth row: average mixing ratio (global, northern and southern hemisphere).

fluxes for most species doubled from 1951 to 1971, with trimethyl benzenes reaching a remarkable 400% growth. Benzene and phenol increased rapidly until 1991, whereupon they stabilized. Toluene and xylene emissions rose during the entire period. Increases in the emissions corresponded to changes in anthropogenic emissions, while biomass burning remained approximately constant; this explains the decrease in the ratio between biomass burning and anthropogenic sources.

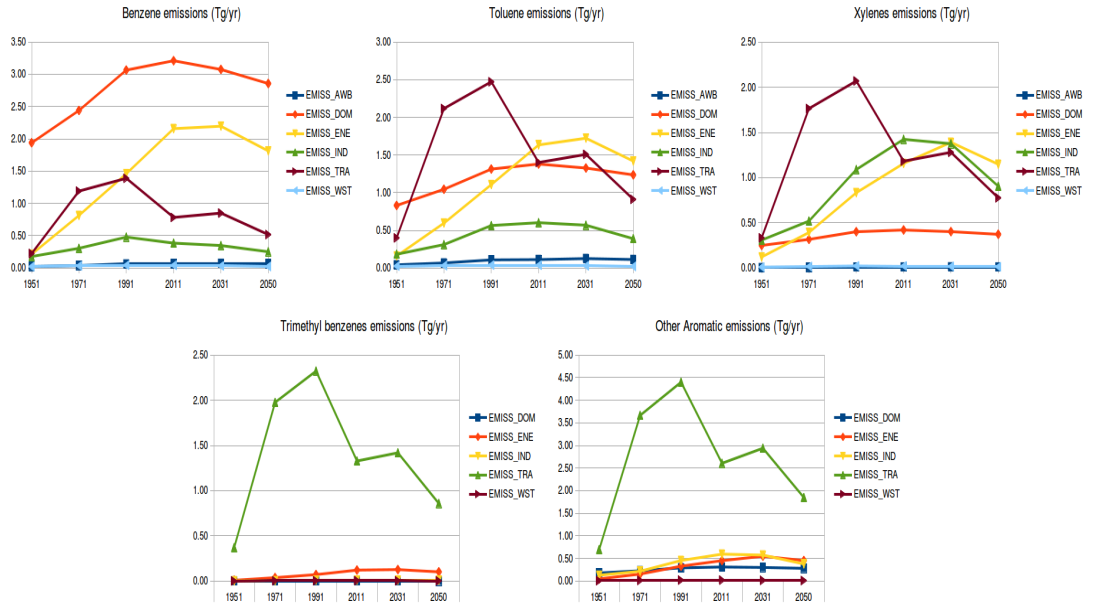

FIGURE 6.2: Emissions trends split by sectors.

In Figure 6.2, emission fluxes are presented by sector. In the case of benzene, the domestic sector dominates emissions, producing more than 50% of total emissions between 1951 and 1991, followed by a stable period (1991–2031), and a decrease until 2050. Relative to 1951, energy sector emissions increased until 2010, plateaued in 2030, and then declined slightly until 2050. Transport emissions exceeded energy emissions for the first 20 years (i.e. 1951–1971), with both sources being approximately equal in strength in 1991. Transport emissions then decreased, with energy emissions being almost two times stronger than transport emissions from 2011 onwards. The remaining sectors played only minor roles. Toluene emissions were dominated by transport emissions, with an almost three-fold increase in their flux by 1991, as compared to 1951; these emissions then fell rapidly in 2011 and 2050. The domestic and energy sectors reproduced the patterns already described for benzene, with the period of 2011–2050 being similarly important as for the transport sector. Xylene emission trends resembled those of toluene, with a major difference being that industrial emissions (instead of domestic sources) had a dominant role. Trimethyl benzenes and other aromatics (which are representative of benzaldehyde, styrene, ethylbenzene, phenol, and higher aromatics), were only governed by transport emissions, with other sectors making only minor contributions to the emissions.

Figure 6.3 presents the annual average mixing ratios of benzene (in ppt) for six different time periods. In 1951, the highest mixing ratios were located in Central Africa, where biomass burning was the main source of benzene. Europe, India, East China, and the US eastern seaboard also presented high mixing ratios. For 1971 to 1991, the areas reaching more than 200 ppt increased, with almost all continental areas increasing approximately 200% by 1991. Contrary to expectations, the emission scenario forecast for the US showed

TABLE 6.1: Surface annual mean mixing ratios at different regions.

	BEN	TOL	XYL	TMB	PHEN	EBEN	BENZAL	STY	HAROM
					Global				
1951	43.9	18.5	6.7	1.2	0.8	1.3	1.2	0.2	2.7
1971	77.8	42.8	18.2	6.7	1.4	5.0	4.5	0.7	4.6
1991	102.1	59.1	27.7	9.1	1.6	6.8	6.8	0.9	6.0
2011	105.6	66.7	34.9	6.5	1.5	5.7	5.9	0.8	5.1
2031	105.1	85.3	49.0	8.4	1.7	7.7	8.3	1.1	6.2
2050	90.5	84.0	47.0	5.2	1.4	5.9	6.8	0.7	5.3
					South-east Asia				
1951	88.2	30.0	8.6	0.8	1.3	1.5	1.5	0.3	3.1
1971	137.8	53.1	18.5	4.4	2.6	4.5	4.4	0.9	5.8
1991	197.8	89.2	38.9	10.0	3.6	9.3	9.8	1.4	10.2
2011	211.8	132.4	74.0	13.4	4.0	12.3	13.1	2.0	12.6
2031	230.5	190.8	116.8	20.5	4.9	19.4	20.9	3.2	16.6
2050	202.6	182.7	106.8	11.3	3.9	14.1	16.6	1.7	13.4
					Europe				
1951	128.5	104.0	68.0	9.4	1.0	8.0	7.3	1.4	5.7
1971	235.4	277.0	190.9	56.7	5.5	36.0	32.2	8.1	25.0
1991	206.1	316.5	240.5	58.6	7.7	37.4	33.3	10.4	27.2
2011	92.1	204.9	160.1	14.2	2.1	14.3	14.7	2.9	9.9
2031	60.5	144.9	118.9	8.0	1.0	9.9	9.6	1.5	6.5
2050	56.5	131.0	106.9	6.7	0.9	8.7	6.9	1.2	5.6
					S.America				
1951	11.6	11.7	2.9	1.4	1.9	0.8	0.7	0.5	2.0
1971	23.0	22.2	8.5	4.8	4.9	2.8	2.4	1.5	5.4
1991	24.8	25.1	10.7	5.2	4.8	3.1	2.8	1.3	6.0
2011	24.3	25.4	10.7	4.0	4.3	2.5	2.3	1.1	5.0
2031	25.3	29.7	13.5	3.4	4.0	2.3	2.1	1.0	4.8
2050	21.1	36.2	18.7	2.9	3.9	2.3	2.0	1.0	4.6
					Africa				
1951	54.0	23.8	6.0	0.9	4.7	1.6	3.6	0.4	23.1
1971	81.6	36.2	10.1	1.8	10.2	2.8	6.3	0.8	39.2
1991	105.7	44.7	12.7	2.6	11.9	3.5	7.6	0.9	43.4
2011	121.1	47.2	13.3	2.4	8.4	3.3	6.5	0.7	36.1
2031	122.5	51.8	16.1	2.4	8.0	3.4	6.6	0.7	35.7
2050	124.8	67.6	26.3	2.4	7.8	3.9	7.2	0.7	35.4
					US				
1951	72.0	66.2	41.3	14.4	1.4	8.1	7.3	1.8	5.9
1971	178.7	238.4	152.4	84.6	6.3	41.8	40.1	9.2	27.2
1991	166.6	239.5	157.1	71.4	5.5	36.4	36.2	7.4	24.0
2011	50.6	110.9	81.2	8.1	1.1	7.3	5.9	1.5	4.8
2031	27.5	74.5	54.3	4.0	0.6	4.2	3.9	0.8	2.8
2050	18.6	55.1	39.7	2.8	0.5	3.0	2.8	0.6	2.1

a large decrease in mixing ratios (down to 30 ppt), approaching 1951 values. In contrast, ratios in Africa did not decrease during the entire period (1950–2050), and from 2011 to 2050, there was practically no change (see Table 6.1). Benzene mixing ratios in Europe decreased quickly by 2011 (100 ppt less than in 1971), but these decreases were smaller than those in the US. Mixing ratios in Southeast Asia continuously increased, except by 2050.

Toluene mean mixing ratios are shown in Figure 6.4. In 1951, high mixing ratios were present in Europe, China, the eastern US, and Central Africa; everywhere else mixing

ratios were below 10 ppt. In 1971, mixing ratios rapidly increased, exceeding 200 ppt. These increases were exceptionally remarkable in Europe, the US, and India. In contrast, mixing ratios in the southern hemisphere remained practically unaltered. From 1991 to 2050, toluene mixing ratios continued rising steadily in the northern hemisphere, with the US being the only area that presented a decrease (this occurred after 2010). In Africa, mixing ratios also increased steadily.

Xylene mixing ratios increased rapidly in the US, the Arabian Peninsula, India, and Southeast Asia for 1951–1991 (see Figure 6.5), then mixing ratios dropped in the US and Europe from 1991 to 2050. The southern hemisphere had relatively stable mixing ratios during the full 100-year period, with only local areas of Africa and eastern South America presenting increases in the mixing ratios. Figure 6.6 shows the mixing ratios of benzaldehyde. We distinguished two regions in terms of mixing-ratio temporal evolution: The first region comprised eastern and Southeast Asia and the Arabian Peninsula, where mixing ratios increased from 1951 to 2050. The second region comprised the US and Europe, where mixing ratios increased starting in 1951, reaching their maximum in 1991, and then decreased almost to values modelled for 1951. Southern hemisphere mixing ratios did not show a clear trend, as they were dominated by biomass burning.

Finally, as phenol mixing ratios were dominated by biomass burning, no large changes were observed that did not correspond with variability in biomass burning. Significant increases were found only in a few specific regions (e.g. Southeast Asia), where there was an increase in anthropogenic emissions and where benzene mixing ratios were high. This occurred because benzene is the main source of phenol, upon chemical oxidation.

6.3 Sources of uncertainty/ Discussion

These simulation results should be interpreted as possible developments in mixing ratios, but not as a forecast. RCPs generally assume an increasingly strict air pollution control policy, which implies that the RCPs would not be valid for analysis of possible trends in air pollution under less optimistic assumptions (van Vuuren et al., 2011). In addition to the influence of the scenario chosen, a further concern is the lack of annual seasonality of the inventory.

As an RCP emission inventory gathers information for 1950–2000 from different databases (Lamarque et al., 2010), it acquires any problems associated with each database. For instance, the RETRO inventory reported issues such as shifts in the geographical distribution of international ship traffic and aircraft and a lack of emissions reported from cement manufacturing (van het Bolscher et al.); these issues are now present in the RCP.

Performing a single simulation covering the full period would allow for a more detailed analysis of the trends and would remove this source of possible error.

6.4 Summary

In this study we used an AC-GCM model to simulate the mixing ratio trends of aromatic compounds from a global to a regional scale. The outcome is therefore classified into two parts: global and regional scale. At the global scale:

- By 2050 mixing ratios for most aromatics have doubled relative to 1951.
- Benzene mixing ratios are expected to decrease by 2050 but toluene and xylenes will keep rising. Benzaldehyde, phenol, and trimethyl benzene mixing ratios will drop to 1951-level concentrations.

At the regional scale we found three different trends:

- The US and Europe exhibit the following trends: mixing ratios rise from 1951 until 1991, then decrease until 2050.
- Mixing ratios continuously increase from 1951 to 2050 in areas like Southeast Asia and the Arabian Peninsula.
- In the southern hemisphere, a relatively small increase in mixing ratios occurs from 1951 to 1991, and then ratios stabilize.

With regard to air pollution, India and China are the countries exposed to the highest mixing ratios of aromatics. It would be beneficial for those countries to stablish air pollution control strategies to prevent the scenarios presented in the simulations.

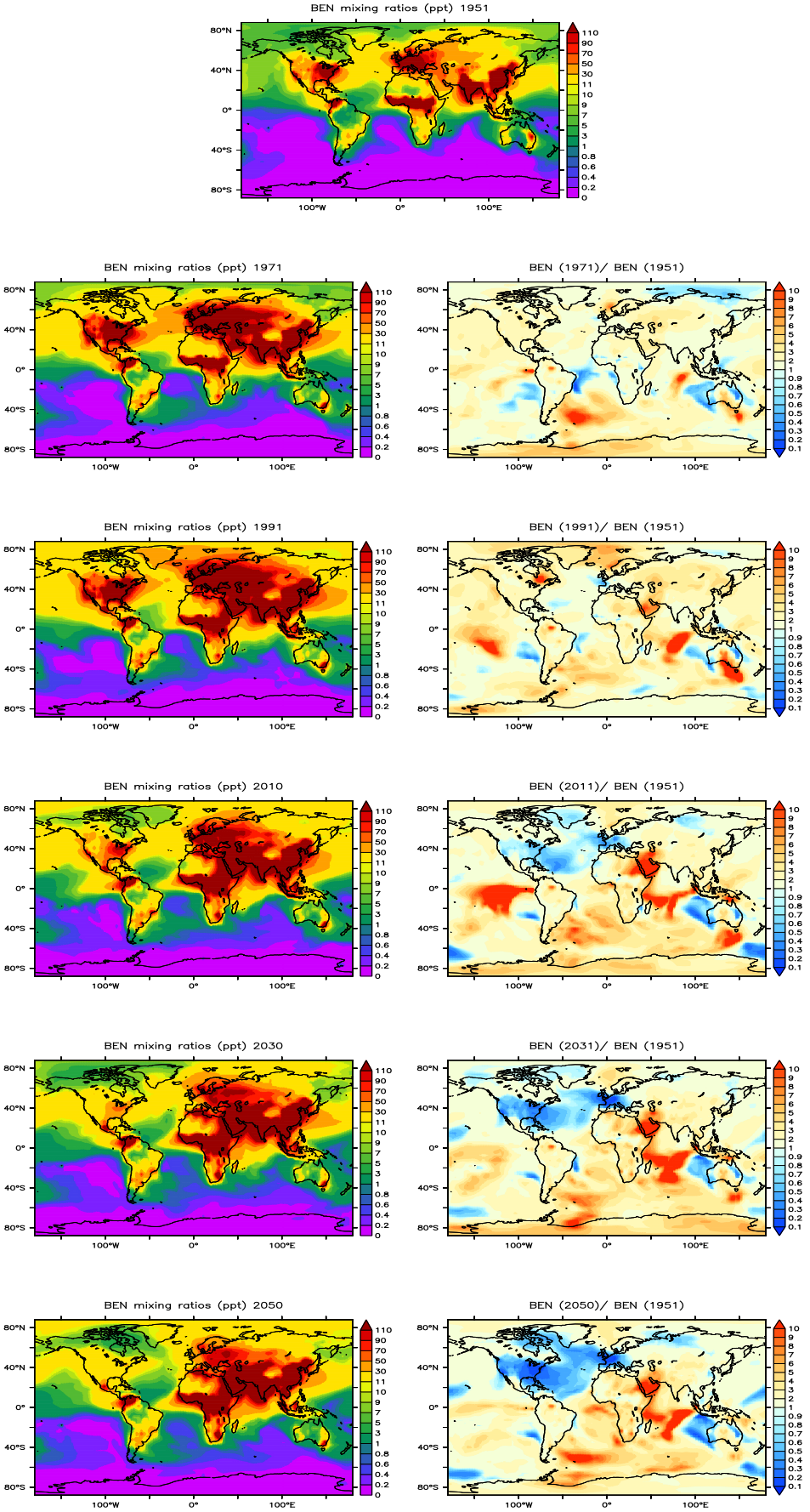

FIGURE 6.3: Benzene mixing ratios ppt on an annual basis in different years of the period 1950-2050

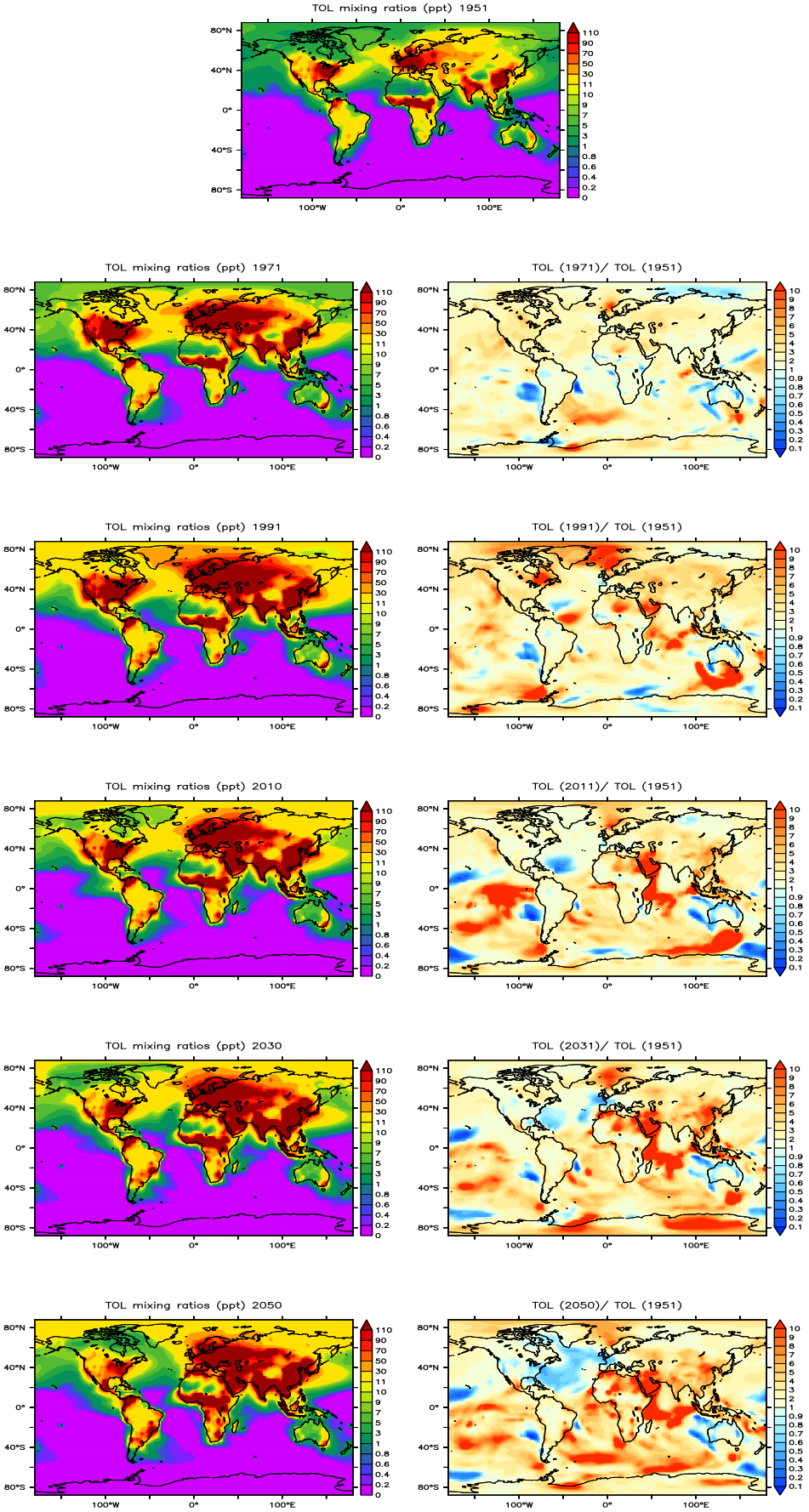

FIGURE 6.4: Toluene mixing ratios ppt on an annual basis in different years of the period 1950-2050.

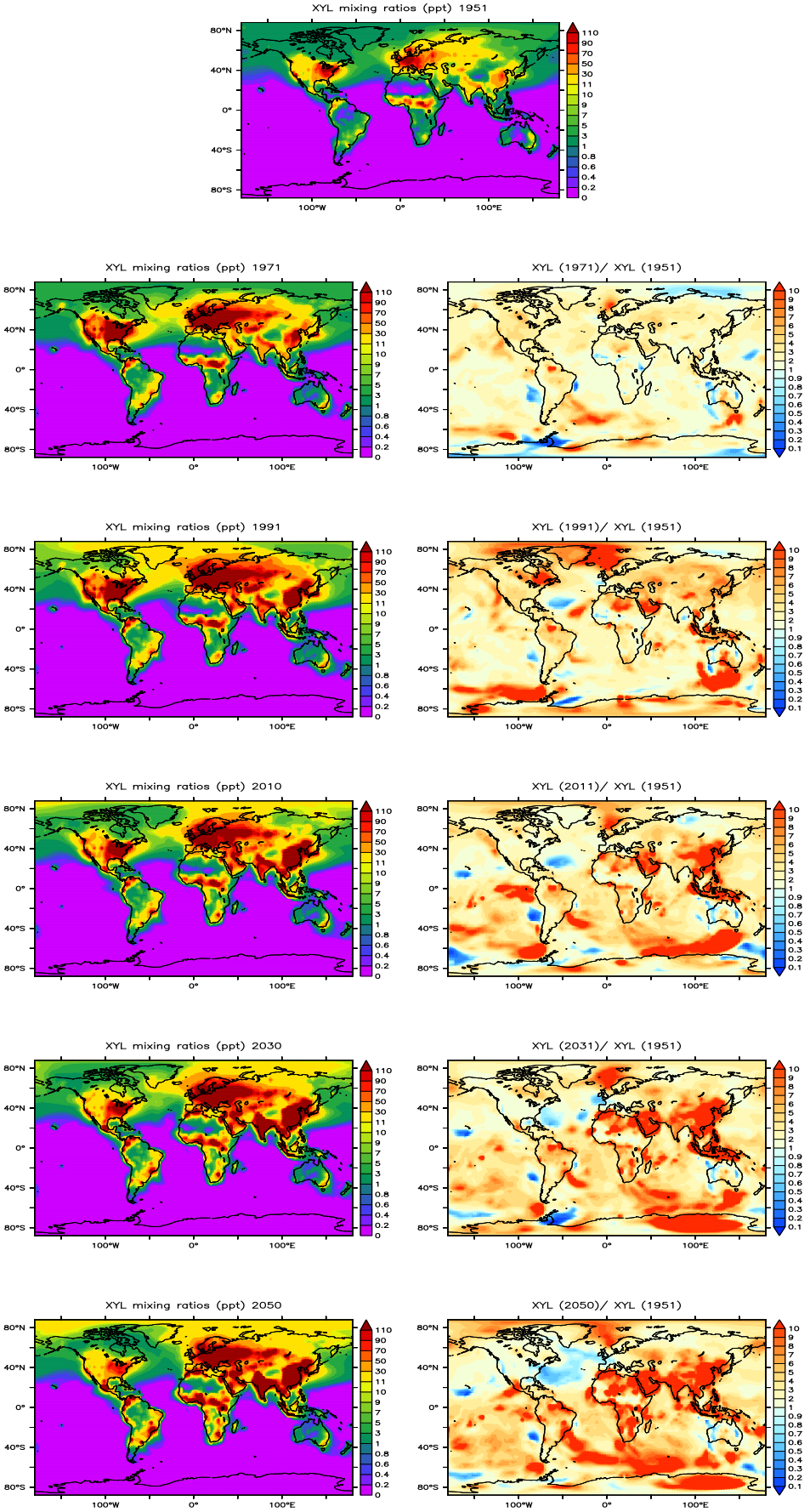

FIGURE 6.5: Xylenes (lumped) mixing ratios ppt on an annual basis in different years of the period 1950-2050.

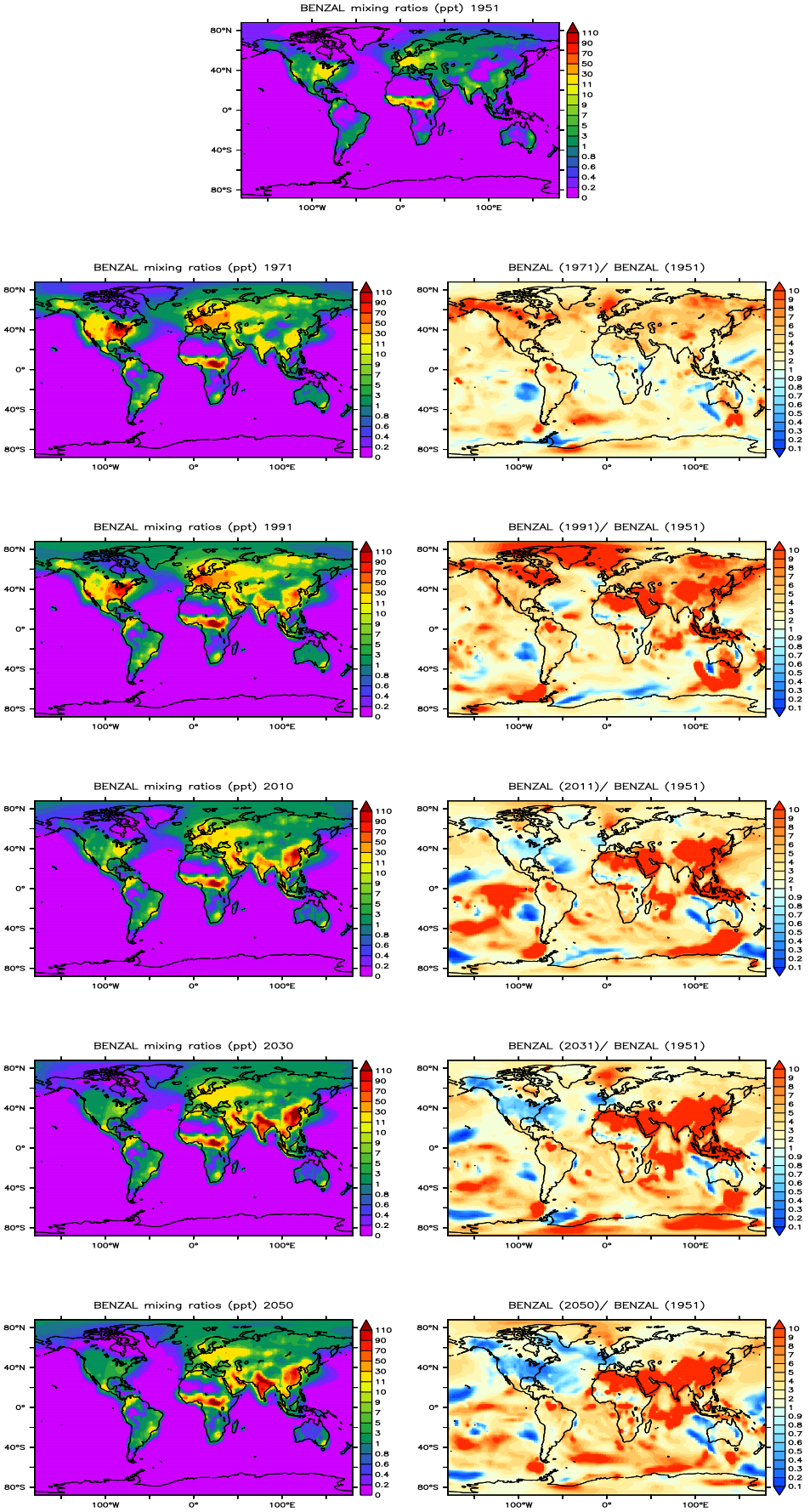

FIGURE 6.6: Benzaldehyde mixing ratios ppt on an annual basis in different years of the period 1950-2050.

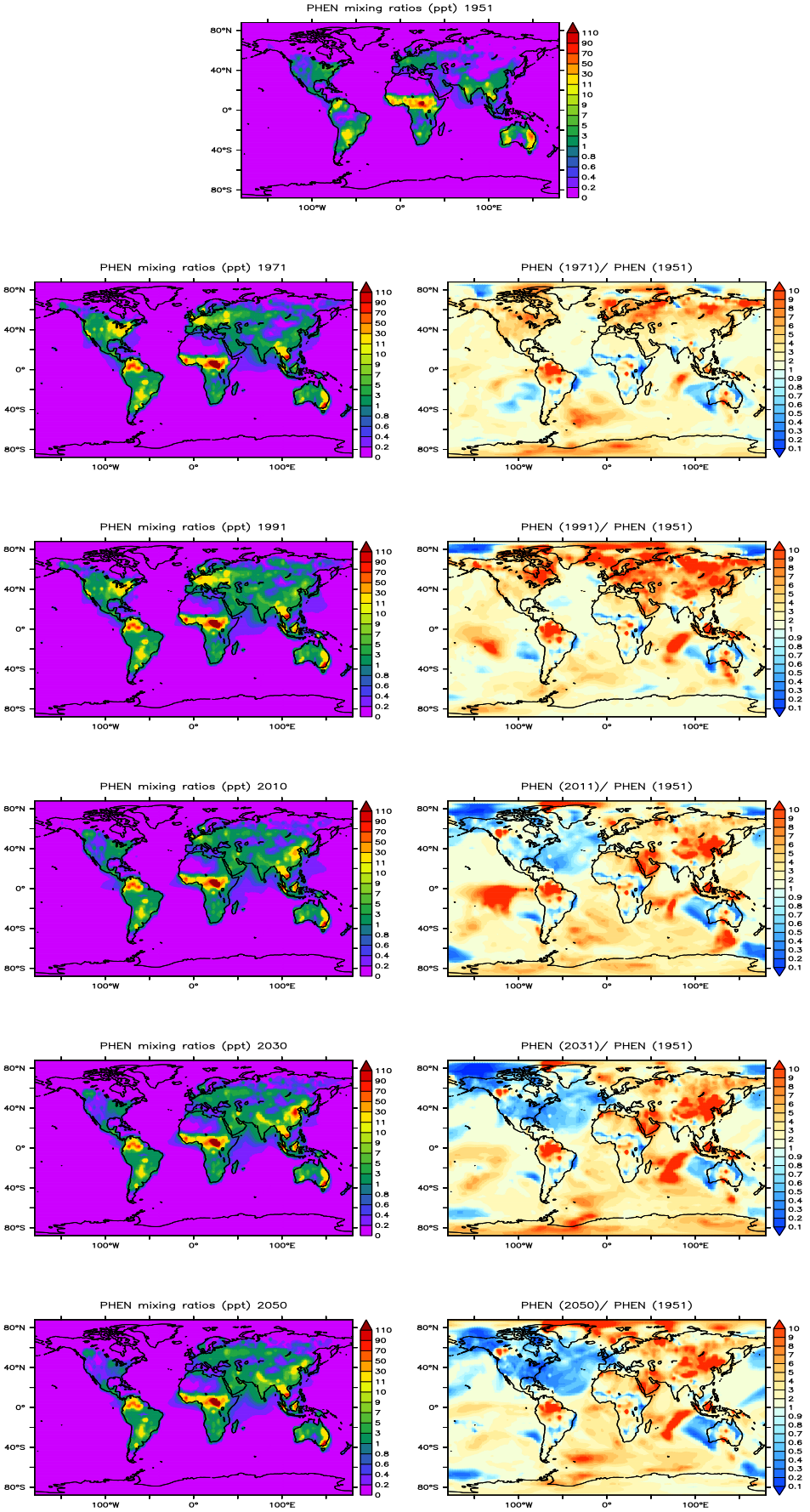

FIGURE 6.7: Phenol mixing ratios ppt on an annual basis in different years of the period 1950-2050

Chapter 7

Conclusions

The aim of this thesis is to investigate aromatic VOC compounds in the atmosphere on a global scale. This work accomplishes three things: first, it gives a quantitative description of the atmospheric budget and the mixing ratio spatial distribution of aromatic VOCs. Second, it identifies the impacts of aromatics in the most important atmospheric photooxidants (i.e. OH and ozone), as well as the HO_x and NO_x cycles, and VOCs. Finally, it reports trends for 1950–2050 and the relationship between emissions and mixing ratio trends. The aromatics chosen for this study are those that contain fewer than nine carbon atoms, and that have the simplest structures (as described and enumerated in Chapter 1). A three-dimensional atmospheric chemistry global circulation model (AC-GCM) was used to achieve the aforementioned points.

A chemical mechanism that can simultaneously represent the atmospheric oxidation of aromatic compounds and enable computations in a global model has been developed. The mechanism is based on the Master Chemical Mechanism (MCM), and the number of reactions and species from the MCM has been reduced by more than half. Comparing the MCM, the CRI mechanism, and the reduced MCM mechanism with the MECCA box model yielded good agreement on the simulated mixing ratios for most compounds. However, discrepancies for some species were found due to the addition or removal of specific channels (e.g. HONO formation yields in CRI and MCM were lower than for the created mechanism because the latter includes more channels, leading to HONO formation). The last step of the mechanism implementation in the model was to include the Henry's law coefficient for each new species added into the system. This step was crucial to model calculations of wet and dry deposition processes. The Henry's law coefficient of each aromatic species was retrieved from the literature, or, if it was not available, was estimated based on species with known coefficients that were structurally similar.

Emissions are another key way to properly characterize gas tracers in global models. We therefore included the sources of aromatic compounds in the atmosphere (i.e. biogenic, anthropogenic, and biomass burning emissions) in the model. For biomass burning emissions, a new submodel, *BioBurn*, was developed. The aim of this submodel is to reproduce the satellite-based GFAS emissions. The GFAS algorithm for the calculation of the emission fluxes was therefore adapted to the MESSy model. Biogenic emissions are calculated by the MEGAN model (as a submodel in the AC-GCM). MEGAN emission rates were evaluated under different EMAC model resolutions to quantify the annual flux resolution dependency. We found that emission rates increased incrementally with resolution. However, these increments are not linear, as the differences are larger between lower resolutions (e.g. T21, T42) and relatively stable at higher resolutions (e.g. T85, T106). With respect to anthropogenic emissions, we created a general tool that can be used for any anthropogenic database, because several anthropogenic databases do not provide VOC speciation or the speciation is always limited to the species selected by the database. In this thesis, we developed a speciation method featuring a simple mass conserving approach (i.e. total VOC mass remains unaltered) to be used for any database. This method can be used to create speciation or to tune an existing speciation. We used the RCP8.5 database for all simulations, as it provides speciation for aromatic compounds and covers the period 1950–2050.

After the emissions and chemistry of aromatic compounds were introduced in the AC-GCM model, we simulated the global atmospheric budget and distribution of monocyclic aromatic compounds. Simulation results were evaluated with a mix ensemble of surface and aircraft observations, with the goal of understanding the emission, production, and removal of these compounds. Additionally, two scenarios with different anthropogenic emissions were studied, one with the emissions from the RCP database, and a second with tuned annual global emissions based on the RCP database.

Our simulations reveal that anthropogenic emissions represent the largest source of aromatics ($\simeq 23\,\mathrm{TgC\,year^{-1}}$), and biomass burning represent the second largest ($\simeq 5\,\mathrm{TgC\,year^{-1}}$). The simulated chemical production of aromatics accounts for $\simeq 5\,\mathrm{TgC\,year^{-1}}$. The atmospheric burden of aromatics sums to 0.3 TgC. The main removal process of aromatics is photochemical decomposition ($\simeq 27\,\mathrm{TgC\,year^{-1}}$), while wet and dry deposition are responsible for a removal of $\simeq 4\,\mathrm{TgC\,year^{-1}}$. Simulated mixing ratios at the surface and elsewhere in the troposphere show good spatial and temporal agreement with the observations for benzene, although the model generally underestimates mixing ratios. Toluene is generally well reproduced by the model at the surface, but mixing ratios in the free troposphere are underestimated. Finally, larger discrepancies are found for xylenes: Surface mixing ratios are not only overestimated, but a low temporal correlation is also found

with respect to in situ observations. The scenario that used tuned anthropogenic emissions had lower agreement with the observations, underestimating the observations. This underestimation was due to the lower anthropogenic emissions as compared to in the RCP scenario.

Mixing ratios for simulated aromatics showed similar spatial distributions, with higher concentrations in the northern hemisphere than the southern hemisphere and very low concentrations in oceanic areas. The largest mixing ratios are found in China and India, areas that produce large amounts of anthropogenic emissions. In the southern hemisphere, the highest mixing ratios were in Central Africa and the Amazon, where biomass burning is frequent.

The evaluated model configuration was then used to quantify global-scale impacts of aromatic compounds on the gas-phase composition. This method consisted of comparing different scenarios that included or excluded the aromatic compound degradation scheme. When aromatic compounds are included in the chemical mechanism, we found a small annual average (less than 3%) net decrease on global OH, ozone, and NO_x mixing ratios. In contrast, significant regional differences were observed in high NO_x regime areas, with an increase of up to 4% in O_3 mixing ratios and 8% in OH concentrations. Conversely, the Amazon region had the largest decreases, of more than 10%. Globally, the inclusion of aromatics (i.e. more organic tracers) results in CO mixing ratio increases, which cause a general decrease in OH. Large increases in formaldehyde were found in urban areas. Glyoxal is the organic compound with the largest changes, with a global increase of 20%. Although the relative impact of aromatics at global scale is limited, at a regional level they are important players in atmospheric chemistry.

Finally, we studied the evolution of mixing ratios at surface from 1950–2050. The future emission scenario used is the RCP8.5; this scenario is characterized by a very high baseline emission, assuming no change in global climate policy and a high population. The analysis showed large increases in the second half of the twentieth century, followed by a stabilization period and a drop in concentrations by 2050. At the regional scale, Europe and North America have decreasing mixing ratios after 2010, leading to values close to those modelled in 1950. In contrast, Southeast Asia was predicted to increase over the whole period, with a slight decrease only in 2050. For most species, the increases in mixing ratios can be explained by the proportion of emissions coming from the energy and transport sectors (except benzene, whose emissions are dominated by domestic emissions). In general, biomass burning was less relevant than anthropogenic emissions during this time period, excluding Africa.

Outlook

This study on aromatic compounds from the global scale perspective raised several points that extend current knowledge:

- To better evaluate model simulations, a larger array of measurements is desirable. While numerous measurements exist for benzene and toluene, for the other aromatic compounds examined in this study, the number of measurements was much lower, and no permanent station is currently measuring them. Using tropospheric flights could be one options, but this would be technically difficult as the lifetime of this species is short and mixing ratios are expected to fall below present instrumentation detection limits.

- As the master chemical mechanism is based on experimental data, there are limitations in the information available on the multiple oxidation sequences, as well as uncertainties in the initial oxidation steps (Jenkin et al., 2003). Future experiments will clarify this issue.

- Further research should be carried out to expand knowledge on the influence of gas-phase aromatic chemistry on secondary aerosol formation. This could be done using the EMAC model, with the help of the ORACLE submodel (Tsimpidi et al., 2014). This research would also extend the work by Henze et al. (2008), in which SOA formation is studied at the global scale, but without detailed gas-phase chemistry. Newer SOA yields are also available, which were not available at the time of Henze's study. This updated analysis would also allow a model inter-comparison.

- Emissions are a key factor in correctly simulating mixing ratios. Current emission inventories estimate aromatic fluxes by scaling the total VOC flux. A direct estimation of the emissions fluxes would allow a more accurate approximation. This would be possible if a large enough matrix of observations were to be available.

Appendix A

Chemical reactions of aromatics

TABLE A.1: Gas phase reactions used in MECCA for the oxidation of aromatic VOC. First column is the enumeration of the equation; the second, labels whether the reactions belong to the troposphere "TR", gas phase "G", contains more than 3 carbon atoms "C"; and nitrogen "N". TEMP correspond to temperature in Kelvin. Detailed description about the labels (and MECCA model) can be found in http://www.rolf-sander.net/messy/mecca/caaba_mecca_manual.pdf. All species and reactions constant are named following MCM nomenclature http://mcm.leeds.ac.uk/MCM/.

reaction			rate coefficient	reference
G11006	TrGC	C5DICARBO2 + HO2 → C5DICAROOH	KRO2HO2*0.706*(1-rcoch2o2_oh-rchohch2o2_oh)	(Rickard and Pascoe, 2009)
G11006b	TrGC	C5DICARBO2 + HO2 → MGLYOX + GLYOX + HO2 + OH	KRO2HO2*0.706*(rcoch2o2_oh-rchohch2o2_oh)	(Rickard and Pascoe, 2009)*
G11007	TrGCN	C5DICARBO2 + NO → MGLYOX + GLYOX + HO2 + NO2	KRO2NO	(Rickard and Pascoe, 2009)*
G11008	TrGCN	C5DICARBO2 + NO3 → MGLYOX + GLYOX + HO2 + NO2	KRO2NO3	(Rickard and Pascoe, 2009)*
G11009	TrGC	C5DICARBO2 → MGLYOX + GLYOX + HO2	KRO2sHORO2*RO2	(Rickard and Pascoe, 2009)*
G11010	TrGC	MCOCOMOOOH + OH → MCOCOMOXO2	2.00E-11	(Rickard and Pascoe, 2009)
G11013	TrGC	C33CO + OH → CO + CO + CO + HO2	5.77E-11	(Rickard and Pascoe, 2009)
G11015	TrGC	C3DIALOOH + OH → C33CO + OH	1.44E-10	(Rickard and Pascoe, 2009)
G11018	TrGC	C3DIALO2 + HO2 → C3DIALOOH	KRO2HO2*0.520*(1-rcoch2o2_oh)	(Rickard and Pascoe, 2009)
G11018b	TrGC	C3DIALO2 + HO2 → GLYOX + CO + HO2 + OH	KRO2HO2*0.520*rcoch2o2_oh	(Rickard and Pascoe, 2009)*
G11019	TrGCN	C3DIALO2 + NO → GLYOX + CO + HO2 + NO2	KRO2NO	(Rickard and Pascoe, 2009)*
G11020	TrGCN	C3DIALO2 + NO3 → GLYOX + CO + HO2 + NO2	KRO2NO3	(Rickard and Pascoe, 2009)*
G11021	TrGC	C3DIALO2 → GLYOX + CO + HO2	8.80E-13*RO2	(Rickard and Pascoe, 2009)*
G11022	TrGC	HCOCOHCO3 + HO2 → GLYOX + HO2 + OH	KAPHO2*rco3_oh	(Rickard and Pascoe, 2009)*
G11023	TrGC	HCOCOHCO3 + HO2 → HCOCOHCO3H	KAPHO2*(rco3_ooh+rco3_o3)	(Rickard and Pascoe, 2009)*
G11024	TrGCN	HCOCOHCO3 + NO → GLYOX + HO2 + NO2	KAPNO	(Rickard and Pascoe, 2009)
G11025	TrGCN	HCOCOHCO3 + NO2 → HCOCOHPAN	k_CH3CO3_NO2	(Rickard and Pascoe, 2009)
G11026	TrGCN	HCOCOHCO3 + NO3 → GLYOX + HO2 + NO2	KRO2NO3*1.74	(Rickard and Pascoe, 2009)
G11027	TrGC	HCOCOHCO3 → GLYOX + HO2	KRO2AP*RO2	(Rickard and Pascoe, 2009)
G11028	TrGC	METACETHO + OH → CH3CO3	9.82E-11	(Rickard and Pascoe, 2009)
G11040	TrGC	C5DIALCO + OH → MALDIALCO3 + CO	4.90E-11	(Rickard and Pascoe, 2009)
G11042	TrGCN	HCOCOHPAN + OH → GLYOX + CO + NO2	6.97E-11	(Rickard and Pascoe, 2009)
G11043	TrGCN	HCOCOHPAN → HCOCOHCO3 + NO2	k_PAN_M	(Rickard and Pascoe, 2009)
G11044	TrGC	C32OH13CO + OH → HCOCOHCO3	1.36E-10	(Rickard and Pascoe, 2009)
G11046	TrGC	HCOCOHCO3H + OH → HCOCOHCO3	7.33E-11	(Rickard and Pascoe, 2009)
G11050	TrGC	MALANHY + OH → MALANHYO2	1.4E-12	(Rickard and Pascoe, 2009)

TABLE A.1: Gas phase reactions (... continued)

reaction			rate coefficient	reference
G11051	TrGC	MALDIALOOH + OH → HOCOC4DIAL + OH	1.22E-10	(Rickard and Pascoe, 2009)
G11052	TrGC	MALDIALOOH + OH → MALDIALO2	1.90E-12*EXP(190/TEMP)	(Rickard and Pascoe, 2009)
G11055	TrGCN	NC4DCO2H + OH → MALANHY + NO2	1.90E-12*EXP(190/TEMP)	(Rickard and Pascoe, 2009)*
G11056	TrGC	CO14O3CO2H + OH → HCOCH2O2	2.19E-11	(Rickard and Pascoe, 2009)
G11057	TrGC	BZFUOOH + OH → BZFUO2	3.68E-11	(Rickard and Pascoe, 2009)
G11059	TrGC	HOCOC4DIAL + OH → CO2C4DIAL + HO2	3.67E-11	(Rickard and Pascoe, 2009)
G11061	TrGC	MALDIALCO3 + HO2 → MALDALCO2H + O3	KAPHO2*rco3_o3	(Rickard and Pascoe, 2009)*
G11062	TrGC	MALDIALCO3 + HO2 → MALDALCO3H	KAPHO2*rco3_ooh	(Rickard and Pascoe, 2009)*
G11063	TrGC	MALDIALCO3 + HO2 → .6 MALANHY + HO2 + .4 GLYOX + .4 CO + OH	KAPHO2*rco3_oh	(Rickard and Pascoe, 2009)*
G11064	TrGCN	MALDIALCO3 + NO → .6 MALANHY + HO2 + .4 GLYOX + .4 CO + NO2	KAPNO	(Rickard and Pascoe, 2009)*
G11065	TrGCN	MALDIALCO3 + NO2 → MALDIALPAN	k_CH3CO3_NO2	(Rickard and Pascoe, 2009)
G11066	TrGCN	MALDIALCO3 + NO3 → .6 MALANHY + HO2 + .4 GLYOX + .4 CO + NO2	KRO2NO3*1.74	(Rickard and Pascoe, 2009)*
G11067	TrGC	MALDIALCO3 → .6 MALANHY + HO2 + .4 GLYOX + .4 CO	KRO2AP*RO2	(Rickard and Pascoe, 2009)*
G11068	TrGCN	BZFUONE + NO3 → NBZFUO2	3.00E-13	(Rickard and Pascoe, 2009)
G11069	TrGC	BZFUONE + O3 → .3125 CO14O3CO2H + .1875 CO14O3CHO + .1875 H2O2 + .5 CO + .5 HCOCH2O2 + .5 OH	2.20E-19	(Rickard and Pascoe, 2009)*
G11070	TrGC	BZFUONE + OH → BZFUO2	4.45E-11	(Rickard and Pascoe, 2009)
G11071	TrGCN	NBZFUOOH + OH → NBZFUO2	6.18E-12	(Rickard and Pascoe, 2009)
G11073	TrGC	MALDALCO3H + OH → MALDIALCO3	4.00E-11	(Rickard and Pascoe, 2009)
G11076	TrGC	EPXDLCO2H + OH → C3DIALO2	2.31E-11	(Rickard and Pascoe, 2009)
G11078	TrGC	EPXDLCO3 + HO2 → C3DIALO2 + OH	KAPHO2*rco3_oh	(Rickard and Pascoe, 2009)*
G11079	TrGC	EPXDLCO3 + HO2 → EPXDLCO2H + O3	KAPHO2*rco3_o3	(Rickard and Pascoe, 2009)*
G11080	TrGC	EPXDLCO3 + HO2 → EPXDLCO3H	KAPHO2*rco3_ooh	(Rickard and Pascoe, 2009)*
G11081	TrGCN	EPXDLCO3 + NO → C3DIALO2 + NO2	KAPNO	(Rickard and Pascoe, 2009)
G11082	TrGCN	EPXDLCO3 + NO2 → EPXDLPAN	k_CH3CO3_NO2	(Rickard and Pascoe, 2009)
G11083	TrGCN	EPXDLCO3 + NO3 → C3DIALO2 + NO2	KRO2NO3*1.74	(Rickard and Pascoe, 2009)
G11084	TrGC	EPXDLCO3 → C3DIALO2	KRO2AP*RO2	(Rickard and Pascoe, 2009)*
G11091	TrGC	MALNHYOHCO + OH → CO + CO + CO + HO2	5.68E-12	(Rickard and Pascoe, 2009)
G11092	TrGCN	MALDIAL + NO3 → MALDIALCO3 + HNO3	2*KNO3AL*2.0	(Rickard and Pascoe, 2009)
G11093	TrGC	MALDIAL + O3 → 1.0675 GLYOX + .125 HCHO + .1125 HCOCO2H + .0675 H2O2 + 0.82 HO2 + .57 OH + 1.265 CO	2.00E-18	(Rickard and Pascoe, 2009)*
G11094	TrGC	MALDIAL + OH → .83 MALDIALCO3 + .17 MALDIALO2	5.20E-11	(Rickard and Pascoe, 2009)*
G11096	TrGC	MALANHYOOH + OH → MALNHYOHCO + OH	4.66E-11	(Rickard and Pascoe, 2009)
G11098	TrGCN	MALDIALPAN + OH → GLYOX + CO + CO + NO2	3.70E-11	(Rickard and Pascoe, 2009)
G11099	TrGCN	MALDIALPAN → MALDIALCO3 + NO2	k_PAN_M	(Rickard and Pascoe, 2009)
G11100	TrGC	MALANHYO2 + HO2 → MALANHYOOH	KRO2HO2*0.625*(1-rcoch2o2_oh-rchohch2o2_oh)	(Rickard and Pascoe, 2009)
G11100b	TrGC	MALANHYO2 + HO2 → HCOCOHCO3 + OH	KRO2HO2*0.625*(rcoch2o2_oh+rchohch2o2_oh)	(Rickard and Pascoe, 2009)*
G11101	TrGCN	MALANHYO2 + NO → HCOCOHCO3 + NO2	KRO2NO	(Rickard and Pascoe, 2009)*
G11102	TrGCN	MALANHYO2 + NO3 → HCOCOHCO3 + NO2	KRO2NO3	(Rickard and Pascoe, 2009)*
G11103	TrGC	MALANHYO2 → HCOCOHCO3	8.80E-13*RO2	(Rickard and Pascoe, 2009)*
G11104	TrGC	EPXDLCO3H + OH → EPXDLCO3	2.62E-11	(Rickard and Pascoe, 2009)
G11106	TrGC	CO2C4DIAL + OH → CO + CO + CO + CO + HO2	2.45E-11	(Rickard and Pascoe, 2009)
G11108	TrGC	NBZFUO2 + HO2 → NBZFUOOH	KRO2HO2*0.625*(1-rcoch2o2_oh)	(Rickard and Pascoe, 2009)
G11108b	TrGC	NBZFUO2 + HO2 → .5 CO14O3CHO + .5 NO2 + .5 NBZFUONE + .5 HO2 + OH	KRO2HO2*0.625*rcoch2o2_oh	(Rickard and Pascoe, 2009)*
G11109	TrGCN	NBZFUO2 + NO → .5 CO14O3CHO + .5 NO2 + .5 NBZFUONE + .5 HO2 + NO2	KRO2NO	(Rickard and Pascoe, 2009)*
G11110	TrGCN	NBZFUO2 + NO3 → .5 CO14O3CHO + .5 NO2 + .5 NBZFUONE + .5 HO2 + NO2	KRO2NO3	(Rickard and Pascoe, 2009)*
G11111	TrGCN	NBZFUO2 → .5 CO14O3CHO + .5 NO2 + .5 NBZFUONE + .5 HO2	8.80E-13*RO2	(Rickard and Pascoe, 2009)*

TABLE A.1: Gas phase reactions (... continued)

reaction			rate coefficient	reference
G11114	TrGC	MALDALCO2H + OH → .6 MALANHY + HO2 + .4 GLYOX + .4 CO	3.70E-11	(Rickard and Pascoe, 2009)*
G11116	TrGCN	EPXC4DIAL + NO3 → EPXDLCO3 + HNO3	2*KNO3AL*4.0	(Rickard and Pascoe, 2009)
G11117	TrGC	EPXC4DIAL + OH → EPXDLCO3	4.32E-11	(Rickard and Pascoe, 2009)
G11119	TrGC	MECOACETO2 + HO2 → MECOACEOOH	KRO2HO2*0.625*(1-rcoch2o2_oh)	(Rickard and Pascoe, 2009)
G11119b	TrGC	MECOACETO2 + HO2 → CH3CO3 + HCHO + OH	KRO2HO2*0.625*(rcoch2o2_oh)	(Rickard and Pascoe, 2009)*
G11120	TrGCN	MECOACETO2 + NO → CH3CO3 + HCHO + NO2	KRO2NO	(Rickard and Pascoe, 2009)*
G11121	TrGCN	MECOACETO2 + NO3 → CH3CO3 + HCHO + NO2	KRO2NO3	(Rickard and Pascoe, 2009)*
G11122	TrGC	MECOACETO2 → CH3CO3 + HCHO	KRO2pORO2*RO2	(Rickard and Pascoe, 2009)*
G11123	TrGCN	CO14O3CHO + NO3 → CO + HCOCH2O2 + HNO3	KNO3AL*8.0	(Rickard and Pascoe, 2009)
G11124	TrGC	CO14O3CHO + OH → CO + HCOCH2O2	3.44E-11	(Rickard and Pascoe, 2009)
G11126	TrGCN	NBZFUONE + OH → BZFUCO + NO2	1.16E-12	(Rickard and Pascoe, 2009)
G11127	TrGC	BZFUO2 + HO2 → BZFUOOH	KRO2HO2*0.706*(1-rcoch2o2_oh-rchohch2o2_oh)	(Rickard and Pascoe, 2009)
G11127b	TrGC	BZFUO2 + HO2 → CO14O3CHO + HO2 + OH	KRO2HO2*0.706*(rcoch2o2_oh+rchohch2o2_oh)	(Rickard and Pascoe, 2009)*
G11128	TrGCN	BZFUO2 + NO → CO14O3CHO + HO2 + NO2	KRO2NO	(Rickard and Pascoe, 2009)*
G11129	TrGCN	BZFUO2 + NO3 → CO14O3CHO + HO2 + NO2	KRO2NO3	(Rickard and Pascoe, 2009)*
G11130	TrGC	BZFUO2 → CO14O3CHO + HO2	8.80E-13*RO2	(Rickard and Pascoe, 2009)*
G11131	TrGC	BZFUCO + OH → CO14O3CHO + HO2	1.78E-11	(Rickard and Pascoe, 2009)
G11132	TrGCN	C23O3CHO + NO3 → CO + CH3CO3 + HNO3	KNO3AL*4.0	(Rickard and Pascoe, 2009)
G11133	TrGC	C23O3CHO + OH → CO + CH3CO3	1.27E-11	(Rickard and Pascoe, 2009)
G11135	TrGC	MALDIALO2 + HO2 → MALDIALOOH	KRO2HO2*0.625*(1-rcoch2o2_oh-rchohch2o2_oh)	(Rickard and Pascoe, 2009)
G11135b	TrGC	MALDIALO2 + HO2 → GLYOX + GLYOX + HO2 + OH	KRO2HO2*0.625*(rcoch2o2_oh+rchohch2o2_oh)	(Rickard and Pascoe, 2009)*
G11136	TrGCN	MALDIALO2 + NO → GLYOX + GLYOX + HO2 + NO2	KRO2NO	(Rickard and Pascoe, 2009)*
G11137	TrGCN	MALDIALO2 + NO3 → GLYOX + GLYOX + HO2 + NO2	KRO2NO3	(Rickard and Pascoe, 2009)*
G11138	TrGC	MALDIALO2 → GLYOX + GLYOX + HO2	8.80E-13*RO2	(Rickard and Pascoe, 2009)*
G11150	TrGCN	NC4MDCO2H + OH → MMALANHY + NO2	1.90E-12*EXP(190/TEMP)	(Rickard and Pascoe, 2009)*
G11151	TrGCN	C54CO + NO3 → CO + CO + CO + CH3CO3 + HNO3	KNO3AL*5.5	(Rickard and Pascoe, 2009)
G11152	TrGC	C54CO + OH → CO + CO + CO + CH3CO3	1.72E-11	(Rickard and Pascoe, 2009)
G11154	TrGCN	NTLFUO2 + HO2 → NTLFUOOH	KRO2HO2*0.706*(1-rcoch2o2_oh)	(Rickard and Pascoe, 2009)
G11154b	TrGC	NTLFUO2 + HO2 → ACCOMECHO + NO2 + OH	KRO2HO2*0.706*rcoch2o2_oh	(Rickard and Pascoe, 2009)*
G11155	TrGCN	NTLFUO2 + NO → ACCOMECHO + NO2 + NO2	KRO2NO	(Rickard and Pascoe, 2009)*
G11156	TrGCN	NTLFUO2 + NO3 → ACCOMECHO + NO2 + NO2	KRO2NO3	(Rickard and Pascoe, 2009)*
G11157	TrGCN	NTLFUO2 → ACCOMECHO + NO2	KRO2tORO2*RO2	(Rickard and Pascoe, 2009)*
G11158	TrGC	C5134CO2OH + OH → C54CO + HO2	7.48E-11	(Rickard and Pascoe, 2009)
G11160	TrGC	MC3CODBCO3 + HO2 → .35 GLYOX + .35 CH3O2 + .35 CO + .65 MMALANHY + .65 HO2 + OH	KAPHO2*rco3_oh	(Rickard and Pascoe, 2009)*
G11161	TrGC	MC3CODBCO3 + HO2 → MC3ODBCO2H + O3	KAPHO2*rco3_o3	(Rickard and Pascoe, 2009)*
G11162	TrGC	MC3CODBCO3 + HO2 → MC3ODBCO3H	KAPHO2*rco3_ooh	(Rickard and Pascoe, 2009)*
G11163	TrGCN	MC3CODBCO3 + NO → .35 GLYOX + .35 CH3O2 + .35 CO + .65 MMALANHY + .65 HO2 + NO2	KAPNO	(Rickard and Pascoe, 2009)*
G11164	TrGCN	MC3CODBCO3 + NO2 → MC3CODBPAN	k_CH3CO3_NO2	(Rickard and Pascoe, 2009)*
G11165	TrGCN	MC3CODBCO3 + NO3 → .35 GLYOX + .35 CH3O2 + .35 CO + .65 MMALANHY + .65 HO2 + NO2	KRO2NO3*1.74	(Rickard and Pascoe, 2009)*
G11166a	TrGCN	MC3CODBCO3 → .35 GLYOX + .35 CH3O2 + .35 CO + .65 MMALANHY + .65 HO2	1.00E-11*RO2*0.90	(Rickard and Pascoe, 2009)*

TABLE A.1: Gas phase reactions (... continued)

reaction			rate coefficient	reference
G11166b	TrGCN	MC3CODBCO3 → MC3ODBCO2H	1.00E-11*RO2*0.1	(Rickard and Pascoe, 2009)*
G11167	TrGCN	C5COO2NO2 + OH → MGLYOX + CO + CO + NO2	5.43E-11	(Rickard and Pascoe, 2009)
G11168	TrGCN	C5COO2NO2 → C5CO14O2 + NO2	k_PAN_M	(Rickard and Pascoe, 2009)*
G11169	TrGC	C5DIALOOH + OH → C5DIALCO + OH	7.52E-11	(Rickard and Pascoe, 2009)
G11172	TrGC	C4CO2DBCO3 + HO2 → C4CO2DCO3H	KAPHO2*(rco3_ooh+rco3_o3)	(Rickard and Pascoe, 2009)*
G11173	TrGC	C4CO2DBCO3 + HO2 → HO2 + CO + C33CO + OH	KAPHO2*rco3_oh	(Rickard and Pascoe, 2009)*
G11174	TrGCN	C4CO2DBCO3 + NO → HO2 + CO + C33CO + NO2	KAPNO	(Rickard and Pascoe, 2009)
G11175	TrGCN	C4CO2DBCO3 + NO2 → C4CO2DBPAN	k_CH3CO3_NO2	(Rickard and Pascoe, 2009)*
G11176	TrGCN	C4CO2DBCO3 + NO3 → HO2 + CO + C33CO + NO2	KRO2NO3*1.74	(Rickard and Pascoe, 2009)
G11177	TrGC	C4CO2DBCO3 → HO2 + CO + C33CO	KRO2AP*RO2	(Rickard and Pascoe, 2009)
G11178	TrGC	MMALANHY + OH → MMALANHYO2	1.50E-12	(Rickard and Pascoe, 2009)
G11179	TrGC	PXYFUO2 + HO2 → PXYFUOOH	KRO2HO2*0.706*(1-rcoch2o2_oh-rchohch2o2_oh)	(Rickard and Pascoe, 2009)
G11179b	TrGC	PXYFUO2 + HO2 → C23O3CCHO + HO2 + OH	KRO2HO2*0.706*rcoch2o2_oh+rchohch2o2_oh	(Rickard and Pascoe, 2009)*
G11180	TrGCN	PXYFUO2 + NO → C23O3CCHO + HO2 + NO2	KRO2NO	(Rickard and Pascoe, 2009)*
G11181	TrGCN	PXYFUO2 + NO3 → C23O3CCHO + HO2 + NO2	KRO2NO3	(Rickard and Pascoe, 2009)*
G11182	TrGC	PXYFUO2 → C23O3CCHO + HO2	KRO2tORO2*RO2	(Rickard and Pascoe, 2009)*
G11183	TrGC	MMALANHYO2 + HO2 → MMALNHYOOH	KRO2HO2*0.706*(1-rcoch2o2_oh-rchohch2o2_oh)	(Rickard and Pascoe, 2009)
G11183b	TrGC	MMALANHYO2 + HO2 → CO2H3CO3 + OH	KRO2HO2*0.706*(rcoch2o2_oh+rchohch2o2_oh)	(Rickard and Pascoe, 2009)*
G11184	TrGCN	MMALANHYO2 + NO → CO2H3CO3 + NO2	KRO2NO	(Rickard and Pascoe, 2009)*
G11185	TrGCN	MMALANHYO2 + NO3 → CO2H3CO3 + NO2	KRO2NO3	(Rickard and Pascoe, 2009)*
G11186	TrGC	MMALANHYO2 → CO2H3CO3	KRO2tORO2*RO2	(Rickard and Pascoe, 2009)*
G11187	TrGCN	NPXYFUOOH + OH → NPXYFUO2	5.16E-12	(Rickard and Pascoe, 2009)
G11189	TrGCN	C23O3CCHO + NO3 → C23O3CCO3 + HNO3	KNO3AL*5.5	(Rickard and Pascoe, 2009)
G11190	TrGC	C23O3CCHO + OH → C23O3CCO3	2.15E-11	(Rickard and Pascoe, 2009)
G11192	TrGCN	C4CO2DBPAN + OH → C33CO + CO + NO2	2.74E-11	(Rickard and Pascoe, 2009)
G11193	TrGCN	C4CO2DBPAN → C4CO2DBCO3 + NO2	k_PAN_M	(Rickard and Pascoe, 2009)*
G11194	TrGC	C5CO14O2 + HO2 → .83 MALANHY + .83 CH3O2 + .17 MGLYOX + .17 HO2 + .17 CO + OH	KAPHO2*rco3_oh	(Rickard and Pascoe, 2009)*
G11195	TrGC	C5CO14O2 + HO2 → C5CO14OH + O3	KAPHO2*rco3_o3	(Rickard and Pascoe, 2009)*
G11196	TrGC	C5CO14O2 + HO2 → C5CO14OOH	KAPHO2*rco3_ooh	(Rickard and Pascoe, 2009)*
G11197	TrGCN	C5CO14O2 + NO → .83 MALANHY + .83 CH3O2 + .17 MGLYOX + .17 HO2 + .17 CO + NO2	KAPNO	(Rickard and Pascoe, 2009)*
G11198	TrGCN	C5CO14O2 + NO2 → C5COO2NO2	k_CH3CO3_NO2	(Rickard and Pascoe, 2009)*
G11199	TrGCN	C5CO14O2 + NO3 → .83 MALANHY + .83 CH3O2 + .17 MGLYOX + .17 HO2 + .17 CO + NO2	KRO2NO3*1.74	(Rickard and Pascoe, 2009)*
G11200	TrGC	C5CO14O2 → .83 MALANHY + .83 CH3O2 + .17 MGLYOX + .17 HO2 + .17 CO	KRO2AP*RO2	(Rickard and Pascoe, 2009)*
G11201	TrGC	PXYFUOOH + OH → PXYFUO2	2.78E-11	(Rickard and Pascoe, 2009)
G11203	TrGCN	MC3CODBPAN + OH → GLYOX + HCHO + CO + NO2	4.37E-11	(Rickard and Pascoe, 2009)
G11204	TrGCN	MC3CODBPAN → MC3CODBCO3 + NO2	k_PAN_M	(Rickard and Pascoe, 2009)*
G11205	TrGC	C5CO14OH + OH → .83 MALANHY + .83 CH3O2 + .17 MGLYOX + .17 HO2 + .17 CO	5.44E-11	(Rickard and Pascoe, 2009)*
G11207	TrGC	NPXYFUO2 + HO2 → NPXYFUOOH	KRO2HO2*0.706*(1-rcoch2o2_oh)	(Rickard and Pascoe, 2009)
G11207b	TrGCN	NPXYFUO2 + HO2 → C23O3CCHO + NO2 + OH	KRO2HO2*0.706*rcoch2o2_oh	(Rickard and Pascoe, 2009)*
G11208	TrGCN	NPXYFUO2 + NO → C23O3CCHO + NO2 + NO2	KRO2NO	(Rickard and Pascoe, 2009)*
G11209	TrGCN	NPXYFUO2 + NO3 → C23O3CCHO + NO2 + NO2	KRO2NO3	(Rickard and Pascoe, 2009)*
G11210	TrGCN	NPXYFUO2 → C23O3CCHO + NO2	KRO2tORO2*RO2	(Rickard and Pascoe, 2009)*
G11211	TrGCN	C5DICARB + NO3 → C5CO14O2 + HNO3	KNO3AL*2.75	(Rickard and Pascoe, 2009)

TABLE A.1: Gas phase reactions (... continued)

reaction			rate coefficient	reference
G11212	TrGC	C5DICARB + O3 → .5338 GLYOX + .063 CH3CHO + .348 CH3CO3 + .918 CO + .57 OH + .473 HO2 + .0563 CH3COCO2H + .5338 MGLYOX +.676 H2O2 + .063 HCHO + .0563 HCOCO2H	2.00E-18	(Rickard and Pascoe, 2009)
G11213	TrGC	C5DICARB + OH → .48 C5CO14O2 + .52 C5DICARBO2	6.2E-11	(Rickard and Pascoe, 2009)
G11215	TrGC	MC3ODBCO2H + OH → .35 GLYOX + .35 CH3O2 + .35 CO + .65 MMALANHY + .65 HO2	4.38E-11	(Rickard and Pascoe, 2009)*
G11217	TrGC	C23O3CCO2H + OH → MCOCOMOXO2	8.76E-13	(Rickard and Pascoe, 2009)
G11218	TrGC	C23O3CCO3 + HO2 → C23O3CCO2H + O3	KAPHO2*rco3_o3	(Rickard and Pascoe, 2009)*
G11219	TrGC	C23O3CCO3 + HO2 → C23O3CCO3H	KAPHO2*rco3_ooh	(Rickard and Pascoe, 2009)*
G11230	TrGC	C23O3CCO3 + HO2 → MCOCOMOXO2 + OH	KAPHO2*rco3_oh	(Rickard and Pascoe, 2009)*
G11231	TrGCN	C23O3CCO3 + NO → MCOCOMOXO2 + NO2	KAPNO	(Rickard and Pascoe, 2009)
G11232	TrGCN	C23O3CCO3 + NO2 → C23O3CPAN	k_CH3CO3_NO2	(Rickard and Pascoe, 2009)*
G11233	TrGCN	C23O3CCO3 + NO3 → MCOCOMOXO2 + NO2	KRO2NO3*1.74	(Rickard and Pascoe, 2009)
G11234	TrGC	C23O3CCO3 → MCOCOMOXO2	KRO2AP*RO2	(Rickard and Pascoe, 2009)*
G11235	TrGCN	TLFUONE + NO3 → NTLFUO2	1.00E-12	(Rickard and Pascoe, 2009)
G11236	TrGC	TLFUONE + O3 → .5 CO + .5 OH + .5 MECOACETO2 + .3125 C24O3CCO2H + .1875 ACCOMECHO + .1875 H2O2	8.00E-19	(Rickard and Pascoe, 2009)*
G11237	TrGC	TLFUONE + OH → TLFUO2	6.90E-11	(Rickard and Pascoe, 2009)
G11238	TrGC	ACCOMECO3 + HO2 → ACCOMECO3H	KAPHO2*(rco3_ooh+rco3_o3)	(Rickard and Pascoe, 2009)*
G11239	TrGC	ACCOMECO3 + HO2 → MECOACETO2 + OH	KAPHO2*rco3_oh	(Rickard and Pascoe, 2009)*
G11240	TrGCN	ACCOMECO3 + NO → MECOACETO2 + NO2	KAPNO	(Rickard and Pascoe, 2009)
G11241	TrGCN	ACCOMECO3 + NO2 → ACCOMEPAN	k_CH3CO3_NO2	(Rickard and Pascoe, 2009)*
G11242	TrGCN	ACCOMECO3 + NO3 → MECOACETO2 + NO2	KRO2NO3*1.74	(Rickard and Pascoe, 2009)
G11243	TrGC	ACCOMECO3 → MECOACETO2	KRO2AP*RO2	(Rickard and Pascoe, 2009)
G11244	TrGC	C4CO2DCO3H + OH → C4CO2DBCO3	3.06E-11	(Rickard and Pascoe, 2009)
G11246	TrGCN	EPXDLPAN + OH → C33CO + CO + NO2	2.29E-11	(Rickard and Pascoe, 2009)
G11247	TrGCN	EPXDLPAN → EPXDLCO3 + NO2	k_PAN_M	(Rickard and Pascoe, 2009)*
G11248	TrGC	C4M2ALOHO2 + HO2 → C4MALOHOOH	KRO2HO2*0.706*(1-rcoch2o2_oh-rchohch2o2_oh)	(Rickard and Pascoe, 2009)
G11248b	TrGC	C4M2ALOHO2 + HO2 → GLYOX + MGLYOX + HO2 + OH	KRO2HO2*0.706*rcoch2o2_oh+rchohch2o2_oh	(Rickard and Pascoe, 2009)*
G11249	TrGCN	C4M2ALOHO2 + NO → GLYOX + MGLYOX + HO2 + NO2	KRO2NO	(Rickard and Pascoe, 2009)*
G11250	TrGCN	C4M2ALOHO2 + NO3 → GLYOX + MGLYOX + HO2 + NO2	KRO2NO3	(Rickard and Pascoe, 2009)*
G11251	TrGC	C4M2ALOHO2 → GLYOX + MGLYOX + HO2	KRO2tORO2*RO2	(Rickard and Pascoe, 2009)*
G11252	TrGCN	ACCOMECHO + NO3 → ACCOMECO3 + HNO3	KNO3AL*5.5	(Rickard and Pascoe, 2009)
G11253	TrGC	ACCOMECHO + OH → ACCOMECO3	7.09E-11	(Rickard and Pascoe, 2009)
G11255	TrGC	MMALNHYOOH + OH → MMALANHYO2	1.69E-11	(Rickard and Pascoe, 2009)
G11257	TrGC	C5DICAROOH + OH → C5134CO2OH + OH	1.21E-10	(Rickard and Pascoe, 2009)
G11258	TrGC	C5DICAROOH + OH → C5DICARBO2	1.90E-12*EXP(190/TEMP)	(Rickard and Pascoe, 2009)
G11260	TrGC	C24O3CCO2H + OH → MECOACETO2	8.76E-13	(Rickard and Pascoe, 2009)
G11261	TrGCN	NTLFUOOH + OH → NTLFUO2	4.44E-12	(Rickard and Pascoe, 2009)
G11263	TrGC	MECOACEOOH + OH → MECOACETO2	3.59E-12	(Rickard and Pascoe, 2009)
G11265	TrGCN	ACCOMEPAN + OH → METACETHO + CO + CO + NO2	1.00E-14	(Rickard and Pascoe, 2009)
G11266	TrGCN	ACCOMEPAN → ACCOMECO3 + NO2	k_PAN_M	(Rickard and Pascoe, 2009)*
G11267	TrGC	C4MALOHOOH + OH → GLYOX + MGLYOX + HO2	4.58E-11	(Rickard and Pascoe, 2009)*
G11270	TrGC	C3MCODBCO3 + HO2 → .35 MGLYOX + .35 HO2 + .35 CO + .65 MMALANHY + .65 HO2 + OH	KAPHO2*rco3_oh	(Rickard and Pascoe, 2009)*
G11271	TrGC	C3MCODBCO3 + HO2 → C4CODBCO3H	KAPHO2*(rco3_ooh+rco3_o3)	(Rickard and Pascoe, 2009)*
G11272	TrGCN	C3MCODBCO3 + NO → .35 MGLYOX + .35 HO2 + .35 CO + .65 MMALANHY + .65 HO2 + NO2	KAPNO	(Rickard and Pascoe, 2009)*
G11273	TrGCN	C3MCODBCO3 + NO2 → C3MCODBPAN	k_CH3CO3_NO2	(Rickard and Pascoe, 2009)*

TABLE A.1: Gas phase reactions (... continued)

reaction			rate coefficient	reference
G11274	TrGCN	C3MCODBCO3 + NO3 → NO2 + .35 MGLYOX + .35 HO2 + .35 CO + .65 MMALANHY + .65 HO2	KRO2NO3*1.74	(Rickard and Pascoe, 2009)*
G11275	TrGC	C3MCODBCO3 → .35 MGLYOX + .35 HO2 + .35 CO + .65 MMALANHY + .65 HO2	KRO2AP*RO2	(Rickard and Pascoe, 2009)*
G11276	TrGCN	PXYFUONE + NO3 → NPXYFUO2	1.00E-12	(Rickard and Pascoe, 2009)
G11278	TrGC	PXYFUONE + O3 → OH + CO + MCOCOMOXO2	8.00E-19	(Rickard and Pascoe, 2009)
G11279	TrGC	PXYFUONE + OH → PXYFUO2	2.42E-11	(Rickard and Pascoe, 2009)
G11280	TrGC	TLFUO2 + HO2 → TLFUOOH	KRO2HO2*0.706*(1-rcoch2o2_oh-rchohch2o2_oh)	(Rickard and Pascoe, 2009)
G11280b	TrGC	TLFUO2 + HO2 → ACCOMECHO + HO2 + OH	KRO2HO2*0.706*(rcoch2o2_oh+rchohch2o2_oh)	(Rickard and Pascoe, 2009)*
G11281	TrGCN	TLFUO2 + NO → ACCOMECHO + HO2 + NO2	KRO2NO	(Rickard and Pascoe, 2009)*
G11282	TrGCN	TLFUO2 + NO3 → ACCOMECHO + HO2 + NO2	KRO2NO3	(Rickard and Pascoe, 2009)*
G11283	TrGC	TLFUO2 → ACCOMECHO + HO2	KRO2tORO2*RO2	(Rickard and Pascoe, 2009)*
G11284	TrGC	C5CO14OOH + OH → C5CO14O2	3.59E-12	(Rickard and Pascoe, 2009)
G11286	TrGCN	C23O3CPAN + OH → CO + C23O3CHO + NO2	7.36E-13	(Rickard and Pascoe, 2009)
G11287	TrGCN	C23O3CPAN → C23O3CCO3 + NO2	k_PAN_M	(Rickard and Pascoe, 2009)*
G11294	TrGC	C4CODBCO3H + OH → C3MCODBCO3	4.73E-11	(Rickard and Pascoe, 2009)
G11297	TrGC	TLFUOOH + OH → TLFUO2	2.53E-11	(Rickard and Pascoe, 2009)
G11299	TrGC	C23O3CCO3H + OH → C23O3CCO3	4.34E-12	(Rickard and Pascoe, 2009)
G11301	TrGC	MC3ODBCO3H + OH → MC3CODBCO3	4.73E-11	(Rickard and Pascoe, 2009)
G11304	TrGC	ACCOMECO3H + OH → ACCOMECO3	3.59E-12	(Rickard and Pascoe, 2009)
G11306	TrGC	C5DIALO2 + HO2 → C5DIALOOH	KRO2HO2*0.706*(1-rcoch2o2_oh)	(Rickard and Pascoe, 2009)
G11306b	TrGC	C5DIALO2 + HO2 → MALDIAL + CO + HO2 + OH	KRO2HO2*0.706*rcoch2o2_oh	(Rickard and Pascoe, 2009)*
G11307	TrGCN	C5DIALO2 + NO → MALDIAL + CO + HO2 + NO2	KRO2NO	(Rickard and Pascoe, 2009)*
G11308	TrGCN	C5DIALO2 + NO3 → MALDIAL + CO + HO2 + NO2	KRO2NO3	(Rickard and Pascoe, 2009)*
G11309	TrGC	C5DIALO2 → MALDIAL + CO + HO2	8.80E-13*RO2	(Rickard and Pascoe, 2009)*
G11350	TrGC	PHENOOH + OH → PHENO2	1.16E-10	(Rickard and Pascoe, 2009)
G11352	TrGC	C6CO4DB + OH → CO + CO + HO2 + CO + C33CO	7.70E-11	(Rickard and Pascoe, 2009)
G11354	TrGC	C5CO2DCO3H + OH → C5CO2DBCO3	3.60E-11	(Rickard and Pascoe, 2009)
G11356	TrGCN	NDNPHENOOH + OH → NDNPHENO2	1.90E-12*EXP(190/TEMP)	(Rickard and Pascoe, 2009)
G11358	TrGC	C615CO2O2 + HO2 → C615CO2OOH	KRO2HO2*0.770*(1.-rcoch2o2_oh)	(Rickard and Pascoe, 2009)
G11358b	TrGC	C615CO2O2 + HO2 → C5DICARB + CO + HO2 + OH	KRO2HO2*0.770*rcoch2o2_oh	(Rickard and Pascoe, 2009)*
G11359	TrGCN	C615CO2O2 + NO → C5DICARB + CO + HO2 + NO2	KRO2NO	(Rickard and Pascoe, 2009)*
G11360	TrGCN	C615CO2O2 + NO3 → C5DICARB + CO + HO2 + NO2	KRO2NO3	(Rickard and Pascoe, 2009)*
G11361	TrGC	C615CO2O2 → C5DICARB + CO + HO2	8.80E-13*RO2	(Rickard and Pascoe, 2009)*
G11362	TrGCN	BZEMUCPAN + OH → MALDIAL + CO + NO2	4.05E-11	(Rickard and Pascoe, 2009)
G11363	TrGCN	BZEMUCPAN → BZEMUCCO3 + NO2	k_PAN_M	(Rickard and Pascoe, 2009)*
G11364	TrGCN	BZBIPERNO3 + OH → BZOBIPEROH + NO2	7.30E-11	(Rickard and Pascoe, 2009)
G11366	TrGCN	HOC6H4NO2 + NO3 → NPHEN1O + HNO3	9.00E-14	(Rickard and Pascoe, 2009)
G11367	TrGCN	HOC6H4NO2 + OH → NPHEN1O	9.00E-13	(Rickard and Pascoe, 2009)
G11368	TrGCN	NDNPHENO2 + HO2 → NDNPHENOOH	KRO2HO2*0.770*(1-rchohch2o2_oh)	(Rickard and Pascoe, 2009)
G11368b	TrGC	NDNPHENO2 + HO2 → NC4DCO2H + HNO3 + CO + CO + NO2 + OH	KRO2HO2*0.770*rchohch2o2_oh	(Rickard and Pascoe, 2009)*
G11369	TrGCN	NDNPHENO2 + NO → NC4DCO2H + HNO3 + CO + CO + NO2 + NO2	KRO2NO	(Rickard and Pascoe, 2009)*
G11370	TrGCN	NDNPHENO2 + NO3 → NC4DCO2H + HNO3 + CO + CO + NO2 + NO2	KRO2NO3	(Rickard and Pascoe, 2009)*
G11371	TrGCN	NDNPHENO2 → NC4DCO2H + HNO3 + CO + CO + NO2	8.00E-13*RO2	(Rickard and Pascoe, 2009)*
G11372	TrGC	PBZQCO + OH → C5CO2OHCO3	6.07E-11	(Rickard and Pascoe, 2009)
G11373	TrGCN	CATECHOL + NO3 → CATEC1O + HNO3	9.9E-11	(Rickard and Pascoe, 2009)*
G11374	TrGC	CATECHOL + O3 → MALDALCO2H + HCOCO2H + HO2 + OH	9.2E-18	(Rickard and Pascoe, 2009)

TABLE A.1: Gas phase reactions (... continued)

reaction			rate coefficient	reference
G11375	TrGC	CATECHOL + OH → CATEC1O	1.0E-10	(Rickard and Pascoe, 2009)
G11376	TrGC	C5COOHCO3H + OH → C5CO2OHCO3	8.01E-11	(Rickard and Pascoe, 2009)
G11378	TrGCN	NCATECHOL + NO3 → NNCATECO2	2.60E-12	(Rickard and Pascoe, 2009)
G11379	TrGCN	NCATECHOL + OH → NCATECO2	3.47E-12	(Rickard and Pascoe, 2009)
G11380	TrGC	C5CO2OHCO3 + HO2 → C5COOHCO3H	KAPHO2*(rco3_ooh+rco3_o3)	(Rickard and Pascoe, 2009)*
G11381	TrGC	C5CO2OHCO3 + HO2 → HOCOC4DIAL + HO2 + CO + OH	KAPHO2*rco3_oh	(Rickard and Pascoe, 2009)*
G11382	TrGCN	C5CO2OHCO3 + NO → HOCOC4DIAL + HO2 + CO + NO2	KAPNO	(Rickard and Pascoe, 2009)
G11383	TrGCN	C5CO2OHCO3 + NO2 → C5CO2OHPAN	k_CH3CO3_NO2	(Rickard and Pascoe, 2009)*
G11384	TrGCN	C5CO2OHCO3 + NO3 → HOCOC4DIAL + HO2 + CO + NO2	KRO2NO3*1.74	(Rickard and Pascoe, 2009)
G11385	TrGC	C5CO2OHCO3 → HOCOC4DIAL + HO2 + CO	KRO2AP*RO2	(Rickard and Pascoe, 2009)
G11386	TrGCN	BZEPOXMUC + NO3 → BZEMUCCO3 + HNO3	2*KNO3AL*2.75	(Rickard and Pascoe, 2009)
G11387	TrGC	BZEPOXMUC + O3 → EPXC4DIAL + .125 HCHO + .1125 HCOCO2H + .0675 GLYOX + .0675 H2O2 + .82 HO2 + .57 OH + 1.265 CO	2.00E-18	(Rickard and Pascoe, 2009)*
G11388	TrGC	BZEPOXMUC + OH → .31 BZEMUCCO3 + .69 BZEMUCO2	6.08E-11	(Rickard and Pascoe, 2009)
G11390	TrGCN	NCATECO2 + HO2 → NCATECOOH	KRO2HO2*0.770*(1-rchohch2o2_oh)	(Rickard and Pascoe, 2009)
G11390b	TrGC	NCATECO2 + HO2 → NC4DCO2H + HCOCO2H + HO2 + OH	KRO2HO2*0.770*rchohch2o2_oh	(Rickard and Pascoe, 2009)*
G11391	TrGCN	NCATECO2 + NO → NC4DCO2H + HCOCO2H + HO2 + NO2	KRO2NO	(Rickard and Pascoe, 2009)*
G11392	TrGCN	NCATECO2 + NO3 → NC4DCO2H + HCOCO2H + HO2 + NO2	KRO2NO3	(Rickard and Pascoe, 2009)*
G11393	TrGCN	NCATECO2 → NC4DCO2H + HCOCO2H + HO2	8.00E-13*RO2	(Rickard and Pascoe, 2009)*
G11394	TrGCN	NPHEN1OOH + OH → NPHEN1O2	9.00E-13	(Rickard and Pascoe, 2009)
G11396	TrGCN	NPHENO2 + HO2 → NPHENOOH	KRO2HO2*0.770*(1-rchohch2o2_oh)	(Rickard and Pascoe, 2009)
G11396b	TrGCN	NPHENO2 + HO2 → MALDALCO2H + GLYOX + NO2 + OH	KRO2HO2*0.770*rchohch2o2_oh	(Rickard and Pascoe, 2009)*
G11397	TrGCN	NPHENO2 + NO → MALDALCO2H + GLYOX + NO2 + NO2	KRO2NO	(Rickard and Pascoe, 2009)*
G11398	TrGCN	NPHENO2 + NO3 → MALDALCO2H + GLYOX + NO2 + NO2	KRO2NO3	(Rickard and Pascoe, 2009)*
G11399	TrGCN	NPHENO2 → MALDALCO2H + GLYOX + NO2	8.00E-13*RO2	(Rickard and Pascoe, 2009)*
G11400	TrGC	BENZENE + OH → .352 BZBIPERO2 + .118 BZEPOXMUC + .118 HO2 + .53 PHENOL + .53 HO2	2.3E-12*EXP(-190/TEMP)	(Rickard and Pascoe, 2009)*
G11401	TrGCN	C5CO2OHPAN + OH → HOCOC4DIAL + CO + CO + NO2	7.66E-11	(Rickard and Pascoe, 2009)
G11402	TrGCN	C5CO2OHPAN → C5CO2OHCO3 + NO2	k_PAN_M	(Rickard and Pascoe, 2009)*
G11403	TrGCN	CATEC1O + NO2 → NCATECHOL	2.08E-12	(Rickard and Pascoe, 2009)
G11404	TrGC	CATEC1O + O3 → CATEC1O2	2.86E-13	(Rickard and Pascoe, 2009)
G11405	TrGC	BZEMUCCO + OH → EPXDLCO3 + GLYOX	9.20E-11	(Rickard and Pascoe, 2009)
G11407	TrGCN	NNCATECO2 + HO2 → NNCATECOOH	KRO2HO2*0.770*(1-rchohch2o2_oh)	(Rickard and Pascoe, 2009)
G11407b	TrGCN	NNCATECO2 + HO2 → NC4DCO2H + HCOCO2H + NO2 + OH	KRO2HO2*0.770*(rchohch2o2_oh)	(Rickard and Pascoe, 2009)*
G11408	TrGCN	NNCATECO2 + NO → NC4DCO2H + HCOCO2H + NO2 + NO2	KRO2NO	(Rickard and Pascoe, 2009)*
G11409	TrGCN	NNCATECO2 + NO3 → NC4DCO2H + HCOCO2H + NO2 + NO2	KRO2NO3	(Rickard and Pascoe, 2009)*
G11410	TrGCN	NNCATECO2 → NC4DCO2H + HCOCO2H + NO2	8.00E-13*RO2	(Rickard and Pascoe, 2009)*
G11411	TrGC	BZEMUCCO2H + OH → C5DIALO2	4.06E-11	(Rickard and Pascoe, 2009)
G11413	TrGCN	NNCATECOOH + OH → NNCATECO2	1.90E-12*EXP(190/TEMP)	(Rickard and Pascoe, 2009)
G11415	TrGCN	NPHEN1O + NO2 → DNPHEN	2.08E-12	(Rickard and Pascoe, 2009)
G11416	TrGCN	NPHEN1O + O3 → NPHEN1O2	2.86E-13	(Rickard and Pascoe, 2009)
G11417	TrGCN	DNPHEN + NO3 → NDNPHENO2	2.25E-15	(Rickard and Pascoe, 2009)
G11418	TrGCN	DNPHEN + OH → DNPHENO2	3.00E-14	(Rickard and Pascoe, 2009)
G11419	TrGCN	PHENOL + NO3 → .742 C6H5O + .742 HNO3 + .258 NPHENO2	3.8E-12	(Rickard and Pascoe, 2009)*

TABLE A.1: Gas phase reactions (... continued)

reaction			rate coefficient	reference
G11420	TrGC	PHENOL + OH → .06 C6H5O + .8 CATECHOL + .8 HO2 + .14 PHENO2	4.7E-13*EXP(1220/TEMP)	(Rickard and Pascoe, 2009)*
G11421	TrGCN	PBZQONE + NO3 → NBZQO2	3.00E-13	(Rickard and Pascoe, 2009)
G11422	TrGC	PBZQONE + OH → PBZQO2	4.6E-12	(Rickard and Pascoe, 2009)
G11423	TrGC	PHENO2 + HO2 → PHENOOH	KRO2HO2*0.770*(1-rchohch2o2_oh)	(Rickard and Pascoe, 2009)
G11423b	TrGC	PHENO2 + HO2 → .71 MALDALCO2H + .71 GLYOX + .29 PBZQONE + HO2 + OH	KRO2HO2*0.770*rchohch2o2_oh	(Rickard and Pascoe, 2009)*
G11424	TrGCN	PHENO2 + NO → .71 MALDALCO2H + .71 GLYOX + .29 PBZQONE + HO2 + NO2	KRO2NO	(Rickard and Pascoe, 2009)*
G11425	TrGCN	PHENO2 + NO3 → .71 MALDALCO2H + .71 GLYOX + .29 PBZQONE + HO2 + NO2	KRO2NO3	(Rickard and Pascoe, 2009)*
G11426	TrGC	PHENO2 → .71 MALDALCO2H + .71 GLYOX + .29 PBZQONE + HO2	8.00E-13*RO2	(Rickard and Pascoe, 2009)*
G11427	TrGC	C615CO2OOH + OH → C6125CO + OH	9.42E-11	(Rickard and Pascoe, 2009)
G11430	TrGC	C5CO2DBCO3 + HO2 → C5CO2DCO3H	KAPHO2*(rco3_ooh+rco3_o3)	(Rickard and Pascoe, 2009)*
G11431	TrGC	C5CO2DBCO3 + HO2 → CH3CO3 + C33CO + OH	KAPHO2*rco3_oh	(Rickard and Pascoe, 2009)*
G11432	TrGCN	C5CO2DBCO3 + NO → CH3CO3 + C33CO + NO2	KAPNO	(Rickard and Pascoe, 2009)
G11433	TrGCN	C5CO2DBCO3 + NO2 → C5CO2DBPAN	k_CH3CO3_NO2	(Rickard and Pascoe, 2009)*
G11434	TrGCN	C5CO2DBCO3 + NO3 → CH3CO3 + C33CO + NO2	KRO2NO3*1.74	(Rickard and Pascoe, 2009)
G11435	TrGC	C5CO2DBCO3 → CH3CO3 + C33CO	KRO2AP*RO2	(Rickard and Pascoe, 2009)
G11436	TrGCN	NPHEN1O2 + HO2 → NPHEN1OOH	KRO2HO2*0.770	(Rickard and Pascoe, 2009)
G11437	TrGCN	NPHEN1O2 + NO → NPHEN1O + NO2	KRO2NO	(Rickard and Pascoe, 2009)
G11437b	TrGCN	NPHEN1O2 + NO2 → NPHEN1O + NO3	KPHENO2NO2	(Jagiella and Zabel, 2007)*
G11438	TrGCN	NPHEN1O2 + NO3 → NPHEN1O + NO2	KRO2NO3	(Rickard and Pascoe, 2009)
G11439	TrGCN	NPHEN1O2 → NPHEN1O	KRO2sRO2*RO2	(Rickard and Pascoe, 2009)
G11440	TrGCN	NPHENOOH + OH → NPHENO2	1.07E-10	(Rickard and Pascoe, 2009)
G11442	TrGCN	C6H5O + NO2 → HOC6H4NO2	2.08E-12	(Rickard and Pascoe, 2009)*
G11443	TrGC	C6H5O + O3 → C6H5O2	2.86E-13	(Rickard and Pascoe, 2009)
G11444	TrGCN	NCATECOOH + OH → NCATECO2	1.90E-12*EXP(190/TEMP)	(Rickard and Pascoe, 2009)
G11456	TrGC	PBZQOOH + OH → PBZQCO + OH	1.23E-10	(Rickard and Pascoe, 2009)
G11458	TrGC	PBZQO2 + HO2 → PBZQOOH	KRO2HO2*0.770*(1-rchohch2o2_oh-rcoch2o2_oh)	(Rickard and Pascoe, 2009)
G11458b	TrGC	PBZQO2 + HO2 → C5CO2OHCO3 + OH	KRO2HO2*0.770*(rchohch2o2_oh+rcoch2o2_oh)	(Rickard and Pascoe, 2009)*
G11459	TrGCN	PBZQO2 + NO → C5CO2OHCO3 + NO2	KRO2NO	(Rickard and Pascoe, 2009)*
G11460	TrGCN	PBZQO2 + NO3 → C5CO2OHCO3 + NO2	KRO2NO3	(Rickard and Pascoe, 2009)*
G11461	TrGC	PBZQO2 → C5CO2OHCO3	8.80E-13*RO2	(Rickard and Pascoe, 2009)*
G11462	TrGC	BZOBIPEROH + OH → MALDIALCO3 + GLYOX	8.16E-11	(Rickard and Pascoe, 2009)
G11464	TrGCN	DNPHENO2 + HO2 → DNPHENOOH	KRO2HO2*0.770*(1-rchohch2o2_oh)	(Rickard and Pascoe, 2009)
G11464b	TrGCN	DNPHENO2 + HO2 → NC4DCO2H + HCOCO2H + NO2 + OH	KRO2HO2*0.770*rchohch2o2_oh	(Rickard and Pascoe, 2009)*
G11465	TrGCN	DNPHENO2 + NO → NC4DCO2H + HCOCO2H + NO2 + NO2	KRO2NO	(Rickard and Pascoe, 2009)*
G11466	TrGCN	DNPHENO2 + NO3 → NC4DCO2H + HCOCO2H + NO2 + NO2	KRO2NO3	(Rickard and Pascoe, 2009)*
G11467	TrGCN	DNPHENO2 → NC4DCO2H + HCOCO2H + NO2	8.00E-13*RO2	(Rickard and Pascoe, 2009)*
G11468	TrGC	BZBIPEROOH + OH → BZOBIPEROH + OH	9.77E-11	(Rickard and Pascoe, 2009)
G11470	TrGC	BZEMUCO2 + HO2 → BZEMUCOOH	KRO2HO2*0.770*(1-rchohch2o2_oh-rcoch2o2_oh)	(Rickard and Pascoe, 2009)
G11470b	TrGC	BZEMUCO2 + HO2 → .5 EPXC4DIAL + .5 GLYOX + .5 HO2 + .5 C3DIALO2 + .5 C32OH13CO + OH	KRO2HO2*0.770*(rchohch2o2_oh+rcoch2o2_oh)	(Rickard and Pascoe, 2009)*
G11471	TrGCN	BZEMUCO2 + NO → BZEMUCNO3	KRO2NO*0.105	(Rickard and Pascoe, 2009)
G11472	TrGCN	BZEMUCO2 + NO → .5 EPXC4DIAL + .5 GLYOX + .5 HO2 + .5 C3DIALO2 + .5 C32OH13CO + NO2	KRO2NO*0.895	(Rickard and Pascoe, 2009)*
G11473	TrGCN	BZEMUCO2 + NO3 → .5 EPXC4DIAL + .5 GLYOX + .5 HO2 + .5 C3DIALO2 + .5 C32OH13CO + NO2	KRO2NO3	(Rickard and Pascoe, 2009)*
G11474	TrGC	BZEMUCO2 → .5 EPXC4DIAL + .5 GLYOX + .5 HO2 + .5 C3DIALO2 + .5 C32OH13CO	8.80E-13*RO2	(Rickard and Pascoe, 2009)*
G11475	TrGCN	C5CO2DBPAN + OH → C33CO + CH3CHO + NO2	3.28E-11	(Rickard and Pascoe, 2009)

TABLE A.1: Gas phase reactions (... continued)

reaction			rate coefficient	reference
G11476	TrGCN	C5CO2DBPAN → C5CO2DBCO3 + NO2	k_PAN_M	(Rickard and Pascoe, 2009)*
G11477	TrGCN	NBZQOOH + OH → NBZQO2	6.68E-11	(Rickard and Pascoe, 2009)
G11479	TrGC	CATEC1OOH + OH → CATEC1O2	1.90E-12*EXP(190/TEMP)	(Rickard and Pascoe, 2009)
G11481	TrGC	C6125CO + OH → C5CO14O2 + CO	6.45E-11	(Rickard and Pascoe, 2009)
G11483	TrGCN	NBZQO2 + HO2 → NBZQOOH	KRO2HO2*0.770*(1-rcoch2o2_oh)	(Rickard and Pascoe, 2009)
G11483b	TrGCN	NBZQO2 + HO2 → C6CO4DB + NO2 + OH	KRO2HO2*0.770*rcoch2o2_oh	(Rickard and Pascoe, 2009)*
G11484	TrGCN	NBZQO2 + NO → C6CO4DB + NO2 + NO2	KRO2NO	(Rickard and Pascoe, 2009)*
G11485	TrGCN	NBZQO2 + NO3 → C6CO4DB + NO2 + NO2	KRO2NO3	(Rickard and Pascoe, 2009)*
G11486	TrGCN	NBZQO2 → C6CO4DB + NO2	8.80E-13*RO2	(Rickard and Pascoe, 2009)*
G11487	TrGCN	DNPHENOOH + OH → DNPHENO2	1.90E-12*EXP(190/TEMP)	(Rickard and Pascoe, 2009)
G11489	TrGC	CATEC1O2 + HO2 → CATEC1OOH	KRO2HO2*0.770	(Rickard and Pascoe, 2009)
G11490	TrGCN	CATEC1O2 + NO → CATEC1O + NO2	KRO2NO	(Rickard and Pascoe, 2009)
G11490b	TrGCN	CATEC1O2 + NO2 → CATEC1O + NO3	KPHENO2NO2	(Jagiella and Zabel, 2007)*
G11491	TrGCN	CATEC1O2 + NO3 → CATEC1O + NO2	KRO2NO3	(Rickard and Pascoe, 2009)
G11492	TrGC	CATEC1O2 → CATEC1O	8.80E-13*RO2	(Rickard and Pascoe, 2009)
G11493	TrGC	BZEMUCCO3H + OH → BZEMUCCO3	4.37E-11	(Rickard and Pascoe, 2009)
G11495	TrGC	C6H5OOH + OH → C6H5O2	3.60E-12	(Rickard and Pascoe, 2009)
G11497	TrGC	BZEMUCOOH + OH → BZEMUCCO + OH	1.31E-10	(Rickard and Pascoe, 2009)
G11499	TrGC	BZEMUCCO3 + HO2 → BZEMUCCO2H + O3	KAPHO2*rco3_o3	(Rickard and Pascoe, 2009)*
G11500	TrGC	BZEMUCCO3 + HO2 → BZEMUCCO3H	KAPHO2*rco3_ooh	(Rickard and Pascoe, 2009)*
G11501	TrGC	BZEMUCCO3 + HO2 → C5DIALO2 + OH	KAPHO2*rco3_oh	(Rickard and Pascoe, 2009)*
G11502	TrGCN	BZEMUCCO3 + NO → C5DIALO2 + NO2	KAPNO	(Rickard and Pascoe, 2009)
G11503	TrGCN	BZEMUCCO3 + NO2 → BZEMUCPAN	k_CH3CO3_NO2	(Rickard and Pascoe, 2009)*
G11504	TrGCN	BZEMUCCO3 + NO3 → C5DIALO2 + NO2	KRO2NO3*1.74	(Rickard and Pascoe, 2009)
G11505	TrGC	BZEMUCCO3 → C5DIALO2	1.00E-11*RO2	(Rickard and Pascoe, 2009)*
G11506	TrGC	C6H5O2 + HO2 → C6H5OOH	KRO2HO2*0.770	(Rickard and Pascoe, 2009)
G11507	TrGCN	C6H5O2 + NO → C6H5O + NO2	KRO2NO	(Rickard and Pascoe, 2009)
G11507b	TrGCN	C6H5O2 + NO2 → C6H5O + NO3	KPHENO2NO2	(Jagiella and Zabel, 2007)*
G11508	TrGCN	C6H5O2 + NO3 → C6H5O + NO2	KRO2NO3	(Rickard and Pascoe, 2009)
G11509	TrGC	C6H5O2 → C6H5O	KRO2sRO2*RO2	(Rickard and Pascoe, 2009)
G11510	TrGC	BZEMUCOH + OH → BZEMUCCO + HO2	8.23E-11	(Rickard and Pascoe, 2009)
G11512	TrGCN	BZEMUCNO3 + OH → BZEMUCCO + NO2	4.38E-11	(Rickard and Pascoe, 2009)
G11601	TrGC	TOLUENE + OH → .07 C6H5CH2O2 + .07 PTOL$_C$6H5CH2O2 + .18 CRESOL + .18 PTOL$_C$RESOL + .18 HO2 + .65 TLBIPERO2 + .65 PTOL$_T$LBIPERO2 + .10 TLEPOXMUC + .10 PTOL$_T$LEPOXMUC + .10 HO2	1.8E-12*EXP(340/TEMP)	(Rickard and Pascoe, 2009)*
G11602	TrGC	BZBIPERO2 + HO2 → BZBIPEROOH	KRO2HO2*0.770	(Rickard and Pascoe, 2009)
G11603	TrGCN	BZBIPERO2 + NO → BZBIPERNO3	KRO2NO*0.082	(Rickard and Pascoe, 2009)
G11603b	TrGCN	BZBIPERO2 + NO → NO2 + GLYOX + HO2 + .5 BZFUONE + .5 BZFUONE	KRO2NO*0.918	(Rickard and Pascoe, 2009)*
G11604	TrGCN	BZBIPERO2 + NO3 → NO2 + GLYOX + HO2 + .5 BZFUONE + .5 BZFUONE	KRO2NO3	(Rickard and Pascoe, 2009)*
G11605	TrGC	BZBIPERO2 → GLYOX + HO2 + BZFUONE	8.80E-13*RO2	(Rickard and Pascoe, 2009)*
G11606	TrGC	C6H5CH2O2 + HO2 → C6H5CH2OOH	1.5E-13*EXP(1310/TEMP)	(Rickard and Pascoe, 2009)
G11607	TrGCN	C6H5CH2O2 + NO → C6H5CH2NO3	KRO2NO*0.105	(Rickard and Pascoe, 2009)*
G11607b	TrGCN	C6H5CH2O2 + NO → BENZAL + HO2 + NO2	KRO2NO*0.985	(Rickard and Pascoe, 2009)*
G11608	TrGCN	C6H5CH2O2 + NO3 → BENZAL + HO2 + NO2	KRO2NO3	(Rickard and Pascoe, 2009)*
G11609	TrGC	C6H5CH2O2 → BENZAL + HO2	2*(KCH3O2*2.4E-14*EXP(1620/TEMP))**0.5*RO2	(Rickard and Pascoe, 2009)*
G11610	TrGCN	CRESOL + NO3 → .103 CRESO2 + .103 HNO3 + .506 NCRESO2 + .391 TOL1O + .391 HNO3	1.4E-11	(Rickard and Pascoe, 2009)*
G11611	TrGC	CRESOL + OH → .2 CRESO2 + .727 MCATECHOL + .727 HO2 + .073 TOL1O	4.65E-11	(Rickard and Pascoe, 2009)*
G11612	TrGC	TLBIPERO2 + HO2 → TLBIPEROOH	KRO2HO2*0.820	(Rickard and Pascoe, 2009)
G11613	TrGCN	TLBIPERO2 + NO → NO2 + .6 GLYOX + .4 MGLYOX + HO2 + .2 C4MDIAL + .2 C5DICARB + .2 TLFUONE + .2 BZFUONE + .2 MALDIAL	KRO2NO*0.889	(Rickard and Pascoe, 2009)*
G11614	TrGCN	TLBIPERO2 + NO → TLBIPERNO3	KRO2NO*0.111	(Rickard and Pascoe, 2009)

TABLE A.1: Gas phase reactions (... continued)

reaction			rate coefficient	reference
G11615	TrGCN	TLBIPERO2 + NO3 → NO2 + .6 GLYOX + .4 MGLYOX + HO2 + .2 C4MDIAL + .2 C5DICARB + .2 TLFUONE + .2 BZFUONE + .2 MALDIAL	KRO2NO3	(Rickard and Pascoe, 2009)*
G11616	TrGC	TLBIPERO2 → .6 GLYOX + .4 MGLYOX + HO2 + .2 C4MDIAL + .2 C5DICARB + .2 TLFUONE + .2 BZFUONE + .2 MALDIAL	8.80E-13*RO2	(Rickard and Pascoe, 2009)*
G11617	TrGCN	TLEPOXMUC + NO3 → TLEMUCCO3 + HNO3	KNO3AL*2.75	(Rickard and Pascoe, 2009)
G11618	TrGC	TLEPOXMUC + O3 → EPXC4DIAL + .125 CH3CHO + .695 CH3CO3 + .57 CO + .57 OH + .125 HO2 +.1125 CH3COCO2H + .0675 MGLYOX + .0675 H2O2	5.00E-18	(Rickard and Pascoe, 2009)*
G11619	TrGC	TLEPOXMUC + OH → .31 TLEMUCCO3 + .69 TLEMUCO2	7.99E-11	(Rickard and Pascoe, 2009)*
G11621	TrGC	C6H5CH2OOH + OH → BENZAL + OH	2.05E-11	(Rickard and Pascoe, 2009)
G11623	TrGCN	C6H5CH2NO3 + OH → BENZAL + NO2	6.03E-12	(Rickard and Pascoe, 2009)
G11627	TrGCN	BENZAL + NO3 → C6H5CO3 + HNO3	2.40E-15	(Rickard and Pascoe, 2009)
G11628	TrGC	BENZAL + OH → C6H5CO3	5.9E-12*EXP(225/TEMP)	(Rickard and Pascoe, 2009)
G11629	TrGC	CRESO2 + HO2 → CRESOOH	KRO2HO2*0.820*(1-rchohch2o2_oh)	(Rickard and Pascoe, 2009)
G11629b	TrGC	CRESO2 + HO2 → .68 C5CO14OH + .68 GLYOX + HO2 + .32 PTLQONE + OH	KRO2HO2*0.820*rchohch2o2_oh	(Rickard and Pascoe, 2009)*
G11630	TrGCN	CRESO2 + NO → .68 C5CO14OH + .68 GLYOX + HO2 + .32 PTLQONE + NO2	KRO2NO	(Rickard and Pascoe, 2009)*
G11631	TrGCN	CRESO2 + NO3 → .68 C5CO14OH + .68 GLYOX + HO2 + .32 PTLQONE + NO2	KRO2NO3	(Rickard and Pascoe, 2009)*
G11632	TrGC	CRESO2 → .68 C5CO14OH + .68 GLYOX + HO2 + .32 PTLQONE	8.00E-13*RO2	(Rickard and Pascoe, 2009)*
G11633	TrGCN	NCRESO2 + HO2 → NCRESOOH	KRO2HO2*0.820*(1-rchohch2o2_oh)	(Rickard and Pascoe, 2009)
G11633b	TrGCN	NCRESO2 + HO2 → C5CO14OH + GLYOX + NO2 + OH	KRO2HO2*0.820*rchohch2o2_oh	(Rickard and Pascoe, 2009)*
G11634	TrGCN	NCRESO2 + NO → C5CO14OH + GLYOX + NO2 + NO2	KRO2NO	(Rickard and Pascoe, 2009)*
G11635	TrGCN	NCRESO2 + NO3 → C5CO14OH + GLYOX + NO2 + NO2	KRO2NO3	(Rickard and Pascoe, 2009)*
G11636	TrGCN	NCRESO2 → C5CO14OH + GLYOX + NO2	8.00E-13*RO2	(Rickard and Pascoe, 2009)*
G11637	TrGCN	TOL1O + NO2 → TOL1OHNO2	2.08E-12	(Rickard and Pascoe, 2009)*
G11638	TrGC	TOL1O + O3 → OXYL1O2	2.86E-13	(Rickard and Pascoe, 2009)
G11639	TrGCN	MCATECHOL + NO3 → MCATEC1O + HNO3	1.7E-10*1.0	(Rickard and Pascoe, 2009)
G11640	TrGC	MCATECHOL + O3 → MC3ODBCO2H + HCOCO2H + HO2 + OH	2.8E-17	(Rickard and Pascoe, 2009)*
G11641	TrGC	MCATECHOL + OH → MCATEC1O	2.0E-10*1.0	(Rickard and Pascoe, 2009)
G11642	TrGC	TLBIPEROOH + OH → TLOBIPEROH + OH	9.64E-11	(Rickard and Pascoe, 2009)
G11644	TrGCN	TLBIPERNO3 + OH → TLOBIPEROH + NO2	7.16E-11	(Rickard and Pascoe, 2009)
G11646	TrGC	TLOBIPEROH + OH → C5CO14O2 + GLYOX	7.99E-11	(Rickard and Pascoe, 2009)
G11648	TrGC	TLEMUCCO3 + HO2 → C615CO2O2 + OH	KAPHO2*rco3_oh	(Rickard and Pascoe, 2009)*
G11649	TrGC	TLEMUCCO3 + HO2 → TLEMUCCO2H + O3	KAPHO2*rco3_o3	(Rickard and Pascoe, 2009)*
G11650	TrGCN	TLEMUCCO3 + HO2 → TLEMUCCO3H	KAPHO2*rco3_ooh	(Rickard and Pascoe, 2009)*
G11651	TrGCN	TLEMUCCO3 + NO → C615CO2O2 + NO2	KAPNO	(Rickard and Pascoe, 2009)
G11652	TrGCN	TLEMUCCO3 + NO2 → TLEMUCPAN	k_CH3CO3_NO2	(Rickard and Pascoe, 2009)*
G11653	TrGCN	TLEMUCCO3 + NO3 → C615CO2O2 + NO2	KRO2NO3*1.74	(Rickard and Pascoe, 2009)
G11654	TrGC	TLEMUCCO3 → C615CO2O2	KRO2AP*RO2	(Rickard and Pascoe, 2009)*
G11655	TrGC	TLEMUCO2 + HO2 → TLEMUCOOH	KRO2HO2*0.820*(1-rchohch2o2_oh-rcoch2o2_oh)	(Rickard and Pascoe, 2009)
G11655b	TrGC	TLEMUCO2 + HO2 → .5 C3DIALO2 + .5 CO2H3CHO + .5 EPXC4DIAL + .5 MGLYOX + .5 HO2 + OH	KRO2HO2*0.820*(rchohch2o2_oh+rcoch2o2_oh)	(Rickard and Pascoe, 2009)*
G11656	TrGCN	TLEMUCO2 + NO → TLEMUCNO3	KRO2NO*0.105	(Rickard and Pascoe, 2009)
G11656b	TrGCN	TLEMUCO2 + NO → .5 C3DIALO2 + .5 CO2H3CHO + .5 EPXC4DIAL + .5 MGLYOX + .5 HO2 + NO2	KRO2NO*0.985	(Rickard and Pascoe, 2009)*
G11657	TrGCN	TLEMUCO2 + NO3 → .5 C3DIALO2 + .5 CO2H3CHO + .5 EPXC4DIAL + .5 MGLYOX + .5 HO2 + NO2	KRO2NO3	(Rickard and Pascoe, 2009)*

TABLE A.1: Gas phase reactions (... continued)

reaction			rate coefficient	reference
G11658	TrGCN	TLEMUCO2 → .5 C3DIALO2 + .5 CO2H3CHO + .5 EPXC4DIAL + .5 MGLYOX + .5 HO2	8.80E-13*RO2	(Rickard and Pascoe, 2009)*
G11659	TrGC	C6H5CO3 + HO2 → C6H5CO3H	KAPHO2*0.065	(Roth et al., 2010)*
G11660	TrGC	C6H5CO3 + HO2 → C6H5O2 + OH	KAPHO2*0.20	(Roth et al., 2010)*
G11661	TrGC	C6H5CO3 + HO2 → PHCOOH + O3	KAPHO2*0.15	(Roth et al., 2010)*
G11662	TrGCN	C6H5CO3 + NO → C6H5O2 + NO2	KAPNO	(Rickard and Pascoe, 2009)
G11663	TrGCN	C6H5CO3 + NO2 → PBZN	k_CH3CO3_NO2	(Rickard and Pascoe, 2009)*
G11664	TrGCN	C6H5CO3 + NO3 → C6H5O2 + NO2	KRO2NO3*1.74	(Rickard and Pascoe, 2009)
G11665	TrGC	C6H5CO3 → C6H5O2	KRO2AP*RO2	(Rickard and Pascoe, 2009)
G11666	TrGC	CRESOOH + OH → CRESO2	1.15E-10	(Rickard and Pascoe, 2009)
G11668	TrGCN	NCRESOOH + OH → NCRESO2	1.07E-10	(Rickard and Pascoe, 2009)
G11671	TrGCN	TOL1OHNO2 + NO3 → NCRES1O + HNO3	3.13E-13*1.0	(Rickard and Pascoe, 2009)
G11672	TrGCN	TOL1OHNO2 + OH → NCRES1O	2.8E-12	(Rickard and Pascoe, 2009)
G11673	TrGC	OXYL1O2 + HO2 → OXYL1OOH	KRO2HO2*0.820	(Rickard and Pascoe, 2009)
G11674	TrGCN	OXYL1O2 + NO → TOL1O + NO2	KRO2NO	(Rickard and Pascoe, 2009)
G11674b	TrGCN	OXYL1O2 + NO2 → TOL1O + NO3	KPHENO2NO2	(Jagiella and Zabel, 2007)*
G11675	TrGCN	OXYL1O2 + NO3 → TOL1O + NO2	KRO2NO3	(Rickard and Pascoe, 2009)
G11676	TrGC	OXYL1O2 → TOL1O	KRO2sRO2*RO2	(Rickard and Pascoe, 2009)
G11677	TrGCN	MCATEC1O + NO2 → MNCATECH	2.08E-12	(Rickard and Pascoe, 2009)
G11678	TrGC	MCATEC1O + O3 → MCATEC1O2	2.86E-13	(Rickard and Pascoe, 2009)
G11679a	TrGCAro	C4MDIAL + NO3 → MC3CODBCO3 + HNO3	KNO3AL*4.25	(Rickard and Pascoe, 2009)
G11679b	TrGCAro	C4MDIAL + NO3 → C3MCODBCO3 + HNO3	KNO3AL*4.25	(Rickard and Pascoe, 2009)
G11680	TrGCN	C4MDIAL + O3 → .445 OH + .445 CO + .445 CH3CO3 + .055 MGLYOX + .055 H2O2 + .5 GLYOX + .5 MGLYOX + .0343 HCOCO2H + .0206 GLYOX + .0206 H2O2 + .445 OH + .445 HO2 + .445 CO + .445 CO	5.00E-18	(Rickard and Pascoe, 2009)
G11681	TrGC	C4MDIAL + OH → .385 C3MCODBCO3 + .23 C4M2ALOHO2 + .385 MC3CODBCO3	4.41E-11	(Rickard and Pascoe, 2009)
G11683	TrGC	TLEMUCCO2H + OH → C615CO2O2	5.98E-11	(Rickard and Pascoe, 2009)
G11685	TrGC	TLEMUCCO3H + OH → TLEMUCCO3	6.29E-11	(Rickard and Pascoe, 2009)
G11687	TrGCN	TLEMUCPAN + OH → C5DICARB + CO + NO2	5.96E-11	(Rickard and Pascoe, 2009)
G11688	TrGCN	TLEMUCPAN → TLEMUCCO3 + NO2	k_PAN_M	(Rickard and Pascoe, 2009)*
G11689	TrGC	TLEMUCOOH + OH → TLEMUCCO + OH	7.04E-11	(Rickard and Pascoe, 2009)
G11691	TrGCN	TLEMUCNO3 + OH → TLEMUCCO + NO2	3.06E-11	(Rickard and Pascoe, 2009)
G11693	TrGC	TLEMUCCO + OH → CH3CO3 + EPXC4DIAL + CO	4.06E-11	(Rickard and Pascoe, 2009)
G11695	TrGC	C6H5CO3H + OH → C6H5CO3	4.66E-12	(Rickard and Pascoe, 2009)
G11697	TrGC	PHCOOH + OH → C6H5O2	1.10E-12	(Rickard and Pascoe, 2009)
G11698	TrGCN	PBZN + OH → C6H5OOH + CO + NO2	1.06E-12	(Rickard and Pascoe, 2009)
G11699	TrGCN	PBZN → C6H5CO3 + NO2	k_PAN_M*0.67	(Rickard and Pascoe, 2009)*
G11700	TrGCN	PTLQONE + NO3 → NPTLQO2	1.00E-12	(Rickard and Pascoe, 2009)
G11701	TrGC	PTLQONE + OH → PTLQO2	2.3E-11	(Rickard and Pascoe, 2009)
G11702	TrGCN	NCRES1O + NO2 → DNCRES	2.08E-12	(Rickard and Pascoe, 2009)
G11703	TrGCN	NCRES1O + O3 → NCRES1O2	2.86E-13	(Rickard and Pascoe, 2009)
G11704	TrGC	OXYL1OOH + OH → OXYL1O2	4.65E-11	(Rickard and Pascoe, 2009)
G11706	TrGCN	MNCATECH + NO3 → MNNCATECO2	5.03E-12	(Rickard and Pascoe, 2009)
G11707	TrGCN	MNCATECH + OH → MNCATECO2	6.83E-12	(Rickard and Pascoe, 2009)
G11708	TrGC	MCATEC1O2 + HO2 → MCATEC1OOH	KRO2HO2*0.820*(1-rchohch2o2_oh)	(Rickard and Pascoe, 2009)
G11708b	TrGC	MCATEC1O2 + HO2 → MCATEC1O + OH	KRO2HO2*0.820*rchohch2o2_oh	(Rickard and Pascoe, 2009)*
G11709	TrGCN	MCATEC1O2 + NO → MCATEC1O + NO2	KRO2NO	(Rickard and Pascoe, 2009)
G11709b	TrGCN	MCATEC1O2 + NO2 → MCATEC1O + NO3	KPHENO2NO2	(Jagiella and Zabel, 2007)*
G11710	TrGCN	MCATEC1O2 + NO3 → MCATEC1O + NO2	KRO2NO3	(Rickard and Pascoe, 2009)
G11711	TrGC	MCATEC1O2 → MCATEC1O	8.80E-13*RO2	(Rickard and Pascoe, 2009)
G11712	TrGCN	NPTLQO2 + HO2 → NPTLQOOH	KRO2HO2*0.820*(1-rcoch2o2_oh)	(Rickard and Pascoe, 2009)
G11712b	TrGCN	NPTLQO2 + HO2 → C7CO4DB + NO2 + OH	KRO2HO2*0.820*rcoch2o2_oh	(Rickard and Pascoe, 2009)*
G11713	TrGCN	NPTLQO2 + NO → C7CO4DB + NO2 + NO2	KRO2NO	(Rickard and Pascoe, 2009)*
G11714	TrGCN	NPTLQO2 + NO3 → C7CO4DB + NO2 + NO2	KRO2NO3	(Rickard and Pascoe, 2009)*

TABLE A.1: Gas phase reactions (... continued)

reaction			rate coefficient	reference
G11715	TrGCN	NPTLQO2 → C7CO4DB + NO2	8.80E-13*RO2	(Rickard and Pascoe, 2009)*
G11716	TrGC	PTLQO2 + HO2 → PTLQOOH	KRO2HO2*0.820*(1-rchohch2o2_oh-rcoch2o2_oh)	(Rickard and Pascoe, 2009)
G11716b	TrGC	PTLQO2 + HO2 → C6CO2OHCO3 + OH	KRO2HO2*0.820*(rchohch2o2_oh+rcoch2o2_oh)	(Rickard and Pascoe, 2009)*
G11717	TrGCN	PTLQO2 + NO → C6CO2OHCO3 + NO2	KRO2NO	(Rickard and Pascoe, 2009)*
G11718	TrGCN	PTLQO2 + NO3 → C6CO2OHCO3 + NO2	KRO2NO3	(Rickard and Pascoe, 2009)*
G11719	TrGC	PTLQO2 → C6CO2OHCO3	8.80E-13*RO2	(Rickard and Pascoe, 2009)*
G11720	TrGCN	DNCRES + NO3 → NDNCRESO2	7.83E-15	(Rickard and Pascoe, 2009)
G11721	TrGCN	DNCRES + OH → DNCRESO2	5.10E-14	(Rickard and Pascoe, 2009)
G11722	TrGCN	NCRES1O2 + HO2 → NCRES1OOH	KRO2HO2*0.820	(Rickard and Pascoe, 2009)
G11723	TrGCN	NCRES1O2 + NO → NCRES1O + NO2	KRO2NO	(Rickard and Pascoe, 2009)
G11723b	TrGCN	NCRES1O2 + NO2 → NCRES1O + NO3	KPHENO2NO2	(Jagiella and Zabel, 2007)*
G11724	TrGCN	NCRES1O2 + NO3 → NCRES1O + NO2	KRO2NO3	(Rickard and Pascoe, 2009)
G11725	TrGCN	NCRES1O2 → NCRES1O	KRO2sRO2*RO2	(Rickard and Pascoe, 2009)
G11726	TrGCN	MNNCATECO2 + HO2 → MNNCATCOOH	KRO2HO2*0.820*(1-rchohch2o2_oh)	(Rickard and Pascoe, 2009)
G11726b	TrGCN	MNNCATECO2 + HO2 → NC4MDCO2H + HCOCO2H + NO2 + OH	KRO2HO2*0.820*rchohch2o2_oh	(Rickard and Pascoe, 2009)*
G11727	TrGCN	MNNCATECO2 + NO → NC4MDCO2H + HCOCO2H + NO2 + NO2	KRO2NO	(Rickard and Pascoe, 2009)*
G11728	TrGCN	MNNCATECO2 + NO3 → NC4MDCO2H + HCOCO2H + NO2 + NO2	KRO2NO3	(Rickard and Pascoe, 2009)*
G11729	TrGCN	MNNCATECO2 → NC4MDCO2H + HCOCO2H + NO2	8.00E-13*RO2	(Rickard and Pascoe, 2009)
G11730	TrGCN	MNCATECO2 + HO2 → MNCATECOOH	KRO2HO2*0.820*(1-rchohch2o2_oh)	(Rickard and Pascoe, 2009)
G11730b	TrGCN	MNCATECO2 + HO2 → NC4MDCO2H + HCOCO2H + HO2 + OH	KRO2HO2*0.820*rchohch2o2_oh	(Rickard and Pascoe, 2009)*
G11731	TrGCN	MNCATECO2 + NO → NC4MDCO2H + HCOCO2H + HO2 + NO2	KRO2NO	(Rickard and Pascoe, 2009)*
G11732	TrGCN	MNCATECO2 + NO3 → NC4MDCO2H + HCOCO2H + HO2 + NO2	KRO2NO3	(Rickard and Pascoe, 2009)*
G11733	TrGCN	MNCATECO2 → NC4MDCO2H + HCOCO2H + HO2	8.00E-13*RO2	(Rickard and Pascoe, 2009)*
G11734	TrGC	MCATEC1OOH + OH → MCATEC1O2	2.05E-10	(Rickard and Pascoe, 2009)
G11736	TrGCN	C3MCODBPAN + OH → MGLYOX + CO + CO + NO2	4.37E-11	(Rickard and Pascoe, 2009)
G11737	TrGCN	C3MCODBPAN → C3MCODBCO3 + NO2	k_PAN_M	(Rickard and Pascoe, 2009)*
G11738	TrGC	MCOCOMOXO2 + HO2 → MCOCOMOOOH	KRO2HO2*0.625*(1-.4)	(Rickard and Pascoe, 2009)*
G11738b	TrGC	MCOCOMOXO2 + HO2 → HCHO + CH3CO3 + OH	KRO2HO2*0.625*.4	(Rickard and Pascoe, 2009)*
G11739	TrGCN	MCOCOMOXO2 + NO → HCHO + CH3CO3 + NO2	KRO2NO	(Rickard and Pascoe, 2009)*
G11740	TrGCN	MCOCOMOXO2 + NO3 → HCHO + CH3CO3 + NO2	KRO2NO3	(Rickard and Pascoe, 2009)*
G11741	TrGC	MCOCOMOXO2 → HCHO + CH3CO3	KRO2pORO2*RO2	(Rickard and Pascoe, 2009)*
G11742	TrGCN	NPTLQOOH + OH → NPTLQO2	8.56E-11	(Rickard and Pascoe, 2009)
G11744	TrGC	PTLQOOH + OH → PTLQCO + OH	1.42E-10	(Rickard and Pascoe, 2009)
G11746	TrGC	PTLQCO + OH → C6CO2OHCO3	7.95E-11	(Rickard and Pascoe, 2009)
G11747	TrGCN	NDNCRESO2 + HO2 → NDNCRESOOH	KRO2HO2*0.820*(1-rchohch2o2_oh)	(Rickard and Pascoe, 2009)
G11747b	TrGCN	NDNCRESO2 + HO2 → NC4MDCO2H + HNO3 + CO + CO + NO2 + OH	KRO2HO2*0.820*rchohch2o2_oh	(Rickard and Pascoe, 2009)*
G11748	TrGCN	NDNCRESO2 + NO → NC4MDCO2H + HNO3 + CO + CO + NO2 + NO2	KRO2NO	(Rickard and Pascoe, 2009)*
G11749	TrGCN	NDNCRESO2 + NO3 → NC4MDCO2H + HNO3 + CO + CO + NO2 + NO2	KRO2NO3	(Rickard and Pascoe, 2009)*
G11750	TrGCN	NDNCRESO2 → NC4MDCO2H + HNO3 + CO + CO + NO2	8.00E-13*RO2	(Rickard and Pascoe, 2009)*
G11751	TrGCN	DNCRESO2 + HO2 → DNCRESOOH	KRO2HO2*0.820*(1-rchohch2o2_oh)	(Rickard and Pascoe, 2009)
G11751b	TrGCN	DNCRESO2 + HO2 → NC4MDCO2H + HCOCO2H + NO2 + OH	KRO2HO2*0.820*rchohch2o2_oh	(Rickard and Pascoe, 2009)*
G11752	TrGCN	DNCRESO2 + NO → NC4MDCO2H + HCOCO2H + NO2 + NO2	KRO2NO	(Rickard and Pascoe, 2009)*
G11753	TrGCN	DNCRESO2 + NO3 → NC4MDCO2H + HCOCO2H + NO2 + NO2	KRO2NO3	(Rickard and Pascoe, 2009)*
G11754	TrGCN	DNCRESO2 → NC4MDCO2H + HCOCO2H + NO2	8.00E-13*RO2	(Rickard and Pascoe, 2009)*
G11755	TrGCN	NCRES1OOH + OH → NCRES1O2	1.53E-12	(Rickard and Pascoe, 2009)

TABLE A.1: Gas phase reactions (... continued)

reaction			rate coefficient	reference
G11757	TrGC	MNNCATCOOH + OH → MNNCATECO2	1.90E-12*EXP(190/TEMP)	(Rickard and Pascoe, 2009)
G11759	TrGCN	MNCATECOOH + OH → MNCATECO2	1.90E-12*EXP(190/TEMP)	(Rickard and Pascoe, 2009)
G11761	TrGCN	NO3 + CO23C3CHO → CH3CO3 + CO + CO + HNO3	KNO3AL*4.0	(Rickard and Pascoe, 2009)
G11762	TrGC	OH + CO23C3CHO → CH3CO3 + CO + CO	1.23E-11	(Rickard and Pascoe, 2009)
G11763	TrGC	C7CO4DB + OH → CO + CO + CH3CO3 + C33CO	9.58E-11	(Rickard and Pascoe, 2009)
G11765	TrGC	C6CO2OHCO3 + HO2 → C5134CO2OH + HO2 + CO + OH	KAPHO2*rco3_oh	(Rickard and Pascoe, 2009)*
G11766	TrGC	C6CO2OHCO3 + HO2 → C6COOHCO3H	KAPHO2*(rco3_ooh+rco3_o3)	(Rickard and Pascoe, 2009)*
G11767	TrGCN	C6CO2OHCO3 + NO → C5134CO2OH + HO2 + CO + NO2	KAPNO	(Rickard and Pascoe, 2009)
G11768	TrGCN	C6CO2OHCO3 + NO2 → C6CO2OHPAN	k_CH3CO3_NO2	(Rickard and Pascoe, 2009)*
G11769	TrGCN	C6CO2OHCO3 + NO3 → C5134CO2OH + HO2 + CO + NO2	KRO2NO3*1.74	(Rickard and Pascoe, 2009)
G11770	TrGC	C6CO2OHCO3 → C5134CO2OH + HO2 + CO	KRO2AP*RO2	(Rickard and Pascoe, 2009)
G11771	TrGCN	NDNCRESOOH + OH → NDNCRESO2	1.90E-12*EXP(190/TEMP)	(Rickard and Pascoe, 2009)
G11773	TrGCN	DNCRESOOH + OH → DNCRESO2	1.90E-12*EXP(190/TEMP)	(Rickard and Pascoe, 2009)
G11775	TrGC	C6COOHCO3H + OH → C6CO2OHCO3	9.29E-11	(Rickard and Pascoe, 2009)
G11777	TrGCN	C6CO2OHPAN + OH → C5134CO2OH + CO + CO + NO2	8.96E-11	(Rickard and Pascoe, 2009)
G11778	TrGCN	C6CO2OHPAN → C6CO2OHCO3 + NO2	k_PAN_M	(Rickard and Pascoe, 2009)*
G11800	TrGC	LXYL + OH → TLEPOXMUC + HO2 + $PXYL_T$LEPOXMUC + LCARBON	0.401E-11	(Rickard and Pascoe, 2009)*
G11801	TrGC	LXYL + OH → C6H5CH2O2 + $PXYL_C$6H5CH2O2 + LCARBON	0.101E-11	(Rickard and Pascoe, 2009)*
G11802	TrGC	LXYL + OH → CRESOL + $PXYL_C$RESOL + LCARBON	0.261E-11	(Rickard and Pascoe, 2009)*
G11803	TrGC	LXYL + OH → TLBIPERO2 + HO2 + $PXYL_T$LBIPERO2 + LCARBON	0.932E-11	(Rickard and Pascoe, 2009)*
G11805	TrGCN	LXYL + NO3 → C6H5CH2O2 + HNO3 + $PXYL_C$6H5CH2O2 + LCARBON	3.9E-16	(Rickard and Pascoe, 2009)*
G11806	TrGC	LTMB + OH → TLEPOXMUC + HO2 + $PTMB_T$LEPOXMUC + 2 LCARBON	0.827E-11	(Rickard and Pascoe, 2009)*
G11807	TrGC	LTMB + OH → C6H5CH2O2 + $PTMB_C$6H5CH2O2 + 2 LCARBON	0.189E-11	(Rickard and Pascoe, 2009)*
G11808	TrGC	LTMB + OH → CRESOL + $PTMB_C$RESOL + 2 LCARBON	0.141E-11	(Rickard and Pascoe, 2009)*
G11809	TrGC	LTMB + OH → TLBIPERO2 + HO2 + $PTMB_T$LBIPERO2 + 2 LCARBON	2.917E-11	(Rickard and Pascoe, 2009)*
G11810	TrGCN	LTMB + NO3 → C6H5CH2O2 + HNO3 + $PTMB_C$6H5CH2O2 + 2 LCARBON	1.52E-15	(Rickard and Pascoe, 2009)*
G11811	TrGC	EBENZ + OH → .10 TLEPOXMUC + .07 C6H5CH2O2 + .18 CRESOL + .65 TLBIPERO2 + 0.28 HO2 + LCARBON	7.00E-12	(Rickard and Pascoe, 2009)*
G11812	TrGCN	EBENZ + NO3 → C6H5CH2O2 + HNO3 + LCARBON	1.20E-16	(Rickard and Pascoe, 2009)*
G11813	TrGC	HAROM + OH → .14 TLEPOXMUC + .03 C6H5CH2O2 + .04 CRESOL + .79 TLBIPERO2 + 0.18 HO2 + 4 LCARBON	5.67E-11	(Rickard and Pascoe, 2009)*
G11814	TrGCN	HAROM + NO3 → C6H5CH2O2 + HNO3 + 4 LCARBON	2.60E-15	(Rickard and Pascoe, 2009)*
G11900	TrGCN	NO3 + STYRENE → NSTYRENO2	1.50E-12	(Rickard and Pascoe, 2009)
G11901	TrGC	O3 + STYRENE → .545 HCHO + .1 BENZENE + .28 C6H5O2 + .56 CO + .36 OH + .28 HO2 + .075 PHCOOH + .545 BENZAL + .09 H2O2 + .075 HCOOH	1.70E-17	(Rickard and Pascoe, 2009)*
G11902	TrGC	OH + STYRENE → STYRENO2	5.80E-11	(Rickard and Pascoe, 2009)
G11903	TrGCN	NSTYRENO2 + HO2 → NSTYRENOOH	KRO2HO2*0.859	(Rickard and Pascoe, 2009)
G11904	TrGCN	NSTYRENO2 + NO → NO2 + NO2 + HCHO + BENZAL	KRO2NO	(Rickard and Pascoe, 2009)*
G11905	TrGCN	NSTYRENO2 + NO3 → NO2 + NO2 + HCHO + BENZAL	KRO2NO3	(Rickard and Pascoe, 2009)*
G11906	TrGCN	NSTYRENO2 → NO2 + HCHO + BENZAL	KRO2sRO2*RO2	(Rickard and Pascoe, 2009)*
G11907	TrGCN	OH + NSTYRENOOH → NSTYRENO2	6.16E-11	(Rickard and Pascoe, 2009)
G11914	TrGC	STYRENO2 + HO2 → STYRENOOH	KRO2HO2*0.859*(1-rchohch2o2_oh)	(Rickard and Pascoe, 2009)
G11914b	TrGCN	STYRENO2 + HO2 → NO2 + OH + HCHO + BENZAL	KRO2HO2*0.859*rchohch2o2_oh	(Rickard and Pascoe, 2009)*

TABLE A.1: Gas phase reactions (... continued)

reaction			rate coefficient	reference
G11915	TrGCN	STYRENO2 + NO → NO2 + HO2 + HCHO + BENZAL	KRO2NO	(Rickard and Pascoe, 2009)*
G11916	TrGCN	STYRENO2 + NO3 → NO2 + HO2 + HCHO + BENZAL	KRO2NO3	(Rickard and Pascoe, 2009)*
G11917	TrGC	STYRENO2 → HO2 + HCHO + BENZAL	KRO2sRO2*RO2	(Rickard and Pascoe, 2009)*
G11918	TrGC	OH + STYRENOOH → STYRENO2	6.16E-11	(Rickard and Pascoe, 2009)

Aromatic gas phase reactions notes:

G11006b: reactions with KRO2Ho2

G11007: MGLYOX + GLYOX + HO2 from KDEC substitution

G11008: MGLYOX + GLYOX + HO2 from KDEC substitution

G11009: permutation reaction (minor channels removed)

G11018b: reactions with KRO2Ho2

G11019: KDEC C3DIALO → GLYOX + CO + HO2

G11020: KDEC C3DIALO → GLYOX + CO + HO2

G11021: permutation reaction (minor channels removed)

G11022: rco3_oh updated

G11023: rco3_ooh+rco3_o3 updated

G11055: KDEC NC4DCO2→ MALANHY + NO2

G11061: rco3_o3 updated

G11062: rco3_ooh updated

G11063: rco3_oh updated + KDEC MALDIALCO2 → .6 MALANHY + HO2 + .4 GLYOX + .4 CO

G11064: KDEC MALDIALCO2 → .6 MALANHY + HO2 + .4 GLYOX + .4 CO

G11066: KDEC MALDIALCO2 → .6 MALANHY + HO2 + .4 GLYOX + .4 CO

G11067: KDEC MALDIALCO2 → .6 MALANHY + HO2 + .4 GLYOX + .4 CO

G11069: KDEC BZFUONOOA → .5 BZFUONOO + .5 CO + .5 HCOCH2O2 + .5 OH and BZFUONOO → .625 CO14O3CO2H + .375 CO14O3CHO + .375 H2O2

G11078: updated rco3_oh

G11079: updated rco3_o3

G11080: updated rco3_ooh

G11084: Only major channel taken

G11093: KDEC: GLYOOA → .125 HCHO + .18 GLYOO + 0.82 HO2 + .57 OH + 1.265 CO and H2O substitution GLYOO → .625 HCOCO2H + .375 GLYOX + .375 H2O2

G11094: merged equations

G11100b: reactions with KRO2Ho2

G11101: KDEC MALANHYO → HCOCOHCO3

G11102: KDEC MALANHYO → HCOCOHCO3

G11103: Only major channel taken and KDEC MALANHYO → HCOCOHCO3

G11108b: reactions with KRO2Ho2

G11109: KDEC NBZFUO → .5 CO14O3CHO + .5 NO2 + .5 NBZFUONE + .5 HO2

G11110: KDEC NBZFUO → .5 CO14O3CHO + .5 NO2 + .5 NBZFUONE + .5 HO2

G11111: KDEC NBZFUO → .5 CO14O3CHO + .5 NO2 + .5 NBZFUONE + .5 HO2 and RO2 Only major channel taken

G11114: KDEC MALDIALCO2 → .6 MALANHY + HO2 + .4 GLYOX + .4 CO

G11119b: reactions with KRO2Ho2

G11120: KDEC MECOACETO → CH3CO3 + HCHO

G11121: KDEC MECOACETO → CH3CO3 + HCHO

G11122: KDEC MECOACETO → CH3CO3 + HCHO

G11127b: reactions with KRO2Ho2

G11128: KDEC BZFUO → CO14O3CHO + HO2

G11129: KDEC BZFUO → CO14O3CHO + HO2

G11130: KDEC BZFUO → CO14O3CHO + HO2 and Only major channel taken

G11135b: reactions with KRO2Ho2

G11136: KDEC MALDIALO → GLYOX + GLYOX + HO2

G11137: KDEC MALDIALO → GLYOX + GLYOX + HO2

G11138: KDEC MALDIALO → GLYOX + GLYOX + HO2 and Only major channel taken

G11150: KDEC NC4MDCO2 → MMALANHY + NO2

G11154b: reactions with KRO2Ho2

G11155: KDEC NTLFUO → ACCOMECHO + NO2

G11156: KDEC NTLFUO → ACCOMECHO + NO2

G11157: KDEC NTLFUO → ACCOMECHO

G11160: KDEC MC3CODBCO2 → .35 GLYOX + .35 CH3O2 + .35 CO + .65 MMALANHY + .65 HO2 and updated rco3_oh

G11161: updated rco3_o3

G11162: updated rco3_ooh

G11163: KDEC MC3CODBCO2 → .35 GLYOX + .35 CH3O2 + .35 CO + .65 MMALANHY + .65 HO2

G11165: KDEC MC3CODBCO2 → .35 GLYOX + .35 CH3O2 + .35 CO + .65 MMALANHY + .65 HO2

G11166a: KDEC MC3CODBCO2 → .35 GLYOX + .35 CH3O2 + .35 CO + .65 MMALANHY + .65 HO2 and Only major channel taken

G11166b: product distribution of the RCO3 + RO2 reactions

G11172: updated rco3_ooh+ rco3_o3

G11173: updated rco3_oh

G11179b: reactions with KRO2Ho2

G11180: KDEC NPXYFUO → C23O3CCHO + NO2

G11181: KDEC NPXYFUO → C23O3CCHO + NO2

G11182: KDEC NPXYFUO → C23O3CCHO + NO2

G11183b: reactions with KRO2Ho2

G11184: KDEC MMALANHYO→CO2H3CO3

G11185: KDEC MMALANHYO→CO2H3CO3

G11186: KDEC MMALANHYO→CO2H3CO3 and Only major channel taken

G11194: updated rco3_oh and KDEC C5CO14CO2 →.83 MALANHY + .83 CH3O2 + .17 MGLYOX + .17 HO2 + .17 CO

G11195: updated rco3_o3

G11196: updated rco3_ooh

G11197: KDEC C5CO14CO2 →.83 MALANHY + .83 CH3O2 + .17 MGLYOX + .17 HO2 + .17 CO

G11199: KDEC C5CO14CO2 →.83 MALANHY + .83 CH3O2 + .17 MGLYOX + .17 HO2 + .17 CO

G11200: KDEC C5CO14CO2 →.83 MALANHY + .83 CH3O2 + .17 MGLYOX + .17 HO2 + .17 CO and Only major channel taken

G11205: KDEC C5CO14CO2 → .83 MALANHY + .83 CH3O2 + .17 MGLYOX + .17 HO2 + .17 CO

G11207b: reactions with KRO2Ho2

G11208: KDEC NPXYFUO → C23O3CCHO + NO2

G11209: KDEC NPXYFUO → C23O3CCHO + NO2

G11210: KDEC NPXYFUO → C23O3CCHO + NO2

//1. original //C5DICARB + O3 = GLYOX + MGLOOB : 2.00E-18*0.5 ;

//1. KDEC C5DICARB + O3 = GLYOX + .125 CH3CHO + .695 CH3CO3 + .57 CO + .57 OH + .125 HO2 +.18 MGLOO : 2.00E-18*0.5 ;

//2. original //C5DICARB + O3 = MGLYOX + GLYOOA : 2.00E-18*0.5 ;

//2. KDEC C5DICARB + O3 = MGLYOX + .125 HCHO + .18 GLYOO + 0.82 HO2 + .57 OH + 1.265 CO : 2.00E-18*0.5 ;

//3. All merged C5DICARB + O3 = .5 GLYOX + .063 CH3CHO + .348 CH3CO3 + .285 CO + .285 OH + .063 HO2 +.09 MGLOO + .5 MGLYOX + .063 HCHO + .09 GLYOO + 0.41 HO2 + .285 OH + .633 CO

G11215: KDEC MC3CODBCO2 → .35 GLYOX + .35 CH3O2 + .35 CO + .65 MMALANHY + .65 HO2

G11218: updated rco3_o3

G11219: updated rco3_ooh

G11230: updated rco3_oh

G11234: Only major channel taken

G11236: KDEC TLFUONOOA →.5 CO + .5 OH + .5 MECOACETO2 + .5 TLFUONOO and H2Osubs TLFUONOO →.625 C24O3CCO2H + .375 ACCOMECHO + .375 H2O2

G11238: updated rco3_ooh+rco3_o3

G11239: updated rco3_oh

G11248b: reactions with KRO2Ho2

G11249: KDEC C4M2ALOHO → GLYOX + MGLYOX + HO2

G11250: KDEC C4M2ALOHO → GLYOX

+ MGLYOX + HO2
G11251: Only major channel taken
G11267: KDEC C4M2ALOHO2 →GLYOX + MGLYOX + HO2
G11270: updated `rco3_oh` and KDEC C3MCODBCO2 → .35 MGLYOX + .35 HO2 + .35 CO + .65 MMALANHY + .65 HO2
G11271: updated `rco3_ooh`+`rco3_o3`
G11272: KDEC C3MCODBCO2 → .35 MGLYOX + .35 HO2 + .35 CO + .65 MMALANHY + .65 HO2
G11274: KDEC C3MCODBCO2 → .35 MGLYOX + .35 HO2 + .35 CO + .65 MMALANHY + .65 HO2
G11275: KDEC C3MCODBCO2 → .35 MGLYOX + .35 HO2 + .35 CO + .65 MMALANHY + .65 HO2
G11280b: KDEC NTLFUO → ACCOMECHO + NO2 and reactions with KRO2Ho2
G11281: KDEC NTLFUO → ACCOMECHO + NO2
G11282: KDEC NTLFUO → ACCOMECHO + NO2
G11283: KDEC NTLFUO → ACCOMECHO + NO2
G11306b: KDEC C5DIALO →MALDIAL + CO + HO2 and reactions with KRO2Ho2
G11307: KDEC C5DIALO →MALDIAL
G11308: KDEC C5DIALO →MALDIAL
G11309: KDEC C5DIALO →MALDIAL
G11358b: reactions with KRO2Ho2 and KDEC C615CO2O → C5DICARB + CO + HO2
G11359: KDEC C615CO2O → C5DICARB + CO + HO2
G11360: KDEC C615CO2O → C5DICARB + CO + HO2
G11361: Only major channel taken
G11368b: reactions with KRO2Ho2 and KDEC NDNPHENO → NC4DCO2H + HNO3 + CO + CO + NO2
G11369: KDEC NDNPHENO → NC4DCO2H + HNO3 + CO + CO + NO2
G11370: KDEC NDNPHENO → NC4DCO2H + HNO3 + CO + CO + NO2
G11371: KDEC NDNPHENO → NC4DCO2H + HNO3 + CO + CO + NO2
G11373: KDEC CATECOOA → MALDALCO2H + HCOCO2H + HO2 + OH
G11380: updated `rco3_ooh`+`rco3_o3`
G11381: updated `rco3_oh`
G11387: KDEC GLYOOA → .125 HCHO + .18 GLYOO + .82 HO2 + .57 OH + 1.265 CO
G11390b: reactions with KRO2Ho2 and KDEC NCATECO → NC4DCO2H + HCOCO2H + HO2
G11391: KDEC NCATECO → NC4DCO2H + HCOCO2H + HO2
G11392: KDEC NCATECO → NC4DCO2H + HCOCO2H + HO2
G11393: KDEC NCATECO → NC4DCO2H + HCOCO2H + HO2
G11396b: reactions with KRO2Ho2 and KDEC NPHENO → MALDALCO2H + GLYOX + NO2
G11397: KDEC NPHENO → MALDALCO2H + GLYOX + NO2
G11398: KDEC NPHENO → MALDALCO2H + GLYOX + NO2
G11399: KDEC NPHENO → MALDALCO2H + GLYOX + NO2
G11400: merged equations
G11407b: reactions with KRO2Ho2 and KDEC NNCATECO → NC4DCO2H + HCOCO2H + NO2
G11408: KDEC NNCATECO → NC4DCO2H + HCOCO2H + NO2
G11409: KDEC NNCATECO → NC4DCO2H + HCOCO2H + NO2
G11410: KDEC NNCATECO → NC4DCO2H + HCOCO2H + NO2
G11419: merged equations(same rate c.)
G11420: merged equation(same rate c.)
G11423b: reactions with KRO2Ho2 and KDEC PHENO → .71 MALDALCO2H + .71 GLYOX + .29 PBZQONE + HO2
G11424: KDEC PHENO → .71 MALDALCO2H + .71 GLYOX + .29 PBZQONE + HO2
G11425: KDEC PHENO → .71 MALDALCO2H + .71 GLYOX + .29 PBZQONE + HO2
G11426: KDEC PHENO → .71 MALDALCO2H + .71 GLYOX + .29 PBZQONE + HO2 and Only major channel taken
G11430: updated `rco3_ooh`+`rco3_o3`
G11431: `rco3_oh`
G11437b: new channel
G11442: HOC6H4NO2 is a nitro-phenol
G11458b: reactions with KRO2Ho2 and KDEC PBZQO →C5CO2OHCO3
G11459: KDEC PBZQO →C5CO2OHCO3
G11460: KDEC PBZQO →C5CO2OHCO3
G11461: KDEC PBZQO →C5CO2OHCO3 and Only major channel taken
G11464b: reactions with KRO2Ho2 and KDEC DNPHENO → NC4DCO2H + HCOCO2H + NO2
G11465: KDEC DNPHENO → NC4DCO2H + HCOCO2H + NO2
G11466: KDEC DNPHENO → NC4DCO2H + HCOCO2H + NO2
G11467: KDEC DNPHENO → NC4DCO2H + HCOCO2H + NO2
G11470b: reactions with KRO2Ho2 and KDEC BZEMUCO → .5 EPXC4DIAL + .5 GLYOX + .5 HO2 + .5 C3DIALO2 + .5 C32OH13CO
G11472: KDEC BZEMUCO → .5 EPXC4DIAL + .5 GLYOX + .5 HO2 + .5 C3DIALO2 + .5 C32OH13CO
G11473: KDEC BZEMUCO → .5 EPXC4DIAL + .5 GLYOX + .5 HO2 + .5 C3DIALO2 + .5 C32OH13CO
G11474: KDEC BZEMUCO → .5 EPXC4DIAL + .5 GLYOX + .5 HO2 + .5 C3DIALO2 + .5 C32OH13CO and Only major channel taken
G11483b: reactions with KRO2Ho2 and KDEC NBZQO → C6CO4DB + NO2
G11484: KDEC NBZQO → C6CO4DB + NO2
G11485: KDEC NBZQO → C6CO4DB + NO2
G11486: KDEC NBZQO → C6CO4DB + NO2
G11490b: new channel
G11499: updated `rco3_o3`
G11500: updated `rco3_ooh`
G11501: updated `rco3_oh`
G11505: Only major channel taken
G11507b: new channel
G11601: merged eq. under same rate c.
G11603b: KDEC BZBIPERO → GLYOX + HO2 + .5 BZFUONE + .5 BZFUONE
G11604: KDEC BZBIPERO → GLYOX + HO2 + .5 BZFUONE + .5 BZFUONE
G11605: KDEC BZBIPERO → GLYOX + HO2 + .5 BZFUONE + .5 BZFUONE and Only major channel taken
G11607: KROPRIM*O2 fast reaction C6H5CH2O = BENZAL + HO2
G11607b: KROPRIM*O2 fast reaction C6H5CH2O = BENZAL + HO2
G11608: KROPRIM*O2 fast reaction C6H5CH2O = BENZAL + HO2
G11609: KROPRIM*O2 fast reaction C6H5CH2O = BENZAL + HO2 and C6H5CH2OH replaced with its ox. product BENZAL
G11610: merged eq under the same rate C.
G11611: merged eq under the same rate C.
G11613: KDEC TLBIPERO →.6 GLYOX + .4 MGLYOX + HO2 + .2 ZCODC23DBCOD + .2 C5DICARB + .2 TLFUONE + .2 BZFUONE + .2 MALDIAL
G11615: KDEC TLBIPERO →.6 GLYOX + .4 MGLYOX + HO2 + .2 ZCODC23DBCOD + .2 C5DICARB + .2 TLFUONE + .2 BZFUONE + .2 MALDIAL
G11616: Only major channel and KDEC TLBIPERO →.6 GLYOX + .4 MGLYOX + HO2 + .2 ZCODC23DB COD + .2 C5DICARB + .2 TLFUONE + .2 BZFUONE + .2 MALDIAL
G11618: KDEC MGLOOB → .125 CH3CHO + .695 CH3CO3 + .57 CO + .57 OH + .125 HO2 +.18 MGLOO
G11619: merged equations
G11629b: reactions with KRO2Ho2 and KDEC CRESO → .68 C5CO14OH + .68 GLYOX + HO2 + .32 PTLQONE
G11630: KDEC CRESO → .68 C5CO14OH + .68 GLYOX + HO2 + .32 PTLQONE
G11631: KDEC CRESO → .68 C5CO14OH + .68 GLYOX + HO2 + .32 PTLQONE
G11632: KDEC CRESO → .68 C5CO14OH + .68 GLYOX + HO2 + .32 PTLQONE and Only major channel taken
G11633b: reactions with KRO2Ho2 and KDEC NCRESO → C5CO14OH + GLYOX + NO2
G11634: KDEC NCRESO → C5CO14OH + GLYOX + NO2
G11635: KDEC NCRESO → C5CO14OH + GLYOX + NO2
G11636: KDEC NCRESO → C5CO14OH + GLYOX + NO2 and Only major channel taken
G11637: TOL1OHNO2 is a nitro-phenol
G11640: KDEC MCATECOOA → MC3ODBCO2H + HCOCO2H + HO2 + OH
G11648: updated `rco3_oh`
G11649: updated `rco3_o3`
G11650: updated `rco3_ooh`
G11654: Only major channel taken
G11655b: reactions with KRO2Ho2 and KDEC TLEMUCO→ .5 C3DIALO2 +

.5 CO2H3CHO + .5 EPXC4DIAL + .5 MGLYOX + .5 HO2

G11656b: KDEC TLEMUCO→ .5 C3DIALO2 + .5 CO2H3CHO + .5 EPXC4DIAL + .5 MGLYOX + .5 HO2

G11657: KDEC TLEMUCO→ .5 C3DIALO2 + .5 CO2H3CHO + .5 EPXC4DIAL + .5 MGLYOX + .5 HO2

G11658: KDEC TLEMUCO→ .5 C3DIALO2 + .5 CO2H3CHO + .5 EPXC4DIAL + .5 MGLYOX + .5 HO2 and Only major channel taken

G11659: branching ratios from Roth et al 2010

G11660: branching ratios from Roth et al 2010

G11661: branching ratios from Roth et al 2010

G11665: Only major channel taken

G11674b: new channel

G11680: already in MIM3

G11681: already in MIM3

G11708b: reactions with KRO2Ho2

G11709b: new channel

G11712b: reactions with KRO2Ho2 and KDEC NPTLQO → C7CO4DB + NO2

G11713: KDEC NPTLQO → C7CO4DB + NO2

G11714: KDEC NPTLQO → C7CO4DB + NO2

G11715: KDEC NPTLQO → C7CO4DB + NO2

G11716b: reactions with KRO2Ho2 and KDEC PTLQO → C6CO2OHCO3

G11717: KDEC PTLQO → C6CO2OHCO3

G11718: KDEC PTLQO → C6CO2OHCO3

G11719: Only major channel taken and KDEC PTLQO → C6CO2OHCO3

G11723b: new channel

G11726b: reactions with KRO2Ho2 and KDEC MNNCATECO → NC4MDCO2H + HCOCO2H + NO2

G11727: KDEC MNNCATECO → NC4MDCO2H + HCOCO2H + NO2

G11728: KDEC MNNCATECO → NC4MDCO2H + HCOCO2H + NO2

G11730b: reactions with KRO2Ho2 and KDEC MNCATECO → NC4MDCO2H + HCOCO2H + HO2

G11731: KDEC MNCATECO → NC4MDCO2H + HCOCO2H + HO2

G11732: KDEC MNCATECO → NC4MDCO2H + HCOCO2H + HO2

G11733: KDEC MNCATECO → NC4MDCO2H + HCOCO2H + HO2

G11738: RO2 with ether function.

G11738b: reactions with KRO2Ho2 and KDEC MCOCOMOXO → HCHO + CH3CO3. According to Orlando and Tyndall (2012) 40% of OH and aldehyde results from the reaction with HO2

G11739: KDEC MCOCOMOXO → HCHO + CH3CO3

G11740: KDEC MCOCOMOXO → HCHO + CH3CO3

G11741: KDEC MCOCOMOXO → HCHO + CH3CO3

G11747b: reactions with KRO2Ho2 and KDEC NDNCRESO → NC4MDCO2H + HNO3 + CO + CO + NO2

G11748: KDEC NDNCRESO → NC4MDCO2H + HNO3 + CO + CO + NO2

G11749: KDEC NDNCRESO → NC4MDCO2H + HNO3 + CO + CO + NO2

G11750: KDEC NDNCRESO → NC4MDCO2H + HNO3 + CO + CO + NO2

G11751b: reactions with KRO2Ho2 and KDEC DNCRESO → NC4MDCO2H + HCOCO2H + NO2

G11752: KDEC DNCRESO → NC4MDCO2H + HCOCO2H + NO2

G11753: KDEC DNCRESO → NC4MDCO2H + HCOCO2H + NO2

G11754: KDEC DNCRESO → NC4MDCO2H + HCOCO2H + NO2

G11765: updated `rco3_oh`

G11766: updated `rco3_ooh`+`rco3_o3`

G11800: For consistency, we use the same products as for TOLUENE

G11801: For consistency, we use the same products as for TOLUENE

G11802: For consistency, we use the same products as for TOLUENE

G11803: For consistency, we use the same products as for TOLUENE

G11805: For consistency, we use the same products as for TOLUENE

G11806: For consistency, we use the same products as for TOLUENE

G11807: For consistency, we use the same products as for TOLUENE

G11808: For consistency, we use the same products as for TOLUENE

G11809: For consistency, we use the same products as for TOLUENE

G11810: For consistency, we use the same products as for TOLUENE

G11811: merged under same rate constant

G11812: For consistency, we use the same products as for TOLUENE

G11813: we use DIET35TOL(from MCM) as representative of Higher aromatics

G11814: For consistency, we use the same products as for TOLUENE

G11901: KDEC CH2OOB → .24 CH2OO + .40 CO + .36 HO2 + .36 CO + .36 OH and H2Osubs PHCHOO → .625 PHCOOH + .375 BENZAL + .375 H2O2

G11904: KDEC NSTYRENEO → NO2 + HCHO + BENZAL

G11905: KDEC NSTYRENEO → NO2 + HCHO + BENZAL

G11906: KDEC NSTYRENEO → NO2 + HCHO + BENZAL

G11914b: KDEC STYRENO → HO2 + HCHO + BENZAL and reactions with KRO2Ho2

G11915: KDEC STYRENO → HO2 + HCHO + BENZAL

G11916: KDEC STYRENO → HO2 + HCHO + BENZAL

G11917: KDEC STYRENO → HO2 + HCHO + BENZAL

TABLE A.2: Photolysis reactions. Labels follow same nomenclature as for table 1, with the addition of "J" meaning photolysis equations. Rate coefficients definition are taken from (Taraborrelli et al., 2008).

#	labels	reaction	rate coefficient	reference
J11011	TrGCJ	MCOCOMOOOH + hv → CH3CO3 + HCHO + OH	J_ACETOL+jx(ip_CH3OOH)	(Rickard and Pascoe, 2009)*
J11014	TrGCJ	C33CO + hv → CO + HO2 + CO + CO + HO2	jx(ip_HOCH2CHO)*2	(Rickard and Pascoe, 2009)
J11017	TrGCJ	C3DIALOOH + hv → GLYOX + CO + HO2 + OH	jx(ip_HOCH2CHO)*2+jx(ip_CH3OOH)	(Rickard and Pascoe, 2009)*
J11041	TrGCJ	C5DIALCO + hv → MALDIALCO3 + CO + HO2	jx(ip_MGLYOX)+jx(ip_MACR)	(Rickard and Pascoe, 2009)
J11045	TrGCJ	C32OH13CO + hv → GLYOX + HO2 + HO2 + CO	jx(ip_HOCH2CHO)*2	(Rickard and Pascoe, 2009)
J11047	TrGCJ	HCOCOHCO3H + hv → GLYOX + HO2 + OH	jx(ip_CH3OOH)	(Rickard and Pascoe, 2009)
J11053	TrGCJ	MALDIALOOH + hv → C32OH13CO + CO + OH + HO2	jx(ip_HOCH2CHO)*2	(Rickard and Pascoe, 2009)
J11054	TrGCJ	MALDIALOOH + hv → GLYOX + GLYOX + HO2 + OH	jx(ip_CH3OOH)	(Rickard and Pascoe, 2009)*
J11058	TrGCJ	BZFUOOH + hv → CO14O3CHO + HO2 + OH	jx(ip_CH3OOH)	(Rickard and Pascoe, 2009)*
J11060	TrGCJ	HOCOC4DIAL + hv → HCOCOHCO3 + HO2 + CO	jx(ip_MGLYOX)+jx(ip_HOCH2CHO)	(Rickard and Pascoe, 2009)
J11072	TrGCJN	NBZFUOOH + hv → .5 CO14O3CHO + .5 NO2 + .5 NBZFUONE + .5 HO2 + OH	jx(ip_CH3OOH)	(Rickard and Pascoe, 2009)*
J11074	TrGCJ	MALDALCO3H + hv → HCOCO3H + HO2 + CO + HO2 + CO	jx(ip_MACR)	(Rickard and Pascoe, 2009)
J11075	TrGCJ	MALDALCO3H + hv → .6 MALANHY + HO2 + .4 GLYOX + .4 CO + OH	jx(ip_CH3OOH)	(Rickard and Pascoe, 2009)*
J11077	TrGCJ	EPXDLCO2H + hv → C3DIALO2 + HO2	2.77*jx(ip_HOCH2CHO)	(Rickard and Pascoe, 2009)
J11095	TrGCJ	MALDIAL + hv → .4 BZFUONE + .6 MALDIALCO3 + .6 HO2	4.E3*jx(ip_MVK)*0.14	(Rickard and Pascoe, 2009)
J11097	TrGCJ	MALANHYOOH + hv → HCOCOHCO3 + OH	jx(ip_CH3OOH)	(Rickard and Pascoe, 2009)*
J11105	TrGCJ	EPXDLCO3H + hv → C3DIALO2 + OH	jx(ip_CH3OOH)+2.77*jx(ip_HOCH2CHO)	(Rickard and Pascoe, 2009)
J11107	TrGCJ	CO2C4DIAL + hv → CO + CO + HO2 + HO2 + CO + CO	jx(ip_MGLYOX)*2	(Rickard and Pascoe, 2009)
J11112	TrGCJ	CO23C3CHO + hv → CH3CO3 + CO + CO + HO2	jx(ip_MGLYOX)	(Rickard and Pascoe, 2009)
J11113	TrGCJ	CO23C3CHO + hv → CH3CO3 + HCOCO3	2.15*jx(ip_MGLYOX)	(Rickard and Pascoe, 2009)
J11115	TrGCJ	MALDALCO2H + hv → HCOCO2H + HO2 + CO + HO2 + CO	jx(ip_MACR)	(Rickard and Pascoe, 2009)
J11118	TrGCJ	EPXC4DIAL + hv → C3DIALO2 + CO + HO2	2.77*jx(ip_HOCH2CHO)*2	(Rickard and Pascoe, 2009)
J11125	TrGCJ	CO14O3CHO + hv → HO2 + CO + HCOCH2O2	jx(ip_MGLYOX)	(Rickard and Pascoe, 2009)
J11134	TrGCJ	C23O3CHO + hv → CO + HO2 + CH3CO3	J_ACETOL	(Rickard and Pascoe, 2009)
J11153	TrGCJ	C54CO + hv → HO2 + CO + CO + CO + CH3CO3	jx(ip_MGLYOX)+2.15*jx(ip_MGLYOX)*2	(Rickard and Pascoe, 2009)
J11159	TrGCJ	C5134CO2OH + hv → CO23C3CHO + HO2 + CO + HO2	jx(ip_HOCH2CHO)+2.15*jx(ip_MGLYOX)	(Rickard and Pascoe, 2009)
J11170	TrGCJ	C5DIALOOH + hv → MALDIAL + CO + HO2 + OH	jx(ip_CH3OOH)+jx(ip_MACR)	(Rickard and Pascoe, 2009)*
J11188	TrGCNJ	NPXYFUOOH + hv → C23O3CCHO + NO2 + OH	jx(ip_CH3OOH)	(Rickard and Pascoe, 2009)*
J11191	TrGCJ	C23O3CCHO + hv → CO + MCOCOMOXO2 + HO2	jx(ip_HOCH2CHO)	(Rickard and Pascoe, 2009)
J11202	TrGCJ	PXYFUOOH + hv → C23O3CCHO + HO2 + OH	jx(ip_CH3OOH)	(Rickard and Pascoe, 2009)*
J11206	TrGCJ	C5CO14OH + hv → CH3CO3 + HCOCO2H + HO2 + CO	jx(ip_MVK)	(Rickard and Pascoe, 2009)
J11214	TrGCJ	C5DICARB + hv → .6 C5CO14O2 + .6 HO2 + .4 TLFUONE	jx(ip_NO2)*0.2	(Rickard and Pascoe, 2009)*
J11216	TrGCJ	MC3ODBCO2H + hv → CH3COCO2H + HO2 + CO + HO2 + CO	jx(ip_MACR)	(Rickard and Pascoe, 2009)
J11245	TrGCJ	C4CO2DCO3H + hv → HO2 + CO + C33CO + OH	jx(ip_CH3OOH)+jx(ip_MGLYOX)	(Rickard and Pascoe, 2009)
J11254	TrGCJ	ACCOMECHO + hv → MECOACETO2 + HO2 + CO	jx(ip_HOCH2CHO)	(Rickard and Pascoe, 2009)
J11256	TrGCJ	MMALNHYOOH + hv → CO2H3CO3 + OH	jx(ip_CH3OOH)	(Rickard and Pascoe, 2009)*

TABLE A.2: Photolysis reactions (... continued)

#	labels	reaction	rate coefficient	reference
J11259	TrGCJ	C5DICAROOH + hv → MGLYOX + GLYOX + HO2 + OH	jx(ip_CH3OOH)+jx(ip_HOCH2CHO)+J_ACETOL	(Rickard and Pascoe, 2009)*
J11262	TrGCNJ	NTLFUOOH + hv → ACCOMECHO + NO2 + OH	jx(ip_CH3OOH)	(Rickard and Pascoe, 2009)*
J11264	TrGCJ	MECOACEOOH + hv → CH3CO3 + HCHO + OH	jx(ip_CH3OOH)	(Rickard and Pascoe, 2009)*
J11268	TrGCJ	C4MALOHOOH + hv → GLYOX + MGLYOX + HO2 + OH	jx(ip_CH3OOH)	(Rickard and Pascoe, 2009)
J11269	TrGCJ	C4MALOHOOH + hv → CO2H3CHO + HO2 + CO + OH	2.77*jx(ip_HOCH2CHO)*2	(Rickard and Pascoe, 2009)
J11285	TrGCJ	C5CO14OOH + hv → .83 MALANHY + .83 CH3O2 + .17 MGLYOX + .17 HO2 + .17 CO + OH	jx(ip_CH3OOH)	(Rickard and Pascoe, 2009)*
J11295	TrGCJ	C4CODBCO3H + hv → .35 MGLYOX + .35 HO2 + .35 CO + .65 MMALANHY + .65 HO2 + OH	jx(ip_CH3OOH)	(Rickard and Pascoe, 2009)*
J11296	TrGCJ	C4CODBCO3H + hv → HCOCO3H + HO2 + CO + CH3CO3	jx(ip_MACR)	(Rickard and Pascoe, 2009)
J11298	TrGCJ	TLFUOOH + hv → ACCOMECHO + HO2 + OH	jx(ip_CH3OOH)	(Rickard and Pascoe, 2009)*
J11300	TrGCJ	C23O3CCO3H + hv → OH + MCOCOMOXO2	jx(ip_CH3OOH)	(Rickard and Pascoe, 2009)
J11302	TrGCJ	MC3ODBCO3H + hv → CH3COCO3H + HO2 + CO + HO2 + CO	jx(ip_MACR)	(Rickard and Pascoe, 2009)
J11303	TrGCJ	MC3ODBCO3H + hv → .35 GLYOX + .35 CH3O2 + .35 CO + .65 MMALANHY + .65 HO2 + OH	jx(ip_CH3OOH)	(Rickard and Pascoe, 2009)*
J11305	TrGCJ	ACCOMECO3H + hv → MECOACETO2 + OH	jx(ip_CH3OOH)	(Rickard and Pascoe, 2009)
J11351	TrGCJ	PHENOOH + hv → .71 MALDALCO2H + .71 GLYOX + .29 PBZQONE + HO2 + OH	jx(ip_CH3OOH)	(Rickard and Pascoe, 2009)*
J11353	TrGCJ	C6CO4DB + hv → C4CO2DBCO3 + HO2 + CO	jx(ip_MGLYOX)*2	(Rickard and Pascoe, 2009)
J11355	TrGCJ	C5CO2DCO3H + hv → CH3CO3 + C33CO + OH	jx(ip_CH3OOH)+jx(ip_MGLYOX)	(Rickard and Pascoe, 2009)
J11357	TrGCNJ	NDNPHENOOH + hv → NC4DCO2H + HNO3 + CO + CO + NO2 + OH	jx(ip_CH3OOH)	(Rickard and Pascoe, 2009)*
J11365	TrGCNJ	BZBIPERNO3 + hv → GLYOX + HO2 + .5 BZFUONE + .5 BZFUONE + NO2	J_IC3H7NO3	(Rickard and Pascoe, 2009)*
J11367b	TrGCNJ	HOC6H4NO2 + hv → HONO + PHONOnitrop + CPENTDIENKETENE	jx(ip_HOC6H4NO2)	see note
J11367c	TrGCJ	CPENTDIENKETENE + hv → CO2 + CO + 2 HO2 + MALDIAL	J_KETENE	see note
J11377	TrGCJ	C5COOHCO3H + hv → HOCOC4DIAL + HO2 + CO + OH	jx(ip_CH3OOH)	(Rickard and Pascoe, 2009)
J11389	TrGCJ	BZEPOXMUC + hv → .5 C5DIALO2 + 1.5 HO2 + 1.5 CO + .5 MALDIAL	jx(ip_NO2)*0.1	(Rickard and Pascoe, 2009)
J11395	TrGCJN	NPHEN1OOH + hv → NPHEN1O + OH	jx(ip_CH3OOH)	(Rickard and Pascoe, 2009)
J11406	TrGCJ	BZEMUCCO + hv → HCOCOHCO3 + C3DIALO2	jx(ip_HOCH2CHO)*2+J_ACETOL	(Rickard and Pascoe, 2009)
J11412	TrGCJ	BZEMUCCO2H + hv → C5DIALO2 + HO2	jx(ip_MACR)	(Rickard and Pascoe, 2009)
J11414	TrGCNJ	NNCATECOOH + hv → NC4DCO2H + HCOCO2H + NO2 + OH	jx(ip_CH3OOH)	(Rickard and Pascoe, 2009)*
J11428	TrGCJ	C615CO2OOH + hv → C5DICARB + CO + HO2 + OH	jx(ip_MVK)+jx(ip_CH3OOH)	(Rickard and Pascoe, 2009)
J11441	TrGCNJ	NPHENOOH + hv → MALDALCO2H + GLYOX + OH + NO2	J_IC3H7NO3+jx(ip_CH3OOH)	(Rickard and Pascoe, 2009)
J11445	TrGCNJ	NCATECOOH + hv → NC4DCO2H + HCOCO2H + HO2 + OH	jx(ip_CH3OOH)	(Rickard and Pascoe, 2009)*
J11457	TrGCJ	PBZQOOH + hv → C5CO2OHCO3 + OH	jx(ip_CH3OOH)	(Rickard and Pascoe, 2009)*
J11463	TrGCJ	BZOBIPEROH + hv → MALDIALCO3 + GLYOX + HO2	J_ACETOL	(Rickard and Pascoe, 2009)
J11469	TrGCJ	BZBIPEROOH + hv → GLYOX + HO2 + .5 BZFUONE + .5 BZFUONE + OH	jx(ip_CH3OOH)	(Rickard and Pascoe, 2009)*
J11478	TrGCNJ	NBZQOOH + hv → C6CO4DB + NO2 + OH	jx(ip_CH3OOH)	(Rickard and Pascoe, 2009)*
J11480	TrGCJ	CATEC1OOH + hv → CATEC1O + OH	jx(ip_CH3OOH)	(Rickard and Pascoe, 2009)
J11482	TrGCJ	C6125CO + hv → C5CO14O2 + CO + HO2	jx(ip_MGLYOX)+jx(ip_MVK)	(Rickard and Pascoe, 2009)
J11488	TrGCNJ	DNPHENOOH + hv → NC4DCO2H + HCOCO2H + NO2 + OH	jx(ip_CH3OOH)	(Rickard and Pascoe, 2009)*
J11494	TrGCJ	BZEMUCCO3H + hv → C5DIALO2 + OH	jx(ip_CH3OOH)+jx(ip_MACR)	(Rickard and Pascoe, 2009)
J11496	TrGCJ	C6H5OOH + hv → C6H5O + OH	jx(ip_CH3OOH)	(Rickard and Pascoe, 2009)

TABLE A.2: Photolysis reactions (... continued)

#	labels	reaction	rate coefficient	reference
J11498	TrGCJ	BZEMUCOOH + hv → .5 EPXC4DIAL + .5 GLYOX + .5 HO2 + .5 C3DIALO2 + .5 C32OH13CO + OH	jx(ip_CH3OOH)+jx(ip_HOCH2CHO)*2	(Rickard and Pascoe, 2009)*
J11511	TrGCJ	BZEMUCOH + hv → .5 EPXC4DIAL + .5 GLYOX + .5 HO2 + .5 C3DIALO2 + .5 C32OH13CO + HO2	jx(ip_HOCH2CHO)*2	(Rickard and Pascoe, 2009)*
J11513	TrGCJN	BZEMUCNO3 + hv → EPXC4DIAL + NO2 + GLYOX + HO2	2.77*jx(ip_HOCH2CHO)	(Rickard and Pascoe, 2009)
J11620	TrGCJ	TLEPOXMUC + hv → .5 C615CO2O2 + HO2 + CO + .5 EPXC4DIAL + .5 CH3CO3	jx(ip_NO2)*0.1	(Rickard and Pascoe, 2009)
J11622	TrGCJ	C6H5CH2OOH + hv → BENZAL + HO2 + OH	jx(ip_CH3OOH)	(Rickard and Pascoe, 2009)*
J11624	TrGCJ	C6H5CH2NO3 + hv → BENZAL + HO2 + NO2	0.59*J_IC3H7NO3	(Rickard and Pascoe, 2009)*
J11626	TrGCJ	BENZAL + hv → HO2 + CO + C6H5O2	jx(ip_BENZAL)	(Atkinson et al., 2012)
J11643	TrGCJ	TLBIPEROOH + hv → .6 GLYOX + .4 MGLYOX + HO2 + .2 C4MDIAL + .2 C5DICARB + .2 TLFUONE + .2 BZFUONE + .2 MALDIAL + OH	jx(ip_CH3OOH)	(Rickard and Pascoe, 2009)*
J11645	TrGCJN	TLBIPERNO3 + hv → .6 GLYOX + .4 MGLYOX + HO2 + .2 C4MDIAL + .2 C5DICARB + .2 TLFUONE + .2 BZFUONE + .2 MALDIAL + NO2	J_IC3H7NO3	(Rickard and Pascoe, 2009)*
J11647	TrGCJ	TLOBIPEROH + hv → C5CO14O2 + GLYOX + HO2	J_ACETOL	(Rickard and Pascoe, 2009)
J11667	TrGCJ	CRESOOH + hv → .68 C5CO14OH + .68 GLYOX + HO2 + .32 PTLQONE + OH	jx(ip_CH3OOH)	(Rickard and Pascoe, 2009)*
J11669	TrGCNJ	NCRESOOH + hv → .68 C5CO14OH + .68 GLYOX + HO2 + .32 PTLQONE + OH + NO2	J_IC3H7NO3	(Rickard and Pascoe, 2009)*
J11670	TrGCNJ	NCRESOOH + hv → C5CO14OH + GLYOX + NO2 + OH	jx(ip_CH3OOH)	(Rickard and Pascoe, 2009)*
J11672b	TrGCNJ	TOL1OHNO2 + hv → HONO + PHONOnitrop + MCPENTDIENKETENE	jx(ip_TOL1OHNO2)	see note
J11682	TrGCJ	C4MDIAL + hv → .3 C3MCODBCO3 + .3 HO2 + .3 CO + .3 MC3CODBCO3 + .3 HO2 + .3 CO + .4 PXYFUONE	4.E3*jx(ip_MVK)*0.2	(Rickard and Pascoe, 2009)
J11684	TrGCJ	TLEMUCCO2H + hv → C615CO2O2 + HO2	jx(ip_MACR)	(Rickard and Pascoe, 2009)
J11686	TrGCJ	TLEMUCCO3H + hv → C615CO2O2 + OH	jx(ip_CH3OOH)+jx(ip_MACR)	(Rickard and Pascoe, 2009)
J11690	TrGCJ	TLEMUCOOH + hv → .5 C3DIALO2 + .5 CO2H3CHO + .5 EPXC4DIAL + .5 MGLYOX + .5 HO2 + OH	jx(ip_CH3OOH)+2.77*jx(ip_HOCH2CHO)+J_ACETOL	(Rickard and Pascoe, 2009)*
J11692	TrGCNJ	TLEMUCNO3 + hv → EPXC4DIAL + NO2 + CH3CO3 + CO + HO2	2.77*jx(ip_HOCH2CHO) +J_ACETOL	(Rickard and Pascoe, 2009)
J11694	TrGCJ	TLEMUCCO + hv → CH3CO3 + EPXC4DIAL + CO + HO2	2.77*jx(ip_HOCH2CHO) +2.15*jx(ip_MGLYOX)	(Rickard and Pascoe, 2009)
J11696	TrGCJ	C6H5CO3H + hv → C6H5O2 + OH	jx(ip_CH3OOH)	(Rickard and Pascoe, 2009)
J11705	TrGCJ	OXYL1OOH + hv → TOL1O + OH	jx(ip_CH3OOH)	(Rickard and Pascoe, 2009)
J11707b	TrGCNJ	MNCATECH + hv → HONO + PHONOnitrop + MCPENTDIENKETENE	jx(ip_TOL1OHNO2)	see note
J11707c	TrGCJ	MCPENTDIENKETENE + hv → CO2 + CO + 2 HO2 + C4MDIAL	J_KETENE	see note
J11721b	TrGCNJ	DNCRES + hv → HONO + PHONOnitrop + MNCPENTDIENKETENE + LhvDNCRES + NO2	jx(ip_TOL1OHNO2)	see note
J11721c	TrGCNJ	MNCPENTDIENKETENE + hv → CO2 + CO + 2 HO2 + NC4MDCO2H	J_KETENE	see note
J11734	TrGCNJ	DNPHEN + hv → HONO + MNCPENTDIENKETENE + NO2	jx(ip_HOC6H4NO2)	see note
J11735	TrGCJ	MCATEC1OOH + hv → MCATEC1O + OH	jx(ip_CH3OOH)	(Rickard and Pascoe, 2009)
J11743	TrGCNJ	NPTLQOOH + hv → C7CO4DB + NO2 + OH	jx(ip_CH3OOH)	(Rickard and Pascoe, 2009)*
J11745	TrGCJ	PTLQOOH + hv → C6CO2OHCO3 + OH	jx(ip_CH3OOH)	(Rickard and Pascoe, 2009)*
J11756	TrGCNJ	NCRES1OOH + hv → NCRES1O + OH	jx(ip_CH3OOH)	(Rickard and Pascoe, 2009)
J11758	TrGCNJ	MNNCATCOOH + hv → NC4MDCO2H + HCOCO2H + NO2 + OH	jx(ip_CH3OOH)	(Rickard and Pascoe, 2009)*
J11760	TrGCNJ	MNCATECOOH + hv → NC4MDCO2H + HCOCO2H + HO2 + OH	jx(ip_CH3OOH)	(Rickard and Pascoe, 2009)*
J11764	TrGCJ	C7CO4DB + hv → C5CO2DBCO3 + HO2 + CO	jx(ip_MGLYOX)*2	(Rickard and Pascoe, 2009)

TABLE A.2: Photolysis reactions (... continued)

#	labels	reaction	rate coefficient	reference
J11772	TrGCNJ	NDNCRESOOH + hv → NC4MDCO2H + HNO3 + CO + CO + NO2 + OH	jx(ip_CH3OOH)	(Rickard and Pascoe, 2009)*
J11774	TrGCNJ	DNCRESOOH + hv → NC4MDCO2H + HCOCO2H + NO2 + OH	jx(ip_CH3OOH)	(Rickard and Pascoe, 2009)*
J11776	TrGCJ	C6COOHCO3H + hv → C5134CO2OH + HO2 + CO + OH	jx(ip_CH3OOH)	(Rickard and Pascoe, 2009)
J11919	TrGCJ	STYRENOOH + hv → HO2 + HCHO + BENZAL + OH	jx(ip_CH3OOH)	(Rickard and Pascoe, 2009)*

*Notes:

J-values are calculated with an external module and then supplied to the MECCA chemistry.

Values that originate from the Master Chemical Mechanism (MCM) by Rickard and Pascoe (2009) are translated according in the following way:
J(11) → jx(ip_COH2)
J(12) → jx(ip_CHOH)
J(15) → jx(ip_HOCH2CHO)
J(18) → jx(ip_MACR)
J(22) → jx(ip_ACETOL)
J(23)+J(24) → jx(ip_MVK)
J(31)+J(32)+J(33) → jx(ip_GLYOX)
J(34) → jx(ip_MGLYOX)
J(41) → jx(ip_CH3OOH)
J(53) → J(IC3H7NO3)
J(54) → J(IC3H7NO3)
J(55) → J(IC3H7NO3)
J(56)+J(57) → jx(ip_NOA)

J11011 KDEC MCOCOMOXO → HCHO + CH3CO3
J11017 KDEC C3DIALO → GLYOX + CO + HO2
J11054 KDEC MALDIALO → GLYOX + GLYOX + HO2
J11058 KDEC BZFUO → CO14O3CHO + HO2
J11072 KDEC NBZFUO → .5 CO14O3CHO + .5 NO2 + .5 NBZFUONE + .5 HO2
J11075 KDEC MALDIALCO2 → .6 MALANHY + HO2 + .4 GLYOX + .4 CO
J11097 KDEC MALANHYO → HCOCOHCO3
J11170 KDEC C5DIALO → MALDIAL + CO + HO2
J11188 KDEC NPXYFUO → C23O3CCHO + NO2
J11202 KDEC PXYFUO → C23O3CCHO + HO2
J11214 KDEC TLFUONE → .6 C5CO14O2 + .6 HO2 + .4 TLFUONE
J11256 KDEC MMALANHYO → CO2H3CO3
J11259 KDEC C5DICARBO → MGLYOX + GLYOX + HO2
J11262 KDEC NTLFUO → ACCOMECHO + NO2
J11264 KDEC MECOACETO → CH3CO3 + HCHO
J11285 KDEC C5CO14CO2 → .83 MALANHY + .83 CH3O2 + .17 MGLYOX + .17 HO2 + .17 CO
J11295 KDEC C3MCODBCO2 → .35 MGLYOX + .35 HO2 + .35 CO + .65 MMALANHY + .65 HO2
J11298 KDEC TLFUO → ACCOMECHO + HO2
J11303 KDEC MC3CODBCO2 → .35 GLYOX + .35 CH3O2 + .35 CO + .65 MMALANHY + .65 HO2
J11351 KDEC PHENO → .71 MALDALCO2H + .71 GLYOX + .29 PBZQONE + HO2
J11357 KDEC NDNPHENO → NC4DCO2H + HNO3 + CO + CO + NO2
J11365 KDEC BZBIPERO → GLYOX + HO2 + .5 BZFUONE + .5 BZFUONE
J11367b new channel created for nitrophenol decomposition , jval from literature
J11367c new channel created for nitrophenol decomposition , jval from lit.L. Vereecken personal communication
J11414 KDEC NNCATECO → NC4DCO2H + HCOCO2H + NO2
J11445 KDEC NCATECO → NC4DCO2H + HCOCO2H + HO2
J11457 KDEC PBZQO → C5CO2OHCO3
J11469 KDEC BZBIPERO → GLYOX + HO2 + .5 BZFUONE + .5 BZFUONE
J11478 KDEC NBZQO → C6CO4DB + NO2
J11488 KDEC DNPHENO → NC4DCO2H + HCOCO2H + NO2
J11498 KDEC BZEMUCO → .5 EPXC4DIAL + .5 GLYOX + .5 HO2 + .5 C3DIALO2 + .5 C32OH13CO
J11511 KDEC BZEMUCO → .5 EPXC4DIAL + .5 GLYOX + .5 HO2 + .5 C3DIALO2 + .5 C32OH13CO
J11622 KROPRIM*O2 fast reaction C6H5CH2O = BENZAL + HO2
J11624 KROPRIM*O2 fast reaction C6H5CH2O = BENZAL + HO2
J11643 KDEC TLBIPERO → .6 GLYOX + .4 MGLYOX + HO2 + .2 ZCODC23DBCOD + .2 C5DICARB + .2 TLFUONE + .2 BZFUONE + .2 MALDIAL
J11645 KDEC TLBIPERO → .6 GLYOX + .4 MGLYOX + HO2 + .2 ZCODC23DBCOD + .2 C5DICARB + .2 TLFUONE + .2 BZFUONE + .2 MALDIAL
J11667 KDEC CRESO → .68 C5CO14OH + .68 GLYOX + HO2 + .32 PTLQONE
J11669 KDEC CRESO → .68 C5CO14OH + .68 GLYOX + HO2 + .32 PTLQONE
J11670 KDEC NCRESO → C5CO14OH + GLYOX + NO2
J11672b new channel
J11682 already in MIM 3
J11690 KDEC TLEMUCO → .5 C3DIALO2 + .5 CO2H3CHO + .5 EPXC4DIAL + .5 MGLYOX + .5 HO2
J11707b new channel
J11707c new channel, L. Vereecken personal communication
J11721b new channel, L. Vereecken personal communication
J11721c new channel
J11734 new channel
J11743 KDEC NPTLQO → C7CO4DB + NO2
J11745 KDEC PTLQO → C6CO2OHCO3
J11758 KDEC MNNCATECO → NC4MDCO2H + HCOCO2H + NO2
J11760 KDEC MNCATECO → NC4MDCO2H + HCOCO2H + HO2
J11772 KDEC NDNCRESO → NC4MDCO2H + HNO3 + CO + CO + NO2
J11774 KDEC DNCRESO → NC4MDCO2H + HCOCO2H + NO2
J11919 KDEC STYRENO → HO2 + HCHO + BENZAL

Appendix B

Henry's coefficients used for aromatic compounds

TABLE B.1: Henry's coefficients assigned to aromatic compounds used in the aromatic mechanism

species	**H [M/atm]**	$\Delta_{soln}H/\mathbf{R}$ **[K]**	**specie**	**Reference**
BENZENE	*1.8* 10^{-1}	4100	*Benzene*	*Sander (2015)*
TOLUENE	*1.5* 10^{-1}	4000	*Toluene*	*Sander (2015)*
BENZAL	*3.6* 10^{1}		*Benzaldehyde*	*Sander (2015)*
MALANHY	3.6 10^{1}	0		
TLFUONE	3.6 10^{1}	0	5-Methyl-2(5H)-furanone	
C6H5CH2NO3	3.6 10^{1}	0		
BZFUONE	3.6 10^{1}	0		
PXYFUONE	3.6 10^{1}	0	3-Methyl-2(5H)-furanone	
PHENOL	*2.9* 10^{3}	*6800*	*Phenol*	*Sander (2015)*
C6H5O	2.9 10^{3}	6800	Phenyloxidanyl	
C6H5OOH	2.9 10^{3}	6800	Phenyl hydroperoxide	
C6H5CH2OOH	2.9 10^{3}	6800	Benzyl hydroperoxide	
TOL1O	2.9 10^{3}	6800	(2-Methylphenyl)oxidanyl	
C6H5CH2OH	2.9 10^{3}	6800		
OXYL1OOH	2.9 10^{3}	6800		
BZBIPERNO3	2.9 10^{3}	6800		
CRESOL	2.9 10^{3}	6800	Cresol	
HOC6H4NO2	*7.0* 10^{1}	*4600*	*2-nitrophenol*	Sander (2015)
NPHEN1OOH	7.0 10^{1}	4600		
NPHEN1O	7.0 10^{1}	4600		
TOL1OHNO2	7.0 10^{1}	4600		
NCRES1O	7.0 10^{1}	4600		
NCRES1OOH	7.0 10^{1}	4600		
TLBIPERNO3	7.0 10^{1}	4600		

TABLE B.1: Henry's coefficients (... continued)

species	**H [M/atm]**	$\Delta_{soln}H/\mathbf{R}$ **[K]**	**specie**	**Reference**
PBZN	7.0 10^1	4600	benzoyl nitro peroxide	
NSTYRENOOH	7.0 10^1	4600		
DNPHEN	*2.3* 10^3	*0*	*dinitro-o-cresol*	*Sander (2015)*
NDNPHENOOH	2.3 10^3	0		
NNCATECOOH	2.3 10^3	0		
DNPHENOOH	2.3 10^3	0		
MNNCATCOOH	2.3 10^3	0		
DNCRESOOH	2.3 10^3	0		
NDNCRESOOH	2.3 10^3	0		
DNCRES	2.3 10^3	0	2-Methyl-4,6-dinitrophenol	
PHCOOH	*2.4* 10^4	0	*Benzoic Acid*	*Sander (2015)*
PTLQCO	2.4 10^4	0		
C6H5CO3H	2.4 10^4	0	Perbenzoic acid	
NBZQOOH	2.4 10^4	0		
NPTLQOOH	2.4 10^4	0		
NBZFUOOH	2.4 10^4	0		
STYRENOOH	2.4 10^4	0		
CATECHOL	4.6 10^3	0	Catechol	Sander (2015)
PBZQCO	4.6 10^3	0		
NPHENOH	4.6 10^3	0		
CATEC1O	4.6 10^3	0		
NPHENOOH	4.6 10^3	0		
NCRESOOH	4.6 10^3	0		
NCATECHOL	4.6 10^3	0		
CATEC1OOH	4.6 10^3	0		
MNCATECH	4.6 10^3	0	3-Methyl-6-nitro-1,2-benzenediol	
MCATECHOL	4.6 10^3	0	3-Methylcatechol	
MCATEC1OOH	4.6 10^3	0		
NCRESOH	4.6 10^3	0		
GLYOX	3.6 10^5	0	Glyoxal	Sander (2015)
C5DIALOOH	3.6 10^5	0		
BZEPOXMUC	3.6 10^5	0		
MALDIAL	3.6 10^5	0	2-Butenedial	
CO14O3CHO	3.6 10^5	0		
CO23C3CHO	3.6 10^5	0		
C54CO	3.6 10^5	0	2,3,4-Trioxopentanal	
EPXC4DIAL	3.6 10^5	0		
MGLYOX	3.7 10^3	7500	Methyl glyoxal	Sander (2015)
C5CO2DBPAN	3.7 10^3	7500		
C7CO4DB	3.7 10^3	7500		
GLYPAN	3.7 10^3	7500		
METACETHO	3.7 10^3	7500		
C23O3CHO	3.7 10^3	7500		
C23O3CCHO	3.7 10^3	7500		
C5DICARB	3.7 10^3	7500		

TABLE B.1: Henry's coefficients (... continued)

species	**H [M/atm]**	$\Delta_{soln}H/\mathbf{R}$ **[K]**	**specie**	**Reference**
ACCOMECHO	3.7 10^3	7500		
C4MDIAL	3.7 10^3	7500		
C6125CO	3.7 10^3	7500	2,5-Dioxo-3-hexenal	
PAN	2.8 10^0	6500	peroxyacetylnitrate	Sander (2015)
C5COO2NO2	2.8 10^0	6500		
MC3CODBPAN	2.8 10^0	6500		
EPXDLPAN	2.8 10^0	6500		
ACCOMEPAN	2.8 10^0	6500		
C3MCODBPAN	2.8 10^0	6500		
C23O3CPAN	2.8 10^0	6500		
BZEMUCPAN	2.8 10^0	6500		
TLEMUCPAN	2.8 10^0	6500		
MALDIALPAN	2.8 10^0	6500		
CH3O2NO2	2.8 10^0	6500	(Nitroperoxy)methane	
PHAN	3.9 10^4	8600		Sander (2015)
TLOBIPEROH	3.9 10^4	8600		
C4CO2DBPAN	3.9 10^4	8600		
HCOCOHPAN	3.9 10^4	8600		
NC4DCO2H	3.9 10^4	8600		
C4PAN6	3.9 10^4	8600		
C5CO2OHPAN	3.9 10^4	8600		
BZEMUCNO3	3.9 10^4	8600		
TLEMUCNO3	3.9 10^4	8600		
C6CO2OHPAN	3.9 10^4	8600		
CH3OOH	3.2 10^2	5300	methyl hydroperoxide	Sander (2015)
3-Hexanol	2.0 10^1			Sander (2015)
2,5-hexanediol	2.0 10^6			Sander (2015)
C4M2AL2OH	2.0 10^6			
C4MALOHOOH	2.0 10^6			
C6COOHCO3H	2.0 10^6			
TLEMUCOOH	2.0 10^6			
HCOCOHCO3H	2.0 10^6			
MALDIALOOH	2.0 10^6			
MMALNHY2OH	2.0 10^6			
PHENOH	2.0 10^6			
MNCATECOOH	2.0 10^6			
BZFUOOH	2.0 10^6			
MALNHYOHCO	2.0 10^6			
MALANHYOOH	2.0 10^6			
MALANHY2OH	2.0 10^6			
BZFUOH	2.0 10^6			
PXYFUOOH	2.0 10^6			
TLFUOH	2.0 10^6			
MMALNHYOOH	2.0 10^6			
PXYFUOH	2.0 10^6			
TLFUOOH	2.0 10^6			
PHENOOH	2.0 10^6			

TABLE B.1: Henry's coefficients (... continued)

species	**H [M/atm]**	$\Delta_{soln}H/\mathbf{R}$ **[K]**	**specie**	**Reference**
NCATECOOH	2.0 10^6			
PBZQOOH	2.0 10^6			
BZBIPEROOH	2.0 10^6			
BZBIPER2OH	2.0 10^6			
PBZQOH	2.0 10^6			
PTLQOH	2.0 10^6			
CRESOH	2.0 10^6			
TLBIPER2OH	2.0 10^6			
TLEMUCOH	2.0 10^6			
TLBIPEROOH	2.0 10^6			
MCATEC1O	2.0 10^6			
PTLQOOH	2.0 10^6			
CRESOOH	2.0 10^6			
HOHOC4DIAL	2.0 10^6			
CO2C4DIAL	2.0 10^6			
C514CO23OH	2.0 10^6			
C5DICAROOH	2.0 10^6			
C6CO4DB	2.0 10^6			
BZEMUCOOH	2.0 10^6			
BZEMUCOH	2.0 10^6			
C5COOHCO3H	2.0 10^6			
C4CO2DCO3H	2.0 10^6			
C5CO2DCO3H	2.0 10^6			
1,2,6-hexanetriol	2.0 10^{11}			Sander (2015)
trans-2-hexenal	2.0 10^1			Sander (2015)
MMALANHY	2.0 10^1			
PBZQONE	2.0 10^1		1,4-Benzoquinone	
NBZFUONE	2.0 10^1			
Glyoxylic acid	9.0 10^3			Sander (2015)
NC4MDCO2H	9.0 10^3			
BZEMUCCO2H	9.0 10^3			
BZEMUCCO	9.0 10^3			
BZEMUCCO3H	9.0 10^3			
BZFUCO	9.0 10^3			
MCOCOMOOOH	9.0 10^3			
CO14O3CO2H	9.0 10^3			
BZOBIPEROH	9.0 10^3			
NTLFUOOH	9.0 10^3			
C33CO	9.0 10^3		Oxomalonaldehyde	
C3DIALOOH	9.0 10^3			
C5DIALCO	9.0 10^3			
C32OH13CO	9.0 10^3			
MALDALCO3H	9.0 10^3			
EPXDLCO3H	9.0 10^3			
C615CO2OH	9.0 10^3			
EPXDLCO2H	9.0 10^3			
MALDALCO2H	9.0 10^3		4-Oxo-2-butenoic acid	
C5DIALOH	9.0 10^3			Sander (2015)

TABLE B.1: Henry's coefficients (... continued)

species	**H [M/atm]**	$\Delta_{soln}H/\mathbf{R}$ **[K]**	**specie**	**Reference**
MC3ODBCO3H	9.0 10^3			
CH3COCO2H	3.1 10^5	5100	Piruvic Acid	Sander (2015)
C5134CO2OH	3.1 10^5	5100		
C23O3CCO2H	3.1 10^5	5100		
C24O3CCO2H	3.1 10^5	5100		
MECOACEOOH	3.1 10^5	5100		
C5CO14OOH	3.1 10^5	5100		
C4CODBCO3H	3.1 10^5	5100		
C23O3CCO3H	3.1 10^5	5100		
ACCOMECO3H	3.1 10^5	5100		
C615CO2OOH	3.1 10^5	5100		
CH3COCO3H	3.1 10^5	5100		
HOCOC4DIAL	3.1 10^5	5100		
TLEMUCCO	3.1 10^5	5100		
pentanoic acid	2.2 10^3	6583		Sander (2015)
C5CO14OH	2.2 10^3	6583		
MC3ODBCO2H	2.2 10^3	6583		
TLEMUCCO2H	2.2 10^3	6583		
TLEMUCCO3H	2.2 10^3	6583		
NPXYFUOOH	2.2 10^3	6583		
MVK	4.1 10^1			Sander (2015)
TLEPOXMUC	4.1 10^1			
PTLQONE	4.1 10^1		2-Methyl-1,4-benzoquinone	
TLEMUCCO	4.1 10^4			Warneck (2005)
LXYL	1.7 10^{-1}		xylene (averaged)	
O	1.9 10^{-1}		o-xylene	Sander (2015)
M	1.6 10^{-1}		m-xylene	Sander (2015)
P	1.6 10^{-1}		p-xylene	Sander (2015)
LTMB	2.2 10^{-1}		trimethylbenzene (ave)	
1,2,3	3.1 10^{-1}		1,2,3-trimethylbenzene	Sander (2015)
1,2,4	1.7 10^{-1}		1,2,4-trimethylbenzene	Sander (2015)
1,3,5	1.7 10^{-1}		1,2,5-trimethylbenzene	Sander (2015)
EBENZ	1.2 10^{-1}		ethylbenzene	Sander (2015)
HAROM	1.2 10^{-1}		3,5-dimethyl ethyl benzene	Sander (2015)
STYRENE	3.7 10^{-1}			Sander (2015)

The henry's coefficient is expressed as H (M/atm). The value that are assigned are taken from the compilation of Henry's coefficients by Rolf Sander unless specified otherwise. Many species are managed choosing surrogate species. Those species that have H $> 10^8$

need to be treated in SCAV as if they had H = 10^8 in order to avoid too high numerical stiffness.

The first row of each box is written in italics. This row is the reference structure value and chemical structure in which we have based our approximation for other species.

The criteria for choosing the Henry's coefficient for those species which is not defined is summarized in the following points:

1. Non-aromatic ring products: Hexanol (1OH), Hexanediol (2OH or OOH), Hexantril(3OH)
2. Conjugated carbonyls: Glyox (Doble aldehyde), Crotonaldehyde/trans-2-hexena (C5dicarb), 3-methyl butanoic acid (=O + -OH)
3. glyoxilic acid (aldehyde+carbonyl)
4. For species with more of 2-OH, the value is in the order of 10^6, which in the model is enough for an uptake of 90% (Lawrence and Crutzen. MATCH)
5. -O- we consider it inert (epoxy group doesn't contribute efficiently. Epoxypropane Hr=5.3)
6. Not Hr for peroxy radicals (they react enough fast).They are not shown in the table.
7. We will tend to attach species to those of higher Rh (in case of doubt)

Appendix C

Literate of global annual emission fluxes

TABLE C.1: Biogenic annual average emissions for important VOC. Units are Tg/yr.

Species	TgC/yr (Range)	Tg(tracer)/yr (Range)	Best Estimate Tg/yr (range)
Ethane – C2H6			1.58 (0.56-3.9)
Ayddin et al 2011	-	-	
Pozzer et al 2010	-	-	
Etiope et al2009	1.26	1.58	
Xiao et al 2008	-	-	
Pozzer et al 2007	0.45	0.56	
Folberth et al 2006	0.8	1	
Von Kuhlman et al 2003	-	-	
Granier et al 2001	1.6	2	
Bey et al 2001	-	-	
Poisson et al 2000	3.1	3.9	
Propane – C3H8			2.96 (0.36-3.68)
Pozzer et al 2010	-	-	
Etiope et al 2009	2.2	2.69	
Fu et al 2008	-	-	
Pozzer et al 2007	0.29	0.36	
Folberth et al 2006	1.6	1.96	
Von Kuhlman et 2003	-	-	
Granier et al 2001	2.7	3.3	
Bey 2001	-	-	
Poisson et al 2000	3	3.68	
Acetone – CH3COCH3			32 (4-76)
Fischer et al 2012	19.9	32	
Fu et al 2008	32.9	53	
Pozzer et al 2007	25.6	41.29	

Folberth et al 2006	47.11	76	
Von Kuhlman et al2003a,b	24.8	40	
Jacob et al 2002	38.43	62	
Bey et al 2001	15	24.1	
Singh et al 2000	13 (8.7-17.4)	21 (14-28)	
Reissell et al 99	(6.2-6.8)	(10-11)	
Collins et al 99	-	-	
Brasseur et al 98	11.2	18	
Wang et al 98a	14.9	24	
Singh et al 94	5.6(2.4-11.2)	9 (4-18)	
Methanol – CH3OH			300 (42-320)
Pozzer et al 2007	22.2	61.89	
Folberth et al 2006	99.94	268.8	
Jacob et al 2005	55.9 (38.9 – 74.1)	151 (105-200)	
Tie et al 2003	(39-117)	(104-312)	
von Kuhlman et al 2003a,b	28.9	77	
Heikes et al 2002	111.1 (22.2 – 118.5)	300 (60-320)	
Galbally and Kirstine 2002	41.9 (15.6 – 90)	113 (42-243)	
Singh et al 2000	35.2 (22.2-61.1)	95 (60-165)	
Ethene – C2H4			12.55 (5.91-23.5)
Pozzer et al 2007	10.7	12.55	
Fu et al 2008	8.2	9.6	
Folberth et al 2006	4.97	5.91	
Poisson et al 2000	20.1	23.5	
Propene – C3H6			3.53 (1.33-16.48)
Pozzer et al 2007	2	3.53	
Folberth et al 2006	1.14	1.33	
Poisson et al 2000	14.1	16.48	
Butanes(lumped) – C4H10			0.4
Pozzer et al 2007	0.37	0.41	
von Kuhlman et al 2003a,b	0.3	0.4	
Poisson et al 2000	67.5	81.73	
Formic Acid – HCOOH	*Gmol/yr		2.6 (0.92-7.1)
Paulot et al 2011	56	2.6	
Ito et al. 2007	-	-	
Pozzer et al 2007	124	5.78	
Lathiere et al 2006	125	5.75	
von Kuhlmann 2003a,b	122	5.6	
Kesselmeier&Staudt99	(14-156)	(0.92-7.1)	
Kesselmeier'98b	(20-130)	(1.2-6)	
Acetic Acid – CH3COOH	*Gmol/yr		2.58 (0.54-5.64)
Paulot et al 2011	43	2.58	
Pozzer et al 2007	58.5	3.51	
Ito et al. 2007	-	-	
Lathiere et al 2006	25	1.5	
von Kuhlmann 2003a,b	56	3.36	

Kesselmeier'98b	(10-33)	(0.6-2)	
Bode et al '97	(9-94)	(0.54-5.64)	
Acetaldehyde – CH3CHO			80 (20-160)
Millet et al 2010	43	80	
Singh et al 2004	86	160	
Isoprene – CH2=CCH=CH2			583 (466-681)
Pozzer et al 2007	(305-340)	(346-385)	
Arneth et al. (2007a)	412	466	
Wiedinmyer et al. (2006)	459	520	
Lathiere (2006)	460	521	
Guenther et al. (2006)	503	570	
Kaplan et al. (2006)	541	613	
Tao and Jain (2005)	601	681	
Valdes et al. (2005)	594	673	
Shim et al. (2005)	566	641	
Naik et al. (2004)	454	514	
Sanderson et al. (2003)	483	547	
Potter et al. (2001)	559	633	
Adams et al. (2001)	561	635	
Wang and Shallcross (2000)	530	600	
Levis et al. (1999)	507	574	
Guenther 1995	503	570	
Benzene – C6H6			
Fu et al 2008	-	-	-
Henze et al 2008	-	-	
Toluene - C7H8			
Fu et al 2008	-	-	-
Henze et al 2008	-	-	
Xylene – C6H4(CH3)2			
Fu et al 2008	-	-	-
Henze et al 2008	-	-	
Formaldehyde –HCHO			
Pozzer et al 2007	-	-	-
Folberth et al 2006	-	-	-
Von Kuhlman et al 2003	-	-	
MEK			7 (0-10)
Pozzer et al 2007	0	0	-
Singh et al 2004		(5-10)	
Von Kuhlman et al 2003 (Mek + ketones)	0	0	

TABLE C.2: Biomass burning annual average emissions for important VOC. Units are Tg/yr.

Species	TgC/yr (Range)	Tg(tracer)/yr (Range)	Best Estimate Tg/yr (range)
Ethane – C2H6			2.8 (2.29 – 6.5)
Ayddin et al 2011	-	-	
Pozzer et al 2010	2.2	2.8	
Etiope et al2009	1.8	2.29	
Xiao et al 2008	1.9	2.4	
Pozzer et al 2007	2.2	2.8	
Folberth et al 2006	4.61	5.8	
Von Kuhlman et al 2003	5.2	6.5	
Granier et al 2001	3.9	4.9	
Bey et al 2001	3	3.8	
Poisson et al 2000	2.9	3.7	
Propane – C3H8			1.1 (0.41 – 2.45)
Pozzer et al 2010	0.9	1.1	
Etiope et al 2009	0.3	0.41	
Fu et al 2008	1.7	2.1	
Pozzer et al 2007	0.7	0.86	
Folberth et al 2006	1.26	1.5	
Von Kuhlman et 2003	1.7	2	
Granier et al 2001	2	2.45	
Bey 2001	0.9	1.1	
Poisson et al 2000	0.8	0.98	
Acetone – CH3COCH3			2.8 (1.76 - 14)
Fischer et al 2012	1.7	2.8	
Fu et al 2008	1.9	3	
Pozzer et al 2007	1.1	1.76	
Folberth et al 2006	2	3.2	
Von Kuhlman et al2003a,b	2.6	4.2	
Jacob et al 2002	2.8	4.5	
Bey et al 2001	8.7	14.0	
Singh et al 2000	3.1 (1.86-6.2)	5 (3 – 10)	
Reissell et al 99	-	-	
Collins et al 99	-	-	
Brasseur et al 98	8.7	14	
Wang et al 98a	8.7	14	
Singh et al 94	6.2 (4.96 – 7.44)	10 (8 – 12)	
Methanol – CH3OH			12 (2 – 32)
Pozzer et al 2007	2.3	6.24	
Folberth et al 2006	4.3	11.6	
Jacob et al 2005	4.81 (3.7 – 7.41)	13 (10 – 20)	
Tie et al 2003	-	-	
von Kuhlman et al 2003a,b	5.6	15	
Heikes et al 2002	4.44 (0.74 – 11.85)	12 (2 – 32)	

Galbally and Kirstine 2002	4.81 (2.22 - 7.04)	13 (6 – 19)	
Singh et al 2000	2.22 (1.11- 6.30)	6 (3 – 17)	
Ethene – C2H4			10.1 (4.84 – 10.1)
Pozzer et al 2007	4.1	4.84	
Fu et al 2008	-	-	
Folberth et al 2006	8.63	10.1	
Poisson et al 2000	7.7	9.0	
Propene – C3H6			3.7 (2.16 – 3.7)
Pozzer et al 2007	1.8	2.16	
Folberth et al 2006	3.14	3.7	
Poisson et al 2000	2.6	3.0	
Butanes(lumped) – C4H10			1.1 (1.1 – 4.0)
Pozzer et al 2007	0.9	1.1	
von Kuhlman et al 2003a,b	2.1	2.6	
Poisson et al 2000	3.3	4.0	
Formic Acid – HCOOH	*Gmol/yr		1.5 (1.5 – 8.5)
Paulot et al 2011	32.5	1.5	
Ito et al. 2007	183	8.5	
Pozzer et al 2007	73.2	3.37	
Lathiere et al 2006	-	-	
von Kuhlmann 2003a,b	174	8.1	
Kesselmeier&Staudt99	-	-	
Kesselmeier'98b	-	-	
Acetic Acid – CH3COOH	*Gmol/yr		11.2 (6.18 – 16.8)
Paulot et al 2011	187	11.2	
Pozzer et al 2007	102.9	6.18	
Ito et al. 2007	279	16.8	
Lathiere et al 2006	-	-	
von Kuhlmann 2003a,b	243	14.6	
Kesselmeier'98b	-	-	
Bode et al '97	-	-	
Acetaldehyde – CH3CHO			3 (3 – 10)
Millet et al 2010	1.6	3	
Singh et al 2004	4	10	
Isoprene – CH2=CCH=CH2			
Pozzer et al 2007	-	-	-
Arneth et al. (2007a)	-	-	
Wiedinmyer et al. (2006)			
Lathiere (2006)	-	-	
Guenther et al. (2006)	-	-	
Kaplan et al. (2006)	-	-	
Tao and Jain (2005)	-	-	
Valdes et al. (2005)	-	-	
Shim et al. (2005)	-	-	
Naik et al. (2004)	-	-	
Sanderson et al. (2003)	-	-	

Potter et al. (2001)	-	-	
Adams et al. (2001)	-	-	
Wang and Shallcross (2000)	-	-	
Levis et al. (1999)	-	-	
Guenther 1995	-	-	
Benzene – C6H6			2.7 (1.5 – 2.7)
Fu et al 2008	1.4	1.5	
Henze et al 2008	2.5	2.7	
Toluene - C7H8			1.5 (0.93 – 1.5)
Fu et al 2008	1.0	0.93	
Henze et al 2008	1.6	1.5	
Xylene – C6H4(CH3)2			0.8 (0.28 – 0.8)
Fu et al 2008	0.3	0.28	
Henze et al 2008	0.7	0.8	
Formaldehyde –HCHO			5.98 (3.3-7.8)
Pozzer et al 2007	1.32	3.3	
Folberth et al 2006	2.4	5.98	
Von Kuhlman et 2003	3.1	7.8	
MEK			1.5 (1-9.9)
Pozzer et al 2007		4.19	
Singh et al 2004		(1-3)	
Von Kuhlman et 2003 (Mek + ketones)	6.6	9.9	

Appendix D

Complementary figures of the comparison with observations

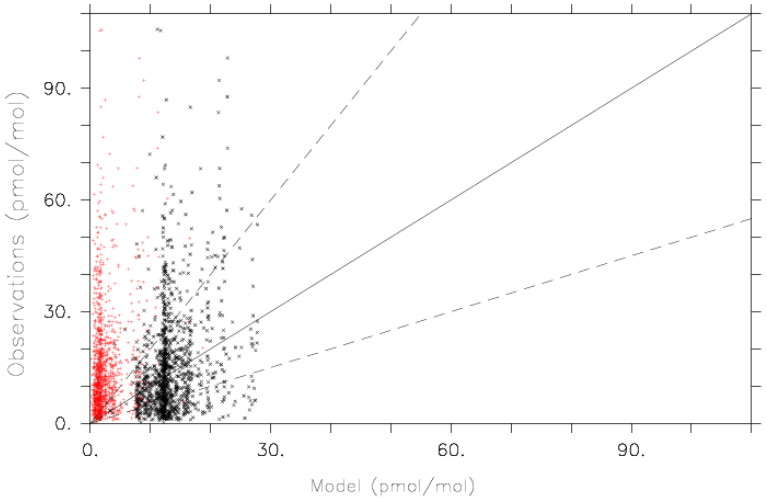

FIGURE D.1: Scatter diagram of CARIBIC vs simulations (for benzene). In red LIT scenario, in black RCP scenario. Units are in pmol/mol

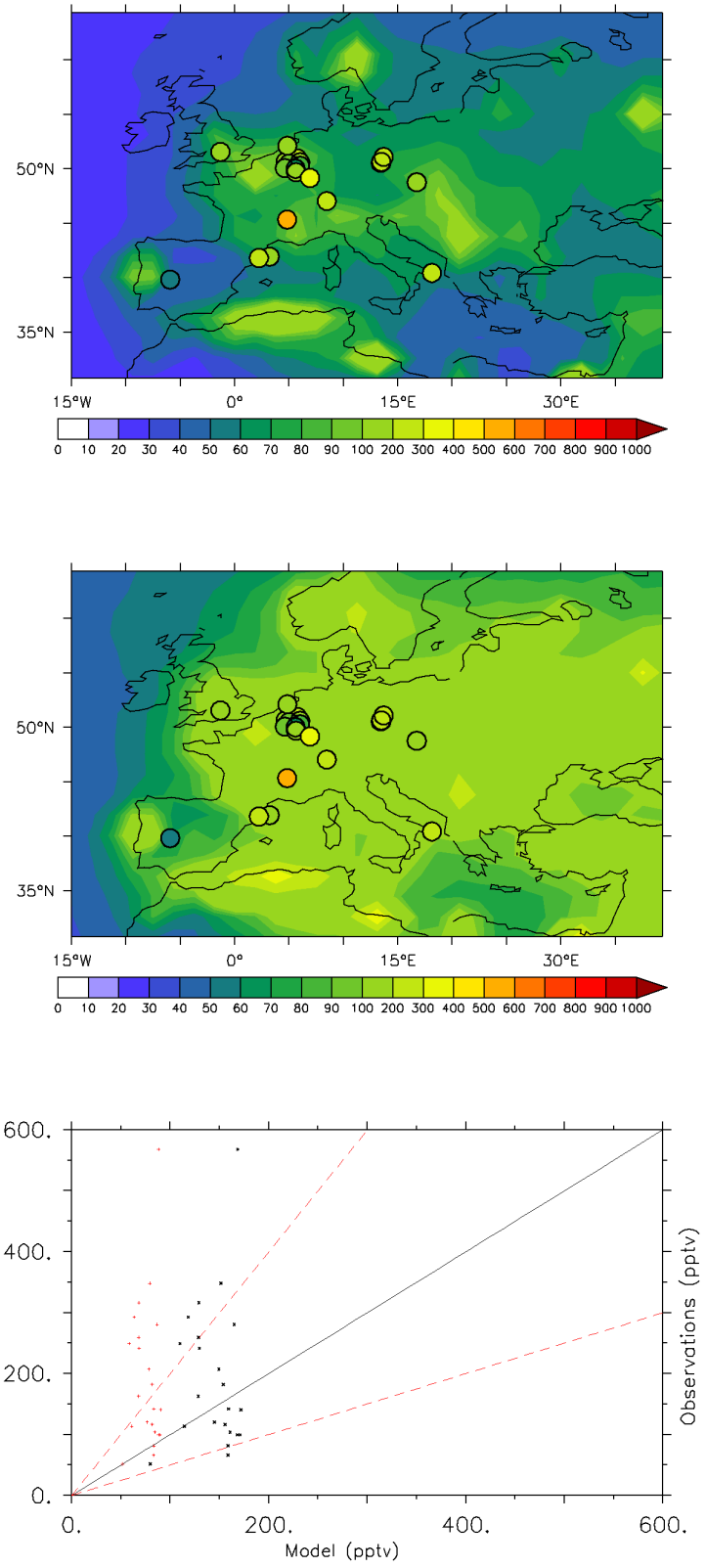

FIGURE D.2: On top, benzene annual averaged mixing ratios for Europe (left LIT scenario, right RCP scenario). In circles, annual average mixing ratios of EEA dataset. Units are in pmol/mol. On the bottom, scatter plot of observations vs simulations. In red LIT scenario, in black RCP

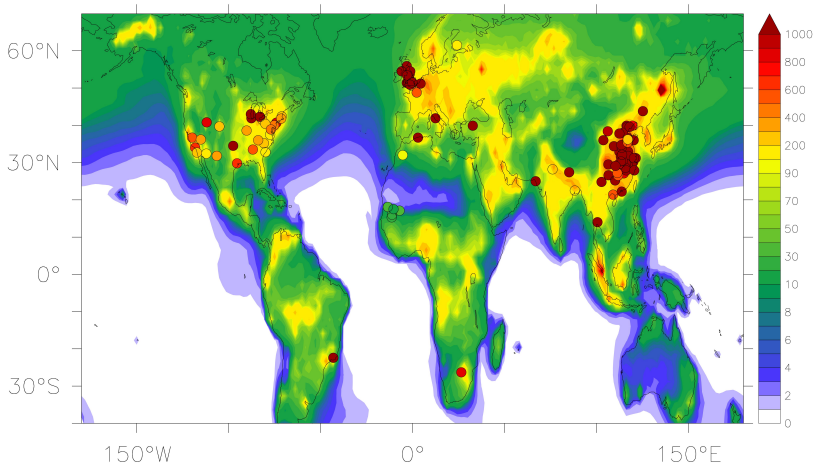

FIGURE D.3: Toluene mixing ratios from literature in pmol/mol (each work covers different time spans). In background model annual average mixing ratios.

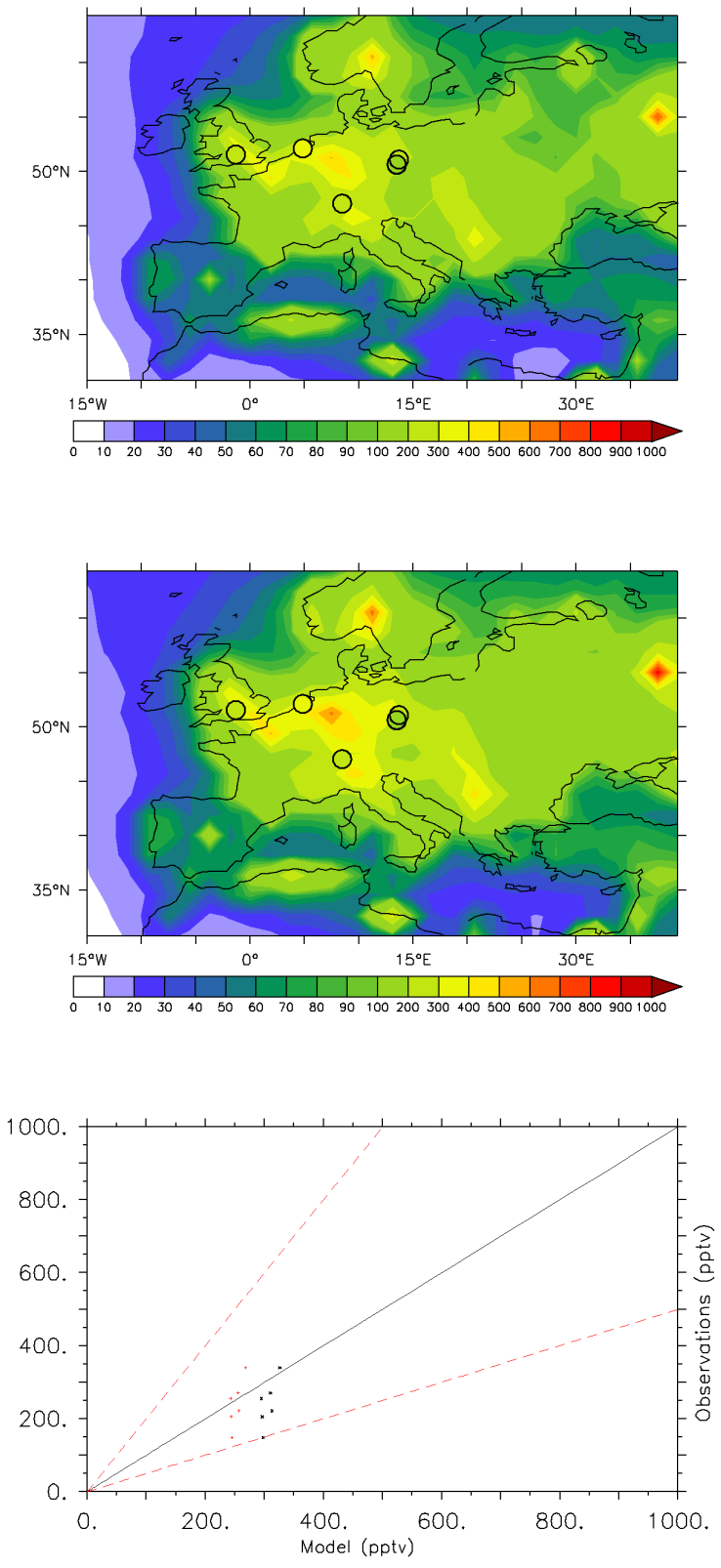

FIGURE D.4: On top, toluene annual averaged mixing ratios for Europe (left LIT scenario, right RCP scenario). In circles, annual average mixing ratios of EEA. Units are in pmol/mol. On the bottom, scatter plot, in red LIT scenario, in black RCP

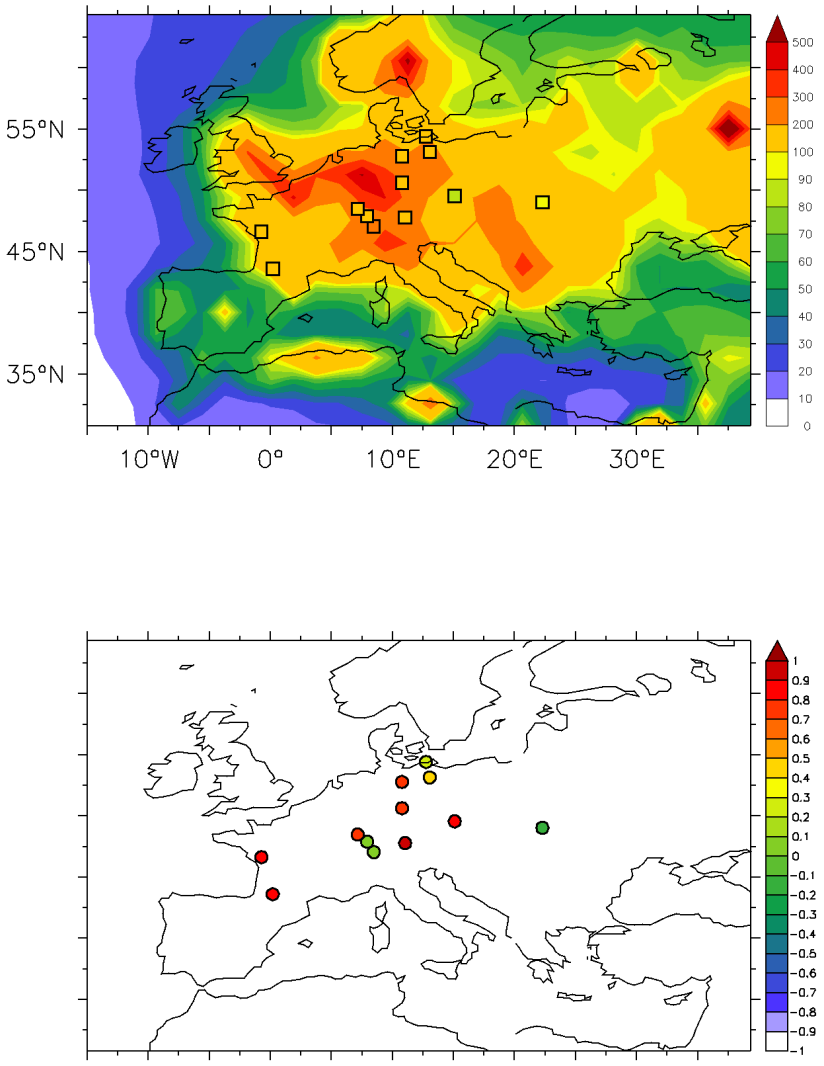

FIGURE D.5: Left: In squares, toluene annual averaged mixing ratios of EMEP stations, in background LIT scenario annual averaged mixing ratios (in units of pmol/mol). Right: Temporal correlation between observations and simulated mixing ratios.

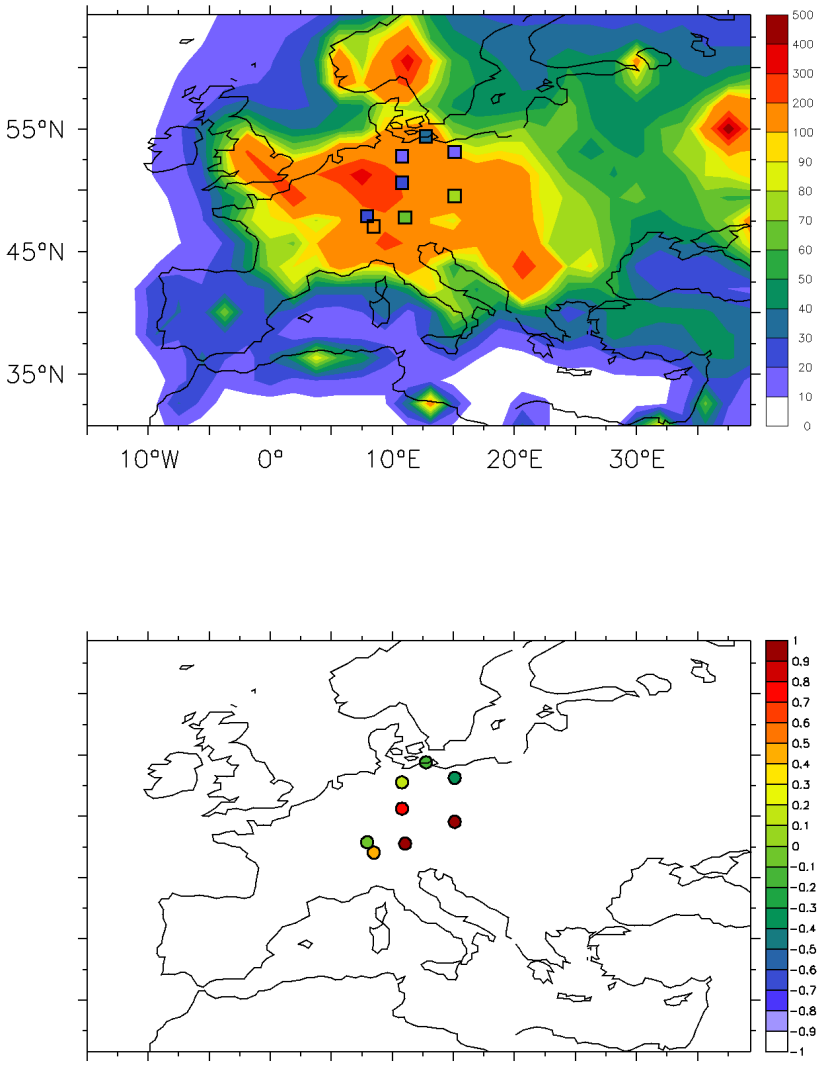

FIGURE D.6: Left: In squares, xylene annual averaged mixing ratios of EMEP stations, in background LIT scenario annual averaged mixing ratios (in units of pmol/mol). Right: Temporal correlation between observations and simulated mixing ratios.

Appendix E

Emission factors and chemical mechanism modification

TABLE E.1: Emission factors used for the biomass burning emission flux of Higher aromatic species. * This is the average of the molar masses of the different compounds. We use the average value of Pine-forest understory and coniferous canopy as representative for extra-tropical forest.

Species	Semiarid Shrubland	Pine-forest understory	Coniferous canopy	Organic soil	number of carbon atoms	molar mass
Naphthalene PTR	0.71	0.20	0.29	0.82	10	128
1-Butenylbenzene	0.00	0.00	0.00	0.00	10	132
Ethylstyrene	0.00	0.00	0.01	0.00	10	132
1-Methyl-1-Propenylbenzene	0.03	0.01	0.01	0.01	10	132
p-Cymene	0.12	0.06	0.05	0.06	10	134
Isobutylbenzene	0.01	0.01	0.01	0.01	10	134
n-Butylbenzene	0.00	0.01	0.01	0.00	10	134
1,4-Diethylbenzene	0.01	0.01	0.01	0.01	10	134
Ethyl Xylene isomer 1	0.01	0.01	0.01	0.00	10	134
Ethyl Xylene isomer 2	0.00	0.00	0.00	0.00	10	134
C11 Aromatics PTR	0.05	0.08	0.11	0.23	10	134
Sum	0.95	0.40	0.50	1.14	11	134*

TABLE E.2: Reactions modified to account for potential SOA loss. Reaction containing XXXSOA, are new species created to simulate the SOA formation channel.

Reaction	Rate constant
BENZENE + OH= .352BZBIPERO2 + .118BZEPOXMUC +.53HO2 + .118HO2	$2.3x10^{-12} * EXP(-190/TEMP) * 0.72$
BENZENE + OH= BENSOA	$2.3x10^{-12} * EXP(-190/TEMP) * 0.28$
PHENOL + NO3= PHENOLSOA	$3.8x10^{-12} * 0.23$
PHENOL + OH= .06C6H5O + .8CATECHOL + .8HO2 +.14PHENO2	$4.7x10^{-13} * EXP(1220/TEMP) * 0.77$
TOLUENE + OH= .07C6H5CH2O2 + .18CRESOL + .18HO2 + .65TLBIPERO2 + .10TLEPOXMUC + .10HO2	$1.8x10^{-12} * EXP(340/TEMP) * 0.82$
TOLUENE + OH= TOLSOA	$1.8x10^{-12} * EXP(340/TEMP) * 0.18$
BENZAL + NO3= C6H5CO3 + HNO3	$2.40x10^{-15} * 0.77$
BENZAL + NO3= BENZALSOA	$2.40x10^{-15} * 0.23$
BENZAL + OH= C6H5CO3	$5.9x10^{-12} * EXP(225/TEMP) * 0.77$
BENZAL + OH= BENZALSOA	$5.9x10^{-12} * EXP(225/TEMP) * 0.23$
LXYL + OH= TLEPOXMUC + HO2 + PXYL$_T$LEPOXMUC + LCARBON	$0.401x10^{-11} * 0.74$
LXYL + OH= XYLSOA	$1.695x10^{-11} * 0.26$
LTMB + OH= TLEPOXMUC + HO2 + PTMB$_T$LEPOXMUC + 2LCARBON	$0.827x10^{-11} * 0.77$
LTMB + OH= LTMBSOA	$3.345x10^{-11} * 0.23$
LTMB + NO3= C6H5CH2O2 + HNO3 + PTMB$_C$6H5CH2O2 + 2LCARBON	$1.52x10^{-15} * 0.77$
LTMB + NO3= LTMBSOA	$1.52x10^{-15} * 0.23$
EBENZ + OH= .10TLEPOXMUC + .07C6H5CH2O2 + .18CRESOL + .65TLBIPERO2 + 0.28HO2 + LCARBON	$7.00x10^{-12} * 0.77$
EBENZ + OH= EBENZSOA	$7.00x10^{-12} * 0.23$
EBENZ + NO3= C6H5CH2O2 + HNO3 + LCARBON	$1.20x10^{-16} * 0.77$
EBENZ + NO3= EBENZSOA	$1.20x10^{-16} * 0.23$
HAROM + OH= .14TLEPOXMUC + .03C6H5CH2O2 + .04CRESOL + .79TLBIPERO2 + 0.18HO2 + 4LCARBON	$5.67x10^{-11} * 0.77$
HAROM + OH= HAROMSOA	$5.67x10^{-11} * 0.23$
HAROM + NO3= C6H5CH2O2 +HNO3 + 4LCARBON	$2.60x10^{-15} * 0.77$
HAROM + NO3= HAROMSOA	$2.60x10^{-15} * 0.23$
NO3 + STYRENE= NSTYRENO2	$1.50x10^{-12} * 0.77$
NO3 + STYRENE= STYRENESOA	$1.50x10^{-12} * 0.23$
O3 + STYRENE= .545HCHO + .1BENZENE + .28C6H5O2 +.56CO + .36OH + .28HO2 + .075PHCOOH + .545BENZAL + .09H2O2 + .075HCOOH	$1.70x10^{-17} * 0.77$
O3 + STYRENE= STYRENESOA	$1.70x10^{-17} * 0.23$
OH + STYRENE= STYRENO2	$5.80x10^{-11} * 0.77$
OH + STYRENE= STYRENESOA	$5.80x10^{-11} * 0.23$

Appendix F

Chapter 5 supplementary figures

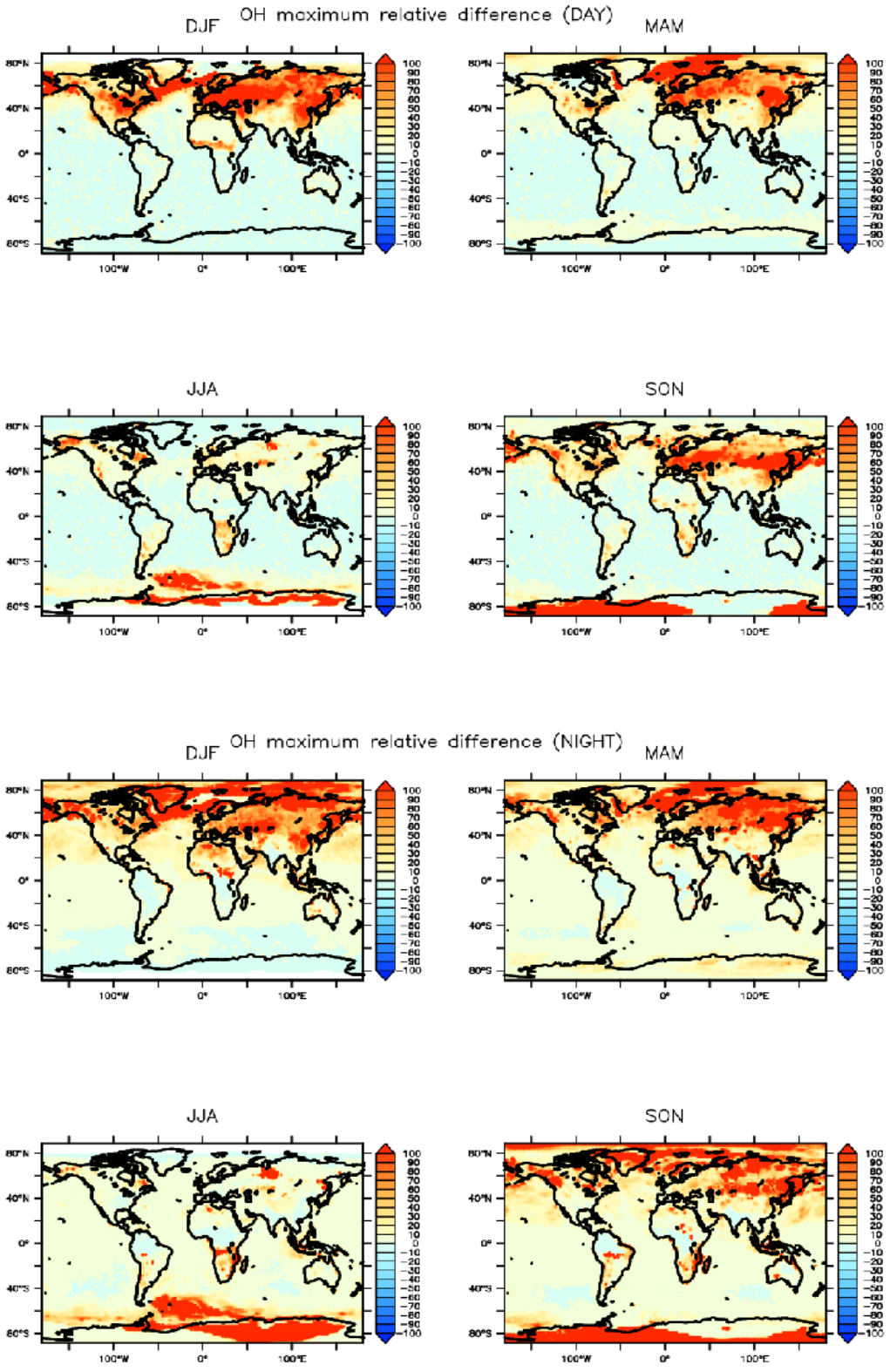

FIGURE F.1: Maximum instantaneous relative differences for OH.

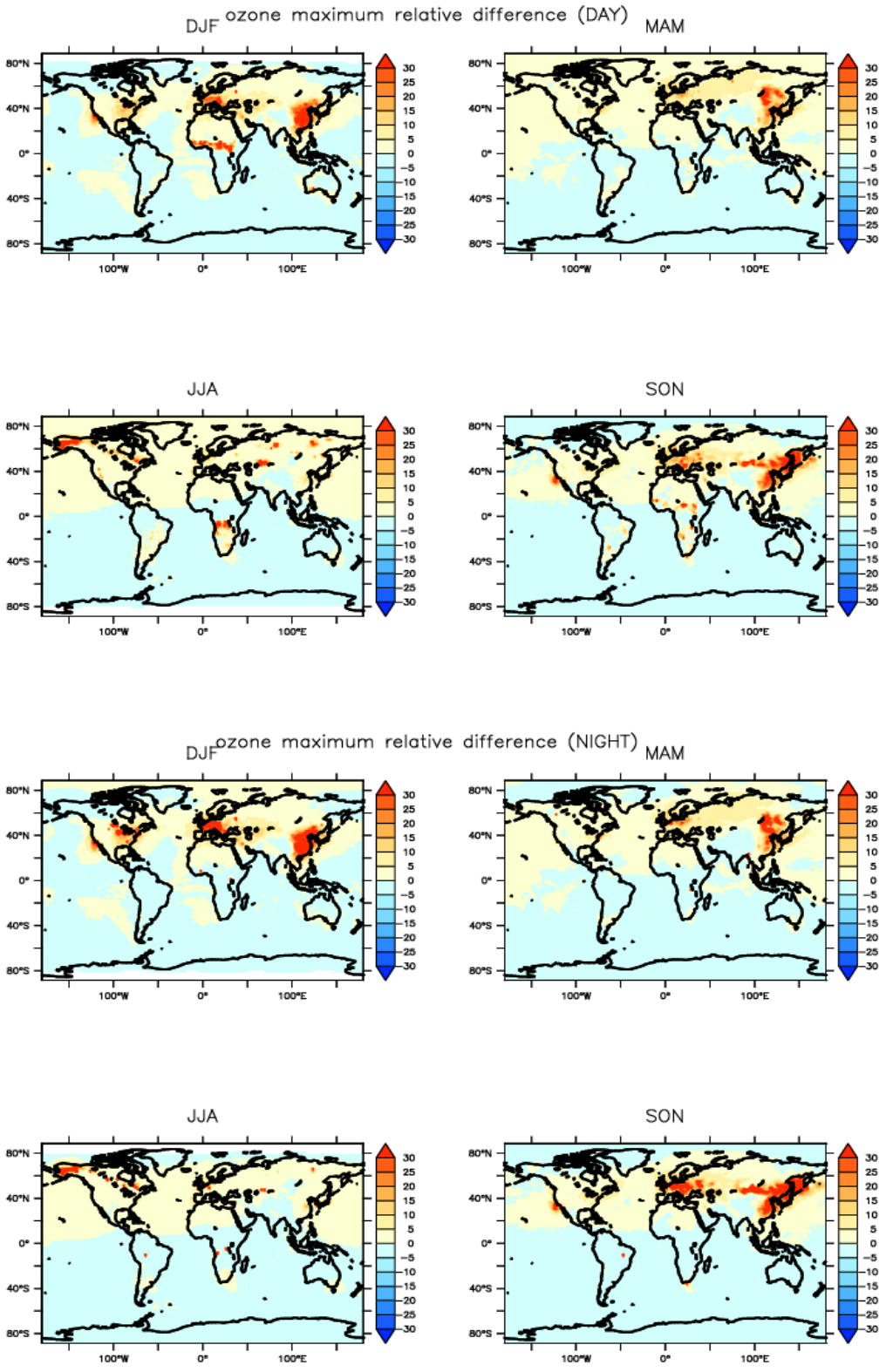

FIGURE F.2: Maximum instantaneous relative differences for ozone.

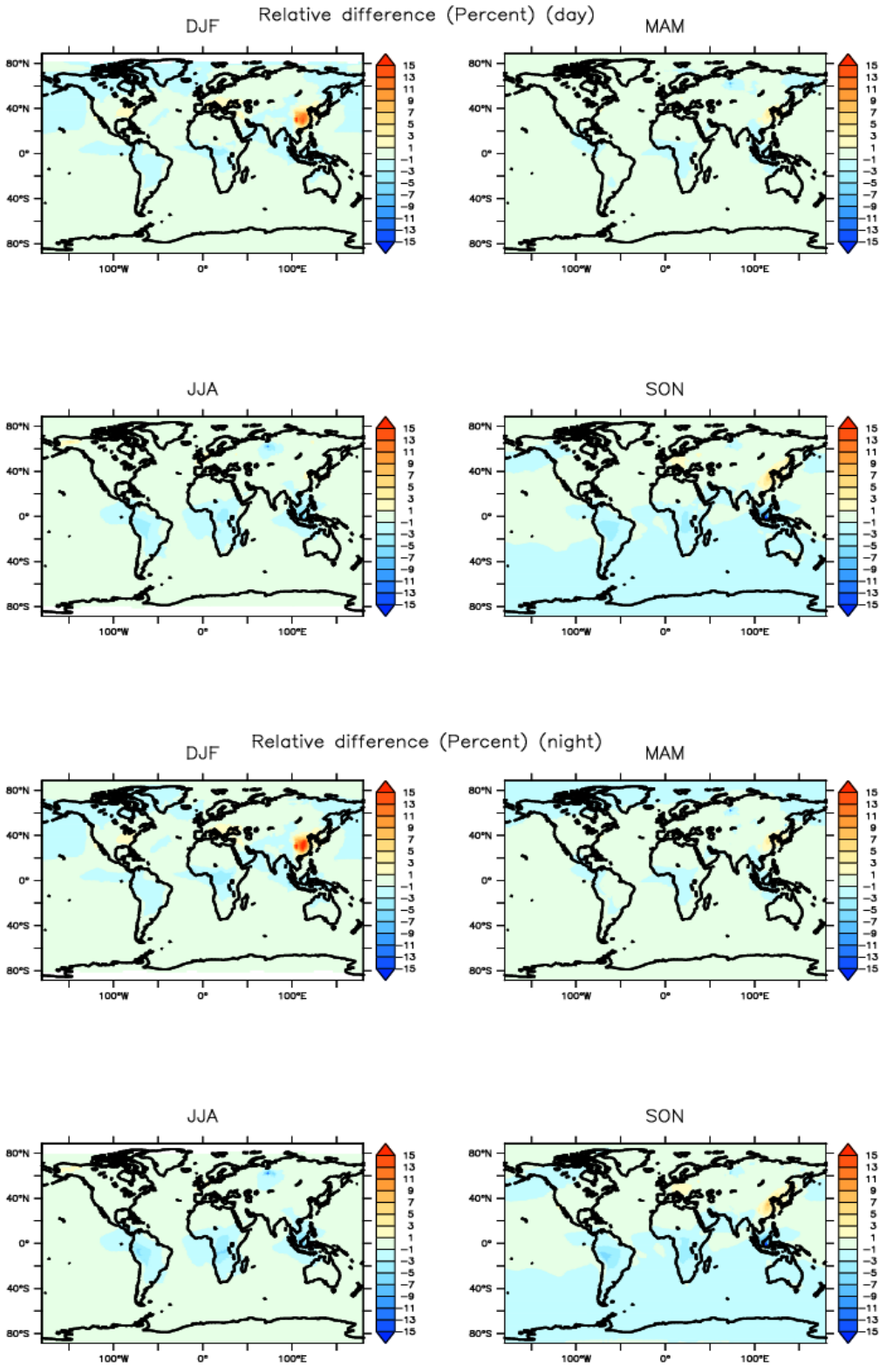

FIGURE F.3: Relative differences for ozone, split in four seasons.

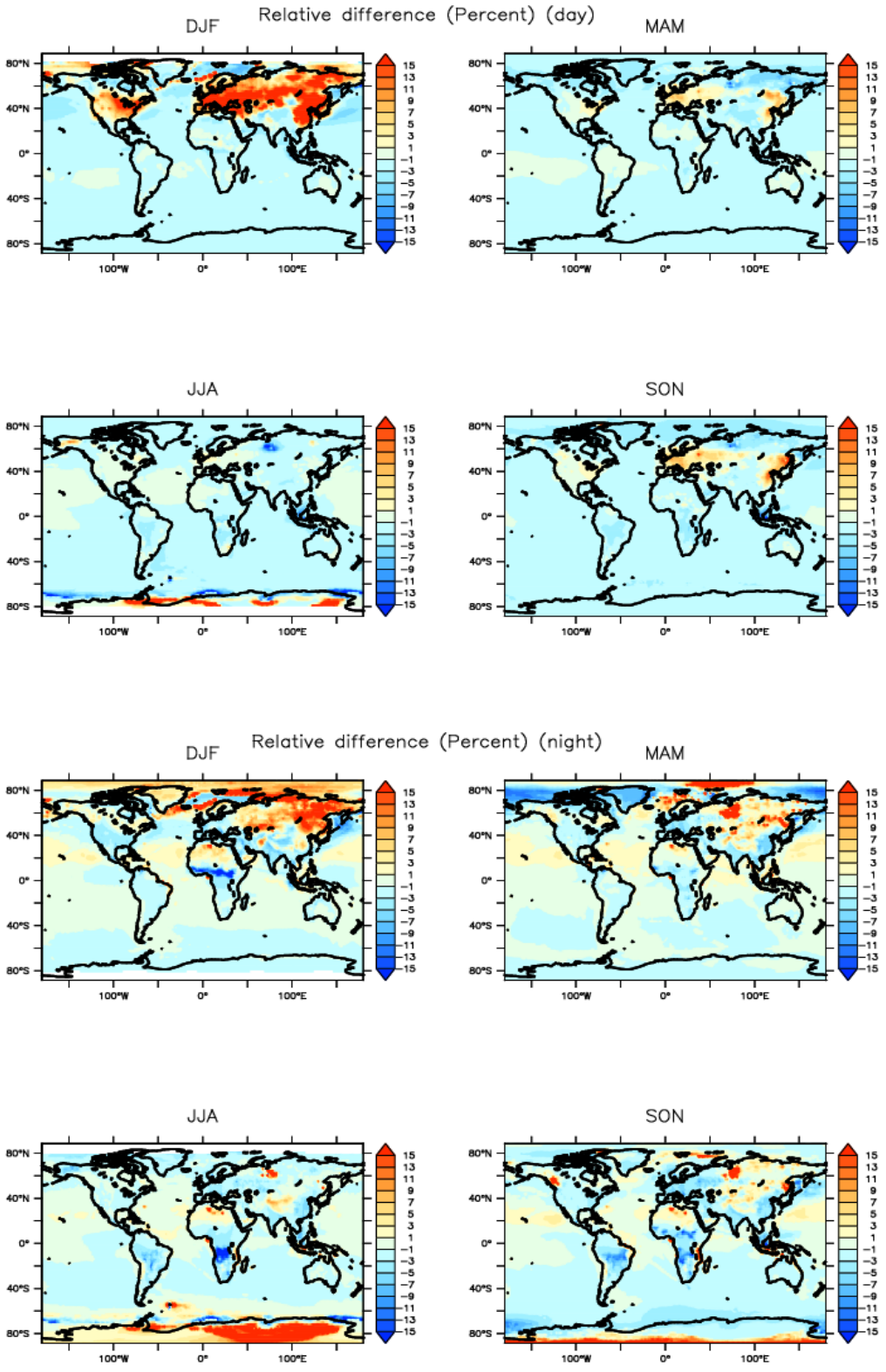

FIGURE F.4: Relative differences for OH, split in four seasons.

Bibliography

Akagi, S., Yokelson, R. J., Wiedinmyer, C., Alvarado, M., Reid, J., Karl, T., Crounse, J., and Wennberg, P.: Emission factors for open and domestic biomass burning for use in atmospheric models, Atmospheric Chemistry and Physics, 11, 4039–4072, 2011.

Akimoto, H.: Global air quality and pollution, Science, 302, 1716–1719, 2003.

Andreae, M. O. and Merlet, P.: Emission of trace gases and aerosols from biomass burning, Global biogeochemical cycles, 15, 955–966, 2001.

Andrés-Hernández, M., Kartal, D., Reichert, L., Burrows, J., Meyer Arnek, J., Lichtenstern, M., Stock, P., and Schlager, H.: Peroxy radical observations over West Africa during AMMA 2006: photochemical activity in the outflow of convective systems, Atmospheric Chemistry and Physics, 9, 3681–3695, 2009.

Arakawa, A. and Schubert, W. H.: Interaction of a cumulus cloud ensemble with the large-scale environment, Part I, Journal of the Atmospheric Sciences, 31, 674–701, 1974.

Arneth, A., Monson, R., Schurgers, G., Niinemets, Ü., and Palmer, P.: Why are estimates of global terrestrial isoprene emissions so similar (and why is this not so for monoterpenes)?, Atmospheric Chemistry and Physics, 8, 4605–4620, 2008.

Asselin, R.: Frequency filter for time integrations, Monthly Weather Review, 100, 487–490, 1972.

Atkinson, R.: Atmospheric chemistry of VOCs and NO_x, Atmospheric environment, 34, 2063–2101, 2000.

Atkinson, R. and Arey, J.: Atmospheric degradation of volatile organic compounds, Chemical reviews, 103, 4605–4638, 2003.

Atkinson, R., Baulch, D. L., Cox, R. A., Hampson, Jr., R. F., Kerr, J. A., Rossi, M. J., and Troe, J.: Summary of evaluated kinetic and photochemical data for atmospheric chemistry: Web version August 2014, http://iupac.pole-ether.fr, 2012.

Baek, S.-O. and Jenkins, R. A.: Characterization of trace organic compounds associated with aged and diluted sidestream tobacco smoke in a controlled atmosphere—volatile organic compounds and polycyclic aromatic hydrocarbons, Atmospheric Environment, 38, 6583–6599, 2004.

Baker, A., Slemr, F., and Brenninkmeijer, C.: Analysis of non-methane hydrocarbons in air samples collected aboard the CARIBIC passenger aircraft, Atmospheric Measurement Techniques, 3, 311–321, 2010.

Baker, A. K., Beyersdorf, A. J., Doezema, L. A., Katzenstein, A., Meinardi, S., Simpson, I. J., Blake, D. R., and Rowland, F. S.: Measurements of nonmethane hydrocarbons in 28 United States cities, Atmospheric Environment, 42, 170–182, 2008.

Barker, M., Hengst, M., Schmid, J., Buers, H.-J., Mittermaier, B., Klemp, D., and Koppmann, R.: Volatile organic compounds in the exhaled breath of young patients with cystic fibrosis, European respiratory journal, 27, 929–936, 2006.

Barletta, B., Meinardi, S., Simpson, I. J., Khwaja, H. A., Blake, D. R., and Rowland, F. S.: Mixing ratios of volatile organic compounds (VOCs) in the atmosphere of Karachi, Pakistan, Atmospheric Environment, 36, 3429–3443, 2002.

Barletta, B., Meinardi, S., Sherwood Rowland, F., Chan, C.-Y., Wang, X., Zou, S., Yin Chan, L., and Blake, D. R.: Volatile organic compounds in 43 Chinese cities, Atmospheric Environment, 39, 5979–5990, 2005.

Barna, M. and Lamb, B.: Improving ozone modeling in regions of complex terrain using observational nudging in a prognostic meteorological model, Atmospheric Environment, 34, 4889–4906, 2000.

Bejan, I., El Aal, Y. A., Barnes, I., Benter, T., Bohn, B., Wiesen, P., and Kleffmann, J.: The photolysis of ortho-nitrophenols: a new gas phase source of HONO, Physical Chemistry Chemical Physics, 8, 2028–2035, 2006.

Bengtsson, L., Hodges, K. I., and Hagemann, S.: Sensitivity of large-scale atmospheric analyses to humidity observations and its impact on the global water cycle and tropical and extratropical weather systems in ERA40, Tellus A, 56, 202–217, 2004.

Bloss, C., Wagner, V., Bonzanini, A., Jenkin, M. E., Wirtz, K., Martin-Reviejo, M., and Pilling, M. J.: Evaluation of detailed aromatic mechanisms (MCMv3 and MCMv3.1) against environmental chamber data, Atmospheric Chemistry and Physics, 5, 623–639, doi:10.5194/acp-5-623-2005, URL http://www.atmos-chem-phys.net/5/623/2005/, 2005a.

Bloss, C., Wagner, V., Jenkin, M. E., Volkamer, R., Bloss, W. J., Lee, J. D., Heard, D. E., Wirtz, K., Martin-Reviejo, M., Rea, G., Wenger, J. C., and Pilling, M. J.: Development of a detailed chemical mechanism (MCMv3. 1) for the atmospheric oxidation of aromatic hydrocarbons, Atmospheric Chemistry and Physics, 5, 641–664, 2005b.

Bousquet, P., Ciais, P., Miller, J. B., Dlugokencky, E. J., Hauglustaine, D. A., Prigent, C., Van der Werf, G. R., Peylin, P., Brunke, E.-G., Carouge, C., Langenfelds, R. L., Lathiere, J., Papa, F., Ramonet, M., Schmidt, M., Steele, L. P., Tyler, S. C., and White, J.: Contribution of anthropogenic and natural sources to atmospheric methane variability, Nature, 443, 439–443, URL http://dx.doi.org/10.1038/nature05132http://www.nature.com/nature/journal/v443/n7110/suppinfo/nature05132{_}S1.html, 2006.

Brenninkmeijer, C. A. M., Crutzen, P., Boumard, F., Dauer, T., Dix, B., Ebinghaus, R., Filippi, D., Fischer, H., Franke, H., Frieβ, U., Heintzenberg, J., Helleis, F., Hermann, M., Kock, H. H., Koeppel, C., Lelieveld, J., Leuenberger, M., Martinsson, B. G., Miemczyk, S., Moret, H. P., Nguyen, H. N., Nyfeler, P., Oram, D., O'Sullivan, D., Penkett, S., Platt, U., Pupek, M., Ramonet, M., Randa, B., Reichelt, M., Rhee, T. S., Rohwer, J., Rosenfeld, K., Scharffe, D., Schlager, H., Schumann, U., Slemr, F., Sprung, D., Stock, P., Thaler, R., Valentino, F., van Velthoven, P., Waibel, A., Wandel, A., Waschitschek, K., Wiedensohler, A., Xueref-Remy, I., Zahn, A., Zech, U., and Ziereis, H.: Civil Aircraft for the regular investigation of the atmosphere based on an instrumented container: The new CARIBIC system, Atmospheric Chemistry and Physics, 7, 4953–4976, 2007.

Broadgate, W. J., Liss, P. S., and Penkett, S. A.: Seasonal emissions of isoprene and other reactive hydrocarbon gases from the ocean, Geophysical Research Letters, 24, 2675–2678, 1997.

Brocco, D., Fratarcangeli, R., Lepore, L., Petricca, M., and Ventrone, I.: Determination of aromatic hydrocarbons in urban air of Rome, Atmospheric Environment, 31, 557–566, 1997.

Buchholz, J.: Simulations of physics and chemistry of polar stratospheric clouds with a general circulation model, Sierke, 2005.

Buczynska, A. J., Krata, A., Stranger, M., Godoi, A. F. L., Kontozova-Deutsch, V., Bencs, L., Naveau, I., Roekens, E., and Van Grieken, R.: Atmospheric BTEX-concentrations in an area with intensive street traffic, Atmospheric Environment, 43, 311–318, 2009.

Butler, T., Lawrence, M., Taraborrelli, D., and Lelieveld, J.: Multi-day ozone production potential of volatile organic compounds calculated with a tagging approach, Atmospheric Environment, 45, 4082–4090, 2011.

Cabrera-Perez, D., Taraborrelli, D., Sander, R., and Pozzer, A.: Global atmospheric budget of simple monocyclic aromatic compounds, Atmospheric Chemistry and Physics Discussions, 2016, 1–25, doi:10.5194/acp-2015-996, URL http://www.atmos-chem-phys-discuss.net/acp-2015-996/, 2016.

Chen, J., Wenger, J. C., and Venables, D. S.: Near-ultraviolet absorption cross sections of nitrophenols and their potential influence on tropospheric oxidation capacity, The Journal of Physical Chemistry A, 115, 12 235–12 242, 2011.

Cheng, S.-B., Zhou, C.-H., Yin, H.-M., Sun, J.-L., and Han, K.-L.: OH produced from o-nitrophenol photolysis: a combined experimental and theoretical investigation., The Journal of chemical physics, 130, 234 311–234 311, 2009.

Ciarrocca, M., Tomei, G., Fiaschetti, M., Caciari, T., Cetica, C., Andreozzi, G., Capozzella, A., Schifano, M. P., Andre', J.-C., Tomei, F., and Sancini, A.: Assessment of occupational exposure to benzene, toluene and xylenes in urban and rural female workers, Chemosphere, 87, 813–819, 2012.

Clifford, G. M., Thüner, L. P., Wenger, J. C., and Shallcross, D. E.: Kinetics of the gas-phase reactions of OH and NO 3 radicals with aromatic aldehydes, Journal of Photochemistry and Photobiology A: Chemistry, 176, 172–182, 2005.

Courant, R., Friedrichs, K., and Lewy, H.: Über die partiellen Differenzengleichungen der mathematischen Physik, Mathematische annalen, 100, 32–74, 1928.

Cremer, S., Sledge, M. F., and Heinze, J.: Chemical mimicry: male ants disguised by the queen's bouquet, Nature, 419, 897–897, 2002.

Crutzen, P. J. and Andreae, M. O.: Biomass burning in the tropics: impact on atmospheric chemistry and biogeochemical cycles., Science, 250, 1669–1678, 1990.

Crutzen, P. J. and Zimmermann, P. H.: The changing photochemistry of the troposphere, Tellus B, 43, 136–151, 1991.

Damian, V., Sandu, A., Damian, M., Potra, F., and Carmichael, G. R.: The kinetic preprocessor KPP-a software environment for solving chemical kinetics, Computers & Chemical Engineering, 26, 1567–1579, 2002.

Daniel, J. S. and Solomon, S.: On the climate forcing of carbon monoxide, Journal of Geophysical Research: Atmospheres, 103, 13 249–13 260, 1998.

Deckert, R., Jöckel, P., Grewe, V., Gottschaldt, K.-D., and Hoor, P.: A quasi chemistry-transport model mode for EMAC, Geoscientific Model Development, 4, 195–206, 2011.

Derwent, R., Davies, T., Delaney, M., Dollard, G., Field, R., Dumitrean, P., Nason, P., Jones, B., and Pepler, S.: Analysis and interpretation of the continuous hourly monitoring data for 26 C_2-C_8 hydrocarbons at 12 United Kingdom sites during 1996, Atmospheric Environment, 34, 297–312, 2000.

Dietmüller, S., Jöckel, P., Tost, H., Kunze, M., Gellhorn, C., Brinkop, S., Frömming, C., Ponater, M., Steil, B., Lauer, A., and Hendricks, J.: A new radiation infrastructure for the Modular Earth Submodel System (MESSy, based on version 2.51), Geoscientific Model Development, 9, 2209–2222, doi:10.5194/gmd-9-2209-2016, URL http://www.geosci-model-dev.net/9/2209/2016/, 2016.

Dignon, J. and Logan, J.: Biogenic emissions of isoprene: A global inventory, EOS, Trans. AGU, 71, 1260, 1990.

Dodge, M.: Combined use of modeling techniques and smog chamber data to derive ozone-precursor relationships, in: International conference on photochemical oxidant pollution and its control: Proceedings, vol. 2, pp. 881–889, US Environmental Protection Agency, Environmental Sciences Research Laboratory Research Triangle Park, NC, 1977.

Dolgorouky, C., Gros, V., Sarda-Esteve, R., Sinha, V., Williams, J., Marchand, N., Sauvage, S., Poulain, L., Sciare, J., and Bonsang, B.: Total OH reactivity measurements in Paris during the 2010 MEGAPOLI winter campaign, Atmospheric Chemistry and Physics, 12, 9593–9612, 2012.

Dutta, C., Som, D., Chatterjee, A., Mukherjee, A., Jana, T., and Sen, S.: Mixing ratios of carbonyls and BTEX in ambient air of Kolkata, India and their associated health risk, Environmental monitoring and assessment, 148, 97–107, 2009.

Emmons, L. K., Walters, S., Hess, P. G., Lamarque, J.-F., Pfister, G. G., Fillmore, D., Granier, C., Guenther, A., Kinnison, D., Laepple, T., Orlando, J., Tie, X., Tyndall, G., Wiedinmyer, C., Baughcum, S. L., and Kloster, S.: Description and evaluation of the Model for Ozone and Related chemical Tracers, version 4 (MOZART-4), Geoscientific Model Development, 3, 43–67, 2010.

Ervens, B., George, C., Williams, J. E., Buxton, G. V., Salmon, G. A., Bydder, M., Wilkinson, F., Dentener, F., Mirabel, P., Wolke, R., and Herrmann, H.: CAPRAM 2.4 (MODAC mechanism): An extended and condensed tropospheric aqueous phase mechanism and its application, Journal of Geophysical Research: Atmospheres, 108, 2003.

Faraday, M.: On new compounds of carbon and hydrogen, and on certain other products obtained during the decomposition of oil by heat, Philosophical Transactions of the Royal Society of London, 115, 440–466, 1825.

Finlayson-Pitts, B. J. and Pitts Jr, J. N.: Atmospheric chemistry. Fundamentals and experimental techniques, John Wiley and Sons, New York, NY, 1986.

Fischer, E., Jacob, D., Yantosca, R., Sulprizio, M., Millet, D., Mao, J., Paulot, F., Singh, H., Roiger, A., Ries, L., et al.: Atmospheric peroxyacetyl nitrate (PAN): a global budget and source attribution, Atmospheric Chemistry and Physics, 14, 2679–2698, 2014.

Friedrich, R. and Obermeier, A.: Anthropogenic emissions of volatile organic compounds, Reactive hydrocarbons in the atmosphere, 1, 39, 1999.

Fu, T.-M., Jacob, D. J., Wittrock, F., Burrows, J. P., Vrekoussis, M., and Henze, D. K.: Global budgets of atmospheric glyoxal and methylglyoxal, and implications for formation of secondary organic aerosols, Journal of Geophysical Research: Atmospheres (1984–2012), 113, 2008.

Ganzeveld, L. and Lelieveld, J.: Dry deposition parameterization in a chemistry general circulation model and its influence on the distribution of reactive trace gases, Journal of Geophysical Research: Atmospheres (1984–2012), 100, 20 999–21 012, 1995.

Ganzeveld, L., Lelieveld, J., and Roelofs, G.-J.: A dry deposition parameterization for sulfur oxides in a chemistry and general circulation model, Journal of Geophysical Research: Atmospheres, 103, 5679–5694, 1998.

Gery, M. W., Whitten, G. Z., Killus, J. P., and Dodge, M. C.: A photochemical kinetics mechanism for urban and regional scale computer modeling, Journal of Geophysical Research: Atmospheres, 94, 12 925–12 956, 1989.

Giglio, L.: MODIS collection 5 active fire product user's guide version 2.4, Science Systems and Applications, Inc, 2010.

Goliff, W. S., Stockwell, W. R., and Lawson, C. V.: The regional atmospheric chemistry mechanism, version 2, Atmospheric Environment, 68, 174–185, 2013.

Granier, C., Pétron, G., Müller, J.-F., and Brasseur, G.: The impact of natural and anthropogenic hydrocarbons on the tropospheric budget of carbon monoxide, Atmospheric Environment, 34, 5255–5270, 2000.

Granier, C., Artaxo, P., and Reeves, C. E.: Emissions of atmospheric trace compounds, vol. 18, Springer Science & Business Media, 2004.

Granier, C., Bessagnet, B., Bond, T., D'Angiola, A., van der Gon, H. D., Frost, G. J., Heil, A., Kaiser, J. W., Kinne, S., Klimont, Z., Kloster, S., Lamarque, J. F., Liousse, C., Masui, T., Meleux, F., Mieville, A., Ohara, T., Raut, J. C., Riahi, K., Schultz, M. G., Smith, S. J., Thompson, A., van Aardenne, J., van der Werf, G. R., and van Vuuren, D. P.: Evolution of anthropogenic and biomass burning emissions of air pollutants at global and regional scales during the 1980–2010 period, Climatic Change, 109, 163–190, doi:10.1007/s10584-011-0154-1, 2011.

Grewe, V., Brunner, D., Dameris, M., Grenfell, J., Hein, R., Shindell, D., and Staehelin, J.: Origin and variability of upper tropospheric nitrogen oxides and ozone at northern mid-latitudes, Atmospheric Environment, 35, 3421–3433, 2001.

Groene, T.: Biogenic production and consumption of dimethylsulfide (DMS) and dimethylsulfoniopropionate (DMSP) in the marine epipelagic zone: a review, Journal of Marine Systems, 6, 191–209, 1995.

Guenther, A.: The contribution of reactive carbon emissions from vegetation to the carbon balance of terrestrial ecosystems, Chemosphere, 49, 837–844, 2002.

Guenther, A., Hewitt, C., Erickson, D., Fall, R., Geron, C., Graedel, T., Harley, P., Klinger, L., Lerdau, M., McKay, W., Pierce, T., Scholes, B., Steinbrecher, R., Tallamraju, R., Taylor, J., and Zimmerman, P.: A global model of natural volatile organic compound emissions, Journal of Geophysical Research: Atmospheres, 100, 8873–8892, doi:10.1029/94JD02950, URL http://onlinelibrary.wiley.com/doi/10.1029/94JD02950/full{%}5Cnhttp://doi.wiley.com/10.1029/94JD02950, 1995.

Guenther, a., Karl, T., Harley, P., Wiedinmyer, C., Palmer, P. I., and Geron, C.: Estimates of global terrestrial isoprene emissions using MEGAN (Model of Emissions of Gases and Aerosols from Nature), Atmospheric Chemistry and Physics, 6, 3181–3210, 2006.

Guenther, A. B., Jiang, X., Heald, C. L., Sakulyanontvittaya, T., Duhl, T., Emmons, L. K., and Wang, X.: The Model of Emissions of Gases and Aerosols from Nature version 2.1 (MEGAN2.1): an extended and updated framework for modeling biogenic emissions, Geoscientific Model Development, 5, 1471–1492, doi:10.5194/gmd-5-1471-2012, URL http://www.geosci-model-dev.net/5/1471/2012/, 2012.

Guo, H., Wang, T., Blake, D., Simpson, I., Kwok, Y., and Li, Y.: Regional and local contributions to ambient non-methane volatile organic compounds at a polluted rural/coastal site in Pearl River Delta, China, Atmospheric Environment, 40, 2345–2359, 2006.

Haagen-Smit, A.: Chemistry and physiology of Los Angeles smog, Industrial & Engineering Chemistry, 44, 1342–1346, 1952.

Hack, J. J.: Parameterization of moist convection in the National Center for Atmospheric Research community climate model (CCM2), Journal of Geophysical Research: Atmospheres, 99, 5551–5568, 1994.

Hagemann, S., Arpe, K., and Roeckner, E.: Evaluation of the hydrological cycle in the ECHAM5 model, Journal of Climate, 19, 3810–3827, 2006.

Hakola, H., Tarvainen, V., Laurila, T., Hiltunen, V., Hellén, H., and Keronen, P.: Seasonal variation of VOC concentrations above a boreal coniferous forest, Atmospheric Environment, 37, 1623–1634, 2003.

Heiden, A., Kobel, K., Komenda, M., Koppmann, R., Shao, M., and Wildt, J.: Toluene emissions from plants, Geophysical Research Letters, 26, 1283–1286, 1999a.

Heiden, A. C., Kobel, K., Komenda, M., Koppmann, R., Shao, M., and Wildt, J.: Toluene emissions from plants, Geophysical Research Letters, 26, 1283–1286, doi:10.1029/1999GL900220, URL http://dx.doi.org/10.1029/1999GL900220, 1999b.

Helsel, D. R.: Less than obvious-statistical treatment of data below the detection limit, Environmental Science & Technology, 24, 1766–1774, 1990.

Henze, D., Seinfeld, J., Ng, N., Kroll, J., Fu, T.-M., Jacob, D. J., and Heald, C.: Global modeling of secondary organic aerosol formation from aromatic hydrocarbons: high-vs. low-yield pathways, Atmospheric Chemistry and Physics, 8, 2405–2420, 2008.

Hofmann, A. W.: On Insolinic Acid., Proceedings of the Royal Society of London, 8, 1–3, 1856.

Hoque, R. R., Khillare, P., Agarwal, T., Shridhar, V., and Balachandran, S.: Spatial and temporal variation of BTEX in the urban atmosphere of Delhi, India, Science of the Total Environment, 392, 30–40, 2008.

Ichoku, C. and Kaufman, Y. J.: A method to derive smoke emission rates from MODIS fire radiative energy measurements, IEEE transactions on Geoscience and Remote Sensing, 43, 2636–2649, 2005.

Inomata, S., Tanimoto, H., Kato, S., Suthawaree, J., Kanaya, Y., Pochanart, P., Liu, Y., and Wang, Z.: PTR-MS measurements of non-methane volatile organic compounds during an intensive field campaign at the summit of Mount Tai, China, in June 2006, Atmospheric Chemistry and Physics, 10, 7085–7099, 2010.

Jaars, K., Beukes, J. P., Van Zyl, P. G., Venter, A. D., Josipovic, M., Pienaar, J. J., Vakkari, V., Aaltonen, H., Laakso, H., Kulmala, M., Tiitta, P., Guenther, A., Hellén, H., Laakso, L., and Hakola, H.: Ambient aromatic hydrocarbon measurements at Welgegund, South Africa, Atmospheric Chemistry and Physics, 14, 7075–7089, 2014.

Jacob, D. J., Field, B. D., Jin, E. M., Bey, I., Li, Q., Logan, J. A., Yantosca, R. M., and Singh, H. B.: Atmospheric budget of acetone, Journal of Geophysical Research: Atmospheres, 107, ACH 5–1–ACH 5–17, doi:10.1029/2001JD000694, URL http://dx.doi.org/10.1029/2001JD000694, 2002.

Jagiella, S. and Zabel, F.: Reaction of phenylperoxy radicals with NO 2 at 298 K, Physical Chemistry Chemical Physics, 9, 5036–5051, 2007.

Jenkin, M., Saunders, S., Wagner, V., and Pilling, M.: Protocol for the development of the Master Chemical Mechanism, MCM v3 (Part B): tropospheric degradation of aromatic volatile organic compounds, Atmospheric Chemistry and Physics, 3, 181–193, 2003.

Jenkin, M., Watson, L., Utembe, S., and Shallcross, D.: A Common Representative Intermediates (CRI) mechanism for VOC degradation. Part 1: Gas phase mechanism development, Atmospheric Environment, 42, 7185–7195, 2008.

Jeuken, A., Siegmund, P., Heijboer, L., Feichter, J., and Bengtsson, L.: On the potential assimilating meteorological analyses in a global model for the purpose of model validation, Journal of Geophysical Research, 101, 939–16, 1996.

Jöckel, P., Sander, R., Kerkweg, A., Tost, H., and Lelieveld, J.: Technical note: the modular earth submodel system (MESSY)-a new approach towards earth system modeling, Atmospheric Chemistry and Physics, 5, 433–444, 2005.

Jöckel, P., Tost, H., Pozzer, A., Brühl, C., Buchholz, J., Ganzeveld, L., Hoor, P., Kerkweg, A., Lawrence, M. G., Sander, R., Steil, B., Stiller, G., Tanarhte, M., Taraborrelli, D., van Aardenne, J., and Lelieveld, J.: The atmospheric chemistry general circulation model ECHAM5/MESSy1: consistent simulation of ozone from the surface to the mesosphere, Atmospheric Chemistry and Physics Discussions, 6, 6957–7050, 2006.

Jöckel, P., Kerkweg, A., Buchholz-Dietsch, J., Tost, H., Sander, R., and Pozzer, A.: Technical note: Coupling of chemical processes with the Modular Earth Submodel System (MESSy) submodel TRACER, Atmospheric Chemistry and Physics, 8, 1677–1687, 2008.

Jöckel, P., Kerkweg, A., Pozzer, A., Sander, R., Tost, H., Riede, H., Baumgaertner, A., Gromov, S., and Kern, B.: Development cycle 2 of the modular earth submodel system (MESSy2), Geoscientific Model Development, 3, 717–752, 2010.

Jöckel, P., Tost, H., Pozzer, A., Kunze, M., Kirner, O., Brenninkmeijer, C. A. M., Brinkop, S., Cai, D. S., Dyroff, C., Eckstein, J., Frank, F., Garny, H., Gottschaldt, K.-D., Graf, P., Grewe, V., Kerkweg, A., Kern, B., Matthes, S., Mertens, M., Meul, S., Neumaier, M., Nützel, M., Oberländer-Hayn, S., Ruhnke, R., Runde, T., Sander, R., Scharffe, D., and Zahn, A.: Earth System Chemistry integrated Modelling (ESCiMo) with the Modular Earth Submodel System (MESSy) version 2.51, Geoscientific Model Development, 9, 1153–1200, doi:10.5194/gmd-9-1153-2016, URL http://www.geosci-model-dev.net/9/1153/2016/, 2016.

Johnson, T. J., Sams, R. L., Profeta, L. T., Akagi, S. K., Burling, I. R., Yokelson, R. J., and Williams, S. D.: Quantitative IR spectrum and vibrational assignments for glycolaldehyde vapor: glycolaldehyde measurements in biomass burning plumes, The Journal of Physical Chemistry A, 117, 4096–4107, 2013.

Justice, C., Giglio, L., Korontzi, S., Owens, J., Morisette, J., Roy, D., Descloitres, J., Alleaume, S., Petitcolin, F., and Kaufman, Y.: The MODIS fire products, Remote Sensing of Environment, 83, 244–262, 2002.

Kaiser, J., Flemming, J., Schultz, M., Suttie, M., and Wooster, M.: The macc global fire assimilation system: First emission products (GFASv0), ECMWF Technical Memoranda, pp. 1–16, 2009.

Kaiser, J. W., Heil, A., Andreae, M. O., Benedetti, A., Chubarova, N., Jones, L., Morcrette, J. J., Razinger, M., Schultz, M. G., Suttie, M., and Van Der Werf, G. R.: Biomass burning emissions estimated with a global fire assimilation system based on observed fire radiative power, Biogeosciences, 9, 527–554, 2012.

Kalabokas, P., Bartzis, J., and Papagiannakopoulos, P.: Atmospheric levels of nitrogen oxides at a Greek oil refinery compared with the urban measurements in Athens, Water, Air and Soil Pollution: Focus, 2, 703–716, 2002.

Kansal, A.: Sources and reactivity of NMHCs and VOCs in the atmosphere: A review, Journal of hazardous materials, 166, 17–26, 2009.

Kerbachi, R., Boughedaoui, M., Bounoua, L., and Keddam, M.: Ambient air pollution by aromatic hydrocarbons in Algiers, Atmospheric Environment, 40, 3995–4003, 2006.

Kerkweg, A., Buchholz, J., Ganzeveld, L., Pozzer, A., Tost, H., and Jöckel, P.: Technical Note: an implementation of the dry removal processes DRY DEPosition and SEDImentation in the Modular Earth Submodel System (MESSy), Atmospheric Chemistry and Physics, 6, 4617–4632, 2006a.

Kerkweg, A., Sander, R., Tost, H., and Jöckel, P.: Technical note: Implementation of prescribed (OFFLEM), calculated (ONLEM), and pseudo-emissions (TNUDGE) of chemical species in the Modular Earth Submodel System (MESSy), Atmospheric Chemistry and Physics, 6, 3603–3609, 2006b.

Kesselmeier, J. and Staudt, M.: Biogenic volatile organic compounds (VOC): an overview on emission, physiology and ecology, Journal of atmospheric chemistry, 33, 23–88, 1999.

Kim, K.-H. and Kim, M.-Y.: The distributions of BTEX compounds in the ambient atmosphere of the Nan-Ji-Do abandoned landfill site in Seoul, Atmospheric Environment, 36, 2433–2446, 2002.

Kleinman, L. I.: Low and high NOx tropospheric photochemistry, Journal of Geophysical Research: Atmospheres, 99, 16 831–16 838, 1994.

Koppmann, R.: Volatile organic compounds in the atmosphere, John Wiley & Sons, 2008.

Kroll, J. H. and Seinfeld, J. H.: Chemistry of secondary organic aerosol: Formation and evolution of low-volatility organics in the atmosphere, Atmospheric Environment, 42, 3593–3624, 2008.

Lamarque, J. F., Bond, T. C., Eyring, V., Granier, C., Heil, A., Klimont, Z., Lee, D., Liousse, C., Mieville, A., Owen, B., Schultz, M. G., Shindell, D., Smith, S. J., Stehfest, E., Van Aardenne, J., Cooper, O. R., Kainuma, M., Mahowald, N., McConnell, J. R., Naik, V., Riahi, K., and Van Vuuren, D. P.: Historical (1850–2000) gridded anthropogenic and biomass burning emissions of reactive gases and aerosols: methodology and application, Atmospheric Chemistry and Physics, 10, 7017–7039, 2010.

Landgraf, J. and Crutzen, P.: An efficient method for online calculations of photolysis and heating rates, Journal of the atmospheric sciences, 55, 863–878, 1998.

Lauer, A., Eyring, V., Hendricks, J., Jöckel, P., and Lohmann, U.: Global model simulations of the impact of ocean-going ships on aerosols, clouds, and the radiation budget, Atmospheric Chemistry and Physics, 7, 5061–5079, 2007.

Lawrence, M., Jöckel, P., and Kuhlmann, R. v.: What does the global mean OH concentration tell us?, Atmospheric Chemistry and Physics, 1, 37–49, 2001.

Lawrence, M. G. and Rasch, P. J.: Tracer transport in deep convective updrafts: Plume ensemble versus bulk formulations, Journal of the atmospheric sciences, 62, 2880–2894, 2005.

Lee, S., Chiu, M., Ho, K., Zou, S., and Wang, X.: Volatile organic compounds (VOCs) in urban atmosphere of Hong Kong, Chemosphere, 48, 375–382, 2002.

Lelieveld, J., Berresheim, H., Borrmann, S., Crutzen, P., Dentener, F., Fischer, H., Feichter, J., Flatau, P., Heland, J., Holzinger, R., Korrmann, R., Lawrence, M., Levin, Z., Markowicz, K., Mihalopoulos, N., Minikin, A., Ramanathan, V., De Reus, M., Roelofs, G., Scheeren, H., Sciare, J., Schlager, H., Schultz, M., Siegmund, P., Steil, B., Stephanou, E., Stier, P., Traub, M., Warneke, C., Williams, J., and Ziereis, H.: Global air pollution crossroads over the Mediterranean, Science, 298, 794–799, 2002.

Lelieveld, J., Brühl, C., Jöckel, P., Steil, B., Crutzen, P. J., Fischer, H., Giorgetta, M. A., Hoor, P., Lawrence, M. G., Sausen, R., and Tost, H.: Stratospheric dryness: model simulations and satellite observations, Atmospheric Chemistry and Physics, 7, 1313–1332, 2007.

Lelieveld, J., Gromov, S., Pozzer, A., and Taraborrelli, D.: Global tropospheric hydroxyl distribution, budget and reactivity, Atmospheric Chemistry and Physics Discussions, 2016, 1–25, doi:10.5194/acp-2016-160, URL http://www.atmos-chem-phys-discuss.net/acp-2016-160/, 2016.

Lewis, A. C., Carslaw, N., Marriott, P. J., Kinghorn, R. M., Morrison, P., Lee, A. L., Bartle, K. D., and Pilling, M. J.: A larger pool of ozone-forming carbon compounds in urban atmospheres, Nature, 405, 778–781, 2000.

Lightfoot, P. D., Cox, R., Crowley, J., Destriau, M., Hayman, G., Jenkin, M., Moortgat, G., and Zabel, F.: Organic peroxy radicals: kinetics, spectroscopy and tropospheric chemistry, Atmospheric Environment. Part A. General Topics, 26, 1805–1961, 1992.

Lin, S.-J. and Rood, R. B.: Multidimensional flux-form semi-Lagrangian transport schemes, Monthly Weather Review, 124, 2046–2070, 1996.

Lobert, J. M. and Warnatz, J.: Emissions from the combustion process in vegetation, Fire in the Environment, 13, 15–37, 1993.

Lohmann, U. and Roeckner, E.: Design and performance of a new cloud microphysics scheme developed for the ECHAM general circulation model, Climate Dynamics, 12, 557–572, 1996.

Lovelock, J.: Natural halocarbons in the air and in the sea, Nature, 256, 193–194, 1975.

Manzini, E., Giorgetta, M., Esch, M., Kornblueh, L., and Roeckner, E.: The influence of sea surface temperatures on the northern winter stratosphere: Ensemble simulations with the MAECHAM5 model, Journal of climate, 19, 3863–3881, 2006.

Martins, E. M., Arbilla, G., Bauerfeldt, G. F., and de Paula, M.: Atmospheric levels of aldehydes and BTEX and their relationship with vehicular fleet changes in Rio de Janeiro urban area, Chemosphere, 67, 2096–2103, 2007.

Mayer, B. and Kylling, A.: Technical note: The libRadtran software package for radiative transfer calculations-description and examples of use, Atmospheric Chemistry and Physics, 5, 1855–1877, 2005.

McDonald, J. D., Zielinska, B., Fujita, E. M., Sagebiel, J. C., Chow, J. C., and Watson, J. G.: Emissions from charbroiling and grilling of chicken and beef, Journal of the Air & Waste Management Association, 53, 185–194, 2003.

Michałowicz, J. and Duda, W.: Phenols—sources and toxicity, Polish Journal of Environmental Studies, 16, 347–362, 2007.

Miller, L., Xu, X., Grgicak-Mannion, A., Brook, J., and Wheeler, A.: Multi-season, multi-year concentrations and correlations amongst the BTEX group of VOCs in an urbanized industrial city, Atmospheric Environment, 61, 305–315, 2012.

Millet, D. B., Jacob, D. J., Custer, T. G., de Gouw, J. A., Goldstein, A. H., Karl, T., Singh, H. B., Sive, B. C., Talbot, R. W., Warneke, C., and Williams, J.: New constraints on terrestrial and oceanic sources of atmospheric methanol, Atmospheric Chemistry and Physics, 8, 6887–6905, doi:10.5194/acp-8-6887-2008, URL http://www.atmos-chem-phys.net/8/6887/2008/, 2008.

Millet, D. B., Guenther, A., Siegel, D. a., Nelson, N. B., Singh, H. B., de Gouw, J. a., Warneke, C., Williams, J., Eerdekens, G., Sinha, V., Karl, T., Flocke, F., Apel, E., Riemer, D. D., Palmer, P. I., and Barkley, M.: Global atmospheric budget of acetaldehyde: 3-D model analysis and constraints from in-situ and satellite observations, Atmospheric Chemistry and Physics, 10, 3405–3425, 2010.

Misztal, P., Hewitt, C., Wildt, J., Blande, J., a.S.D. Eller, Fares, S., Gentner, D., Gilman, J., Graus, M., Greenberg, J., a.B. Guenther, Hansel, a., Harley, P., Huang, M., Jardine, K., Karl, T., Kaser, L., Keutsch, F., Kiendler-Scharr, a., Kleist, E., Lerner, B., Li, T., Mak, J., a.C. Nölscher, Schnitzhofer, R., Sinha, V., Thornton, B., Warneke, C., Wegener, F., Werner, C., Williams, J., Worton, D., Yassaa, N., and a.H. Goldstein: Atmospheric benzenoid emissions from plants rival those from fossil fuels, Scientific reports, 5, 2015.

Mohr, C., Lopez-Hilfiker, F. D., Zotter, P., Prévoît, A. S. H., Xu, L., Ng, N. L., Herndon, S. C., Williams, L. R., Franklin, J. P., Zahniser, M. S., Worsnop, D. R., Knighton, W. B., Aiken, A. C., Gorkowski, K. J., Dubey, M. K., Allan, J. D., and Thornton, J. A.: Contribution of nitrated phenols to wood burning brown carbon light absorption in Detling, United Kingdom during winter time, Environmental science & technology, 47, 6316–6324, 2013.

Montzka, S. A., Krol, M., Dlugokencky, E., Hall, B., Jöckel, P., and Lelieveld, J.: Small interannual variability of global atmospheric hydroxyl, Science, 331, 67–69, 2011.

Moss, R. H., Nakicenovic, N., and O'Neill, B.: Towards new scenarios for analysis of emissions, climate change, impacts, and response strategies, IPCC, 2008.

Müller, J.-F.: Geographical distribution and seasonal variation of surface emissions and deposition velocities of atmospheric trace gases, Journal of Geophysical Research: Atmospheres, 97, 3787–3804, 1992.

Myriokefalitakis, S., Vrekoussis, M., Tsigaridis, K., Wittrock, F., Richter, A., Brühl, C., Volkamer, R., Burrows, J., and Kanakidou, M.: The influence of natural and anthropogenic secondary sources on the glyoxal global distribution, Atmospheric Chemistry and Physics, 8, 4965–4981, 2008.

Na, K., Kim, Y. P., Moon, I., and Moon, K.-C.: Chemical composition of major VOC emission sources in the Seoul atmosphere, Chemosphere, 55, 585–594, 2004.

Naik, V., Fiore, A. M., Horowitz, L. W., Singh, H. B., Wiedinmyer, C., Guenther, A., De Gouw, J. A., Millet, D. B., Goldan, P. D., Kuster, W. C., and Goldstein, A.: Observational constraints on the global atmospheric budget of ethanol, Atmospheric Chemistry and Physics, 10, 5361–5370, 2010.

Natangelo, M., Mangiapan, S., Bagnati, R., Benfenati, E., and Fanelli, R.: Increased concentrations of nitrophenols in leaves from a damaged forestal site, Chemosphere, 38, 1495–1503, 1999.

Nehr, S., Bohn, B., Dorn, H.-P., Fuchs, H., Häseler, R., Hofzumahaus, A., Li, X., Rohrer, F., Tillmann, R., and Wahner, A.: Atmospheric photochemistry of aromatic hydrocarbons: OH budgets during SAPHIR chamber experiments, Atmospheric Chemistry and Physics, 14, 6941–6952, doi:10.5194/acp-14-6941-2014, URL http://www.atmos-chem-phys.net/14/6941/2014/, 2014.

Ng, N., Kroll, J., Chan, A., Chhabra, P., Flagan, R., and Seinfeld, J.: Secondary organic aerosol formation from m-xylene, toluene, and benzene, Atmospheric Chemistry and Physics, 7, 3909–3922, 2007.

Nordeng, T. E.: Extended versions of the convective parametrization scheme at ECMWF and their impact on the mean and transient activity of the model in the tropics, European Centre for Medium-Range Weather Forecasts, 1994.

NRC, N. R. C.: Rethinking the ozone problem in urban and regional air pollution, Washington: National Academies Press, p. 489, 1991.

Odum, J. R., Jungkamp, T., Griffin, R. J., Forstner, H., Flagan, R. C., and Seinfeld, J. H.: Aromatics, reformulated gasoline, and atmospheric organic aerosol formation, Environmental Science & Technology, 31, 1890–1897, 1997.

Pickering, K. E., Wang, Y., Tao, W.-K., Price, C., and Müller, J.-F.: Vertical distributions of lightning NOx for use in regional and global chemical transport models, Journal of Geophysical Research: Atmospheres, 103, 31 203–31 216, 1998.

Pierce, T. E. and Waldruff, P. S.: PC-BEIS: a personal computer version of the biogenic emissions inventory system, Journal of the air & waste management association, 41, 937–941, 1991.

Pöschl, U., von Kuhlmann, R., Poisson, N., and Crutzen, P. J.: Development and intercomparison of condensed isoprene oxidation mechanisms for global atmospheric modeling, Journal of Atmospheric Chemistry, 37, 29–52, 2000.

Pozzer, A., Jöckel, P., Sander, R., Williams, J., Ganzeveld, L., and Lelieveld, J.: Technical Note: The MESSy-submodel AIRSEA calculating the air-sea exchange of chemical species, Atmospheric Chemistry and Physics, 6, 5435–5444, 2006.

Pozzer, A., Jöckel, P., Tost, H., Sander, R., Ganzeveld, L., Kerkweg, A., and Lelieveld, J.: Simulating organic species with the global atmospheric chemistry general circulation model ECHAM5/MESSy1: a comparison of model results with observations, Atmospheric Chemistry and Physics, 7, 2527–2550, 2007.

Pozzer, A., Jöckel, P., and Aardenne, J. V.: The influence of the vertical distribution of emissions on tropospheric chemistry, Atmospheric Chemistry and physics, 9, 9417–9432, 2009.

Pozzer, A., Pollmann, J., Taraborrelli, D., Joeckel, P., Helmig, D., Tans, P., Hueber, J., and Lelieveld, J.: Observed and simulated global distribution and budget of atmospheric C_2-C_5 alkanes, Atmospheric Chemistry and Physics, 10, 4403–4422, 2010.

Pozzer, A., Meij, A. d., Pringle, K., Tost, H., Doering, U., Aardenne, J. v., and Lelieveld, J.: Distributions and regional budgets of aerosols and their precursors simulated with the EMAC chemistry-climate model, Atmospheric Chemistry and Physics, 12, 961–987, 2012.

Prather, M. and Spivakovsky, C. M.: Tropospheric OH and the lifetimes of hydrochlorofluorocarbons, Journal of Geophysical Research: Atmospheres, 95, 18 723–18 729, 1990.

Price, C. and Rind, D.: Modeling global lightning distributions in a general circulation model, Monthly Weather Review, 122, 1930–1939, 1994.

Ramaswamy, V., Boucher, O., Haigh, J., Hauglustaine, D., Haywood, J., Myhre, G., Nakajima, T., Shi, G., and Solomon, S.: Radiative forcing of climate change, Tech. rep., Pacific Northwest National Laboratory (PNNL), Richland, WA (US), 2001.

Ran, L., Zhao, C., Geng, F., Tie, X., Tang, X., Peng, L., Zhou, G., Yu, Q., Xu, J., and Guenther, A.: Ozone photochemical production in urban Shanghai, China: Analysis based on ground level observations, Journal of Geophysical Research: Atmospheres (1984–2012), 114, 2009.

Riahi, K., Grübler, A., and Nakicenovic, N.: Scenarios of long-term socio-economic and environmental development under climate stabilization, Technological Forecasting and Social Change, 74, 887–935, 2007.

Rickard, A. and Pascoe, S.: The Master Chemical Mechanism (MCM), http://mcm.leeds.ac.uk, 2009.

Robert, A.: The integration of a spectral model of the atmosphere by the implicit method, in: Proc. WMO/IUGG Symposium on NWP, Tokyo, Japan Meteorological Agency, vol. 7, pp. 19–24, 1969.

Rocke, A. J.: It Began with a Daydream: The 150th Anniversary of the Kekulé Benzene Structure, Angewandte Chemie International Edition, 54, 46–50, doi:10.1002/anie.201408034, URL http://dx.doi.org/10.1002/anie.201408034, 2015.

Roeckner, E., Bäuml, G., Bonaventura, L., Brokopf, R., Esch, M., Giorgetta, M., Hagemann, S., Kirchner, I., Kornblueh, L., Rhodin, A., Schlese, U., Schulzweida, U., and Tompkins, A.: The atmospheric general circulation model ECHAM 5. PART I: Model description, 2003.

Roeckner, E., Brokopf, R., Esch, M., Giorgetta, M., Hagemann, S., Kornblueh, L., Manzini, E., Schlese, U., and Schulzweida, U.: Sensitivity of simulated climate to horizontal and vertical resolution in the ECHAM5 atmosphere model, Journal of Climate, 19, 3771–3791, 2006.

Roesch, A. and Roeckner, E.: Assessment of snow cover and surface albedo in the ECHAM5 general circulation model, Journal of Climate, 19, 3828–3843, 2006.

Roth, E., Chakir, A., and Ferhati, A.: Study of a Benzoylperoxy Radical in the Gas Phase: Ultraviolet Spectrum and C6H5C (O) O2+ HO2 Reaction between 295 and 357 K, The Journal of Physical Chemistry A, 114, 10 367–10 379, 2010.

Sack, T. M., Steele, D. H., Hammerstrom, K., and Remmers, J.: A survey of household products for volatile organic compounds, Atmospheric Environment. Part A. General Topics, 26, 1063–1070, 1992.

Sanadze, J.: Emission of organic matters by leaves of Robinia pseudoacacia L, Soobshch Akad Nauk Gruz SSR, 19, 83–86, 1957.

Sander, R.: Compilation of Henry's law constants for inorganic and organic species of potential importance in environmental chemistry, 1999.

Sander, R.: Compilation of Henry's law constants (version 4.0) for water as solvent, Atmospheric Chemistry and Physics, 15, 4399–4981, doi:10.5194/acp-15-4399-2015, URL http://www.atmos-chem-phys.net/15/4399/2015/, 2015.

Sander, R., Kerkweg, A., Jöckel, P., and Lelieveld, J.: Technical note: The new comprehensive atmospheric chemistry module MECCA, Atmospheric Chemistry and Physics, 5, 445–450, 2005.

Sander, R., Baumgaertner, A., Gromov, S., Harder, H., Jöckel, P., Kerkweg, A., Kubistin, D., Regelin, E., Riede, H., Sandu, A., Taraborrelli, D., Tost, H., and Xie, Z.-Q.: The atmospheric chemistry box model CAABA/MECCA-3.0, 4, 373–380, http://www.geosci-model-dev.net/4/373, 2011.

Sandu, A. and Sander, R.: Technical note: Simulating chemical systems in Fortran90 and Matlab with the Kinetic PreProcessor KPP-2.1, Atmospheric Chemistry and Physics, 6, 187–195, 2006.

Sanford, R. L., Saldarriaga, J., Clark, K. E., Uhl, C., and Herrera, R.: Amazon rain-forest fires, Science, 227, 53–55, 1985.

Sarigiannis, D. A. and Gotti, A.: Biology-based dose-response models for health risk assessment of chemical mixtures, Fresenius Environmental Bulletin, 17, 1439–1451, 2008.

Saunders, S., Jenkin, M., Derwent, R., and Pilling, M.: Protocol for the development of the Master Chemical Mechanism, MCM v3 (Part A): tropospheric degradation of non-aromatic volatile organic compounds, Atmospheric Chemistry and Physics, 3, 161–180, 2003.

Seinfeld, J. H. and Pandis, S. N.: Atmospheric chemistry and physics: from air pollution to climate change, John Wiley & Sons, 2012.

Shiojiri, K., Maeda, T., Arimura, G. I., Ozawa, R., Shimoda, T., and Takabayashi, J.: Functions of plant infochemicals in tritrophic interactions between plants, herbivores and carnivorous natural enemies, Japanese Journal of Applied Entomology and Zoology, 46, 117–133, 2002.

Sindelarova, K., Granier, C., Bouarar, I., Guenther, A., Tilmes, S., Stavrakou, T., Müller, J. F., Kuhn, U., Stefani, P., and Knorr, W.: Global dataset of biogenic VOC emissions calculated by the MEGAN model over the last 30 years, Atmos. Chem. Phys. Discuss, 14, 10 725–10 788, 2014.

Snyder, R., Witz, G., and Goldstein, B. D.: The toxicology of benzene., Environmental health perspectives, 100, 293, 1993.

Stevenson, D., Dentener, F., Schultz, M., Ellingsen, K., Van Noije, T., Wild, O., Zeng, G., Amann, M., Atherton, C., Bell, N., et al.: Multimodel ensemble simulations of present-day and near-future tropospheric ozone, Journal of Geophysical Research: Atmospheres, 111, 2006.

Stier, P., Feichter, J., Kinne, S., Kloster, S., Vignati, E., Wilson, J., Ganzeveld, L., Tegen, I., Werner, M., Balkanski, Y., Schulz, M., Boucher, O., Minikin, A., and Petzold, A.: The aerosol-climate model ECHAM5-HAM, Atmospheric Chemistry and Physics, 5, 1125–1156, 2005.

Stockwell, W. R., Middleton, P., Chang, J. S., and Tang, X.: The second generation regional acid deposition model chemical mechanism for regional air quality modeling, Journal of Geophysical Research: Atmospheres, 95, 16 343–16 367, 1990.

Stockwell, W. R., Kirchner, F., Kuhn, M., and Seefeld, S.: A new mechanism for regional atmospheric chemistry modeling, Journal of geophysical research: Atmospheres, 102, 25 847–25 879, 1997.

Suthawaree, J., Tajima, Y., Khunchornyakong, A., Kato, S., Sharp, A., and Kajii, Y.: Identification of volatile organic compounds in suburban Bangkok, Thailand and their potential for ozone formation, Atmospheric Research, 104, 245–254, 2012.

Tan, J.-H., Guo, S.-J., Ma, Y.-L., Yang, F.-M., He, K.-B., Yu, Y.-C., Wang, J.-W., Shi, Z.-B., and Chen, G.-C.: Non-methane hydrocarbons and their ozone formation potentials in Foshan, China, Aerosol Air Qual Res, 12, 387–398, 2012.

Tanre, D., Geleyn, J., and Slingo, J.: First results of the introduction of an advanced aerosol-radiation interaction in the ECMWF low resolution global model, Aerosols and their climatic effects, pp. 133–177, 1984.

Taraborrelli, D., Lawrence, M. G., Butler, T. M., Sander, R., and Lelieveld, J.: Mainz Isoprene Mechanism 2 (MIM2): an isoprene oxidation mechanism for regional and global atmospheric modelling, Atmospheric Chemistry and Physics Discussions, 8, 14 033–14 085, doi:10.5194/acpd-8-14033-2008, 2008.

Tiedtke, M.: A comprehensive mass flux scheme for cumulus parameterization in large-scale models, Monthly Weather Review, 117, 1779–1800, 1989.

Tompkins, A. M.: A prognostic parameterization for the subgrid-scale variability of water vapor and clouds in large-scale models and its use to diagnose cloud cover, Journal of the atmospheric sciences, 59, 1917–1942, 2002.

Tørseth, K., Aas, W., Breivik, K., Fjæraa, A., Fiebig, M., Hjellbrekke, A., Lund Myhre, C., Solberg, S., and Yttri, K.: Introduction to the European Monitoring and Evaluation Programme (EMEP) and observed atmospheric composition change during 1972–2009, Atmospheric Chemistry and Physics, 12, 5447–5481, 2012.

Tost, H., Jöckel, P., Kerkweg, A., Sander, R., and Lelieveld, J.: Technical note: A new comprehensive SCAVenging submodel for global atmospheric chemistry modelling, Atmospheric Chemistry and Physics, 6, 565–574, 2006a.

Tost, H., Jöckel, P., and Lelieveld, J.: Influence of different convection parameterisations in a GCM, Atmospheric Chemistry and Physics, 6, 5475–5493, 2006b.

Tost, H., Jöckel, P., and Lelieveld, J.: Lightning and convection parameterisations–uncertainties in global modelling, Atmospheric Chemistry and Physics, 7, 4553–4568, 2007.

Tost, H., Lawrence, M. G., Brühl, C., Jöckel, P., Team, T. G., and Team, T. S.-O.-D.: Uncertainties in atmospheric chemistry modelling due to convection parameterisations and subsequent scavenging, Atmospheric Chemistry and Physics, 10, 1931–1951, 2010.

Tremp, J., Mattrel, P., Fingler, S., and Giger, W.: Phenols and nitrophenols as tropospheric pollutants: emissions from automobile exhausts and phase transfer in the atmosphere, Water, Air, and Soil Pollution, 68, 113–123, 1993.

Tsimpidi, A., Karydis, V., Pozzer, A., Pandis, S., and Lelieveld, J.: ORACLE (v1. 0): module to simulate the organic aerosol composition and evolution in the atmosphere, Geoscientific Model Development, 7, 3153–3172, 2014.

van Aalst, M. K., van den Broek, M. M. P., Bregman, A., Brühl, C., Steil, B., Toon, G. C., Garcelon, S., Hansford, G. M., Jones, R. L., Gardiner, T. D., Roelofs, G. J., Lelieveld, J., and

Crutzen, P. J.: Trace gas transport in the 1999/2000 Arctic winter: comparison of nudged GCM runs with observations, Atmospheric Chemistry and Physics, 4, 81–93, 2004.

Van der Werf, G. R., Randerson, J. T., Giglio, L., Collatz, G., Mu, M., Kasibhatla, P. S., Morton, D. C., DeFries, R., Jin, Y. v., and van Leeuwen, T. T.: Global fire emissions and the contribution of deforestation, savanna, forest, agricultural, and peat fires (1997–2009), Atmospheric Chemistry and Physics, 10, 11 707–11 735, 2010.

van het Bolscher, M., Pulles, T., Roel Brand, T., Pereira, A. J., Bernardo Mota, I., Spessa, L. A., Dalsøren, S., Twan van Nojie, K., Bilt, D., and Sophie Szopa, L.: Emission data sets and methodologies for estimating emissions Work Package 1, Deliverable D1-6.

van Vuuren, D. P., Feddema, J., Lamarque, J.-F., Riahi, K., Rose, S., Smith, S., and Hibbard, K.: Work plan for data exchange between the integrated assessment and climate modeling community in support of phase-0 of scenario analysis for climate change assessment (representative community pathways), assessment (Representative Community Pathways), 3, 4, 2008.

van Vuuren, D. P., Edmonds, J., Kainuma, M., Riahi, K., Thomson, A., Hibbard, K., Hurtt, G. C., Kram, T., Krey, V., Lamarque, J. F., Masui, T., Meinshausen, M., Nakicenovic, N., Smith, S. J., and Rose, S. K.: The representative concentration pathways: an overview, Climatic Change, 109, 5–31, 2011.

Voulgarakis, A., Naik, V., Lamarque, J. F., Shindell, D. T., Young, P. J., Prather, M. J., Wild, O., Field, R. D., Bergmann, D., Cameron-Smith, P., Cionni, I., Collins, W. J., Dalsoren, S. B., Doherty, R. M., Eyring, V., Faluvegi, G., Folberth, G. A., Horowitz, L. W., Josse, B., MacKenzie, I. A., Nagashima, T., Plummer, D. A., Righi, M., Rumbold, S. T., Stevenson, D. S., Strode, S. A., Sudo, K., Szopa, S., and Zeng, G.: Analysis of present day and future OH and methane lifetime in the ACCMIP simulations, Atmospheric Chemistry and Physics, 13, 2563–2587, 2013.

Wagner, W. P., Nemecek-Marshall, M., and Fall, R.: Three distinct phases of isoprene formation during growth and sporulation of Bacillus subtilis, Journal of bacteriology, 181, 4700–4703, 1999.

Warneck, P.: Multi-phase chemistry of C2 and C3 organic compounds in the marine atmosphere, Journal of Atmospheric Chemistry, 51, 119–159, 2005.

Went, F.: Blue hazes in the atmosphere, Nature, 187, 641–643, 1960.

Wesely, M.: Parameterization of surface resistances to gaseous dry deposition in regional-scale numerical models, Atmospheric Environment (1967), 23, 1293–1304, 1989.

Wild, M. and Roeckner, E.: Radiative fluxes in the ECHAM5 general circulation model, Journal of Climate, 19, 3792–3809, 2006.

WMO: International Meteorological Vocabulary (2nd ed.), doi:ISBN92-63-02182-1., 1992.

WMO: Air quality guidelines for Europe, Air Management Information System (AMIS) (World Health Organization, Geneva), 2000.

Wooster, M. J., Roberts, G., Perry, G., and Kaufman, Y.: Retrieval of biomass combustion rates and totals from fire radiative power observations: FRP derivation and calibration relationships between biomass consumption and fire radiative energy release, Journal of Geophysical Research: Atmospheres, 110, 2005.

Yanai, M., Esbensen, S., and Chu, J.-H.: Determination of bulk properties of tropical cloud clusters from large-scale heat and moisture budgets, Journal of the Atmospheric Sciences, 30, 611–627, 1973.

Yarwood, G., Rao, S., Yocke, M., and Whitten, G.: Updates to the carbon bond chemical mechanism: CB05, Final report to the US EPA, RT-0400675, 8, 2005.

Yassaa, N., Ciccioli, P., Brancaleoni, E., Frattoni, M., and Meklati, B. Y.: Ambient measurements of selected VOCs in populated and remote sites of the Sahara desert, Atmospheric Research, 100, 141–146, 2011.

Yokelson, R. J., Griffith, D. W., and Ward, D. E.: Open-path Fourier transform infrared studies of large-scale laboratory biomass fires, Journal of Geophysical Research: Atmospheres, 101, 21 067–21 080, 1996.

Yokelson, R. J., Susott, R., Ward, D. E., Reardon, J., and Griffith, D. W.: Emissions from smoldering combustion of biomass measured by open-path Fourier transform infrared spectroscopy, Journal of Geophysical Research: Atmospheres, 102, 18 865–18 877, 1997.

Yokelson, R. J., Burling, I. R., Gilman, J. B., Warneke, C., Stockwell, C. E., De Gouw, J., Akagi, S. K., Urbanski, S. P., Veres, P., Roberts, J. M., Kuster, W. C., Reardon, J., Griffith, D. W. T., Johnson, T. J., Hosseini, S., Miller, J. W., Cocker, D. R., Jung, H., and Weise, D. R.: Coupling field and laboratory measurements to estimate the emission factors of identified and unidentified trace gases for prescribed fires, Atmospheric Chemistry and Physics, 13, 89–116, 2013.

You, X. I., Senthilselvan, A., Cherry, N. M., Hyan, G., Kim, M., and Burstyn, I.: Determinants of airborne concentrations of volatile organic compounds in rural areas of Western Canada, Journal of Exposure Science and Environmental Epidemiology, 18, 117–128, 2008.

Yu, Y., Panday, A., Hodson, E., Galle, B., and Prinn, R.: Monocyclic aromatic hydrocarbons in Kathmandu during the winter season, Water, air, and soil pollution, 191, 71–81, 2008.

Yurdakul, S., Civan, M., and Tuncel, G.: Volatile organic compounds in suburban Ankara atmosphere, Turkey: sources and variability, Atmospheric Research, 120, 298–311, 2013.

Zimmerman, P. R.: Testing of hydrocarbon emissions from vegetation, leaf litter and aquatic surfaces, and development of a methodology for compiling biogenic emission inventories, EPA-450-4-70-004U.S. Environ. Prot. Agency, Research Triangle Park, N.C.,, 1979.